ORNL-3210
UC-80 - Reactor Technology

GAS-COOLED REACTOR PROGRAM

QUARTERLY PROGRESS REPORT

FOR PERIOD ENDING SEPTEMBER 30, 1961

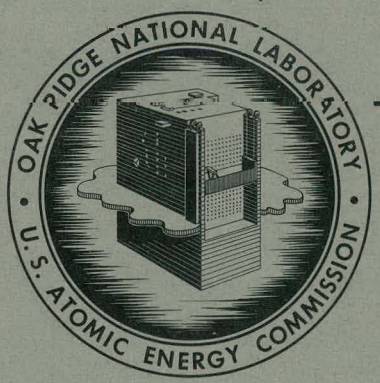

OAK RIDGE NATIONAL LABORATORY
operated by
UNION CARBIDE CORPORATION
for the
U.S. ATOMIC ENERGY COMMISSION

DISCLAIMER

Printed in USA. Price $3.50 . Available from the
Office of Technical Services
Department of Commerce
Washington 25, D.C.

ORNL-3210

Reactor Technology
TID-4500 (16th ed.)

Contract No. W-7405-eng-26

GAS-COOLED REACTOR PROGRAM

QUARTERLY PROGRESS REPORT

For Period Ending September 30, 1961

W. D. Manly, Program Director

DATE ISSUED

FEB - 5 1962

OAK RIDGE NATIONAL LABORATORY
Oak Ridge, Tennessee
operated by
UNION CARBIDE CORPORATION
for the
U. S. ATOMIC ENERGY COMMISSION

THIS PAGE

WAS INTENTIONALLY

LEFT BLANK

CONTENTS

PART 3. ADVANCED REACTOR DESIGN AND DEVELOPMENT

THIS PAGE

WAS INTENTIONALLY

LEFT BLANK

INTRODUCTION AND SUMMARY

This issue of the Oak Ridge National Laboratory's Gas-Cooled Reactor Program Quarterly Progress Report has been organized by project subdivisions, rather than by the previously used breakdown by scientific and engineering subject matter. The major subdivisions of this report are:

Part 1. Investigations in Support of the Experimental Gas-Cooled Reactor

Part 2. Pebble-Bed Reactor Experiment

Part 3. Advanced Reactor Design and Development

Part 4. Test Facilities, Components, and Materials

Future reports in this series will be organized by project in this manner, with appropriate changes as projects are completed and new ones are initiated.

Part 1. Investigations in Support of the Experimental Gas-Cooled Reactor

1. EGCR Physics

The multiplication factors for the through-tube experiment in the Hanford Physical Constants Test Reactor were calculated for the actual experimental system using the methods now being used for EGCR core calculations. The agreement between the measured and calculated values was excellent.

Two groups of calculations were made of the multiplication factor of the EGCR without steel through-tubes. The first group of calculations gave information on the minimum shutdown margin and the number of rods which may be removed from the core or fail to function properly when a shutdown of the cold reactor is required. The results indicated the relative insensitivity of Δk on the location of a withdrawn control rod. The second group of calculations gave data on the conditions that will be encountered during operation of the first core.

A model has been developed for the calculation of the thermal-neutron spectra in graphite that is based on the free gas model for scattering kernels. It was assumed that the flux could be represented by the sum of two components, a Maxwellian distribution and an epithermal residue that approaches 1/E in the asymptotic region. It has been found that the problem reduces to one of finding a good approximation to f(E) and that no more than two free parameters are required to produce an extremely good fit to the epithermal residue.

2. EGCR Performance Analyses

Two cases of the effect of coolant flow interruption because of total failure of the EGCR power supply were considered. In the first case it was assumed that the service machine was attached to the reactor vessel, with all tools withdrawn into the service machine, and that the service machine isolation valve was open and inoperative. In this case it was found that the nozzle and service machine temperatures would remain within safe limits. In the second case it was assumed that the concrete shielding plugs were in place in the nozzles; the service machine was not attached. It was found that after 1 hr the nozzle temperature would be approximately 800°F. An evaluation of the effect of this temperature should be made.

An investigation was made of the flow distribution that could be obtained in the EGCR following loss of normal power if the vessel cooling compressor were supplied with emergency power. The data obtained will be used in an evaluation of core flow in relation to hazards problems.

Analog computer studies of EGCR transient conditions were made to predict the behavior of the system for several scram conditions. The effect of maintaining a constant steam throttle valve position and the effect of a constant turbine pressure were investigated for scrams in which the gas flow decreased at the maximum rate allowed by the blower specifications. For both cases the rate of change of steam generator inlet gas temperature (reactor outlet gas temperature) was less than 150°F/min (the design maximum); however, the rate of change of steam generator outlet gas temperature exceeded the design rate for the first 15 to 20 sec. Another test showed that the steam generator outlet gas temperature was insensitive to changes in reactor power. Studies of two modes of control

(constant flux or load following) showed that the plant was basically stable; that is, it did not oscillate when control rod position, gas flow rate, and throttle valve position were held constant. Under various automatic control conditions the plant was generally sluggish.

Experiments have been conducted for determining whether coating the graphite sleeves of the EGCR fuel element with siliconized silicon carbide would prevent runaway oxidation, contingent on continued operation of one primary coolant blower after the maximum credible accident. Direct comparison tests of coated and uncoated graphite and the results of calculations have failed to prove that the coating, even if of the order of 95% effective, could prevent runaway oxidation under the conditions considered. It has therefore been recommended that the sleeves not be coated.

3. Structural Investigations

The stress analysis program coded by Battelle Memorial Institute for analyzing bodies under plane-strain conditions was used for calculating the thermal stresses that will exist in an EGCR graphite column during steady-state operation at design power. An examination of the results indicated that a reduction in the in-plane stresses could be obtained through the use of an 8-in. by 8-in. column; however, a smaller mesh spacing would have to be used to fully investigate the influence of such a change in geometry.

Graphite thermal rupture studies were initiated as a means of studying the effect of fast-neutron exposure and the resultant Wigner growth on the EGCR graphite moderator columns. A thick-walled cylinder heated by electrical resistance and cooled on the outer surface appeared to be the most attractive for this study from the standpoint of the temperature difference required, the power input, and complexity of the test equipment. It was found, however, that the temperature of such a specimen would be well above the usual upper limit of 1000°F considered for moderator structures in current reactor designs. Different test specimens will be considered.

4. EGCR Component Development and Testing

Endurance tests of a production model of the EGCR control rod and rod drive assembly in a simulated EGCR environment are being planned. The facility for these tests is to be ready for installation of the rod drive mechanism by January 1962.

Fabrication of the casings for the main coolant blowers for the EGCR is substantially behind schedule. Delays have resulted primarily from machining errors, and the repairs have consumed considerable time. The work on other phases of this contract are proceeding without apparent difficulty. Work is also under way on the pressure vessel cooling system compressors.

Four instrumented fuel assemblies are being fabricated for the EGCR. The instrumentation includes a Venturi, with its associated transducer, and 18 thermocouples.

Corrosion tests were conducted on metals of interest in the study of equipment decontamination. Methods for decontaminating from ruthenium and iodine deposited under simulated EGCR conditions are being studied.

5. EGCR Materials Development

The rupture strengths of graphite support sleeves coated with siliconized SiC were determined by the "brittle-ring" test. In all cases the rupture strength was much higher than the estimated tensile stress of 1300 psi during service. There was some indication that the strength was improved by an increase in the coating thickness, but it was also noted that the stronger specimens showed more penetration of the coating material into the graphite. A comparison of the thickness of pyrolytic-graphite coatings, as measured optically and by the eddy-current technique, indicated that eddy-current measurements are accurate to ±0.25 mil over the range from 0.5 to 5 mils.

A report was issued describing the development of suitable designs and fabrication techniques for the burst-slug-detection tube and thermocouple penetrations of the EGCR vessel. The testing of 14-in.-diam pipes containing dissimilar-metal welds is continuing. After heating through 60 thermal cycles, cracks were detected in the ferritic side of the dissimilar joints that were welded with type 347 stainless steel filler wire.

Metallographic examination showed extensive cracks and oxidation in the cracks. No cracks have been observed in similar test welds made with BP-85 filler wire.

Stainless steel coupons were exposed to small concentrations of pure CO_2 in helium to investigate the carburizing tendencies of CO_2. The results obtained at two concentrations indicate that CO_2 is both carburizing and decarburizing, depending on the temperature. The maximum carbon content was observed in specimens tested at ~1600°F. Additional oxidation tests were conducted to determine the effect of pressure on the rate of oxidation of stainless steel at 1800°F in CO-CO_2 mixtures. It was observed that the rate depends on the concentration when a nonprotective oxide is formed, as in pure CO_2, but is relatively independent of the concentration in CO-CO_2 mixtures that favor the formation of a protective oxide.

The effect of the restraint of the UO_2 column on the bowing of fuel elements was studied. The results showed that the extent of the temperature gradient was more important than the temperature level and that the UO_2 column reduced the calculated deflection. A maximum deflection of 0.004 in. was observed.

The fabrication of instrumented irradiation capsules for ORR loop No. 1 and the ORR Poolside Facility is proceeding. Techniques were developed for installing four internal thermocouples for measuring cladding temperatures along the 18-in.-long capsules. The thermocouples were brazed in place with copper.

The expected release of fission gases from ORR-irradiated group I and II capsules was calculated for two assumed conditions: (1) a 0.003-in. gap between the cladding and the UO_2, and (2) no gap between cladding and fuel. The release-rate parameter D′ was estimated from surface-area measurements on control samples of the UO_2 in each capsule. A report was issued in which these calculated values were shown to compare favorably with the measured release of Kr^{85} from the capsules. From this comparison it was concluded that the methods used for calculating release of fission gases are valid.

In graphite-metal diffusion studies, strong dependence of carburization depth on contact pressure has been noted. All bare stainless steel

surfaces bonded to the graphite, whereas copper-plated and black-oxidized surfaces did not. Serious embrittlement of the specimens that bonded was indicated in bend tests.

A final test of gas-metal reactions between type 304 stainless steel and CO-CO_2 impurities in helium in a thermal-convection loop at 1500°F was conducted. The CO_2-to-CO ratio in the helium was 4.0. The steel specimens had gray-green oxidation films, in contrast to the gray-to-black films developed in predominantly CO mixtures. Electron diffraction studies have identified the films as predominantly Mn_2CrO_4.

The degassing studies of EGCR graphite were completed with tests of two specimens to establish the release of sulfur compounds as a function of temperature and to provide volume-time relationships at temperatures other than the 300, 600, and 1000°C points that have been employed. The data indicated that SO_2 was released at 200°C (and probably below), but it disappeared above 600°C; H_2S and CS_2 were released in various amounts over the entire temperature range studied. The volume-time relationship studies confirmed the previously noted essentially linear relationship between the volume of gas evolved and the log of time.

A diffusion model for the transport of gases in porous media has been developed. Only two parameters are required to define a given binary gas-porous medium system in terms of the model. These are an effective normal diffusion coefficient (characteristic of both gases and the medium) and an effective Knudsen coefficient for one of the gases in the same medium. An experimental method for the determination of the required parameters for helium and argon in various types of graphite is being evaluated. Tentative experimental results indicate that the model is applicable over a wide range of gas temperatures, pressures, and media pore sizes.

6. Irradiation Testing of EGCR Components and Materials

Fuel capsule irradiations were continued in the ORR Poolside Facility. It has been determined that the radiation-monitoring system presently in use is inadequate to detect fission gases from cladding leaks in UO_2 specimens operated at low temperatures. Plans have been completed for increasing the monitoring sensitivity. Further, the positioning mechanism became inoperative, and modified equipment is being prepared for installation.

Pertinent design data and planned operating conditions for the next set of capsules to be irradiated have been developed, and the operational flow diagram has been prepared. A new method for establishing and maintaining the desired specimen temperature is being developed.

Additional examinations of group I capsules have confirmed previously reported results. One group III capsule (01-3) leaked NaK when pierced for fission-gas release. Efforts are being made to locate the leak. Post-irradiation determinations of the oxygen-to-uranium ratios of some of the fuel pellets have indicated no increase attributable to irradiation.

Metallographic examinations were made of a longitudinal section of the cladding from ETR capsule E-9. The heavy precipitate found at a pellet-to-pellet interface was tentatively identified as a nitride.

Metallographic examinations have been made, when possible, of a UO_2 pellet from the center of each LITR-irradiated capsule. The irradiated specimens were compared in each case with unirradiated control specimens, but there appears to be no direct correlation of grain size increase and the integrity of the UO_2 pellet with irradiation temperature. Possibly the samples were not representative of fuel irradiated at the estimated temperatures, either because of leaks in the capsules or reactions of the UO_2 with the tantalum thermocouple sheaths, or the recorded temperatures may not have been accurate because of thermocouple drift.

An investigation is being made of the effect of radiation on the notch ductility of the heat-affected zones of large welded structures such as pressure vessels for nuclear reactors. Radiation-induced increases in the notch-impact transition temperature have been detected, and samples are to be given a postirradiation heat treatment to determine the manner and extent of annealing of the radiation effects.

The thin-plate samples of UO_2 sandwiched between ThO_2 plates that were used in the LITR instantaneous fission-gas-release experiments have been removed and examined. As expected, the oxygen-to-uranium ratio of the samples had increased during irradiation. Another thin-plate sample of UO_2 was installed, and a sweep gas (argon or helium) that contained 3% hydrogen was used in an attempt to prevent oxidation. This atmosphere has been effective, and the gamma-ray spectrum of the fission gas being released is markedly different from that of the fission gas released from UO_2 in a nonreducing atmosphere.

7. EGCR Experimental Facilities

The preliminary design report for the EGCR experimental in-pile loops was completed. Studies were carried out to evaluate the credibility of reactor depressurization for several assumed loop experiments. Procurement has been initiated on the in-pile loop materials to be obtained by ORNL, and many subassemblies have been received.

A preliminary design analysis of a hydrogen-cooled in-pile loop to operate in the EGCR at a pressure of 300 psig at a power level of 500 kw has shown that the problems of handling hydrogen as a loop coolant are not as formidable as first predicted. The loop would contain a maximum of 4 lb of hydrogen gas, and the mixture of this small quantity of gas with the cell atmosphere would give a hydrogen concentration well below the limits of combustion.

Further development tests have been run on the through-tube bearings. A 6-in. hermetically sealed gate valve and a 1-in. hermetically sealed harmonic-drive globe valve are being subjected to thermal cycling tests at EGCR operating conditions.

Part 2. Pebble-Bed Reactor Experiment

8. PBRE Physics

Physics calculations have indicated that the critical core of the 30-in.-diam, 48-in.-high PBRE core will have a composition, expressed as the atomic ratios of carbon to thorium to U^{235}, of 590:1.4:1. Preliminary studies have indicated that four control rods, each 3 in. in diameter, located in the reflector, will be required. Approximate calculations have been made of the fast flux in the inner portions of the reflector for use in graphite-damage studies.

9. PBRE Design Studies

Preliminary core design parameters were established based on a system pressure of 500 psia, the requirement that the core flow be upward, and that the pressure drop across the core not exceed 80% of the weight of the bed, thus eliminating the need to hold the bed down to prevent levitation of the fuel pellets.

The effect of irradiation-induced stresses in graphite bodies on the design of the reflector of the PBRE in being studied, because the cracking and rupture associated with differential Wigner growth indicate that the reflector pieces above and below the fuel region must be replaceable. For the chosen design of closely packed 2-in.-diam cylindrical rods with their axes parallel to the core, however, calculations show that if the design lifetime of the reactor is 20 years of full power operation, the graphite should not need to be replaced because of differential Wigner growth alone.

A heat transfer analysis and a comparison of the pebble-bed reactor with the prismatic-core reactor was made. The comparison indicated that the fuel handling, and perhaps the reactor maintenance, for the pebble-bed reactor will have to be considerable easier and more economical than that for the prismatic reactors if the pebble-bed reactor is to be competitive.

10. PBRE Equipment Development and Testing

Preliminary studies were initiated to determine the general size and arrangement of the main PBRE blowers. Tests were initiated on bearings for a compressor for an in-pile loop for testing PBRE components. Means for isolating components for decontamination are being studied.

Part 3. Advanced Reactor Design and Development

11. Fueled-Graphite Investigations

Two batches of enriched carbon-coated UC_2 particles were received from the National Carbon Company for evaluation. Metallographic examination revealed that the coating on the particles has an unusual duplex structure which consists of a layer of pyrolytic graphite over a thin inner layer of pyrolytic carbon. In one batch of particles an extensive reaction was observed between the fuel and the inner layer of the coating. Although the surface contamination of particles in the other batch is higher than desirable, material from this second batch will be further evaluated by irradiation in the LITR in order to study the duplex coating.

Graphite-matrix fuel pellets for irradiation in the two ORR poolside sweep capsules were selected and encapsulated. Out-of-pile evaluation of these and similar miniature fuel pellets is being performed by standard techniques, including thermal cycling to 1500°C. Fuel distribution is poor in some pellets, but acid leaching after thermal cycling has indicated little damage to particles.

In a series of high-temperature experiments on neutron-activated specimens, the release of fission products from coated particles of batch HTM-1 was shown to occur by diffusion. A diffusion coefficient was calculated on the basis of diffusion through a uniform spherical shell.

A mathematical model was developed to describe the release of fission products through low-permeability containers. The model was confirmed by predicting within reasonable limits the relative release of three nuclides in the MTR-48-2 experiment.

The release of fission gases from miniature fueled-graphite bodies containing approximately 850 coated fuel particles was determined by heating neutron-activated samples to temperatures as high as 2100°C. The release of Xe^{133} below 2000°C was less than 10^{-3}; the data also indicate that two or more particles in each fuel body was either uncoated or had cracked. Similar release data are being obtained on control specimens of the fuel pellets used in the MTR-48 experiments. The gas released during heating of the 1-in.-diam pellets to a given temperature was much larger than the release during a long period at the same temperature. The effect of CO on the mechanism of release is being studied in attempts to explain the rapid release during heating.

Postirradiation examinations have been made of fuel pellets and the graphite cans irradiated in MTR capsules 48-1 and -2. It was found that the UC_2 particles in irradiated capsule 48-1 were not as angular as those of the control specimen and that no UC_2 "fingers" were present after irradiation. A fuel pellet from capsule 48-2 showed a similar microstructure. The low-permeability graphite cans used in assemblies MTR-48-1, -2, and -3 were also examined. It was found that each of the three silicon-sealed plugs had a spiral void because the roots of the threads had not filled. At best, only the first thread was completely sealed.

Miniature-capsule fission-gas-release experiments were continued in the LITR, and experimental assembly MTR-48-5 containing pyrolytic-carbon-coated UC_2 particles dispersed in a graphite matrix was inserted in the MTR.

Chemical processing methods are being developed for recovering uranium and thorium from irradiated high-temperature fuel elements containing coated fuel particles. Dissolution procedures that serve as head-end methods for decontamination and recovery of fissile and fertile material by tributyl phosphate–nitric acid solvent-extraction processes are being given first consideration, but alternative techniques, such as chloride volitility, are also being evaluated.

12. Clad Fuel Development

The preliminary design of a beryllium-clad 19-element fuel assembly for insertion in the EGCR has been completed. The fuel will consist of UO_2 pellets. This assembly is designed to produce 1.63 times the average channel power in the EGCR when a column of six assemblies is installed in a fuel channel. In order to achieve the design power, the enrichment will have to be increased in comparison with that of the standard EGCR fuel assembly. The temperature variations in the beryllium-clad assembly will be minimized by selecting a fuel channel in the high-flux region of the core in which to install the fuel assembly column so that the least amount of increased enrichment will be required.

In materials investigations for advanced fuel element design, the low-temperature release of fission products from UO_2 was studied between 500 and 800°C in vacuum and at 400°C in hydrogen. The calculated activation energy for release in the temperature range 400 to 800°C was 14.7 kcal/mole, in contrast to the accepted value of 70 to 80 kcal/mole at higher temperatures (greater than 1200°C).

The metallographic examination of UO_2 pellets fabricated for planned irradiation experiments showed a second phase in pellets containing 110- to 290-ppm iron and 100- to 240-ppm silicon. The second phase was tentatively identified by x-ray diffraction as Fe_3O_4 and alpha iron. In the fabrication of fueled BeO, preheating in vacuum to remove the binder was

found to be helpful in eliminating cracks during sintering. Crack-free specimens containing 20 vol % UO_2 as 150- to 250-μ-diam particles were sintered to 95% of theoretical density.

Studies of the thermal conductivity of 93.4% dense UO_2 by radial heat flow gave results of 0.0732 w/cm·°C near room temperature that decreased to 0.0582 w/cm·°C at 195°C. Determinations at higher temperatures are in progress.

Methods are being studied for producing dispersion-strengthened iron-aluminum-chromium alloys for cladding materials, using dispersions of oxides as the strengthening agents. Methods of preparing alloy powders are being studied. The mechanical fragmentation of higher alloys, followed by mixing with iron, looks favorable.

The correlation of all available tube-burst data at 1300 to 1600°F by means of the Dorn parameter shows good comparison for periods up to 1000 hr. However, the experimental results from longer test periods deviate from linear behavior.

A "break-away" reaction of hot-extruded beryllium tubing in helium containing 4 vol % water vapor was observed in several tests at 650°C. In previous tests of Pechiney Flake under similar conditions no "break-away" reaction occurred.

A batch of 200 ft of 0.300-in.-o.d., 0.040-in.-wall, beryllium tubing from Imperial Chemical Industries is being evaluated by nondestructive tests. While scattered contamination and a few defects have been observed, the tubing appears to be among the best examined to date. In order to correlate the mechanical properties of the tubing with the defects observed during inspection, numerous tubes that showed definite indications were re-examined to identify and mark sections for preparation of test specimens.

A comparison of the room-temperature shear strength of beryllium end-closure welds prepared by the arc-fusion and electron-beam processes showed that the arc-fusion welds are somewhat stronger. Thermal cycling from 1380 to 380°F of arc-fusion welds on eight types of beryllium tubing did not produce leakage after 500 cycles.

Six beryllium-clad UO_2-fueled capsules that were irradiated in the ORR were examined. Four of the capsules had not leaked, but two of the

capsules were completely filled with NaK from the heat transfer bath in which they were irradiated. The NaK was contaminated with fission products. All the capsules and pellets showed small increases in dimensions. Sections have been taken for metallographic examination.

Postirradiation examinations were conducted on a series of BeO-UO_2 pellets. All the pellets remained intact, but there was a general increase in dimensions. The fission-gas release was less than for UO_2 pellets.

Irradiation testing of beryllium sheet specimens manufactured by several techniques and containing various percentages of oxide and carbide gave no evidence for composition-dependent swelling. Several in-pile stress-rupture experiments on beryllium tubing were completed. The fractional decrease in the 100-hr rupture strength at 600°C, when plotted as a function of the exposure, showed good correlation for several samples. Similar data obtained at 700°C showed considerable scatter, perhaps because of the effects of corrosion.

A second experimental assembly containing ten tube-burst specimens of "boron-adjusted" heats of Inconel was tested in the ORR poolside facility. The data did not show that the rupture strength of Inconel is impaired by the helium generated during thermal-neutron bombardment of the B^{10}, as has been postulated.

Specimens of beryllium oxide are being irradiated in the ETR to study the stability of BeO under irradiation. Serious deterioration has occurred as a result of fast-neutron doses of 1×10^{20} to 2×10^{21} neutrons/cm^2. The greatest damage occurs with high doses at low temperatures. An evaluation of the temperature-annealing effects is planned.

13. Design Studies of Advanced Power Plants

Conceptual design studies of four gas-cooled reactor plants have been prepared to investigate the possibility of reducing capital costs by exploiting the advantages of all-ceramic fuel elements. In all four reactors the steam generator was placed directly over the reactor so that the two could be housed in a common pressure vessel. A new type of axial-tube steam generator was evolved. The studies indicated that major savings in the weight and cost of the pressure vessel, steam generator, shield, and containment vessel could be effected.

An analytical approach and an IBM machine code were prepared for the design of once-through steam generators. The results indicate that the size and cost of steam generators can be reduced by increasing the gas system pressure and temperature. Charts have been prepared to facilitate preliminary design calculations for a wide variety of steam generators for gas-cooled reactor applications.

A comparison of gas-turbine and steam power plants for use with all-ceramic gas-cooled reactors was made. The maintenance problems posed by the contaminated system were found to be more serious for the gas turbine and compressor than for the gas-circulator of the corresponding steam plant.

14. Experimental Investigations of Heat Transfer and Fluid Flow

Circumferential temperature distributions were obtained as a function of the axial distance along the cluster for all seven tubes of the downstream cluster in an apparatus containing two full-scale models of the EGCR Title II fuel bundle. In the initial experiments, the upstream cluster was unheated. Because of faulty electrical circuitry, a difference in heat generation of ~±4% around the mean existed between the individual tubes in the cluster. As a result, a gross discrepancy of 5% was found in the heat-transfer coefficients calculated for the six peripheral tubes. A shift observed in the relative positions of the peripheral and central tube heat-transfer coefficient curves for the upstream and downstream sections of the cluster was consistent with earlier results obtained in gas-mixing studies on the influence of the mid-cluster spacer in flow redistribution. Rewiring of the apparatus resulted in mean temperature distributions for the peripheral tubes which were uniform to within ±0.75%; heat-transfer coefficients calculated for tube 6 were ~4% greater than those obtained with nonuniform heating.

A unified correlation of both the heat-transfer and the mass-transfer data to include axial variations was developed by assuming that entrance-region heat or mass transfer in the EGCR cluster geometry could be treated from the viewpoint of boundary-layer growth on a flat plate. Empirical constants were developed from a composite of the data obtained on the several apparatuses used in the course of the experimental program. The

resulting equations, being expressed in terms of axial distance from the apparent channel inlet, are independent of the equivalent channel diameter and the tube ligament spacing, and they characterize the available data to within ±6.4% for heat transfer and ±15% for mass transfer. Both the heat transfer and mass transfer correlations yield coefficients ~30% greater than those found theoretically for flat plates.

15. Development of Equipment and Test Facilities

Experiments are being conducted with a gas chromatograph for the purpose of evaluating its usefulness in continuously monitoring low-pressure (100 mm Hg) helium for H_2, O_2, N_2, CH_4, CO, and CO_2. A modified process chromatograph obtained from Beckman Instruments has given excellent resolution of the six contaminants.

Additional tests of the emf drifts of sheathed Chromel-P vs Alumel thermocouples have shown that hydrogen penetration of the sheath resulted in development of marginally oxidizing conditions inside the sheath. Sheathed thermocouples exposed to hydrogen at 865°C developed emf drifts of −2.7 mv (−67.5°C) in 98 days. Exposure of similar couples to a CO atmosphere resulted in the usual, slight, positive emf drift. Low-temperature tests (704°C, 1300°F) on sheathed couples in a graphite-helium atmosphere have shown no trend in drift after 18 days of exposure. High-pressure hydrogen tests have been set up in an attempt to accelerate the development of negative emf drifts.

Studies have been made of expendable, self-contained, gas-cooled in-pile loops for testing fission-product deposition from unclad reactor fuels. Package loops for use in the LITR, ORR, and EGCR were considered.

Part 4. Test Facilities, Components, and Materials

16. Test Facilities Design and Construction

Construction of GCR-ORR loop No. 2 has been essentially completed, and modified loop No. 1 has been installed and is operating as designed. Pressure-vessel-steel weld samples are being irradiated.

The bearings of the two compressors that had operated for 3300 hr in loop No. 1 were examined, and it was found that they could have

continued to operate without relubrication. A gas-bearing compressor was received from Bristol Siddeley for experimentation.

A subcontract has been arranged with the University of Tennessee for development of basic information on the design and operation of shaft seals.

17. Fabrication Studies

Numerous BeO specimens were fabricated and characterized for use in irradiation experiments. The bulk density of sintered specimens was observed to be strongly affected by the heating rate when the sintering was done in hydrogen; the density was reduced from 96 to 64% when the time to reach the sintering temperature was increased from 2 to 24 hr.

In a study of the compatibility of ceramics and metals, several combinations of refractory materials were shown to be compatible at 1400°C. However, reactions of tantalum and molybdenum with pyrolytic graphite were observed after 345 hr at this temperature.

A nozzle slip-joint test assembly consisting of a T section with two dissimilar metal welds and an Al_2O_3-coated inner tube was fabricated for ORR loop No. 2. The assembly is being tested by thermal cycling to 1550°F.

PART 1. INVESTIGATIONS IN SUPPORT OF THE EXPERIMENTAL GAS-COOLED REACTOR

THIS PAGE

WAS INTENTIONALLY

LEFT BLANK

1. EGCR PHYSICS

A. M. Perry

Reactivity Effects of EGCR Experimental Loop Through-Tubes

D. R. Gilfillan

Experimental data on the reactivity effects of the experimental loop through-tubes have been obtained with the use of the Hanford Physical Constants Test Reactor. As reported previously,[1] the reactivity effect was calculated prior to the experiment in order to approximate the multiplication factor that would be produced by the tube, since this information was needed for planning. Since the tube dimensions used in the calculations did not precisely match those of the tube subsequently used in the experiment, the experimental system has been reanalyzed using the methods now being used for EGCR core calculations.[2] The results of the new calculations are compared with the measurements in Table 1.1. The experimental configuration represented an infinite lattice with one steel tube cell for each eight fuel cells at an enrichment of 1.8%.

[1] GCR Quar. Prog. Rep. Dec. 31, 1959, ORNL-2888, p. 8.

[2] GCR Quar. Prog. Rep. March 31, 1961, ORNL-3102, p. 3.

Table 1.1. Comparison of Calculated and Measured Multiplication Factors for Through-Tube Experiment in Hanford PCTR

Experimental Conditions	Multiplication Factor	
	Calculated	Measured
No steel tube	1.141	1.146 ± 0.004
Empty steel tube	1.032	1.029 ± 0.010
Steel tube containing 2.6% enriched EGCR fuel element	1.070	1.067 ± 0.006

EGCR Control Rod Patterns

C. A. Preskitt D. R. Gilfillan

The multiplication factor of the EGCR without steel through-tubes has been calculated for a large number of different control rod patterns. These were two-group, two-dimensional calculations in which each control rod was represented as a separate region, with the current-to-flux ratio specified as a boundary condition on the surface.[3] The graphite fuel element sleeves were assumed to be coated with 2.5 wt % silicon carbide. Subsequent to the completion of these calculations, the coating was removed from the design, with the result that all values of the multiplication factor reported here are low by an amount $\Delta k/k = 0.0025$.

These studies have been divided into two groups, one in which all control rods are fully inserted, with the exception of a selected few, and a second group in which only a few control rods are inserted and the remainder are fully withdrawn. All calculations in the first group represent the initial core loading at room temperature without fission products. Since this condition has the highest multiplication factor ever attained by the EGCR, these calculations give information on the minimum shutdown margin and the number of rods which may be removed from the core or fail to function properly when a shutdown of the cold reactor is required. The results of these calculations are shown in Table 1.2. The identification of the control rods is shown in Fig. 1.1; it should be noted that no control rods will be installed in positions A, Q, Z, and K.

One interesting observation to be made from these results is the relatively insensitive dependence of Δk on the location of the withdrawn control rod. This flattening of the rod importance results from the deletion of rods A, Q, Z, and K from the array, leaving a larger than average number of fuel channels per control rod near the core boundary, and from the tendency toward reflector moderation of the core when all control rods are inserted.

---

[3]GCR Quar. Prog. Rep. June 30, 1961, ORNL-3166, p. 3.

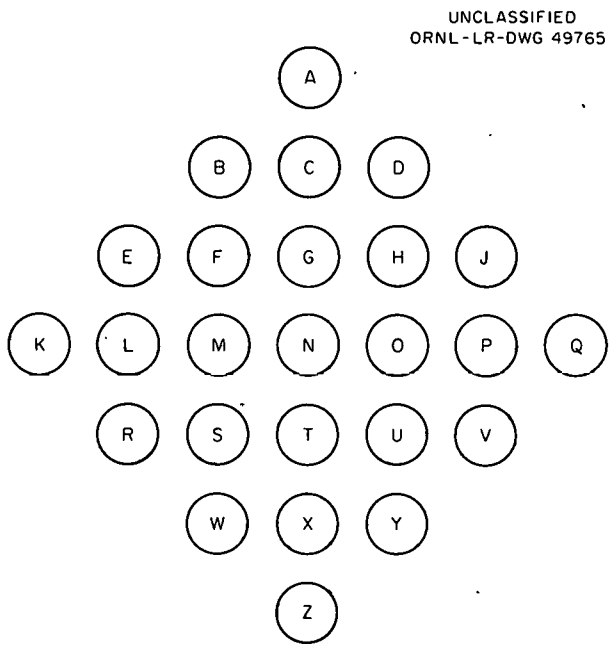

Fig. 1.1. Identification of EGCR Control Rods.

Calculations with the second group of control rod patterns, with a few selected rods fully inserted, were done for the initial core at operating temperature with equilibrium concentrations of xenon and samarium. This part of the study provided information on the reactivity effect and power distribution for the various configurations of fully inserted control rods that will be encountered during operation of the first core. The results of this group of calculations are given in Table 1.3.

A number of interesting effects were observed in the studies summarized in Table 1.3. For example, with rods GOTM inserted, the power distribution is extremely flat, with the peak falling near the radius of the inserted rods. When the central rod (rod N) is inserted together with GOTM, the peak power occurs near the core boundary, and the worth per rod is considerably less for this

Table 1.2. Multiplication Factor of EGCR Initial Core at Room Temperature and Clean

Core Condition	k_{eff}	Δk per Withdrawn Rod
No rods withdrawn	0.9214	
All 21 rods withdrawn	1.1631	0.0115
Rod N withdrawn	0.9376	0.0162
Rods GOTM withdrawn	0.9856	0.0161
Rods FHUS withdrawn	0.9723	0.0127
Rods CPXL withdrawn	0.9769	0.0139

Table 1.3. Multiplication Factor and Radial Peak-to-Average Power Ratio of EGCR Initial Core at Operating Temperature with Equilibrium Concentrations of Xenon and Samarium

Control Rods Fully Inserted	k_{eff}	Δk per Inserted Rod	Radial Peak-to-Average Power Ratio
None	1.0892		1.446
O	1.0750	0.0142	1.450
MO	1.0592	0.0150	1.280
GOTM	1.0330	0.0141	1.127
GOTMLP	1.0162	0.0122	1.303
NGOTM	1.0273	0.0124	1.149
FHUS	1.0352	0.0135	1.385
NFHUS	1.0216	0.0135	1.174
FHUSLP	1.0186	0.0118	1.519
FSP	1.0550	0.0114	1.619
NCPXL	1.0318	0.0115	1.382

configuration. It may also be noted that rods NFHUS are worth slightly more than NGOTM, in spite of the fact that the rods are inserted at a greater radius. As in the previous comparison, the difference between the two power distributions is such as to favor the fuel more in one case than the other.

Neutron Thermalization

E. A. Nephew C. A. Preskitt

Calculations of thermal-neutron spectra in graphite using the free-gas model for scattering kernels have been used to study the accuracy with which the spectrum can be approximated with simple models. In the absence of any perturbation in the spectrum, such as would be caused by a large Pu^{239} concentration, for example, it was assumed that the flux could be represented by the sum of two components, a Maxwellian distribution and an epithermal residue that approaches 1/E in the asymptotic region, that is,

$$\phi(E) = \frac{E}{(kT_N)^2} e^{-E/kT_N} + \lambda F(E) \quad ,$$

where k is Boltzmann's constant and T_N is the neutron temperature. The function F(E) will be referred to as the epithermal residue. For any computed thermal-neutron spectrum the function F(E) is determined by a least squares fitting of a Maxwellian to the total flux in the region of its peak, thus obtaining the neutron temperature. It has been found that the Maxwellian spectrum is a very good fit to the total spectrum up to an energy corresponding to 1.6 kT_N and that the epithermal residues obtained over a wide range of moderator temperatures and absorption cross section have quite similar characteristics. The most important of these characteristics are:

1. The residue contains a $(1/E)^2$ component whose sign and magnitude depend on the temperature and absorption cross section.
2. The peak of the residue occurs at approximately 5.9 kT_N.
3. The residue vanishes at energies below about 1.6 kT_N.

The problem of developing an accurate model for the total spectrum reduces to that of finding a good approximation to F(E). This approximation will, of necessity, contain a number of free parameters, and the utility of a given model depends on minimizing the number of free parameters and obtaining an accurate correlation of the parameters with characteristics of the system.

The present study has shown that no more than two free parameters are required to produce an extremely good fit to the epithermal residue. The region above about $8kT_N$ is well fitted by adding a $(1/E)^2$ term to the well-known 1/E variation usually assumed over this range. The region below $8kT_N$ is difficult to handle accurately, but the inclusion of a Gaussian type of function seems to provide an adequate fit. With this approximation the residue takes the following form:

$$F(E) = \frac{kT_N}{E^2} \left\{ \frac{E}{kT_N} + A - B \exp \left[\alpha \left(\frac{E}{kT_N} - \beta \right)^2 \right] \right\} \quad .$$

In fitting the residue over a very wide range of temperature and absorption cross section it has been found that both β and the difference B − A are very nearly constant, so the equation given above for F(E) actually contains only two free parameters.

A comparison between the exact residues and the function obtained with the present model is shown in Fig. 1.2. The fit is seen to be quite good even for the wide range of conditions represented by the two cases displayed. Additional study will be required in order to determine the accuracy to which the values of the two parameters of the residue may be correlated with the temperature and absorption cross section for a completely general set of conditions.

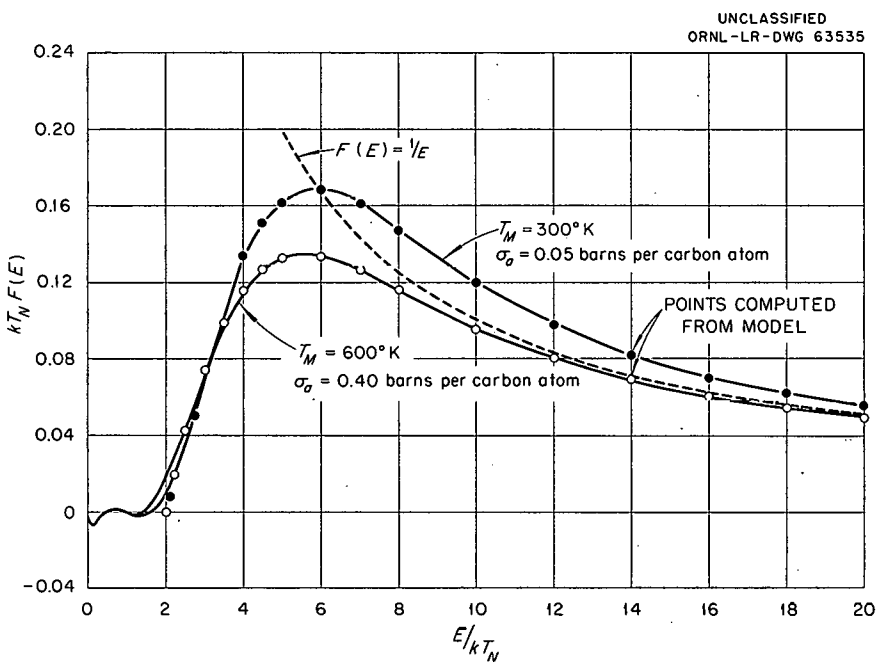

Fig. 1.2. Comparison of Exact Epithermal Residue with that Predicted by Model for Two Values of the Moderator Temperature, T_M, and Absorption Cross Section.

2. EGCR PERFORMANCE ANALYSES

Reactor Nozzle Temperatures Following Total Power Failure

G. Samuels M. E. Lackey

In the event of a total failure of the EGCR power supply, the operation of both the vessel cooling compressors and the reactor coolant blowers will be interrupted. The temperature history to be expected at the reactor top nozzles following this interruption has been investigated. Two cases were analyzed. In the first case it was assumed that the service machine was attached to the reactor vessel, with all tools withdrawn into the service machine, and that the service machine isolation valve was open and inoperative. In the second case it was assumed that the concrete shielding plugs were in place in the nozzles.

Case 1: Service Machine Attached

During normal operation both the service machine and the nozzle to which it is attached are cooled by helium flowing through the service machine and the nozzle into the reactor top plenum. This coolant flow will cease in the event of a total power failure. It was assumed that at the time of the power failure, the service machine, the concrete shield, and the internals of the nozzle were at a temperature of 150°F. The gas in the nozzle would be in contact with the 1050°F gas in the reactor top plenum, and, following the power failure, the nozzle gas would receive heat from the 1050°F gas by diffusion, eddy formation, etc. The nozzle walls and the concrete shield would act as heat sinks and would cool the gas in contact with the nozzle walls to below the bulk temperature of the gas in the nozzle. This cool gas would fall and a thermal-convection current would be started, with the cold gas falling on the outside and the hot gas from the plenum rising through the center of the nozzle.

A simplified model of this system was used for the heatup calculations. The major assumptions are listed below:

1. No time credit was taken for the establishment of thermal circulation.

2. No heat was lost from the nozzle to the concrete.

3. The nozzle was assumed to be at the gas temperature at all times.

4. Heat was transferred from the rising gas to the falling gas.

5. The rising gas entered the service machine and came to equilibrium with the internals of the machine before falling back into the nozzle.

6. No heat was lost from the service machine.

Various gas inlet temperatures from the service machine were assumed and the corresponding gas flow and temperatures entering the service machine were calculated. The initial temperature and flow conditions were assumed to hold for a period of time, after which new gas temperature and flow conditions were calculated from the heat input to the service machine. These temperature and flow conditions were assumed to hold for a period of time, and then the gas temperature and flow conditions were again recalculated. This process was repeated and the gas temperatures were plotted as a function of the total elapsed time. The results are shown in Fig. 2.1. As may be seen from Fig. 2.1, the nozzle will be at approximately 500°F and the service machine will be at approximately 270°F after 1 hr. These

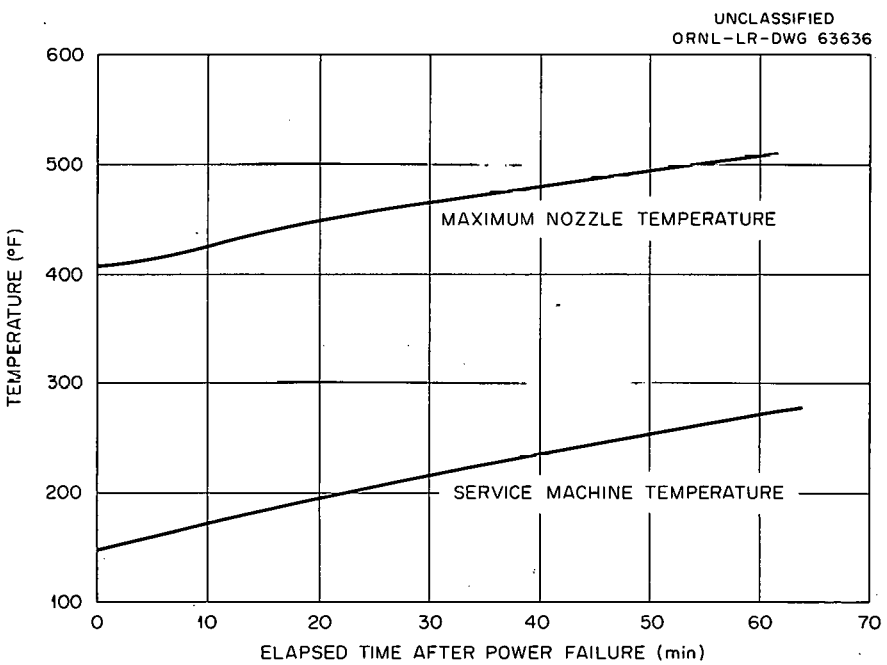

Fig. 2.1. Maximum Nozzle Temperature Following a Total Power Failure with Service Machine Attached.

results are considered to be conservative, since no heat loss from this system was considered, the nozzle was assumed to have zero heat capacity, and no allowance was taken for the establishment of thermal circulation. It appears therefore that under these conditions the nozzle and service machine temperatures will remain within safe limits.

Case 2: Service Machine Unattached

The reactor vessel top nozzles are normally cooled by helium flowing in the annulus formed by the nozzle wall and the insulating cylinder contained with the nozzle. The nozzle temperature is normally about 510°F, that is, the temperature of the helium coolant supply. The mechanism of the beginning of the natural circulation pattern, after the power failure, was assumed to be the same as outlined in case 1.

The major assumption used for the heatup calculations are listed below:

1. No time credit was taken for the establishment of the thermal circulation.

2. No heat was lost from the nozzle to its surroundings.

3. Heat was transferred from the rising hot gas to the cold falling gas in such a manner that they came to equilibrium at the nozzle top.

Various nozzle temperatures were assumed and the corresponding gas flow and temperatures leaving the top nozzle were calculated. The average temperature and flow conditions were assumed to hold during a temperature change of the nozzle. The corresponding time period was calculated assuming the nozzle to be an infinite heat sink during the temperature change. A new time period was then calculated for a new temperature change. The maximum nozzle temperature as a function of time is given in Fig. 2.2. As may be seen from Fig. 2.2 the nozzle temperature will be approximately 800°F after 1 hr. An evaluation of the effect of this temperature should be made.

Emergency Cooling Upon Loss of Normal Power

G. Samuels M. E. Lackey

An investigation has been made of the flow distribution that could be obtained in the reactor under various conditions following loss of normal

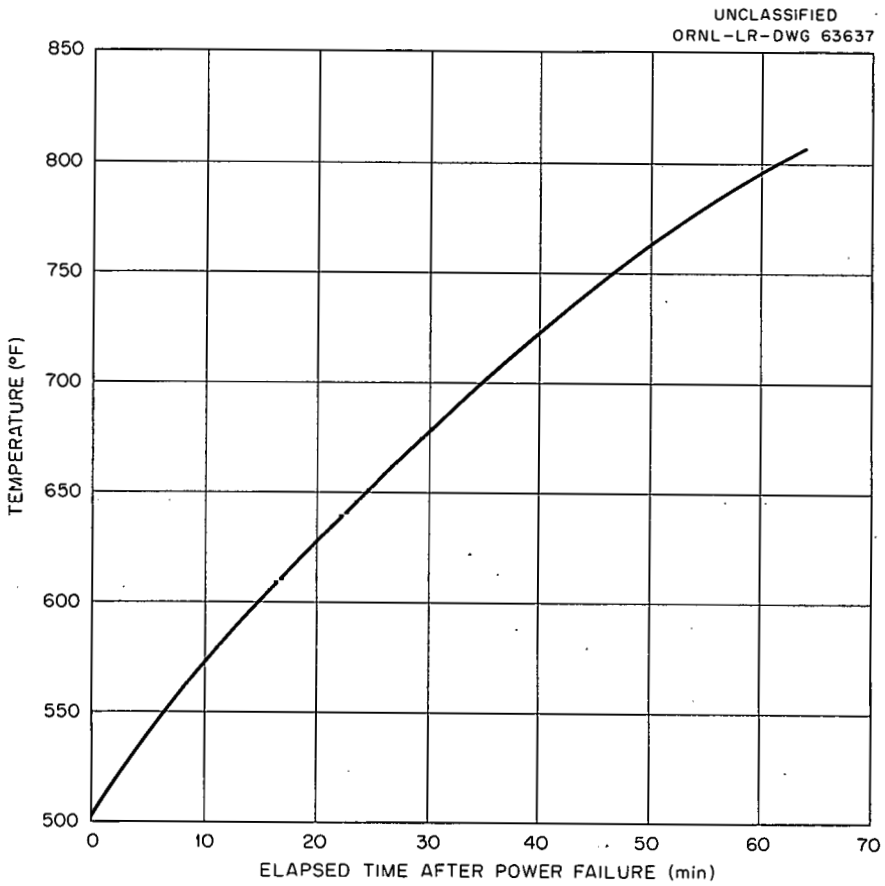

Fig. 2.2. Maximum Nozzle Temperature Following a Total Power Failure with Concrete Shield Plugs in Place.

power if the vessel cooling compressor were supplied with emergency power. The reactor vessel and nozzles are normally cooled by helium supplied by the vessel cooling compressor. This compressor also supplies coolant for the service machine and the charge machine. Four flow cases were investigated:

1. no flow to the charge machine or the service machine,
2. no flow to the charge machine,
3. no flow to the service machine,
4. flow to all service facilities.

A simplified flow diagram of the system is shown in Fig. 2.3. The presently planned system of piping, as shown by the solid lines in Fig. 2.3, and an alternate system of piping, as shown by the dashed lines in Fig. 2.3,

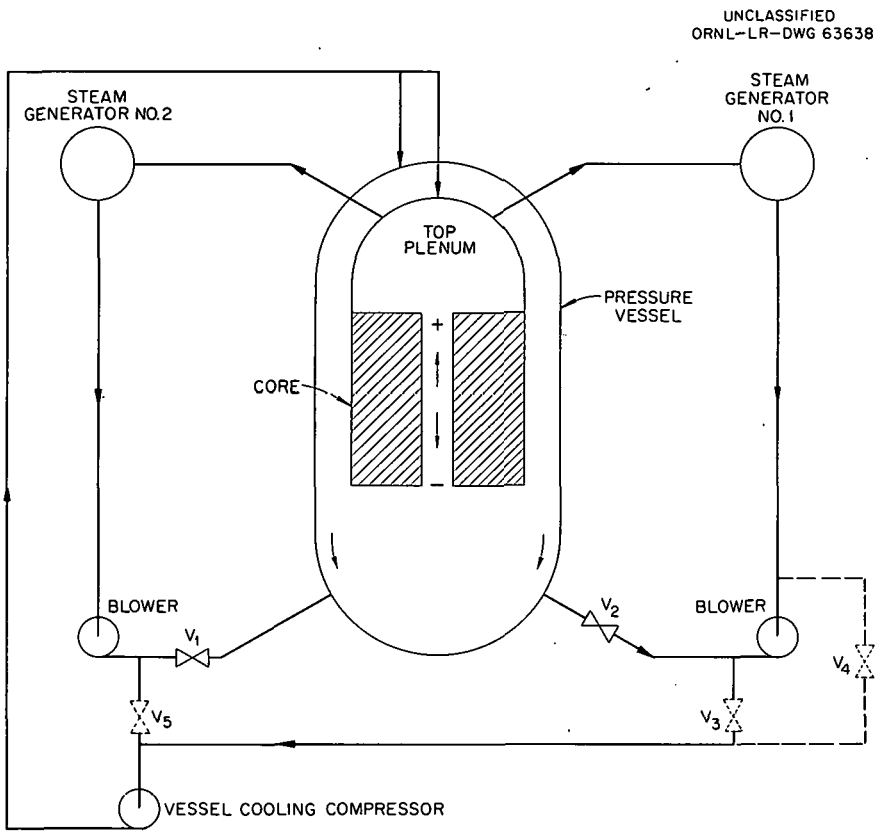

Fig. 2.3. Simplified Flow Diagram of the EGCR Pressure Vessel Cooling Systems.

were investigated. The present system was studied under the assumption that one of the main loop block valves (V_2) had failed to close. The alternate system flows were calculated under the assumption that both main loop block valves (V_1 and V_2) had failed to close. The alternate system requires that valves V_3 and V_5 be closed and valve V_4 be opened after the power failure. These data will permit an evaluation of core flow in relation to hazards problems associated with loss of main blower power. The resulting core and bypass flows for the four cases are listed in Table 2.1. These calculations do not include any thermal forces.

Table 2.1. Coolant Flow After Power Failure with the Vessel Cooling Compressor Operating on Emergency Power

Case	Flow with Present Piping (lb/hr)		Flow with Alternate Piping (lb/hr)	
	Core	Bypass to Top Plenum	Core	Bypass to Top Plenum
1	2 100	5 700	6 100	7 345
2	1 250	6 950	5 900	8 565
3	750	9 900	5 450	10 430
4	1 700	11 150	5 200	12 650

Analog Computer Studies of EGCR Transients

C. S. Walker S. J. Ball

The analog computer models of the EGCR reactor and steam generator developed at ORNL were combined and tested at the Electronic Associates, Incorporated, computing facility. The purpose of the studies was to predict the transient behavior of the plant for several scram conditions and to make preliminary investigations of various over-all plant control systems. Fine-structure representations of both the reactor and steam generator models were employed for all the tests made; however, it was assumed that the behavior of the two gas loops was identical and that the two steam generators operated effectively as a single unit.

The results of two reactor scram tests are shown in Figs. 2.4 and 2.5. In these tests the gas flow was decreased at the maximum rate allowed by the blower specifications.[1] This decrease is called the normal blower coast-down. The effect of maintaining a constant steam throttle valve position is shown in Fig. 2.4, and the effect of a constant turbine pressure is given in Fig. 2.5. The major differences in the two sets of data are in the steam-side behavior; that is, the steam flow rate falls off more rapidly for the case of pressure control. As a result of the lower steam flow rate,

[1]GCR Quar. Prog. Rep. June 30, 1961, ORNL-3166, pp. 30–31.

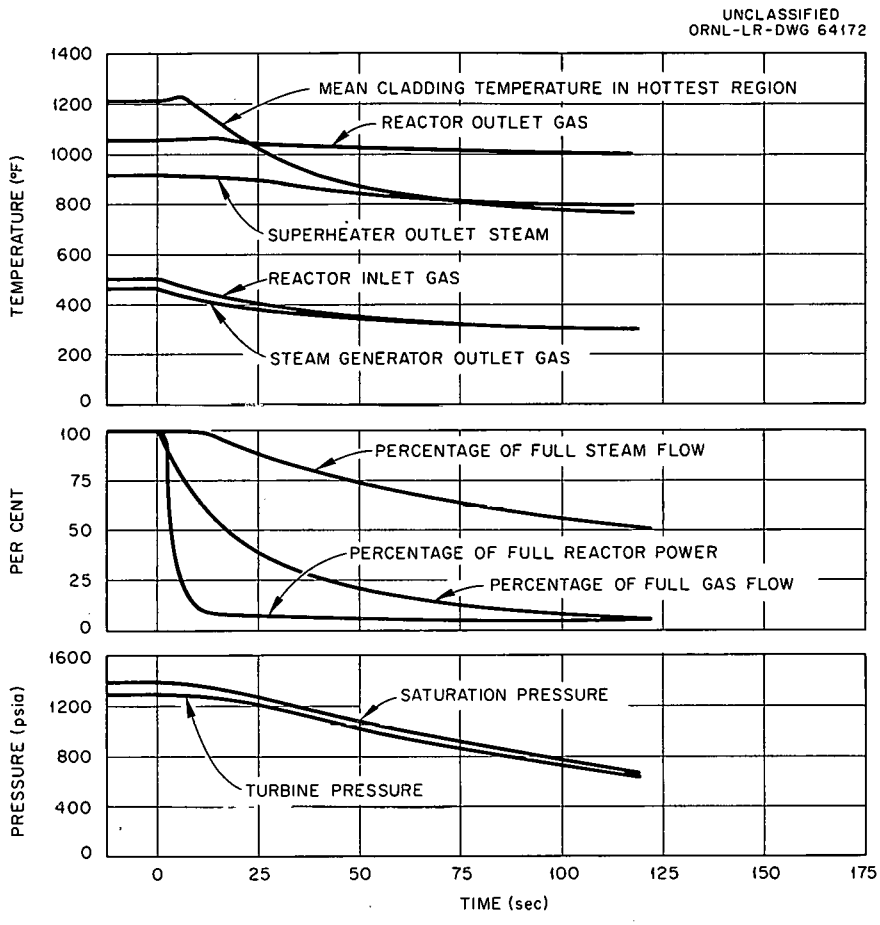

Fig. 2.4. Reactor Response to Scram from Full Power with Gas Flow Decrease as Specified by Normal Blower Coastdown and a Constant Steam Throttle Valve Position.

the superheater outlet steam temperature more closely approaches the reactor outlet gas temperature. The steam generator specifications state that the coolant gas within the steam generator will have a maximum rate of temperature change of 150°F/min. For both cases shown, the rate of change of steam generator inlet gas temperature (reactor outlet gas) is less than 150°F/min; however, the rate of change of steam generator outlet gas temperature exceeds the design rate for the first 15 to 20 sec.

Another point of interest is that other tests showed that for constant gas flow conditions, the steam generator outlet gas temperature is extremely insensitive to changes in reactor power. In a test of a reactor scram from full power with the gas flow rate and the steam throttle valve

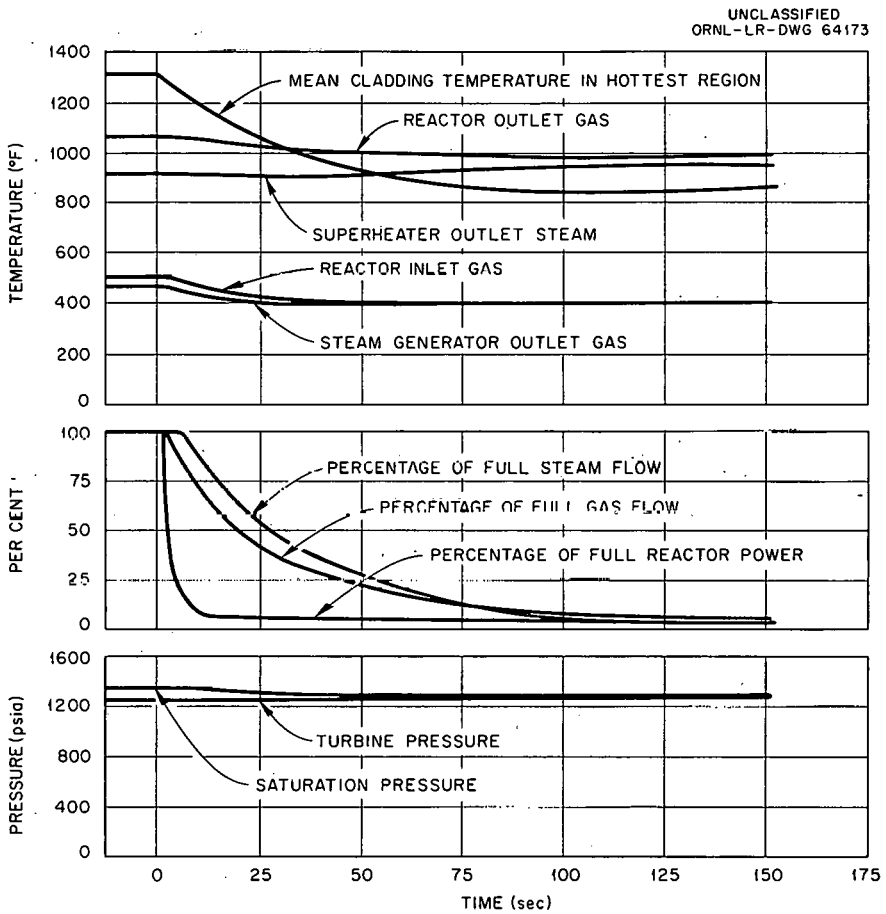

Fig. 2.5. Reactor Response to Scram from Full Power with Gas Flow Decrease as Specified by Normal Blower Coastdown and a Constant Turbine Pressure.

position held constant, a 400°F decrease of reactor outlet temperature within 2 min resulted in less than a 20°F decrease in the steam generator outlet gas temperature.

Control studies were conducted on the basis that the plant is to operate in either of two control modes: (1) a constant-flux mode, in which the reactor power will be maintained at various levels for experimental purposes, and (2) a load-following mode in which the reactor conditions will be varied to accommodate fluctuations in the power demand on the turbine-generator. Since the control requirements for the load-following mode are by far the more difficult, most of the effort was extended in investigating control systems for this mode.

The study showed that the plant was not basically unstable; that is, it did not oscillate when control rod position, gas flow rate, and throttle valve position were held constant. Characteristic oscillations of the plant under various automatic control conditions indicated a generally sluggish response and loose coupling between the reactor and the steam generators. Typical periods of oscillation ranged from 10 to 15 min. While it appeared that any given set of control rod, gas flow, and throttle valve conditions would finally result in a unique set of steam-side conditions, the approach rate of some of the parameters, notably turbine pressure in the load-following mode, was extremely slow. Several of the load-responsive control systems that were investigated showed promise in their ability to control the plant with steam flow as the independent variable. Reset (or integral) control signals from the steam temperature and pressure would be necessary in any case.

Graphite Oxidation

J. O. Kolb W. B. Cottrell

Information pertaining to graphite oxidation in the EGCR has become available from both experiments and calculations since the previous report on this problem.[2] A siliconized silicon carbide coating applied to the sleeve graphite was investigated as a means of preventing runaway oxidation, contingent on continued operation of one primary coolant blower after the maximum credible accident. Experiments for determining the value of the sleeve coating, which is intended to reduce the oxidation by 90 to 95%, have been conducted in the Hanford burning rig.[3] Two experiments with one with uncoated sleeves have been completed. In the latest experiment, coated sleeves were tested which had shear-pin holes and bend-tab slots that were machined into them after the coating was applied. The annulus coolant (air) was preheated to about 150°C for this

[2]GCR Quar. Prog. Rep. March 31, 1961, ORNL-3102, pp. 63–66.

[3]M. H. Fontana, Status Report on Oxidation Analyses for the EGCR, ORNL CF-61-6-28, June 15, 1961.

experiment, whereas in previous experiments the annulus coolant was at the ambient air temperature of about 80°F.

In the burning-rig experiments, the central coolant inlet temperature is between 250 and 400°C. Heat input is constant to the moderator-block Calrod heaters to make up for heat losses, and the heat input of the Globar heater in the center of the channel is programmed to simulate the EGCR afterheat. The Globar heat load is equivalent to the total afterheat generated in the sleeve and the moderator graphite in an EGCR average-power channel. The power to the moderator block heaters is set to establish calculated reactor temperatures. To approach runaway conditions, the initial temperature distribution is normally increased in successive steps, with the air flow rate held constant.

Although the burning-rig conditions are similar to the EGCR fuel channel conditions after the maximum credible accident, the 6-ft-long rig can only mock up part of the actual 14.5-ft-long active fuel channel. Hence the coolant inlet and initial graphite temperatures were chosen to mock up conditions for the top 6 ft of the actual fuel channel.

Direct comparison tests with coated and uncoated sleeves to determine the effectiveness of the coating have been made for only one set of conditions. With no preheating of the annulus air and an unmachined sleeve, similar cooldown was observed for coated and uncoated sleeves with 287-lb/hr coolant flow and an initial graphite temperature of approximatley 600°C. With an initial temperature of approximately 700°C and other conditions the same as above, local moderator block temperatures indicated "runaway" with both coated and uncoated sleeves. Therefore, in the comparable experiments that have been completed, the sleeve coating does not appear to affect significantly the conditions of runaway or the behavior of temperatures during cooldown.

The IBM 7090 graphite oxidation code[3] developed for calculating graphite channel temperatures during a transient by the flow of air through the channel was used for determining the effect of a 95%-effective sleeve coating for various air flow rates, oxidation heat release rates, inlet coolant temperatures, and inlet oxygen concentration conditions. These variables are felt to be the most important in determining a runaway

condition in the EGCR and therefore could determine the value of coating the sleeves, that is, whether or not runaway could be prevented over the expected range of these variables.

The maximum sleeve and moderator block temperatures as a function of time in a maximum-power channel are indicated in Figs. 2.6 through 2.11. The values of the variables of interest are listed below, with an indication of their bases:

Variable	Values Used in Calculations
Air inlet temperature	510°F: normal operating condition
	610°F: arbitrary 100°F increase above normal condition for higher temperature off-design conditions
Central air flow rate	186 lb/hr: average-power channel rate with 43% flow loss through ruptured loop
	365 lb/hr: average-power channel rate with no flow loss through ruptured loop
Inlet oxygen concentration	O_2 concentration in normal air: maximum O_2 concentration possible
	One half O_2 concentration in normal air: arbitrary decrease to investigate effect
Oxidation heat release	Normal EGCR release based on Hanford recommended oxidation rate[3] and Robinson's[4] diffusion-depth expression; changes from normal value were made within possible extreme values

The code was written using a cosine function, centered at the core midplane, to describe the axial-power distribution. For these calculations, the cosine power distribution with the highest peak-to-average ratio was used, that is, zero power at the top and bottom of the active core, since the axial-power distribution calculated for the EGCR has a high peak-to-average ratio. It is not presently known whether the axial

[4]P. J. Robinson, The Effects of Diffusional Control of Oxidation of Graphite on the Highest Safe Temperatures in Air, UKAEA Report 143 (RD/W), 1959.

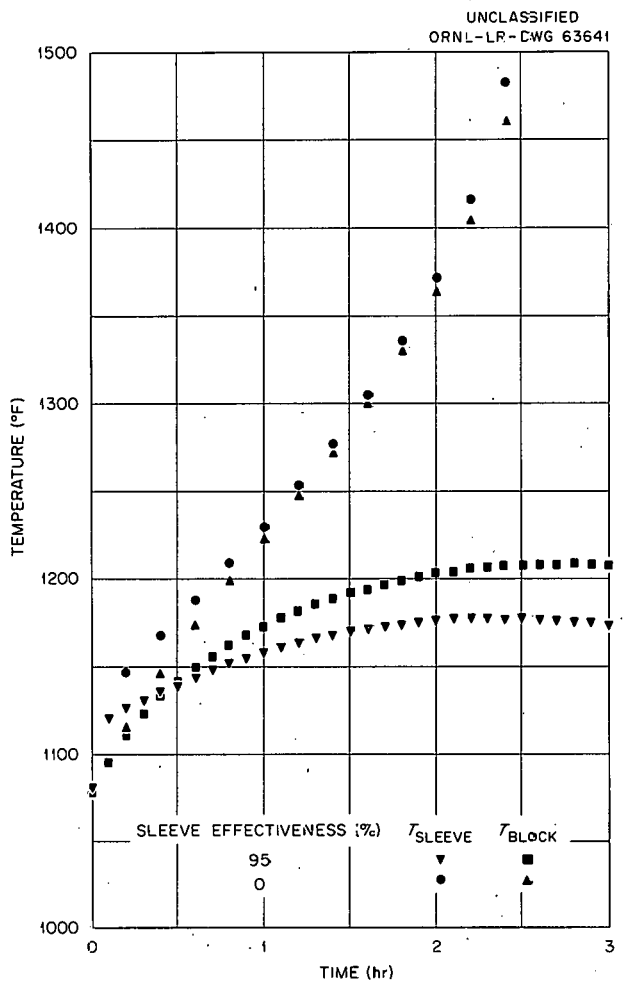

Fig. 2.6. Maximum EGCR Sleeve and Moderator Block Temperatures vs Time for an Inlet Air Temperature of 510°F, a Normal Air O_2 Concentration, a Central Channel Flow Rate of 186 lb/hr, and Normal Oxidation Heat Release.

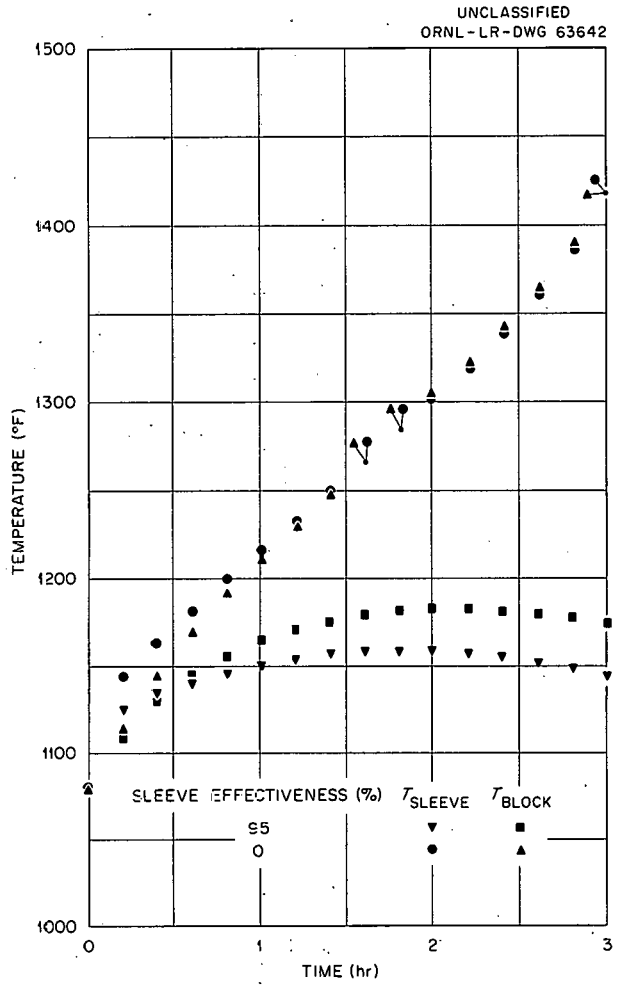

Fig. 2.7. Maximum EGCR Sleeve and Moderator Block Temperatures vs Time for an Inlet Air Temperature of 510°F, One-Half Normal Air O_2 Concentration, a Central Channel Flow Rate of 186 lb/hr, and Normal Oxidation Heat Release.

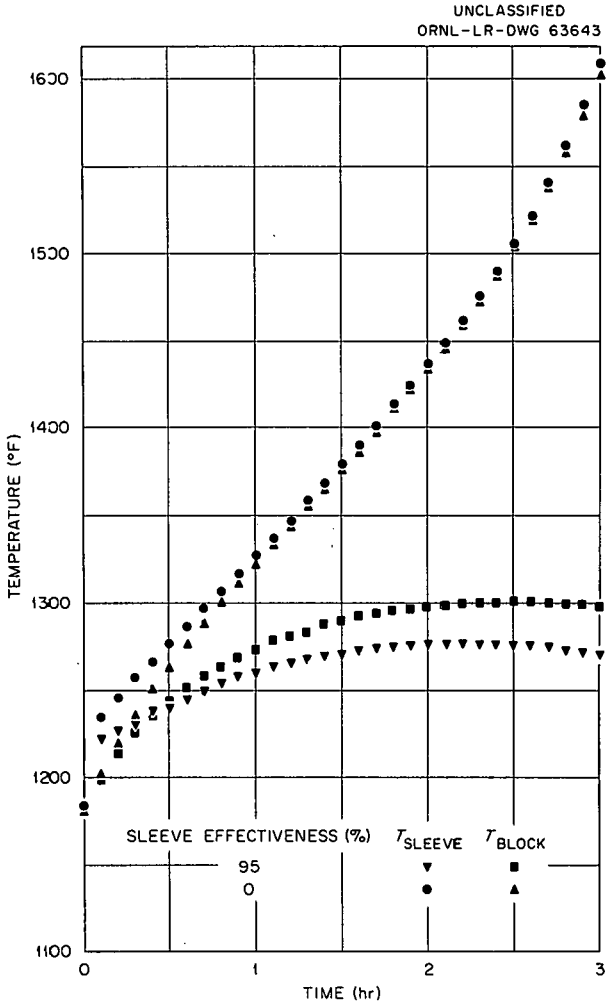

Fig. 2.8. Maximum EGCR Sleeve and Moderator Block Temperatures vs Time for an Inlet Air Temperature of 610°F, a Normal Air O_2 Concentration, a Central Channel Flow Rate of 186 lb/hr, and One-Half Normal Oxidation Heat Release.

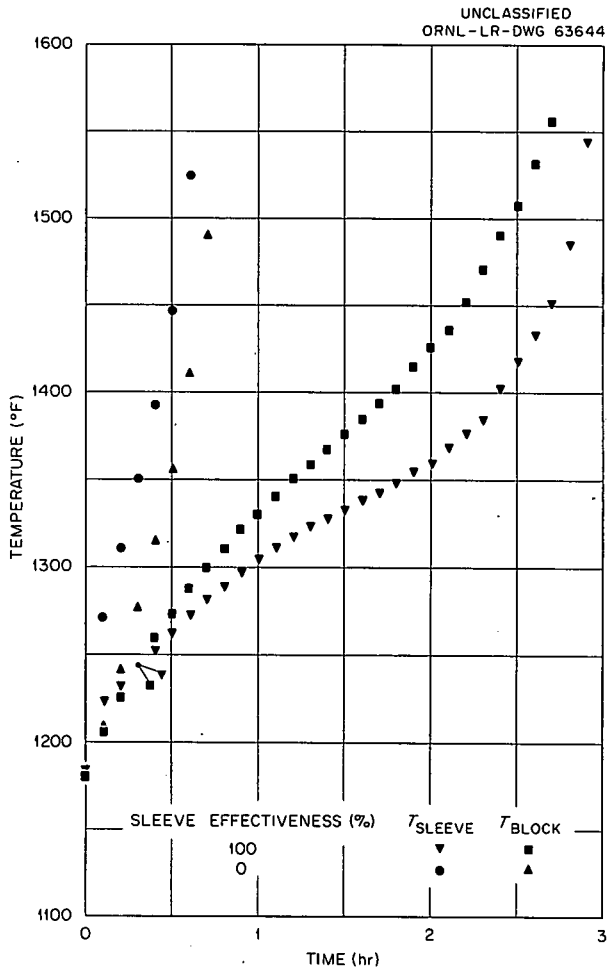

Fig. 2.9. Maximum EGCR Sleeve and Moderator Block Temperatures vs Time for an Inlet Air Temperature of 610°F, a Normal Air O_2 Concentration, a Central Channel Flow Rate of 186 lb/hr, and Twice the Normal Oxidation Heat Release.

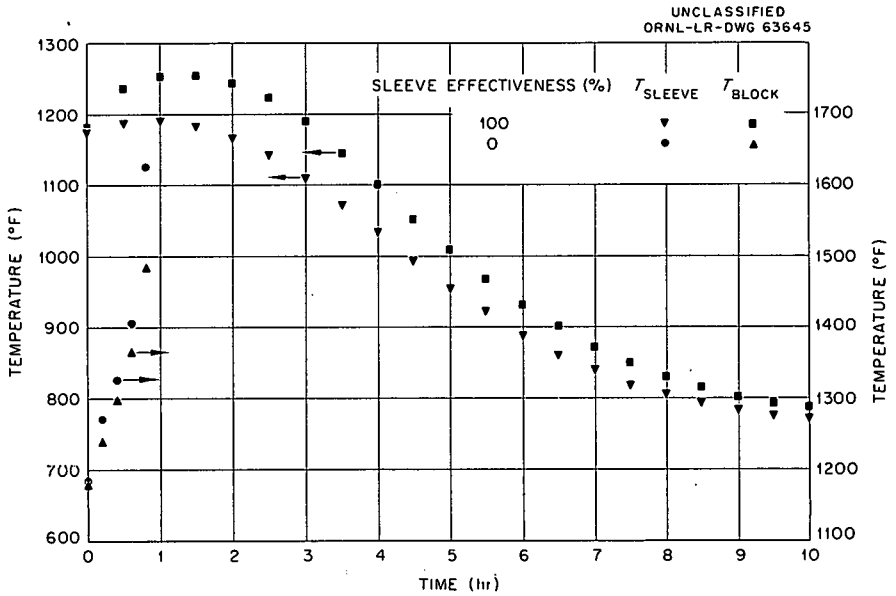

Fig. 2.10. Maximum EGCR Sleeve and Moderator Block Temperatures vs Time for an Inlet Air Temperature of 610°F, a Normal Air O_2 Concentration, a Central Channel Flow Rate of 365 lb/hr, and Twice the Normal Oxidation Heat Release.

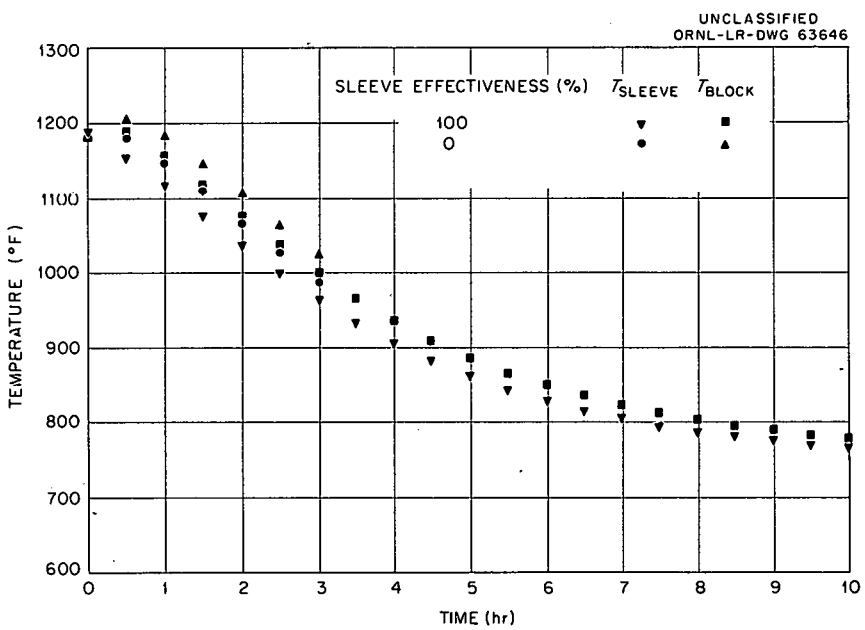

Fig. 2.11. Maximum EGCR Sleeve and Moderator Block Temperatures vs Time for an Inlet Air Temperature of 610°F, a Normal Air O_2 Concentration, a Central Channel Flow Rate of 365 lb/hr, and One-Half Normal Oxidation Heat Release.

distribution used yields higher maximum graphite temperatures than those that would result from the calculated power distributions. The calculations reported here indicate, however, the effect of the sleeve coating under the various other conditions considered.

The air flow rate in the annulus was taken to be 6.5% of the central channel flow rate for all the calculations of the data presented in Figs. 2.6 through 2.11. This flow rate was based on the normal operating condition with helium as the coolant. Further calculations will be made to investigate the effect of varying the annulus flow rate.

An effective sleeve coating (95 to 100% surface coverage) prevents runaway oxidation from occurring in the situations described in Figs. 2.6, 2.7, 2.8, and 2.10. In all cases with a central channel flow rate of 186 lb/hr, runaway occurred with the uncoated sleeve, and, for the condition of Fig. 2.9, runaway occurred with a 100% effective coating. In comparing Figs. 2.9 and 2.10, it may be seen that a central channel flow rate of 365 lb/hr prevented runaway oxidation of the 100%-coated sleeve. For the somewhat lower oxidation heat release of Figs. 2.6 and 2.11, the 365-lb/hr flow rate prevented runaway oxidation of uncoated sleeves, whereas the 186-lb/hr rate did not. The 100°F higher inlet air temperature and factor of 2 lower oxidation heat release of Fig. 2.8 compared with Fig. 2.6 combine to give about the same rate of temperature change as that of Fig. 2.6. It appears from comparing Figs. 2.6 and 2.7 that the inlet oxygen concentration would have to be reduced much more than a factor of 2 to prevent runaway oxidation of an uncoated sleeve. These results indicate, in summary, that an effective sleeve coating could prevent runaway conditions under certain coolant flow rate, oxidation heat release rate, and initial temperature conditions and that these same variables could significantly affect the threshold condition for runaway oxidation and therefore determine whether or not a sleeve coating of a certain effectiveness could prevent runaway oxidation from occurring.

The experimental and calculated data discussed here were considered in detail in deciding whether to coat the graphite sleeves for the first EGCR core. In view of the lack of proof that a sleeve coating, even if of the order of 95% effective, could prevent runaway oxidation in the

EGCR, it was recommended that the sleeves not be coated. The consequent potential hazards should be accommodated as follows: (1) with the presently conceived maximum credible accident, which assumes no runaway oxidation, the graphite operating temperature would have to be degraded to the point where the oxidation would certainly be controlled; or (2) if the graphite temperature degradation unduly derated reactor performance, the possibility of runaway oxidation should be included in the maximum credible accident and the system containment upgraded accordingly.

The present program of graphite oxidation studies includes further experimental determinations of oxidation reaction rates at Hanford and more detailed calculations to determine the effect of initial temperatures, coolant flow rates, and oxidation heat release rates on runaway oxidation conditions. Hanford experimenters have conservatively estimated that the environmental conditions of moisture content, gamma radiation intensity, and surface contamination in the EGCR during a maximum credible accident could increase the oxidation reaction rate a factor of 11 above that which had been previously estimated for EGCR conditions.[5] Hence experimental reaction rate determinations surveying these variables will be carried out by the Hanford Nonmetallic Materials Development group. The calculational program will evaluate whether and under what conditions graphite temperature degradation can prevent runaway oxidation. These calculations are being performed by a combination of the Allis-Chalmers, Bendix G-15, and Oak Ridge IBM 7090 codes.

---

[5]Letter from R. E. Dahl, Hanford Atomic Products Operation, to R. A. Charpie, ORNL, October 31, 1960.

3. STRUCTURAL INVESTIGATIONS

B. L. Greenstreet

Structural Integrity of EGCR Through-Tubes

J. M. Corum

The experimental tube collapse investigation being conducted to provide both instantaneous and time-dependent collapse data applicable to the experimental through-tubes in the EGCR has included tests of 8.0-in.-o.d., 0.25-in.-wall tubes and 4.0-in.-o.d., 0.12-in.-wall tubes, as previously reported.[1] The larger specimens have all been type 304 stainless steel, but the smaller ones have been both types 304 and 347 stainless steel so that the behavior of the two materials can be compared.

The fourth in the series of five 8.0-in.-o.d. tubes is being subjected to an external pressure loading of 460 psi at 1200°F. The specimen is approximately 9 ft long and was purchased in accordance with ASTM A 213 - 58 T grade TP-304 specifications. The average measured mean radius-to-thickness ratio was 15.38 and the ovality ratio was 0.9956. At the end of 1056 hr the specimen had not collapsed, and it was removed from the test vessel for a dimensional check. The diameter of the tube was measured at 30-deg intervals on the perimeter and at 1-ft intervals along the length. By comparing these measurements with the initial measurements at the same positions, the creep deformation of the tube during the first 1056 hr of the test was examined, as shown graphically in Fig. 3.1 for eight positions at 1-ft intervals. A circle corresponding to a perfectly round tube is drawn in each figure to indicate the out of roundness. The data curves were drawn by greatly magnifying the deviations from the nominal 8.0-in. outside diameter. An examination, in consecutive order, of the plots in Fig. 3.1 indicates that each cross section of the tube had an initial pseudo-elliptical shape, with the major axis spiraling counterclockwise around the tube from top to bottom. Furthermore, this initial ellipticity

[1]GCR Quar. Prog. Rep. June 30, 1961, ORNL-3166, p. 39.

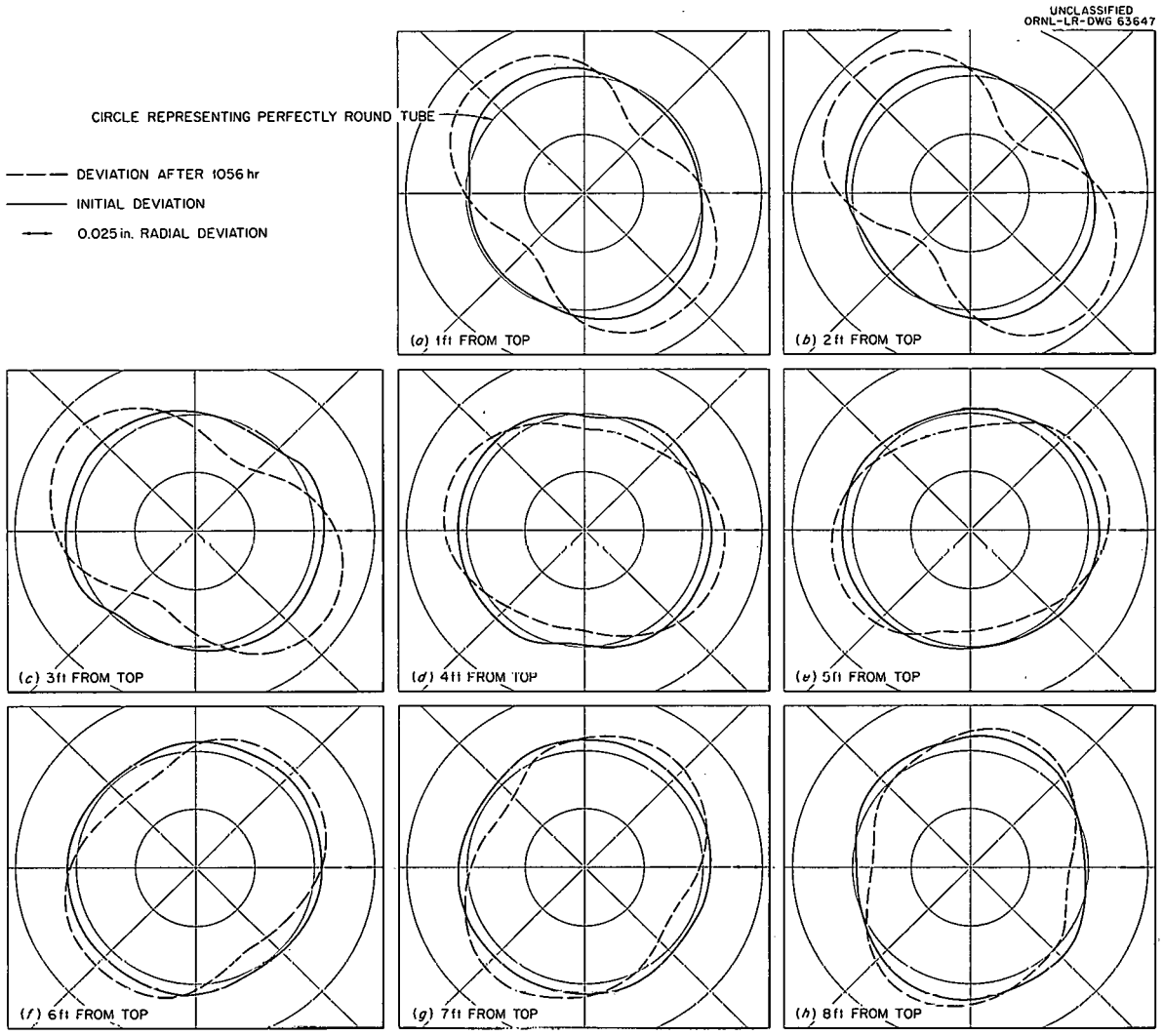

Fig. 3.1. Exaggerated Deviations of the Cross Sections of an 8-in.-o.d., 0.25-in.-Wall Tube from Circles Representing Perfectly Round Tubes Showing Initial Deviations and Deviations After 1056 hr Exposure to an External Pressure of 460 psi at 1200°F.

was simply magnified by creep of the material under the external pressure load. After the measurements were made, the tube was again installed in the test vessel for testing at the above conditions until collapse occurs.

The sixth in the series of 4.0-in.-o.d. tubes is being tested at the University of Tennessee. The specimen is type 304 stainless steel tubing purchased in accordance with ASTM A 312 – 58 T specifications and is approximately 5 ft long. It is being subjected to an external pressure load

of 425 psi at 1200°F, as previously reported.[1] The tube has an average measured mean radius-to-thickness ratio of 15.32 and an ovality ratio of 0.9975. At the end of 871 hr the specimen had not collapsed, and it was removed from the test vessel for a dimensional check. The tube was measured in the same manner as described above for the 8.0-in.-o.d. tube, and the measurements were compared with the initial measurements as in Fig. 3.1. Although the ellipticity for this tube was much less apparent than in the case of the 8.0-in.-o.d. tube, the same type of behavior was observed, with the initial ellipticity being magnified by creep of the material under the external pressure loading. The tube has been reinstalled in the test vessel, and the test is being continued.

Thermal Analysis of Structures Using the Biharmonic Program

F. J. Witt S. E. Moore B. C. Sparks

The stress analysis program[2] coded by Battelle Memorial Institute for analyzing bodies under plane-strain conditions was set up on a production basis. This program solves the nonhomogeneous biharmonic equation numerically for the Airy stress function, and, in turn, evaluates the stresses by numerical differentiation of the function. Since the program will be used extensively in future work, two special problems were solved to check the techniques for programming the input and to check the accuracy of the solutions obtained.

A long, thick-walled cylinder without heat sources or sinks, whose temperature distribution depends only on the radial coordinate, was the first analyzed. The dimensions of the cylinder are shown in Fig. 3.2a where the inner and outer surface temperatures of 0°F and 500°F are indicated. The materials properties used were:

Modulus of elasticity, $E = 17.5 \times 10^6$ psi

Coefficient of thermal expansion, $\alpha = 8.0 \times 10^6$ in./in.·°F

Poisson's ratio, $\mu = 0.3$

---

[2]GCR Quar. Prog. Rep. March 31, 1961, ORNL-3102, pp. 43–50.

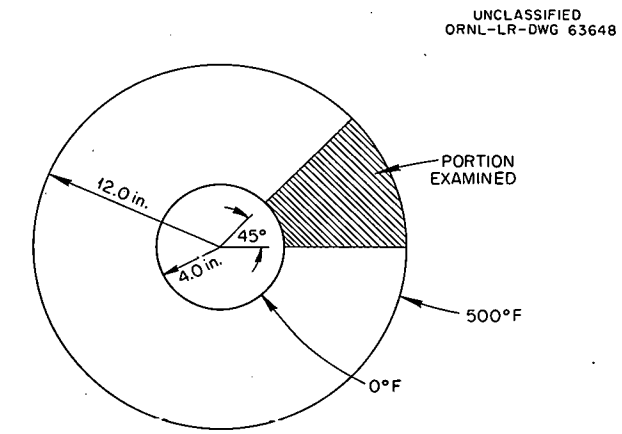

(a) CROSS SECTION OF THICK-WALLED CYLINDER

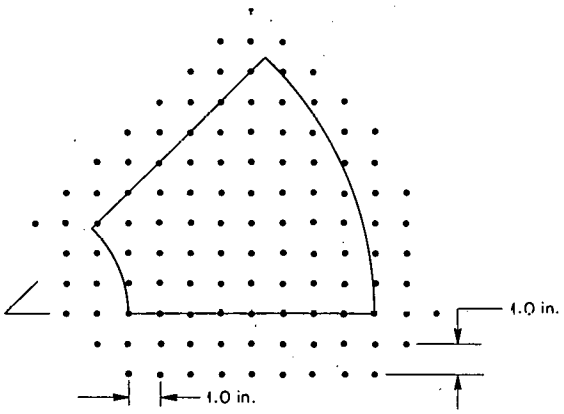

(b) SECTION OF THICK-WALLED CYLINDER SHOWING MESH SPACING

Fig. 3.2. Dimensions of Cylinder Used for Check of Biharmonic Program for Thermal Analysis.

This problem was chosen because analytical results were available[3] in the form needed for a direct comparison with the values obtained numerically. The analytical results include the values of the stress function and the stresses for a particular array of mesh points. Thus, it was necessary only to choose the same array in making the numerical computations.

The use of a symmetrical temperature distribution allowed the computational work to be confined to an examination of one-eighth of the cylinder, as indicated in Fig. 3.2a. The mesh points and the spacing are shown in Fig. 3.2b. Both the analytically and numerically obtained values for the Airy stress function and the tangential stresses along a radial line are listed in Table 3.1.

The good agreement between the two sets of values may be seen. The differences between the stresses are greater than the differences between the values for the stress function because, as stated above, the machine program obtains the stresses by numerical differentiation of the stress function. A reduction in the mesh spacing would bring the two sets of data into closer agreement. However, this refinement is unnecessary in this case.

[3]A. G. Holmes, A Biharmonic Relaxation Method for Calculating Thermal Stresses in Cooled Irregular Cylinders, NACA Report 1059 (1952).

Table 3.1. Comparison of Analytical and Numerical Results

Radius (in.)	Analytical Value of Airy Stress Function	Numerical Value of Airy Stress Function	Analytical Tangential Stress (psi)	Numerical Tangential Stress (psi)
4	−467 627	−464 420	66 988	64 540
5	−439 879	−438 420	36 582	36 020
6	−374 651	−375 400	17 284	17 822
7	−291 678	−294 100	3 636	4 574
8	−204 799	−207 940	−6 746	−5 674
9	−124 507	−127 280	−15 058	−14 423
10	−59 152	−60 880	−21 964	−21 872
11	−15 677	−16 240	−27 864	−28 496
12	0	0	−33 012	−34 470

The stress analysis program was also used to calculate the thermal stresses which will exist in an EGCR graphite column during steady-state operation at design power. The temperature distribution for this case was discussed previously.[4] The cross section of a column is shown in Fig. 3.3a where the portion analyzed is designated.

The boundary conditions which apply to the temperature are identical at all the fuel channel walls, and the outer surface of the column is assumed to be insulated. Thus, the temperature distribution across the entire column may be obtained through the analysis of a portion representing 1/32nd of the cross section. A typical 1/32nd portion is shown in Fig. 3.3b. The degree of symmetry associated with the stress distribution is less than that for the temperature, and one-eighth of the column must be considered in the analysis. For example, the stress distribution is symmetrical about the dashed line in Fig. 3.3b.

The entire one-fourth of the cross section depicted in Fig. 3.3b was analyzed so that the resulting data could be examined for symmetry. The program correctly computed identical numbers for corresponding points. The values for the axial, the shear, and the maximum and minimum in-plane principal stresses corresponding to the numbered mesh points in Fig. 3.3b

[4]GCR Quar. Prog. Rep. June 30, 1961, ORNL-3166, pp. 36–39.

are given in Table 3.2. The values are low, as was expected from the fact that the maximum temperature difference within the body is about 8°F.

The largest in-plane stress is at point 22, which is near the boundary between quadrants. This indicates the importance of the restraint imposed

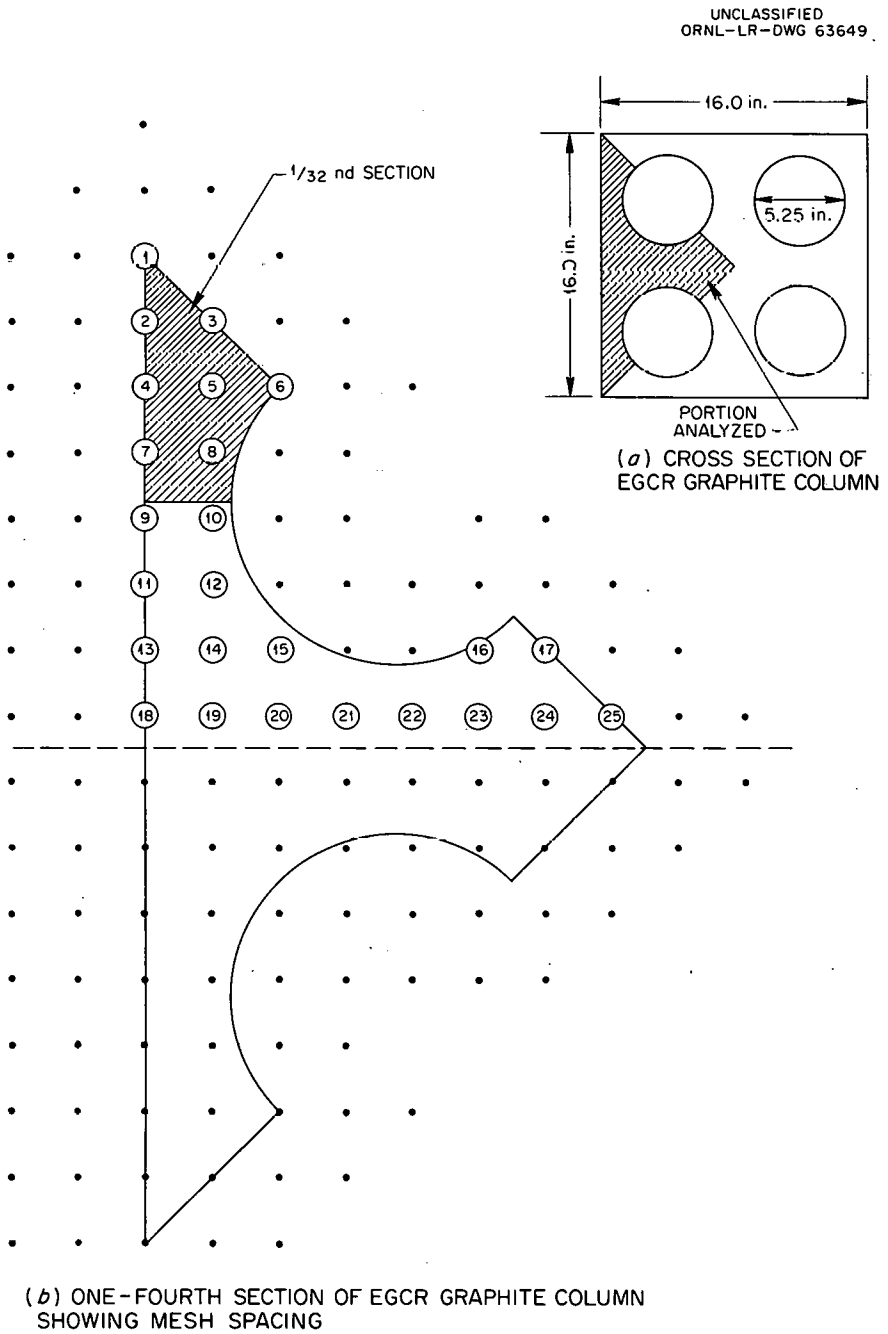

(a) CROSS SECTION OF EGCR GRAPHITE COLUMN

(b) ONE-FOURTH SECTION OF EGCR GRAPHITE COLUMN SHOWING MESH SPACING

Fig. 3.3. Dimensions of EGCR Graphite Column Used in Calculation of Thermal Stresses.

Table 3.2. Principal, Shear, and Axial Thermal Stresses on One-Eight Section of EGCR Graphite Block

Mesh Point Number	Maximum In-Plane Principal Stress (psi)	Minimum In-Plane Principal Stress (psi)	Maximum Shear Stress (psi)	Axial Stress (psi)
1	2	1	0	−8
2	2	−3	3	−9
3	0	−1	0	−6
4	0	−6	3	−8
5	1	0	0	2
6	8	0	4	20
7	1	−6	3	−2
8	3	0	2	9
9	0	−2	1	1
10	4	1	2	12
11	1	−5	3	−4
12	2	1	0	7
13	2	−3	2	−7
14	1	−3	2	−3
15	1	−5	3	5
16	6	−15	11	8
17	0	−5	3	−1
18	7	−1	4	−6
19	1	0	0	−7
20	1	−4	2	−4
21	3	−12	8	−3
22	21	−8	14	12
23	1	−3	2	−1
24	−1	−3	1	−8
25	−2	−2	0	−12

by the adjacent quadrant. The stresses at mesh point 1 through 8 provide an approximate representation of the results for an independent quadrant; that is, one that is not a part of the 16-in. by 16-in. cross section. An examination of these results indicates that a reduction in the in-plane stresses could be obtained through the use of an 8-in. by 8-in. column; however, a smaller mesh spacing would have to be used to fully investigate the influence of such a change in geometry.

Graphite Thermal Rupture Studies

J. M. Corum F. T. Dodge

Wigner growth must be considered in the application of graphite in the core and reflector regions of a nuclear reactor. This type of growth

may produce deformation or cracking, depending upon the restraint imposed. In a case where a potential for cracking exists, the design analyst must predict the amount of fast-neutron exposure required to produce this type of failure.

The reliability of the predicted exposure-to-failure dose depends heavily upon the accuracy of the failure criterion used. Therefore information on the rupture characteristics of graphite under multiaxial stresses is needed. Since strains incurred through Wigner growth are analytically equivalent to thermal strains, a failure criterion applicable to the latter should also apply to the former. On this basis, a study was initiated to determine the feasibility of investigating thermal rupture through tests on bodies with simple geometric shapes.

There are many possible specimen configurations and methods of applying the necessary thermal gradients. There exists in each case, however, an interrelation between the specimen geometry, the temperature gradient necessary to produce rupture, and the heat input necessary to produce the required temperature gradient. Parameter studies involving temperature, power, and geometry were therefore made for several test specimens. The following possibilities were examined:

1. a thick-walled cylinder heated on the inner surface and cooled on the outer surface,
2. a thick-walled cylinder heated internally by electrical resistance and cooled on both the inner and outer surfaces,
3. a thick-walled cylinder heated internally by electrical resistance and cooled on the inner or outer surface only,
4. a solid cylinder heated internally by electrical resistance and surface cooled,
5. a rectangular bar heated internally by electrical resistance and surface cooled,
6. a rectangular bar, as above, cooled on one side only.

A thick-walled cylinder heated by electrical resistance and cooled on the outer surface appeared to be the most attractive for this study from the standpoint of the temperature difference required, the power input, and the complexity of the test equipment. The results of the parameter

study for this particular case are shown graphically in Figs. 3.4 and 3.5. The graphite was assumed to be EGCR needle-type AGOT. Failure was assumed to occur when the strain in the axial or circumferential direction reached the fracture strain corresponding to that direction. The axial fracture strain of 0.205% and the circumferential, or perpendicular, fracture strain of 0.406% noted on the curves in Fig. 3.4 are typical measured values for an EGCR moderator block, while the 0.086% axial fracture strain is a minimum value. The coefficients of thermal expansion were taken to be $0.778 \times 10^{-6}/°F$ and $2.55 \times 10^{-6}/°F$ in the axial and perpendicular directions, respectively. The modulus of elasticity was taken as 1.85×10^{6} psi in the axial direction and 0.74×10^{6} psi in the perpendicular direction, and the thermal conductivity in Btu/hr·ft·°F

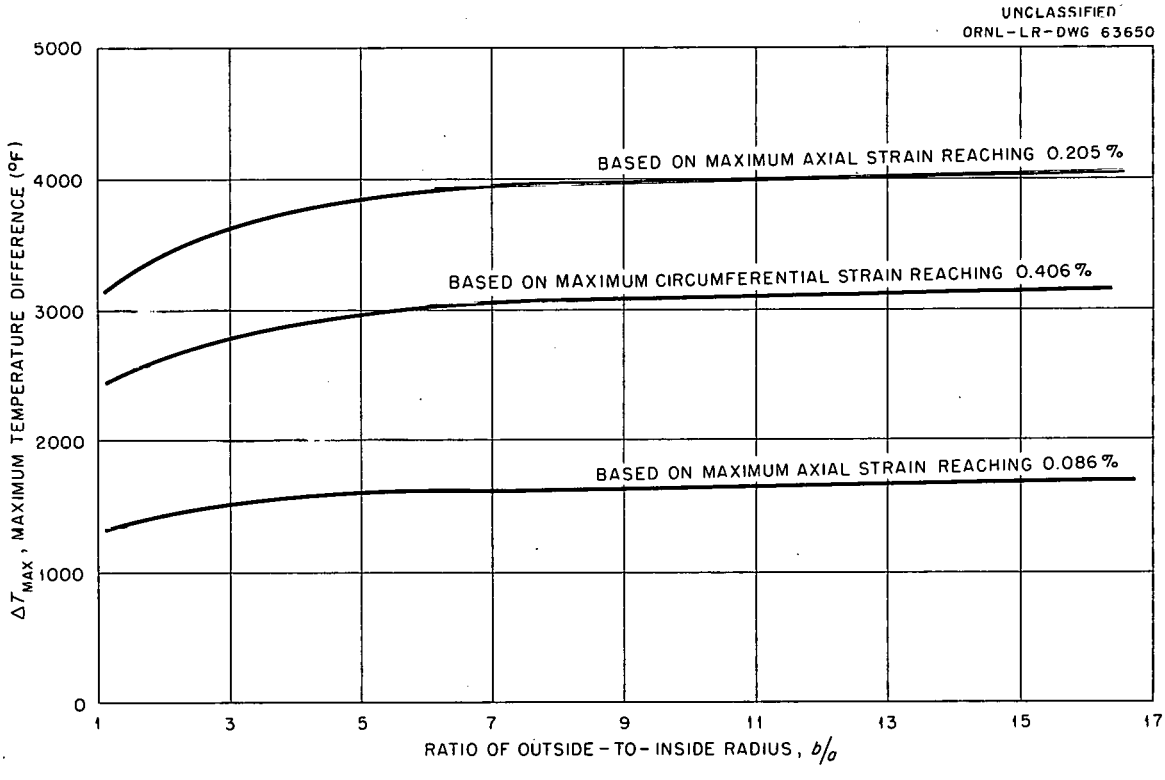

Fig. 3.4. Maximum Temperature Difference Required to Thermally Fracture a Thick Walled Graphite Cylinder Resistance Heated and Cooled on Outer Surface.

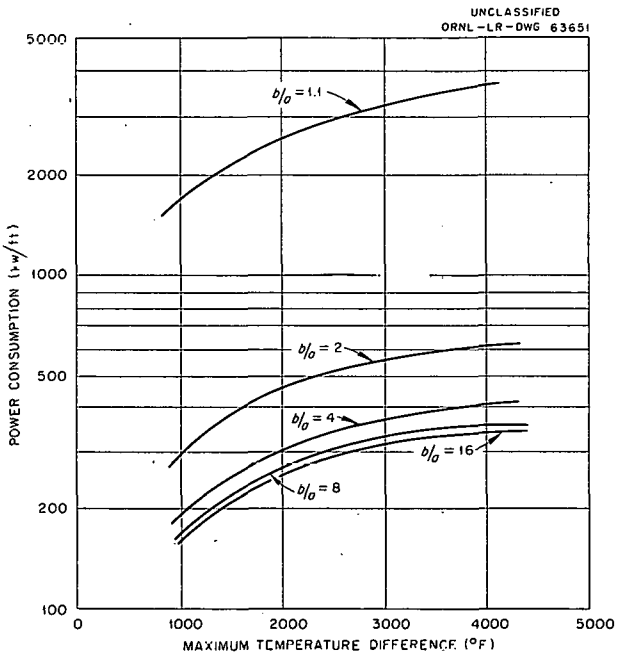

Fig. 3.5. Power Input Required to Achieve Various Maximum Temperature Differences for a Thick-Walled Graphite Cylinder Resistance Heated and Cooled on Outer Surface.

in the perpendicular direction was taken to be the following function of temperature:

$$k = (3.63 \times 10^{-6})t^2 - 0.0267t + 55.44 \quad .$$

The maximum temperature difference necessary to thermally fracture a cylinder with a given ratio of outside to inside radius based on any one of the above three fracture strains being reached is given in Fig. 3.4. The power input required for a given ratio of outside to inside radius, b/a, and a given required maximum temperature difference may be obtained from Fig. 3.5.

As a check of the feasibility of the postulated method, a 1.0-ft-long cylindrical specimen having a 1.0-in. o.d. and a 1/2-in. i.d. (b/a = 2.0) was considered. It was assumed that the cylinder would fracture when the axial strain reached 0.086%, and it was found from Fig. 3.4 that a minimum temperature difference of approximately 1400°F would be required

for fracture. From Fig. 3.5, it was found that a power input of 375 kw (an outer surface heat flux of 4.8×10^6 Btu/hr·ft^2) would correspond to a 1400°F temperature difference in the cylinder. Thus, the temperature difference required and the heat flux associated with it led to the conclusion that, even on the basis of a minimum temperature difference, the temperatures of such a specimen would be well above the usual upper limit of 1000°F considered for moderator structures in current reactor designs.

Experience at the Los Alamos Scientific Laboratory[5] has shown that, in fracture tests of specimens similar to the one described above, surface temperatures on the order of 4000°F may be expected when helium coolant is used. Therefore, in order to utilize the results from thermal rupture tests to predict behavior in the reactor temperature range up to 1000°F, a separate study will be required. The second study will determine the effect of temperature on both fracture stress and fracture strain, or a test specimen must be designed for concentrating the strain so that the temperature difference is reduced and, hence, the over-all temperature load is lowered.

---

[5]Discussions with W. R. Prince of Los Alamos Scientific Laboratory.

4. EGCR COMPONENT DEVELOPMENT AND TESTING

Control Rod Drive Testing Facility

E. Storto

A facility is being designed for conducting endurance tests of a production model of the EGCR control rod and rod drive assembly in a simulated EGCR environment. A schematic diagram of the test facility is shown in Fig. 4.1, with the essential parts and conditions indicated. Detailed designs for all building modifications and most facility hardware have been completed. Design of the instrumentation and controls system is in progress. Some materials and components have been ordered, and construction is expected to start October 1. The facility is to be ready to receive the prototype rod drive mechanism for testing by January 1, 1962.

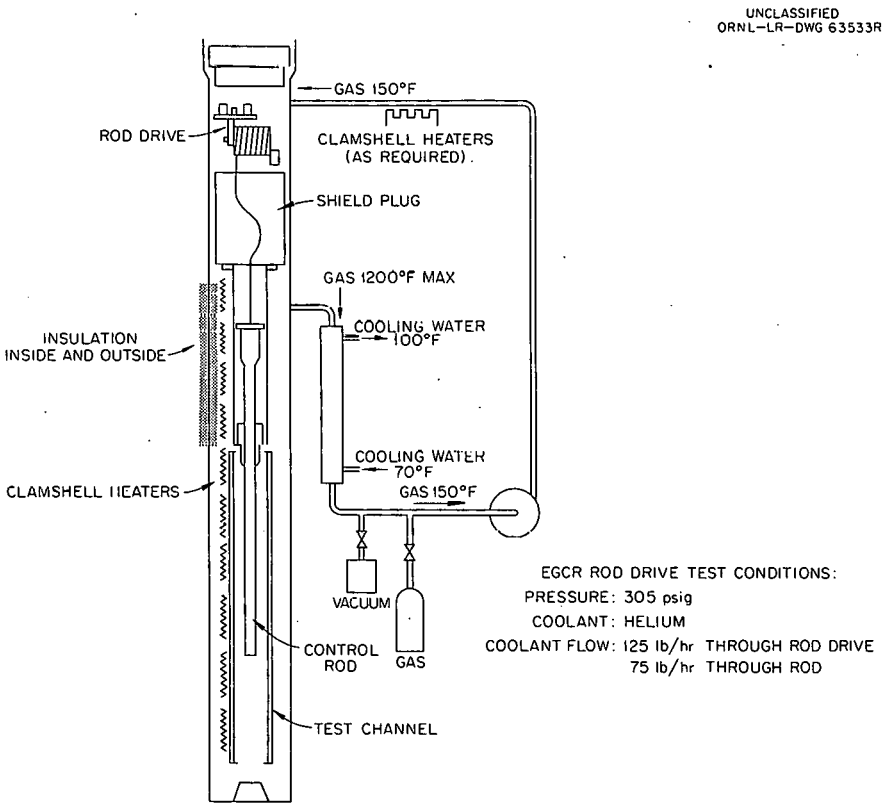

Fig. 4.1. Control Rod Drive Test Facility.

Main Coolant Blowers

E. R. Taylor

The fabrication of the casings for the EGCR blowers is substantially behind schedule. The present Baldwin-Lima-Hamilton schedule states that the first casing will be ready for final tests (hydrostatic, helium leak, and proof) by November 20, 1961. On this basis, the first casing should be shipped to the Joy Manufacturing Co. on December 18, and the second should follow about ten days later.

Numerous delays in the fabrication have resulted from machining errors. The repairs have consumed considerable time because of the postheat treatment requirement for type 405 stainless steel. The complex configuration of the running-seal cavity design, coupled with the type 405 stainless steel end-bell material, present fabrication circumstances which can result in many time-consuming problems.

All other phases of the Joy contract are proceeding without apparent difficulty. The variable-speed fluid couplings have been received, the main drive motors will be shipped by September 1, 1961, and the gear-speed increasers have been shipped to Joy in Buffalo.

Pressure Vessel Cooling System Compressors

E. R. Taylor

The present schedule of the Roots-Connersville Blower Company states a delivery date of November 15, 1961. Delays were encountered in providing a casing design to conform to the requirements of the ASME Boiler and Pressure Vessel Code and to the Nuclear Code Case Interpretations. The Henry Vogt Company, fabricators of the compressor casings, started the initial production welding on August 28, 1961, and it appears that they should be able to proceed without undue difficulty. The fabrication of other basic components is now proceeding normally. Details of design and fabrication on items such as the static seal will be determined in the near future.

Instrumented Fuel Assembly

R. L. Senn

Design and advance procurement are under way for the fabrication and assembly of four instrumented fuel assemblies for the EGCR. These assemblies are scheduled for delivery to the reactor site by October 1962. Each assembly consists of three instrumented subassemblies, a standard fuel element subassembly, a flow-measuring section, and the associated rods and tubing necessary to support the entire unit from the shield plug and Bridgman closure at the reactor vessel top nozzle. The instrumentation includes a Venturi, with its associated transducer, and 18 thermocouples. One thermocouple is located in the shield plug, and the remaining 17 are to be located as indicated in Table 4.1.

The thermocouple elevations and typical locations within the fuel clusters are shown in Figs. 4.2 and 4.3. The central thermocouple, inserted in a molybdenum well, and the internal thermocouples, brazed to the inside of the cladding wall, will extend approximately 5 in. into the fuel can. A similar design and techniques for fabricating instrumented fuel cans have been described previously.[1,2] The thermocouples to measure gas and graphite temperatures are located in grooves and holes drilled through the sleeves.

Detail design work is in progress on the individual fuel rod clusters, the instrumented fuel cans, and the necessary grooving of the graphite sleeves. The flow-measuring section incorporates a Venturi with piezometer rings at the downstream and throat locations, with six pressure taps in each ring. Tubing 1/8 in. in diameter is used to transmit the pressures from the Venturi to the transducer in the Bridgman closure.

Preliminary design work is in progress on a fixture to be used in assembling the column and on shipping crates which will serve both for transportation to the reactor and for handling within the EGCR containment vessel during installation of the assembly in the reactor. Allis-Chalmers will provide the parts shown as Zone 1 in Fig. 4.2, including

---

[1]GCR Quar. Prog. Rep. March 31, 1961, ORNL-3102, pp. 131–3.

[2]GCR Quar. Prog. Rep. June 30, 1961, ORNL-3166, pp. 109–10.

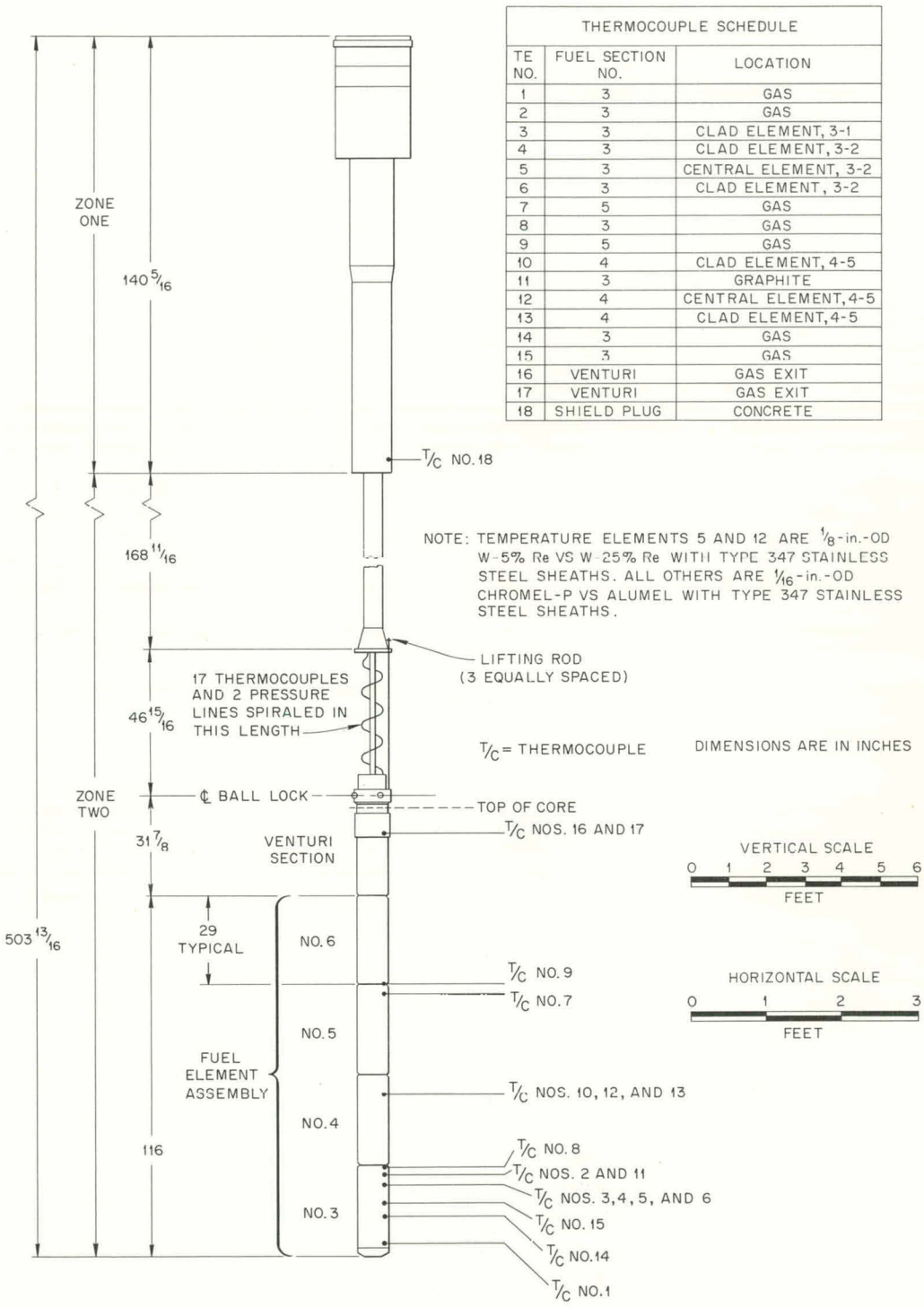

THERMOCOUPLE SCHEDULE		
TE NO.	FUEL SECTION NO.	LOCATION
1	3	GAS
2	3	GAS
3	3	CLAD ELEMENT, 3-1
4	3	CLAD ELEMENT, 3-2
5	3	CENTRAL ELEMENT, 3-2
6	3	CLAD ELEMENT, 3-2
7	5	GAS
8	3	GAS
9	5	GAS
10	4	CLAD ELEMENT, 4-5
11	3	GRAPHITE
12	4	CENTRAL ELEMENT, 4-5
13	4	CLAD ELEMENT, 4-5
14	3	GAS
15	3	GAS
16	VENTURI	GAS EXIT
17	VENTURI	GAS EXIT
18	SHIELD PLUG	CONCRETE

Fig. 4.2. EGCR Instrumented Fuel Assembly.

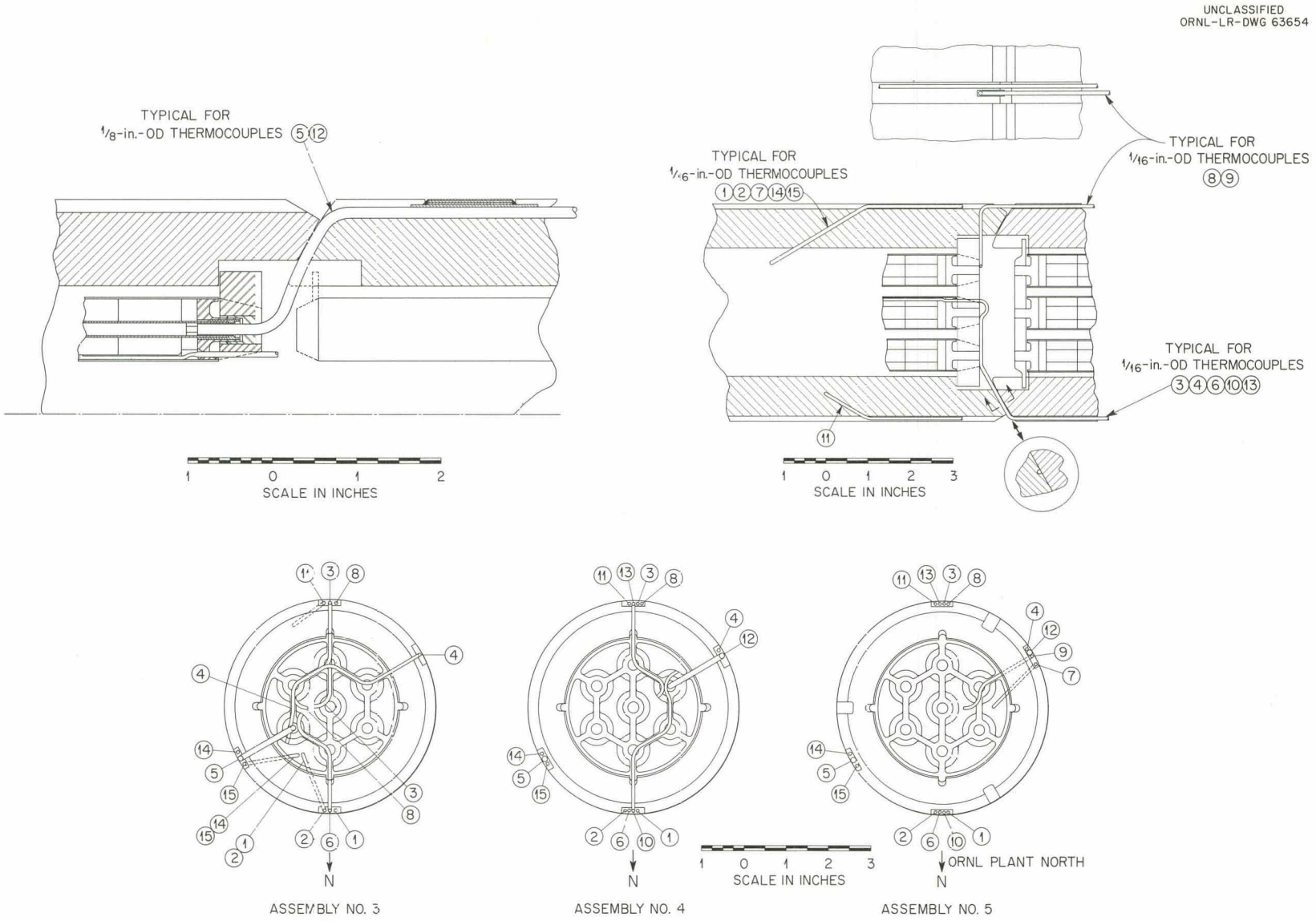

Fig. 4.3. Arrangement of Thermocouples in EGCR Instrumented Fuel Assemblies.

Table 4.1. Thermocouples for EGCR Instrumented Fuel Assemblies

Thermocouple Locations	Size and Type	Number Required per Assembly
Fuel pellet center	1/8-in.-diam, 48-ft-long, type 347 stainless steel-sheathed, MgO-insulated, W–5% Re vs W–25% Re	2
Fuel rod cladding (brazed inside cladding)	1/16-in.-diam, 45-ft-long, type 347 stainless steel-sheathed, MgO-insulated, Chromel-P (type 3G345) vs Alumel (type 3G196)	5
Gas annulus	1/16-in.-diam, 45-ft-long, type 347 stainless steel-sheathed, MgO-insulated, Chromel-P (type 3G345) vs Alumel (type 3G196)	7
Graphite	1/16-in.-diam, 45-ft-long, type 347 stainless steel-sheathed, MgO-insulated, Chromel-P (type 3G345) vs Alumel (type 3G196)	1
Venturi	1/16-in.-diam, 35-ft-long, type 347 stainless steel-sheathed, MgO-insulated, Chromel-P (type 3G345) vs Alumel (type 3G196)	2

the shield plug and the Bridgman closure assembly, which incorporates a pressure transducer and electrical connectors for the thermocouple and transducer leads. ORNL will supply the remaining parts, labeled as Zone 2, and assemble the entire column. All parts and fuel for the fuel element assemblies will be standard EGCR parts modified as necessary to accommodate the instrumentation.

Equipment Decontamination

A. B. Meservey

Corrosion Tests

The effects on metal corrosion rates resulting from varying the H_2O_2 concentration from zero to 0.6 M in 0.3 M oxalate decontamination solutions and oxalate solutions with 0.1 M citrate or acetate were studied

with nine different metals at pH 4.0, 4.5, and 5.0 at 95°C. Acetate, which has been used as a buffer and peroxide stabilizer in oxalate-peroxide solutions at Hanford and Argonne, was found to have more desirable corrosion characteristics than citrate. Low peroxide concentrations accelerated corrosion on mild steels. The corrosion results are listed by metal type below:

Metal Type	Remarks
Types 304 and 347 stainless steel	Corrosion less than 0.0001 mil/hr
Zircaloy-2	Corrosion less than 0.0001 mil/hr
Titanium	Corrosion increased from <0.0001 mil/hr without peroxide to 0.01 mil/hr at 0.6 M H_2O_2.
Aluminum	Corrosion behavior was somewhat complex at low peroxide concentrations, but above 0.1 M H_2O_2 the rate became more stable at 0.02 to 0.05 mil/hr
High-carbon stainless steel, type 440-C (annealed)	Without peroxide as an inhibitor the corrosion rate was 0.06 to 0.9 mil/hr, the higher rates tending to be at the lower pH values; peroxide inhibited corrosion to as low as 0.003 mil/hr
Croloy 2 1/4	In two series of tests with Croloy, corrosion decreased from 0.03 and 0.01 mil/hr without peroxide to 0.0007 and 0.00001 mil/hr at 0.6 M H_2O_2.
Mild steel, types A-109 and 1020	Without peroxide, the corrosion rate was 0.06 to 0.5 mil/hr, the higher values being at the lower pH; at 0.05 M H_2O_2, corrosion increased sharply to 2 to 4 mils/hr in all solutions at pH 4.0; at pH 4.5 and 5.0 corrosion inhibition occurred, except in the presence of 0.1 M citrate; in all solutions above 0.1 M H_2O_2 the corrosion rate decreased to 0.002 to 0.02 mil/hr, the higher rates being at the lower pH values

Decontamination from Ruthenium Baked in Helium

EGCR conditions were simulated by baking Ru^{106} onto several metals in helium at 110°C. Decontamination was significantly more difficult than

with samples dried in air at room temperature. At pH 4.0 and 95°C, oxalate with added peroxide was more effective than without peroxide by a factor of about 6 (example, D.F. = 41 vs 7 on type 347 stainless steel in 20 min). Dilute nitric acid with added peroxide was also more effective than without peroxide, by approximately the same factor. Fluoride did not improve ruthenium decontamination.

Decontamination from Iodine

Carrier-free I^{131} deposited from helium onto metal coupons at 400°C was only 50% removed by 10-min boiling in water. Of several decontamination reagents tested, the best results were obtained from 20-min boiling in 29% potassium hydroxide (D.F. ~1000). In a 2.9% KOH solution the decontamination factor was 64. Reducing agents and oxalate-peroxide were also promising decontaminants.

5. EGCR MATERIALS DEVELOPMENT

J. H. Coobs G. M. Watson

Coatings for Graphite Support Sleeves

F. L. Carlsen, Jr. R. W. McClung

Mechanical Testing of Coated Sleeves

The rupture strengths of siliconized SiC-coated graphite support sleeves were determined using the "brittle ring" test, since stresses in the range of 1200 to 1300 psi may develop in the graphite support sleeves during service in the EGCR because of fast-neutron-induced differential shrinkage.[1] For this test, ring specimens 1 in. thick were cut from two full-size 901S graphite sleeves that had been coated by the American Lava Corporation. The specimens were stressed to rupture by compression loading on the outer surface to produce tensile stresses on the inner surface directly under the points of load application. The results are given in Table 5.1.

These rupture strengths are substantially higher than required by the predicted service stress of 1300 psi and are also higher than the 1870- to 2450-psi rupture strengths determined previously in "brittle ring" tests of uncoated sleeves made from nuclear grades of graphite. Uncoated 901S graphite has not been tested by this method; however, its rupture strength in simple tension has been reported to be approximately 1900 psi perpendicular to the axis of extrusion.

The amount of coating material on the specimens was determined in an attempt to correlate the rupture strength with the amount of coating. The specimens were burned in an open furnace at 1000°C for 48 hr and the residue was weighed. The residue from impurities in the graphite was assumed to be small compared with the amount of coating. The results are given in Table 5.2.

---

[1]GCR Quar. Prog. Rep. June 30, 1960, ORNL-2964, pp. 121–2.

Table 5.1. Rupture Strength of Siliconized-SiC-Coated 901S Graphite Rings

Sleeve No.	Number of Specimens	Rupture Strength (psi)	
		Average	Range
ALC-3	7	3610	2900–4100
ALC-4	12	2550	2300–3300

Table 5.2. Rupture Strength of Siliconized-SiC-Coated 901S Graphite Rings

Sleeve No.	Number of Specimens	Amount of Coating (wt %)	
		Average	Range
ALC-3	7	5.0	4.2–6.0
ALC-4	12	3.8	2.8–4.7

The average rupture strength and average amount of coating for sleeve ALC-3 is higher than for sleeve ALC-4, indicating that the rupture strength may be dependent on the amount of coating. It was noted, however, that there was no consistent correlation between the strength and the amount of coating for specimens from either sleeve.

Perhaps a more important observation is that the coating material penetrated into the graphite approximately 1/8 to 1/4 in. from the inside surface of sleeve ALC-3; whereas, much less penetration occurred on sleeve ALC-4. This observation is considered to be significant because, in the "brittle ring" strength test, the tensile stress is concentrated on the inner surface of the specimen.

Thickness of Coatings on Graphite

Metallographic measurements of the thickness of pyrolytic graphite coatings have been completed. The specimens were EGCR support sleeves

that had been coated by High Temperature Materials, Inc. The pyrolytic coatings were much more uniform than the siliconized SiC coatings that had been previously measured.[2] In addition, it was much easier to make optical measurements on the polished specimens using polarized light. The coating thicknesses for different specimens varied from about 0.5 mil up to about 5 mils. Calibration curves plotted from these data and the eddy-current measurements indicate that the accuracy of the eddy-current technique for the measurement of such pyrolytic graphite coatings is better than ±0.25 mil.

Pressure-Vessel Penetrations

G. M. Slaughter

The development of suitable designs and fabrication techniques for the EGCR burst-slug-detection tubes and thermocouple penetrations was completed. A report describing the recommended procedures was prepared.[3]

Welding of Ferritic Steels to Austenitic Stainless Steels

G. M. Slaughter

Thermal cycling tests of large (14-in.-diam, 1-in.-wall) pipes containing dissimilar-metal welds are being continued. The specimens consist of ASTM A-212, grade B, steel joined to type 304 stainless steel and ASTM A-387, grade D, steel joined to type 304 stainless steel. The welds were made with both BP-85 electrodes and type 347 stainless steel electrodes in order to detect any effects resulting from differences in weld-metal expansion characteristics. All specimens were cycled from room temperature to 1050°F. This temperature range was selected for the tests to correspond with the operating conditions of the ASTM A-387, grade D,

---

[2]GCR Quar. Prog. Rep. June 30, 1961, ORNL-3166, pp. 97–98.

[3]G. M. Slaughter, Fabrication and Inspection Procedures for EGCR Burst-Slug-Detection Tube and Thermocouple Penetrations, ORNL CF-61-8-29, Aug. 14, 1961.

steel to stainless steel welds in the EGCR and because it would probably take a very large number of cycles to obtain cracking of carbon steel to stainless steel welds cycled to 650°F.

An incipient crack was noted in the carbon steel heat-affected zone of the ASTM A-212, grade B, steel to stainless steel joint welded with type 347 stainless steel after 60 thermal cycles. The weld was cycled an additional 17 times, after which dye-penetrant inspection revealed a definite crack. The 3 1/2-in.-diam plug shown in Fig. 5.1a was then machined from the specimen and metallographically examined. Extensive cracking of the type shown in Fig. 5.1b was evident in the heat-affected zone of the carbon steel. The presence of oxide in the cracks indicated that preferential oxidation at the highly stressed weld interface may also have helped promote premature failure of the joint. Evidence of carbon migration from the ferritic steel to the weld metal along the weld interface was also observed. The resultant weakening effect undoubtedly contributed somewhat to failure.

Dye-penetrant inspection also revealed an incipient crack in the ASTM A-387, grade D, steel to stainless steel joint welded with type 347 stainless steel after 60 cycles from 1050°F. A plug was also machined from this sample. The crack at the boundary between the weld metal and the ferritic steel is shown in Fig. 5.2. Extensive oxidation is evident in this crack also, and some decarburization in the heat-affected zone of the ferritic steel was noted.

No cracks can be detected by dye-penetrant inspection of either of the dissimilar-metal specimens welded with BP-85 electrode. These specimens have been subjected to 100 thermal cycles, and cycling of these specimens is continuing.

Reactions of Type 304 Stainless Steel with CO-CO_2 Atmospheres

H. Inouye

On the basis of the data from several tests of type 304 stainless steel in helium containing CO_2 and CO,[4] it appears that CO_2 is decarburizing to type 304 stainless steel and that CO is carburizing. The basis for this

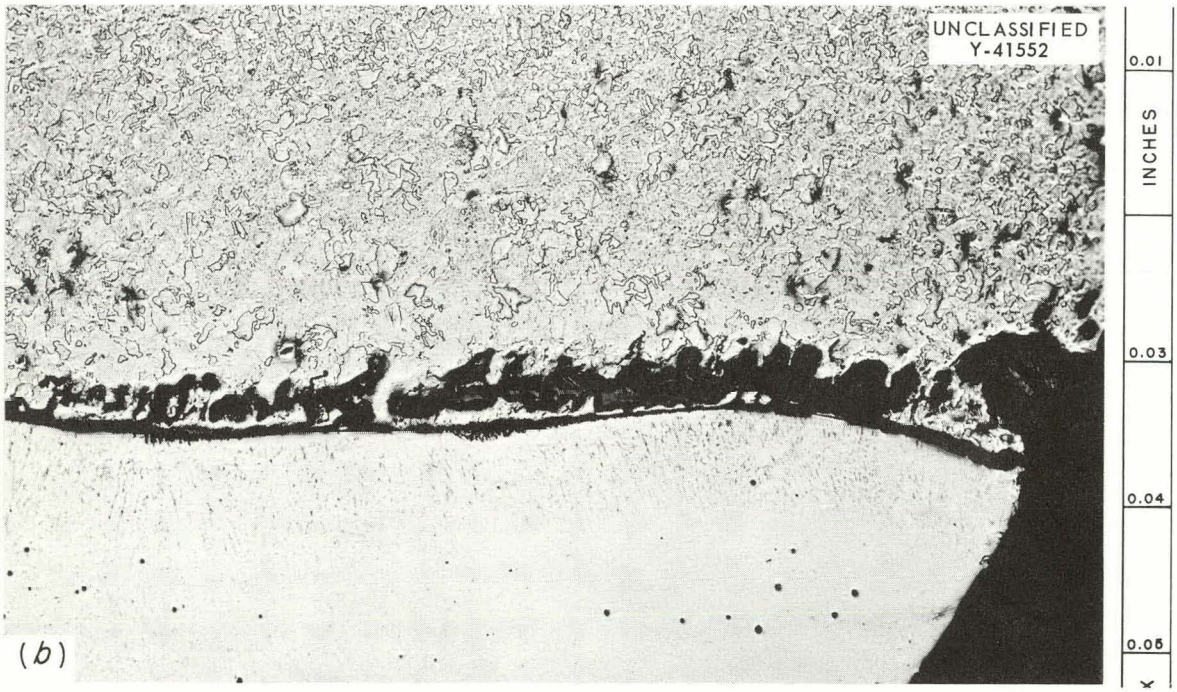

Fig. 5.1. (a) Plug Machined from a Thermal-Cycling Test Specimen Showing a Crack in the Dissimilar-Metal Weld. The dye-penetrant indication on the plug shows the location of the crack in the heat-affected zone of the carbon steel. (b) Photomicrograph of the Crack.

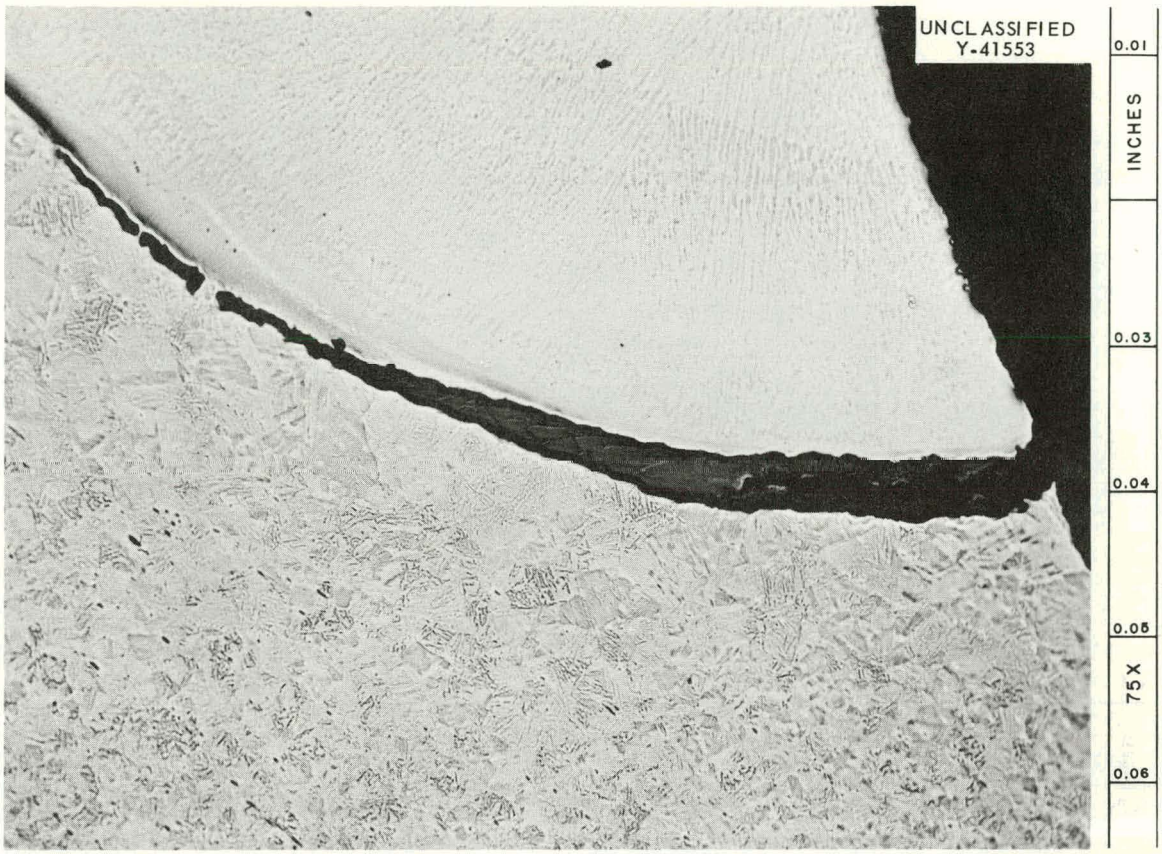

Fig. 5.2. Crack at Boundary Between Type 347 Stainless Steel Weld Metal and ASTM A-387, Grade D, Steel After Thermal-Cycling Test.

conclusion is the correlation observed between the carbon content of metal specimens and the ratio $(P_{CO})^2/P_{CO_2}$, which is proportional to the carbon activity of CO-CO_2 atmospheres. Tests have shown that carburization becomes severe when this ratio exceeds 0.10. To further test the validity of this conclusion and to clarify some contradictory data[5] regarding the effects of CO_2, two tests were conducted in atmospheres in which the only intentional impurity in the helium was CO_2. A further test was conducted in a CO-CO_2 atmosphere in which the ratio $(P_{CO})^2/P_{CO_2}$ was maintained at a value that gave severe carburization to verify the effect of the carbon activity.

---

[4]GCR Quar. Prog. Rep. June 30, 1960, ORNL-2964, pp. 104–6.

[5]GCR Quar. Prog. Rep. June 30, 1961, ORNL-3166, pp. 104–6.

The carbon contents of metal specimens exposed to two concentrations of CO_2 in helium are shown in Table 5.3. A CO_2 concentration of 0.00528 atm corresponds to 0.0247 vol %, based on 315-psi helium plus impurities, while a CO_2 concentration of 0.0524 atm corresponds to 0.244 vol %. The results of these tests indicate that CO_2 was both carburizing and decarburizing, depending on the test temperature. A further point of interest is the occurrence of a maximum in the carbon content at 1607°F (875°C). The apparent lack of correlation between the extent of carburization and the CO_2 pressure signifies that the CO content of the test atmospheres was negligible.

The atmosphere for the CO-CO_2 test of type 304 stainless steel was maintained at P_{CO_2} = 0.0025 atm and P_{CO} = 0.0238 atm, giving a $(P_{CO})^2/P_{CO_2}$ ratio of 0.227. The severe carburization at the higher temperatures predicted on the basis of the previous data is confirmed by the data in Table 5.4.

Oxidation tests were conducted to determine the effect of pressure on the rates of oxidation when protective or nonprotective oxides form on the metal. As shown in Table 5.5, the observed oxidation rates depend

Table 5.3. Carburization of Type 304 Stainless Steel Exposed to CO_2 for 800 hr at Various Temperatures

Test Temperature		Carbon Content (wt %)	
(°F)	(°C)	P_{CO_2} = 0.00528 atm	P_{CO_2} = 0.0524 atm
753	400	0.075	0.062
932	500	0.077	0.062
1112	600	0.080	0.062
1292	700	0.089	0.068
1472	800	0.118	0.096
1517	825	0.132	0.115
1562	850	0.155	0.150
1607	875	0.200	0.230
1652	900	0.190	0.135
1742	950	0.075	0.046
1832	1000	0.030	0.015

Table 5.4. Carburization of Type 304 Stainless Steel Exposed to CO-CO_2 Atmospheres $[(P_{CO})^2/P_{CO_2} = 0.227]$ for 840 hr

Test Temperature (°F)	Carbon Content (wt %)
753	0.072
932	0.072
1112	0.082
1292	0.112
1472	0.200
1652	0.500
1832	1.40

Table 5.5. Effect of Gas Pressure on the Oxidation Rate of Type 304 Stainless Steel at 1800°F

Time (hr)	Weight Gain (mg/cm^2) with Nonprotective Oxide		Weight Gain (mg/cm^2) with Protective Oxide	
	P_{CO_2} = 0.00528 atm	P_{CO_2} = 0.0524 atm	$P_{CO} + P_{CO_2}$ = 0.00435 atm	$P_{CO} + P_{CO_2}$ = 0.0263 atm
50	0.32	1.48	0.42	0.44
100	0.50	1.70	0.60	0.58
200	0.78	2.20	0.85	0.80
300	1.05	3.45	1.05	0.96
400	1.30	7.0	1.20	1.09
500	1.52		1.30	1.22
600	1.68		1.40	1.34
700	1.80		1.48	1.46
800	1.95		1.57	1.58

on the gas concentration when nonprotective oxides form on the metal and are independent of the concentration or pressure when the oxide is protective.

It is not presently clear that the interacting effects of carburization and oxidation may be predicted. The experimental results to date indicate that both phenomena are governed by the composition of the gas; however, this simple mechanism does not take into account the changes occurring at the metal interface. For example, it has been observed metallographically and by chemical analysis that the metal surface is selectively depleted of both chromium and nickel, leaving a thin zone that is high in iron content. Thus, the cross sections of metal specimens exposed to the gases appear to consist of a decarburized surface layer of ferrite on

unaffected austenite, irrespective of whether carburization or decarburization has occurred.

Bowing of a Simulated EGCR Fuel Element

W. R. Martin

Some EGCR fuel elements will be subjected to circumferential thermal gradients because of variations in the coolant flow and the effects of adjacent fuel elements and the graphite sleeve. These gradients may be of the order of 25 to 50°C. Since gradients of this magnitude would cause bowing of the fuel elements, midplane spacers were added to the fuel elements to limit the bowing. The presence of the column of fuel pellets within the fuel element will also reduce the magnitude of the bowing. Analytical studies of the bowing of empty stainless steel tubes have been made,[6] but the effect of the fuel pellets is difficult to predict. The extent of the restraint by the fuel within the tube was studied in an experiment adapted to the thermal apparatus used for the dimensional studies of the EGCR fuel element. Circumferential temperature differences were obtained by placing a furnace longitudinally along the cladding wall as shown in Fig. 5.3. The length of the "hot streak" was 13 in. Dial gages were used to monitor the bowing of the simulated element at temperature as a function of time. The changes in temperature along the circumference of the cladding at various temperature levels are shown in Fig. 5.4 for several typical test conditions.

The results of the tests are shown in Fig. 5.5. The scatter in the data prohibits any detailed analysis of these results; however, the following observations are pertinent:

1. The maximum lateral deflection increased with increasing thermal gradient.

2. The circumferential temperature gradient was more important than the temperature at which the gradient was achieved.

---

[6]J. M. Corum and W. A. Shaw, Restrained Thermal Bowing of Beams Accompanied by Creep with Application to the Experimental Gas-Cooled Reactor Fuel Elements, ORNL CF-60-9-1, December 1960.

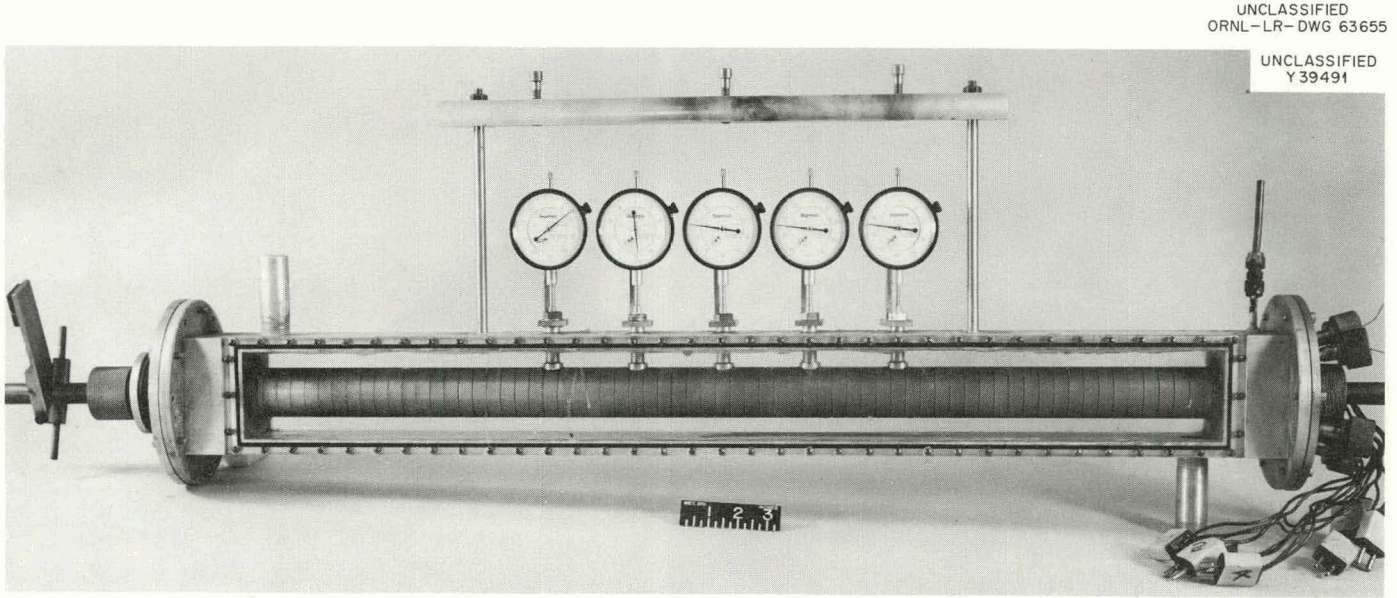

Fig. 5.3. Apparatus for EGCR Fuel Element Bowing Experiments.

3. There was restraint by the UO_2 pellets that resulted in a reduction of the maximum calculated deflection.

4. No difference in bowing was found after the element had been heated through five cycles.

5. The maximum permanent deflection in the element was 0.004 in.

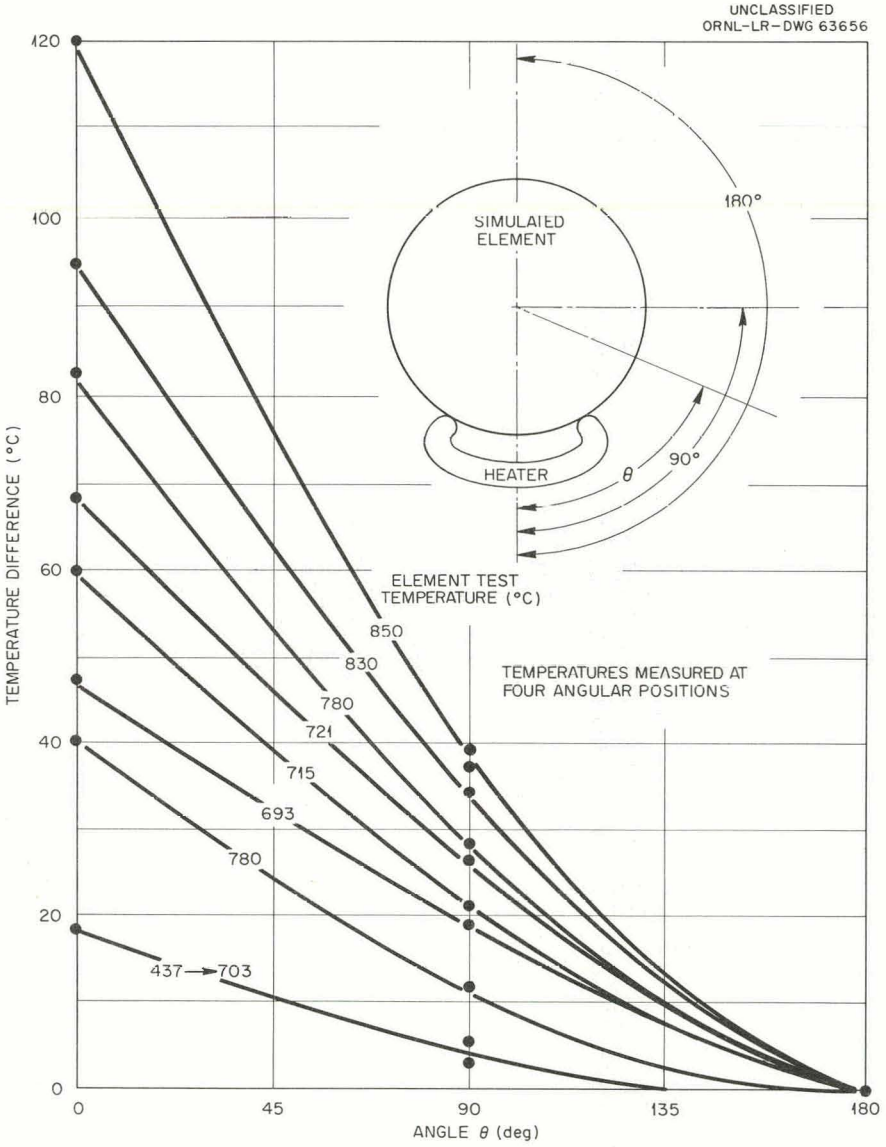

Fig. 5.4. Maximum Temperature Differences Along Circumference of Simulated EGCR Element at Various Temperatures.

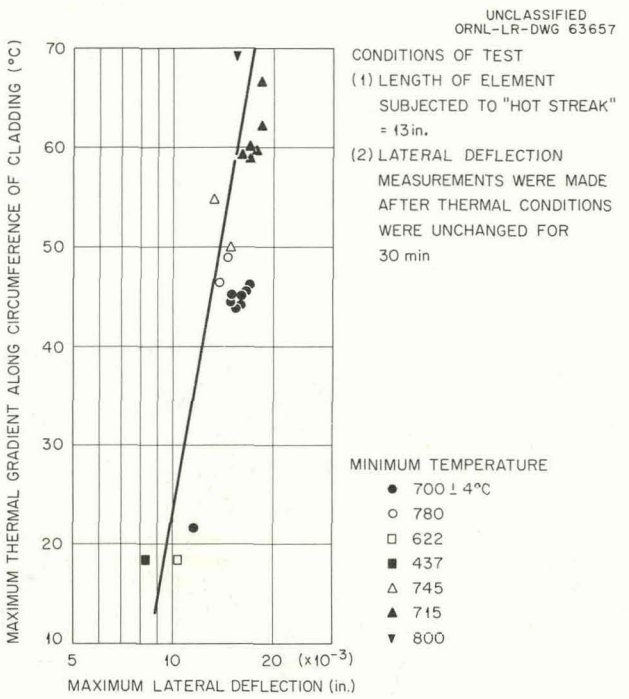

Fig. 5.5. Maximum Lateral Deflection of Simulated EGCR Fuel Element at Various Temperatures.

Fabrication of Instrumented Capsules for Irradiation Tests

E. A. Franco-Ferreira

Capsules for Irradiation in GCR-ORR Loop No. 1

Two capsules for irradiation of UO_2 pellets in GCR-ORR loop No. 1 have been fabricated and a third will be built as a backup unit. An over-all view of a typical capsule is shown in Fig. 5.6a, and a section showing the four internal cladding thermocouples in place is shown in Fig. 5.6b. The central thermocouple well is fabricated of molybdenum. A diagram of an instrumented capsule is presented in Fig. 5.7.

The cladding thermocouples are 0.060-in.-o.d. stainless-steel-sheathed Chromel-Alumel thermocouples with insulated junctions. The portions of the thermocouples that are inside the capsules are swaged to 0.040 in. o.d. in order to minimize the size of the slots which must be cut into the UO_2 pellets to accommodate them. The entire length of the thermocouple must

be brazed to the tube wall with a permissible straightness deviation of only 3 deg. Copper is used as the brazing material and is preplaced on the thermocouple by electroplating to a thickness of 0.001 in. Brazing

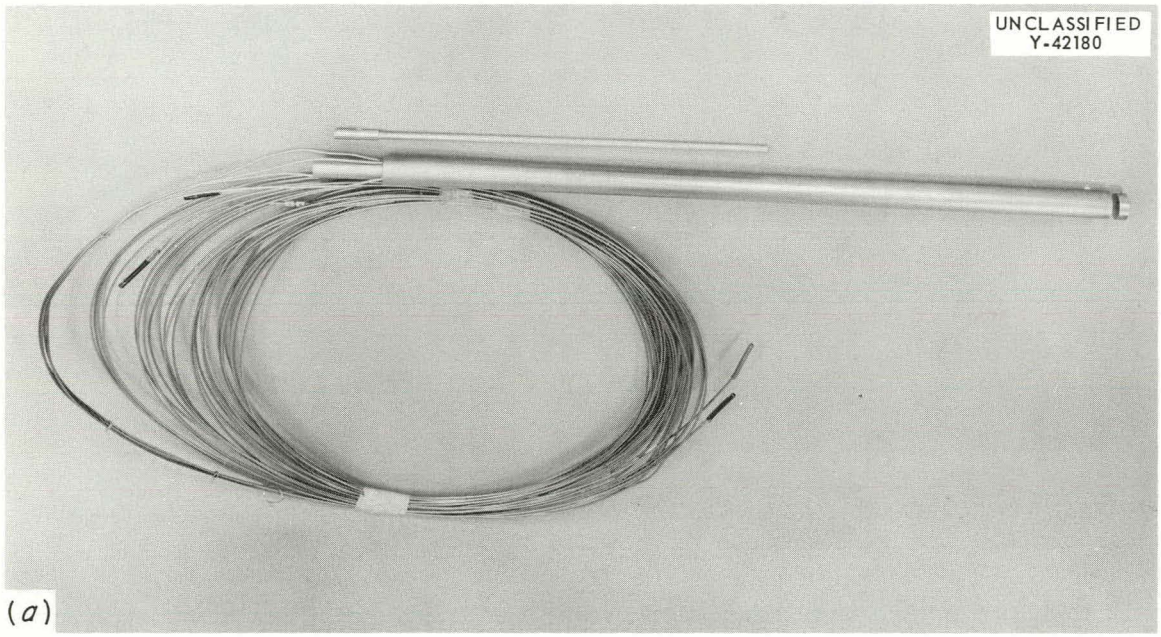

(a)

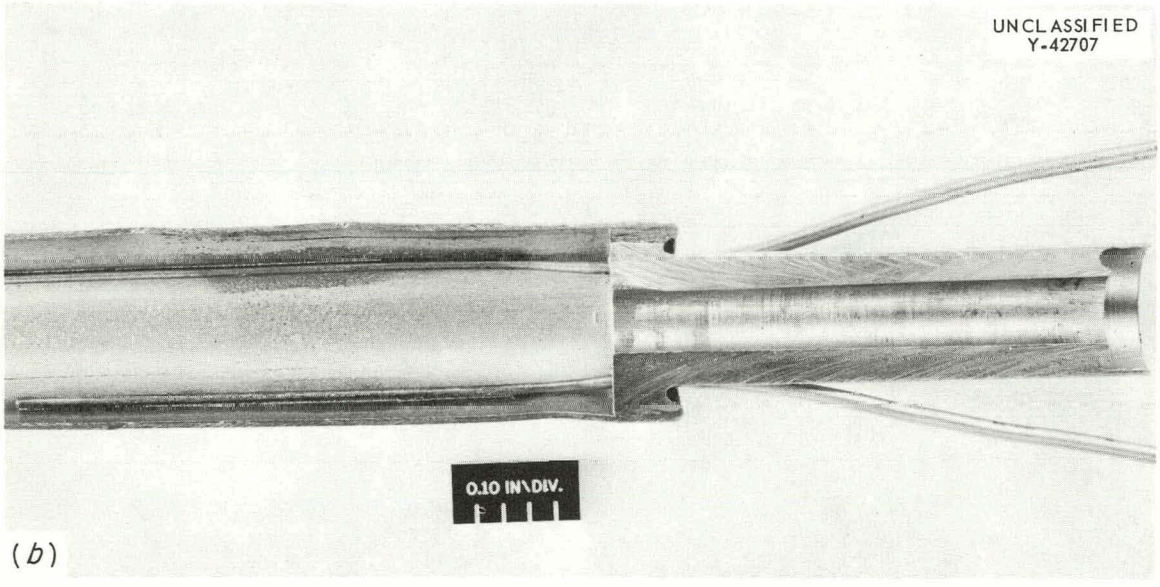

(b)

Fig. 5.6. (a) Over-all View of Typical GCR-ORR Loop No. 1 Capsule. The internal cladding thermocouples have been brazed into place and the central thermocouple well and bottom end cap are shown ready for assembly. (b) Section of Brazed Assembly Showing Attachment of Thermocouple to Cladding.

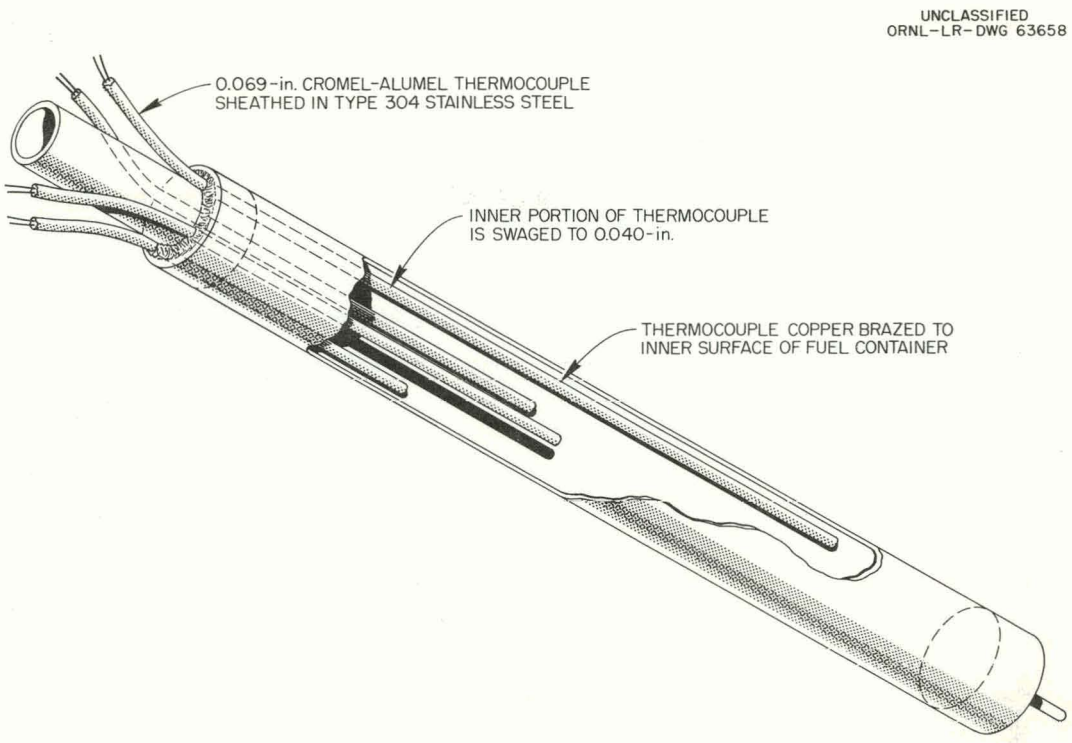

Fig. 5.7. Diagram of Instrumented Capsule for Irradiation in GCR-ORR Loop No. 1.

is carried out in a hydrogen atmosphere using an Inconel X jig to align the thermocouples and hold them in place. Inconel X was selected as the jigging material because the nonreducible aluminum and titanium oxides which form on the surface prevent the jig from inadvertently brazing to the capsule.

Capsules for Irradiation in ORR Poolside Facility

Sixteen capsules are being fabricated for the Group V irradiations in the ORR poolside facility. Four capsules are fueled with graphite bodies containing coated fuel particles, and eight capsules are being loaded with ThO_2-UO_2. The other four capsules are stainless-steel-clad UO_2 fuel elements with a central thermocouple in a tungsten well and a pressure transducer. One of these instrumented capsules is shown in Fig. 5.8a with the top end cap welded in and the transducer tube brazed in place. The central thermocouple well and the bottom end cap are shown

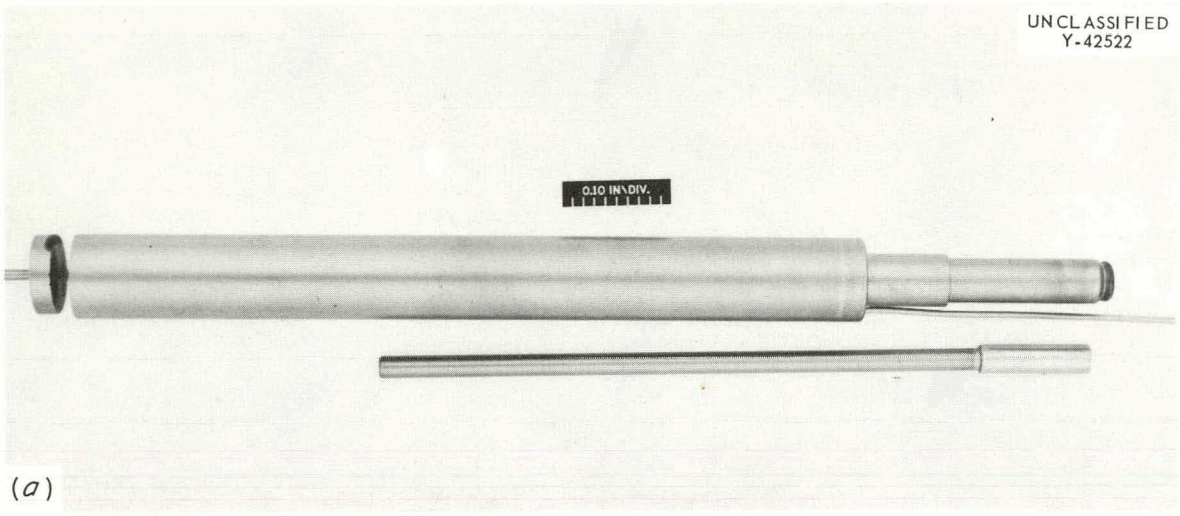

(a)

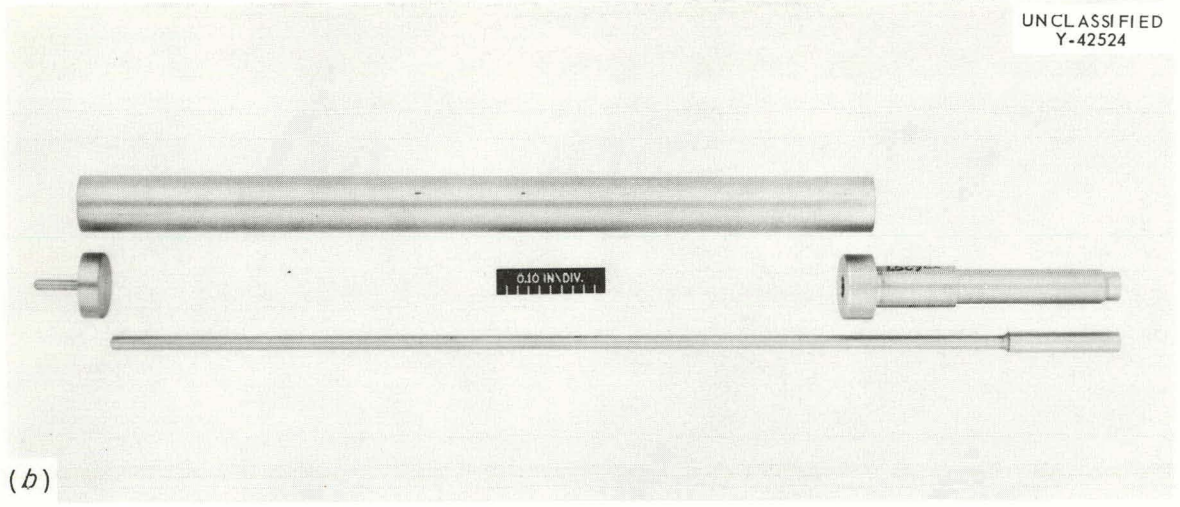

(b)

Fig. 5.8. (a) Instrumented Capsule for Irradiation in ORR Poolside Facility with Top End Cap and Pressure Transducer Tube in Place. Also shown are bottom end cap and central thermocouple well. (b) Components for Capsules Fueled with Vibratory-Compacted ThO_2-UO_2 Granules.

separately. The transducer tube is brazed into the top end cap with NaK-resistant GE-81 brazing alloy.

The eight capsules fueled with vibratory-compacted ThO_2-UO_2 granules incorporate a central thermocouple in a molybdenum well. The components for a capsule of this type are shown in Fig. 5.8b.

Estimates of the Release of Kr^{85} from ORR-Irradiated Capsules

J. L. Scott

In an attempt to test the validity of the method suggested by Cottrell et al.[7] for predicting the release of fission gases from UO_2, calculations were made of the expected release from ORR-irradiated capsules groups I and II. In the calculations, the thermal conductivity of the UO_2 was assumed to be 0.028 w/cm·°C in the range 700 to 1600°C. In the absence of a precise knowledge of the width of the gap between the UO_2 and the cladding, the calculations were made for a 3-mil helium gap and no gap. Values of the release-rate parameter (D′) were estimated from the measured BET surface areas of the UO_2 pellets. The computed values were then compared with the amounts of Kr^{85} actually found in these capsules.[8]

The results showed that the measured values of the percentage of Kr^{85} released generally fell within or close to the limits set by the 3-mil helium gap and no gap cases. Further, most of the measured values were close to those predicted for a 3-mil helium gap when the temperature of the cladding was about 700°C. For capsules with cladding temperatures near 800°C, the measured values corresponded more closely with the assumed condition of no gap between the UO_2 and the cladding. The good agreement between measured and estimated values lends credence to the method of Cottrell et al.[7] and verifies the value of the thermal conductivity of UO_2 which was used in the calculations. In addition, it appears that the surface area of pressed and sintered UO_2 may be used to calculate reliable D′ values for material irradiated up to as much as 2400 Mwd/MT of UO_2.

Graphite-Metal Diffusion Studies

J. H. DeVan

Extensive interdiffusion and bonding occurred, as reported previously,[9] between graphite and type 304L stainless steel diffusion couples at 1300°F. The couples were held for 1000 hr under high vacuum at contact pressures between the specimens of 500 to 2000 psi. Additional metallographic studies

have revealed a strong dependence of carburization depth on the contact pressure. In all cases, carburization depth increased with pressure, reaching a maximum of 0.030 in. at the 2000-psi pressure level. This maximum depth is comparable to the carburization depths (approximately 0.022 in.) reported[10] for type 304 stainless steel specimens exposed to carbon-saturated sodium for 1000 hr at 1300°F. Since the sodium-exposed specimens were presumably under negligible pressure, it would appear that pressure effects in the graphite-stainless steel diffusion couples were associated with improvement in contact area between the graphite and stainless steel surfaces.

Chemical analyses of 0.005-in.-thick stainless steel specimens tested at 1300°F showed a carbon content of 3.59%, which gave a Rockwell C hardness of 48. X-ray analyses revealed $Cr_{23}C_6$ to be the principal carbide on the stainless steel side of the diffusion couple, while Cr_7C_3 was predominant at the graphite-metal interface. Neither Fe_3C nor Cr_3C_2 could be detected.

A second set of diffusion couples has now completed 1000 hr of testing at 1200°F under a vacuum of approximately 3×10^{-6} mm Hg. The calculated contact pressure loads on the faces of the graphite and type 304L stainless steel disk specimens ranged from 500 to 2000 psi. Upon disassembling the apparatus, it was apparent that the pressure loads were not uniformly distributed, and therefore the calculated values were invalid. In order to correct this condition, the present equipment has been realigned, and a new design is being considered.

Visual examination of the specimens used in this test revealed basically the same effects as those of the previous 1300°F test. All bare metal surfaces were bonded to the graphite, whereas copper-plated and black-oxidized surfaces were not. Serious embrittlement of 0.005-in.-

---

[7]W. B. Cottrell et al., Fission-Product Release from UO_2, ORNL-2935, Sept. 13, 1960.

[8]J. L. Scott, The Release of Kr^{85} from UO_2 in ORR Capsules, ORNL-3195, Sept. 21, 1961.

[9]GCR Quar. Prog. Rep. June 30, 1961, ORNL-3166, pp. 168–9.

[10]W. J. Anderson and G. V. Sneesby, Carburization of Austenitic Stainless Steel in Liquid Sodium, Atomics International, NAA-SR-5282.

thick specimens that had bonded to the graphite was indicated in bend tests. Metallographic examinations are presently being performed.

Compatibility Tests of Graphite, Structural Materials, and Coolant

J. H. DeVan

A final investigation[11] of gas-metal reactions between type 304 stainless steel and CO-CO_2 impurities in thermal-convection loops utilized a helium mixture relatively rich in CO_2 (vol % CO_2/vol % CO = 4.0). The stainless steel specimens exposed at 1500°F in this test exhibited gray-green oxidation products, in contrast to the gray-to-black oxidation products developed in predominantly CO mixtures. Adherence of these gray-green films was notably poorer than that displayed in previous tests. Spectrographic analyses of these gray-green films showed chromium and manganese as the strongest components of the scale, with vanadium present in minor amounts. Electron diffraction studies have identified the films as predominantly Mn_2CrO_4.

Evolution of Gas from Graphite

L. G. Overholser J. P. Blakely

The degassing studies of EGCR graphite have been completed. Two specimens were degassed at various temperatures up to 1000°C using primarily 100°C temperature intervals between gas collections. These studies were performed to establish the release of sulfur compounds as a function of temperature and to provide volume-time relationships at temperatures other than the 300, 600, and 1000°C points that had been employed previously.[12,13]

---

[11]GCR Quar. Prog. Rep. March 31, 1961, ORNL-3102, pp. 211–13.

[12]GCR Quar. Prog. Rep. March 31, 1961, ORNL-3102, pp. 216–24.

[13]GCR Quar. Prog. Rep. June 30, 1961, ORNL-3166, pp. 169–77.

The two specimens, 1 1/2 in. in diameter, 2 in. long, and designated C4B-7B and C4B-10B, were machined from the central region of the slab cut from a bar processed as part of a furnace load identified as File No. 3, which was described previously.[13] The results obtained by degassing these two specimens at various temperatures up to 1000°C are given in Table 5.6. These data are in fair agreement, since the periods of time at which the specimens were degassed at the various temperatures were quite different. The temperature spectrum, especially at the higher temperatures, is quite sensitive to the length of time a sample is degassed at some given temperature. Prolonged degassing at 800°C, for example, results in the removal of gas that otherwise would appear at 900°C (or the next highest temperature) if a shorter period of degassing were used at 800°C. The volumes recorded in Table 5.6 at 900°C show a very pronounced effect of time.

The data indicate that SO_2 was released at 200°C (and probably below), but it disappeared above 600°C. A maximum release was observed between 300 and 400°C in the case of specimen C4B-7B, but this release is not confirmed by the results given for specimen C4B-10B. It may be noted that H_2S and CS_2 were released in various amounts over the entire temperature

Table 5.6. Volume and Composition of Gas Evolved by EGCR Graphite at Various Temperatures up to 1000°C

Sample No.	Temperature (°C)	Time (hr)	Gas Volume (cm^3/100 cm^3 of graphite)	Composition of Evolved Gas (vol %)							
				H_2	H_2O	Hydrocarbons	N_2	CO	CO_2	SO_2	$H_2S + CS_2$
C4B-10B	500	23	2.2	3	32	18	12	10	17	4	5
	600	19	1.8	6	18	12	3	19	36	5	0.4
	700	45	2.0	34	10	21	4	21	6		2
	800	69	3.1	34	7	8	2	49	0.7		0.1
	900	47	2.4	34	0.4	4	2	58	0.3		0.6
	1000	42	4.2	30	3	1	1	64	0.2		0.9
	1000	25	1.3	36	1	2	3	56	0.7		0.3
C4B-7B	200	6	0.4	2	57	3	27		3	8	
	300	5	0.4	1	43	8	27	3	8	8	2
	400	10	0.8	2	27	8	19	9	16	18	2
	500	7	0.7	4	36	11	8	14	21	5	
	600	10	1.4	7	15	15	3	30	27	1	
	700	10	1.4	28	8	24	3	26	10		
	800	10	2.0	28	2	9	2	53	3		0.3
	900	25	4.2	39	0.6	5	2	54	0.2		
	1000	41	4.4	40	0.4	2	2	55	0.2		0.5

range studied. Small amounts of these compounds also have been found in the gas released above 1400°C. All the EGCR graphite samples degassed to date have evolved appreciable quantities of sulfur (SO_2, H_2S, CS_2), and there is no reason to believe that the graphite loaded into the EGCR will not do likewise.

The volume-time relationships at 300, 600, and 1000°C have been reported[12,13] for a number of EGCR graphite specimens, and additional data are presented in Table 5.7 and Fig. 5.9 that were obtained by degassing a single specimen of graphite at successively higher temperatures in the range 500 to 1000°C. The general shapes of the 500 and 600°C plots are similar; both show an essentially linear relationship between the volume of gas evolved and the log of time. The slope is larger at 600 than at 500°C, as anticipated. Starting at 700°C, a different type of desorption must occur, as evidenced by the change in the shapes of the curves. As indicated in Table 5.6, this also is the temperature at which a marked increase in the concentration of H_2 in the desorbate is observed. This

Table 5.7. Values for the Constants A and B in the Equation[a] V = A log t + B for EGCR Graphite Sample C4B-10B at Various Temperatures up to 1000°C

Temperature (°C)	Time Interval (min)	A	B
500	90–1620	0.37	1.03
600	100–1100	0.95	−1.18
700	100–300	0.58	−0.92
700	1200–2700	1.9	−4.8
800	125–550	1.3	−2.4
800	1250–3500	2.5	−6.2
900	100–400	1.0	−1.5
900	1250–2800	2.2	−5.1
1000	60–150	1.0	−1.5
1000	1075–2700	4.2	−10.3

[a]Volume expressed as cm^3 (STP) of evolved gas per 100 cm^3 of graphite; time in minutes. The intercepts do not include the gas removed at the lower temperatures.

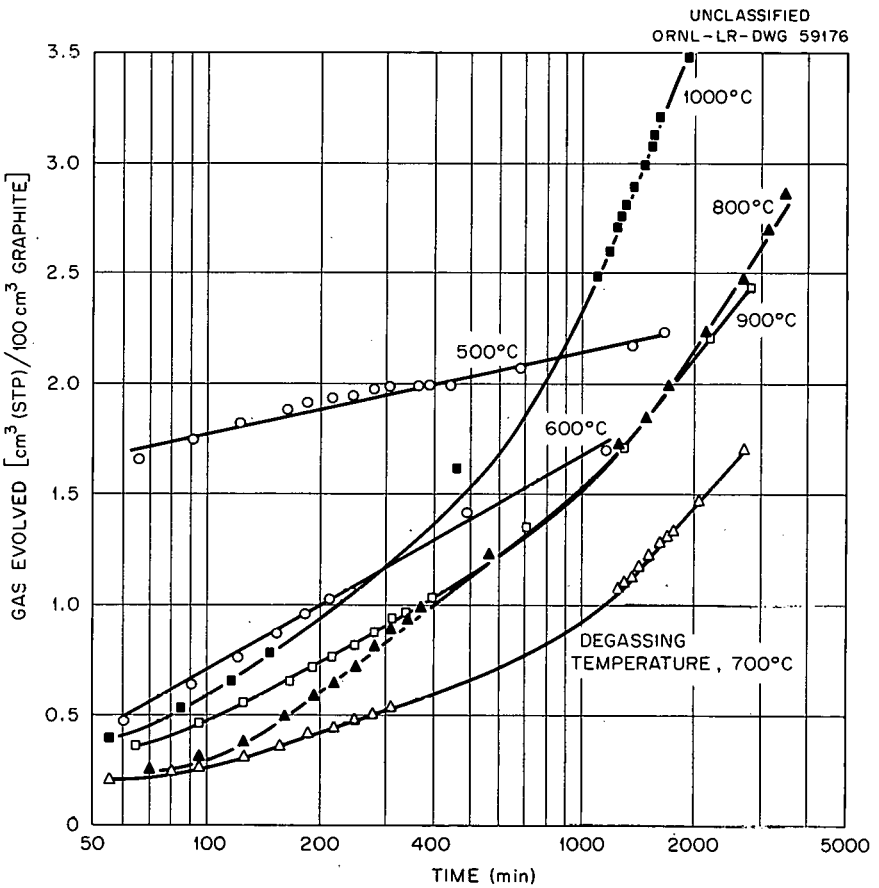

Fig. 5.9. Volume-Time Plots for EGCR Graphite Degassed at 500 to 1000°C.

type of curve, in which the slope increases and then becomes essentially constant, has been observed at 1000°C for other EGCR graphite specimens, as well as for other grades of graphite. No explanation can be offered for the slight decrease in slope which is noted upon going from 800 to 900°C. These data illustrate vividly the changes in the character of the degassing behavior which may occur when a simple specimen of graphite is degassed at various temperatures over prolonged periods of time. Not only may the evolution process change with temperature, but it may also change with time at a constant temperature. This behavior suggests that no simple kinetics formulation is possible. Empirical relationships may be applied, however, over large time intervals to describe the rate of evolution at various temperatures.

A Diffusion Model for the Transport of Gases in Porous Media

J. Truitt R. B. Evans

Pore-diffusion phenomena in porous media are customarily discussed in terms of two basic concepts: Knudsen (or molecular flow) and normal diffusion. Treatment of diffusion in terms of these two concepts restricts the discussion to either of the corresponding limiting cases — gas-gas collisions only (normal diffusion) or gas-wall collisions only (Knudsen) — and is not applicable to the situation in which both collision mechanisms are significant. The primary objective of this investigation was the development of a generalized diffusion model applicable to the more realistic case in which both collision mechanisms are superimposed.

The model[14] is based on (1) the results of a series of uniform-pressure experiments involving the interdiffusion of two gases in a graphite[15] and (2) a theoretical postulation that a portion of the porous media immediately involved in surface collisions behaves as a collection of uniformly distributed "dust" particles. When these particles are treated as large molecules and as the third gas component of the mixture, all the desired results can be obtained from classical multicomponent formulations. These theoretical equations yield the experimentally observed flux ratio, $(m_2/m_1)^{1/2}$, for binary gas mixtures, the Bosanquet interpolation formula, and a differential equation for diffusion that is applicable over the entire pressure range. Application of the model to the results of earlier studies with permeable graphite[16,17] reveals that all conclusions made and equations used previously regarding uniform-pressure measurements remain valid. The model appears to be applicable to all porous media over all pressures ranging from Knudsen to the normal region. The model does not

---

[14]R. B. Evans III, G. M. Watson, and E. A. Mason, J. Chem. Phys., in press (1961).

[15]R. B. Evans III, Jack Truitt, and G. M. Watson, J. Chem. Eng. Data, in press (1961).

[16]GCR Quar. Prog. Rep. March 31, 1960, ORNL-2929, pp. 206–9.

[17]GCR Quar. Prog. Rep. June 30, 1961, ORNL-3166, pp. 177–8.

characterize the porous medium, but, if the interdiffusive rates of a particular binary gas mixture are measured in a certain medium, the diffusive rates for other gas mixtures through this same medium can be predicted. Only two parameters are required to define a given binary gas–porous medium system in terms of the model. These are an effective normal diffusion coefficient (characteristic of both gases and the medium) and an effective Knudsen coefficient for one of the gases in the same medium.

According to the model, portions of the porous medium that are immediately involved in surface collisions are visualized as a collection of very large particles (dust) of mass m_d and radius r_d such that $m_d \gg m_1$ or m_2 and $r_d \gg r_1$ or r_2. This collection is treated as a third gas component. Based on classical multicomponent formulations,[18] the experimentally observed $-J_1/J_2$ condition is developed when the conditions J_d and $dx_d/dz = 0$ are applied to the system. The flux J_1 of either true gas component can be expressed in terms of the relationship

$$J_1 = -D_1 \frac{dn_1}{dz} + \delta_1 \left(\frac{n_1}{n}\right) J \quad ; \qquad \begin{pmatrix} \delta \to 1;\ p \to \infty \\ \delta \to 0;\ p \to 0 \end{pmatrix} ,$$

where

$J = J_1 + J_2$,

$p = nkT$.

The δ_1 replaces the ratio of mean free path to pore radius that is frequently employed in diffusion discussions. When $\delta \to 1$, diffusion is normal; when $\delta \to 0$, diffusion is Knudsen.

It turns out that $1/D_1$ is the sum of a normal diffusion term $1/D_{12}$ and a Knudsen term $1/D_{1k}$. The D_{12} is the normal coefficient D_{12} multiplied

---

[18] J. O. Hirshefelder, C. F. Curtiss, and R. B. Bird, Molecular Theory of Gases and Liquids, p. 517, Eq. (8.1-3), John Wiley and Sons, Inc., New York, 1954.

by the graphite porosity-to-tortuosity ratio of the medium. The normal terms, D_{12}, for the two gases are equal; the Knudsen terms D_{1k} and the δ_1 of the two gases are not equal. The latter can be calculated, however, if D_{1k} and D_{12} are known for one of the gases. The integrated equation for the flux of component 1 through a system of thickness L at $dp/dz = 0$ is

$$\exp\left(\frac{\beta L J_1}{n D_{12}}\right) = \frac{(\delta_1)^{-1} - \beta x_1\ (L)}{(\delta_1)^{-1} - \beta x_1\ (0)} \quad .$$

The β incorporates the $J_1/J_2 = -(m_2/m_1)^{1/2}$ ratio that results from the $dp/dz = 0$ condition, that is, $\beta = J_1/J = 1 - (m_1/m_2)^{1/2}$. The Knudsen contribution appears only through the relationship

$$\frac{1}{\delta_1} = 1 + \frac{D_{12}}{D_{1k}}$$

and does not appear in the exponential term. An experimental method for the determination of these parameters for helium and argon in various types of graphite is currently under evaluation. Tentative experimental results indicate that the model is applicable over a wide range of gas temperatures, pressures, and media pore sizes.

6. IRRADIATION TESTING OF EGCR COMPONENTS AND MATERIALS

D. B. Trauger O. Sisman

Fuel Capsule Irradiations In ORR Poolside Facility

F. R. McQuilkin A. W. Longest
V. A. DeCarlo R. L. Senn

Irradiation of six of the eight group IV capsules, described previously,[1] is continuing in the ORR under the conditions summarized in Table 6.1. The two French beryllium-clad capsules gave indication of fission-gas leakage through the cladding during a routine leak test and were withdrawn during the August 27 shutdown period for disassembly and examination. Temperature oscillations of ±150, ±50, and ±20°F have been encountered with capsules 02-4, 06-4, and 07-4, respectively. During the July reactor shutdown, the 1000-rpm control-gas circulators for these capsules were replaced with similar 1800-rpm units, but no improvement has been observed in the temperature fluctuations. As noted in Table 6.1, five of the six thermocouples on capsule 02-4 have failed.

An evaluation of the radiation-monitoring system indicates that the sensitivity of the ion chambers originally installed is probably insufficient to detect fission gases from cladding leaks in UO_2 fuel specimens operated at low temperatures. Plans have been completed for increasing this sensitivity by replacing the present ion chambers with units having greater sensitivity and supplementing them with highly sensitive GM-tube detectors. A portable GM-tube probe has been installed temporarily and the routine leak checks are being performed immediately following scheduled reactor shutdown rather than 6 hr later. Since the French capsules had not been checked previously with the more sensitive detectors, the time of failure cannot be established.

The positioning mechanisms installed during insertion of the group V capsules became inoperable after limited use. It was determined that

[1]GCR Quar. Prog. Rep. June 30, 1961, ORNL-3166, p. 117.

Table 6.1. Operating Conditions for Group IV Capsules as of August 27, 1961

Capsule No.	Type of Capsule	Cladding Surface Temperature (°F)				Capsule Inner Surface Temperature (°F)		Remarks
		Design	High	Low	Average	Temperature Element No. 2	Temperature Element No. 5	
01-4	UO_2 pellets in instrumented stainless steel tube	1600 (max)	1630	1477	1609	1477	1773	The central thermocouple became inoperable when its temperature reached 1800°F. Later, however, it resumed operation and operated until July 13; temperature recorder No. 6 failed on August 12
02-4	Tamp-packed UO_2 powder in stainless steel tube	1300 (av)			1300			Temperature recorders 1, 2, 5, 4, and 3 failed on May 26, 28, June 3, July 13 and 27, respectively
03-4	Hot-swaged UO_2 powder in stainless steel tube	1300 (av)	1258	1095	1170			On June 13, this capsule was inserted an additional 1 in.
04-4	UO_2 pellets in beryllium tube	1112 (av)	1172	1040	1099			Twenty thermal cycles per month are being applied; temperature element No. 5 failed on May 19
05-4	UO_2 pellets in beryllium tube	1112 (av)	1026	978	1001			Twenty thermal cycles per month are being applied; NaK blanket pressure was increased from 500 to 575 psig on June 5, from 575 to 625 on July 13, and from 625 to 725 on July 30; temperature elements 4 and 2 failed on June 22 and July 13, respectively
06-4	Hot-swaged UO_2 powder in stainless steel tube	1300 (av)	1525	1105	1212			100% N_2 in control gas system
07-4	Hot-swaged UO_2 powder in stainless steel tube	1300 (av)	1367	1270	1315			Temperature element 2 failed on June 13
08B-4	UO_2 pellets in instrumented stainless steel tube	1600 (max)	1610	1430	1487	1680	1428	The central thermocouple operated at 2300°F until it failed on May 27

the spring-loaded stainless-steel detent plunger that locks a capsule at its adjusted position had galled the surface of the positioning-mechanism raceway. Modified mechanisms are being prepared for replacement when the group IV capsules are removed.

Pertinent design data and planned operating conditions for the next set of capsules, group V, have been developed and are summarized in Table 6.2. New equipment designed for use with coated-particle capsules 01-5 and 08-5 provides for a flow of helium to continuously sweep any fission gases released from the coated fuel particles past the new activity monitors. The operational flow diagram for this equipment is shown in Fig. 6.1. The sweep gas will be sampled periodically and analyzed with a gamma-ray spectrometer to determine the quantity and kind of fission gas being released. A 512-channel pulse-height analyzer is being obtained for these measurements. Special equipment for gas sampling and handling is being installed in a new shielded equipment chamber, and additional charcoal traps have been installed to ensure adequate holdup of fission gases before release to the offgas system.

A new method for establishing and maintaining the desired specimen temperature is being instituted. Previously, a fixed location with an estimated neutron flux was established by the choice of fuel enrichment. The desired temperature was obtained by varying the ratio of helium to nitrogen gas in the thermal-barrier gap to adjust the rate of heat transfer from the specimen. This scheme has not been fully satisfactory because the severe thermal gradients cause diffusive separation of the gas mixtures. The gas circulators installed to overcome this effect have performed poorly. Variation in the neutron flux at a fixed irradiation position also occurs because of changes in reactor fuel and experimental loadings, fuel burnup, and shim rod movement. In the revised method, either pure helium or pure nitrogen gas will be used in the thermal-barrier gas gap. Each experimental assembly will be moved, as necessary, by means of the positioning mechanism to obtain the neutron flux required to achieve the desired capsule temperature.

Table 6.2. Summary of Design and Planned Irradiation Conditions for Group V Capsules

Capsule number	01-5	02-5	03-5	04-5	05-5	06-5	07-5	08-5
Origin of fuel specimen	The 3M Co.	ORNL	ORNL	CEA, France	CEA, France	ORNL	ORNL	The 3M Co.
Type of specimen	Pyrolytic carbon-coated UC_2 particles in graphite matrix	UO_2 pellets in P&T[a] instrumented type 304 stainless steel tube	Vibratory compacted ThO_2-UO_2 granules in type 304 stainless steel tube	UO_2 pellets in 0.012-in.-wall type 316 stainless steel tube	UO_2 pellets in 0.012-in.-wall type 316 stainless steel tube	Vibratory compacted ThO_2-UO_2 granules in type 304 stainless steel tube	UO_2 pellets in P&T instrumented type 304 stainless steel tube	Pyrolytic carbon-coated UC_2 particles in graphite matrix
Perturbed thermal-neutron flux, neutrons/cm^3·sec	3.38×10^{13}	1.66×10^{13}	3.0×10^{13}	6.0×10^{13}	6.0×10^{13}	3.0×10^{13}	1.66×10^{13}	3.38×10^{13}
Fuel enrichment in U^{235}, wt % of total uranium	50.0	2.30	93.2	1.9	1.9	93.2	2.30	50.0
Total uranium in fueled specimen, wt %	10.0	88.2	2.5	88.2	88.2	2.5	88.2	10.0
Fuel specimen density								
g/cm^3	1.87	10.47	8.6	10.4	10.4	8.6	10.47	1.87
% of theoretical		95.44	86.0	94.8	94.8	86.0	95.44	
Heat rate, Btu/hr·ft	18 800	30 000	40 000	38 500	38 500	40 000	30 000	18 800
Specific power, w/g of fuel specimen	64.0	13.9	27.1	38.0	38.0	27.1	13.9	64.0
Scheduled burnup, Mwd/MT of fueled specimen	12 500	2 700	5 300	7 400	7 400	5 300	2 700	12 500
Cladding temperature, °F	1 100	1 600	1 300	1 202	1 202	1 000	1 600	700
External pressure on cladding, psig								
Initial	~atmos.	300	300	850	850	300	300	~atmos.
Final	~atmos.	300	300	850	850	300	300	~atmos.
Central temperature measurement	Yes	Yes	Yes	No	No	Yes	Yes	Yes
Type of thermocouple (all with insulated junctions)	1/16-in.-o.d. tantalum-sheathed W-5% Re vs W-25% Re	1/8-in.-o.d. bare W-5% Re vs W-25% Re	1/16-in.-o.d. bare W-5% Re vs W-25% Re			1/16-in.-o.d. bare W-5% Re vs W-25% Re	1/8-in.-o.d. bare W-5% vs W-25% Re	1/16-in.-o.d. tantalum sheathed W-5% Re vs W-25% Re
Thermocouple well	Open molybdenum tube	Tungsten well	Plugged molybdenum tube			Plugged molybdenum tube	Tungsten well	Open molybdenum tube
Capsule internal pressure measurement	No	Yes	No	No	No	No	Yes	No
Shutter thermal cycles	0	0	0	1/day	1/day	0	0	0
Thermal-barrier gas	N_2	N_2	He	He	He	He	N_2	He
Gas gap, in. (hot)	0.005	0.005	0.012	0.011	0.011	0.009	0.005	0.009
Cladding dimensions, in.								
Outside diameter	0.750	0.750	0.625	0.457	0.457	0.625	0.750	0.750
Inside diameter	0.710	0.710	0.585	0.433	0.433	0.585	0.710	0.710
Fuel specimen dimensions, in.								
Outside diameter	0.600[b]	0.706	0.585	0.429	0.429	0.585	0.706	0.600[b]
Inside diameter	0.250	0.323	0.125	0	0	0.125	0.323	0.250
Assembly drawing No.	D-10587	D-10776	D-10731	D-10826	D-10826	D-10731	D-10776	D-10587

[a] P&T refers to capsule internal pressure and central fuel temperature measuring instruments.

[b] A pyrolytic graphite sleeve 0.7055 in. o.d. × 0.605 in. i.d. insulates and spaces the fueled matrix specimen.

Capsule L-27. The central temperatures at the start of irradiation of the a and b sections of capsule L-27 were estimated to be approximately 2000 to 2400°F, respectively. The bottom UO_2 fuel pellet from the a section was selected for metallographic examination. This pellet had not been in contact with the tantalum sheathing on the internal thermocouple and was not damaged to a great extent, as were the upper three pellets. The cross section revealed normal UO_2 fuel, with no evidence of a reaction at either the inner or outer surfaces. Most of the porosity was intergranular, and there was no evidence of grain growth. The top three fuel pellets, which showed evidence of having reacted with the internal thermocouples, were highly fractured, and no suitable sample for mounting for metallographic examination was available.

A UO_2 fuel pellet from the b section which remained intact was also examined. The fuel material did not appear to have undergone significant changes during irradiation. A large amount of intergranular porosity was noted that would seem to indicate a density of less than the measured 95% of theoretical.

Capsule L-28. The central temperatures at the start of irradiation of the a and b sections of capsule L-28 were estimated to be approximately 2200 and 3450°F. A portion of a pellet was selected from the center of the a section for the metallographic specimen. Comparison with the unirradiated control revealed little or no difference in the size of the grains and the amount of porosity.

A transverse section through the UO_2 insulator, UO_2 fuel, and thermocouple region was made at approximately the center of the b section (Fig. 6.10). A reaction of the UO_2 fuel with the tantalum sheath of the thermocouple was evident. The fuel was very porous and the grains were columnar. The columnar grains of the fuel extended into the UO_2 insulator. The second phase material noted in capsule L-24 was not seen.

Capsule L-32. The estimated central temperature at the start of irradiation of the b section of capsule L-32 was 3100°F. No a section central temperature was obtained because of failure of the thermocouple at startup. Very little difference was noted in the microstructures of

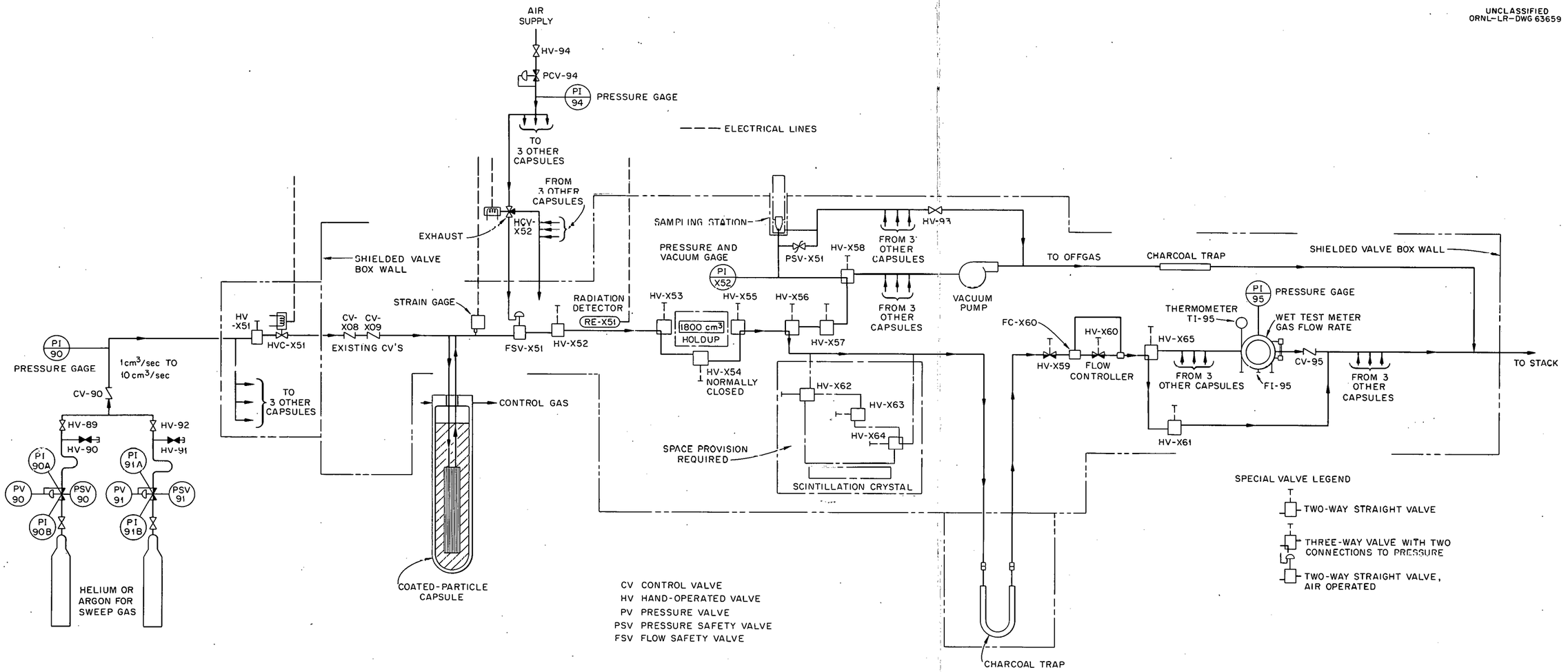

Fig. 6.1. Flow Diagram of Sweep Gas System for Use with Capsules 01-5 and 08-5.

Examination of Irradiated Capsules

J. G. Morgan M. F. Osborne
H. E. Robertson E. L. Long, Jr.

ORR-Irradiated Capsules

Fuel pellets from group I capsules 04-1, 07-1, and 08-1 were examined for changes in UO_2 density. The density changes detected were small and consistent with previously observed changes,[2,3] as shown in Table 6.3. The average diameter of the BeO rod from the center of capsule 04-1 decreased from 0.321 to 0.318 in. in good agreement with previous data.[2] The results of radiochemical analyses of these fuel pellets for uranium burnup are shown in Table 6.4, along with the values calculated from neutron flux data. The higher burnup indicated at the bottom of capsule 04-1 agrees with the gamma scan, which showed an activity peak at the bottom and a depression at the top of the capsule.

Visual examination of group III capsules 01-3, 01A-3, and 08-3 showed a distinct bulge in the 0.020-in.-thick cladding near the bottom of capsule 01-3. The bulge was about 1 in. long and 0.030 in. high. Analysis of the NaK from around these capsules showed a significant quantity of Cs^{137}, indicating fission-product leakage. When the capsules were pierced for fission-gas removal, NaK leaked from capsule 01-3, and NaK was found

[2]GCR Quar. Prog. Rep. March 31, 1961, ORNL-3012, pp. 156–63.

[3]GCR Quar. Prog. Rep. June 30, 1961, ORNL-3166, p. 130.

Table 6.3. Changes in Bulk and Immersion Density of EGCR Prototype Fuel Pellets Irradiated in the ORR

Capsule No.	Pellet No.	Bulk Density[a] (g/cm³)			Immersion Density[b] (g/cm³)		
		Preirradiation	Postirradiation	Change	Preirradiation	Postirradiation	Change
04-1	8	10.38	10.17	−0.21	10.67	10.73	+0.06
07-1	6	10.56	10.44	−0.12	10.61	10.70	+0.09
08-1	7	10.57	10.25	−0.32	10.62	10.70	+0.08

[a]Determined by immersion in mercury.

[b]Determined by immersion in CCl_4.

throughout the capsule when it was opened. Efforts are being made to locate the leak.

Postirradiation determinations were made of the oxygen-to-uranium ratios of some of the fuel pellets. The results for two of the first group and two of the second group of ORR-irradiated capsules are listed in Table 6.5. No increase in the ratio was found as a result of irradiation, within the reproducibility of the analytical method. There is a slight indication of the UO_2 becoming more nearly stoichiometric. Preirradiation values were redetermined using the same technique as that used on the irradiated samples in order to make the values directly comparable.

Table 6.4. Comparison of Burnup Data for Fuel Pellets from ORR-Irradiated Capsules

Capsule No.	Pellet Location	Burnup (Mwd/MT of U)		
		Cs^{137} Analysis	Ce^{144} Analysis	Flux Data
04-1	Second from bottom	2038	1962	1600
04-1	Second from top	1474	1455	1600
07-1	Middle	774	743	580
08-1	Middle	766	708	560

Table 6.5. Oxygen-to-Uranium Ratios of Fuel Pellets from ORR-Irradiated Capsules

Capsule No.	Burnup (Mwd/MT of U)	Oxygen-to-Uranium Ratio of UO_2 Pellets		Calculated Central Temperature (°F)
		Before Irradiation	After Irradiation	
01-1	1710	2.007	2.007	2500
05-1	2700	2.015	2.002	3100
02-2	1400	2.001	2.000	2800
04-2	1680	2.001	2.002	2850

ETR-Irradiated Capsule E-9

Metallographic examination of a longitudinal section of the cladding from ETR capsule E-9 at a pellet-to-pellet interface revealed a heavy precipitate near the inner surface that was tentatively identified as a nitride, since the UO_2 fuel contained an appreciable amount of uranium nitride.[4] At the pellet-to-pellet interfaces the precipitate had penetrated about twice as deep as it had elsewhere in the cladding. Microhardness measurements were made at the outer, central, and inner regions. No change in the microhardness in the outer region was noted (KHN of 165 with a 100-g load). The central region of the cladding showed an increase from a KHN of 152 to approximately 200. The inner region showed a marked increase from a KHN of 130 to approximately 270. A typical area is shown in Fig. 6.2.

[4] Ibid., p. 134.

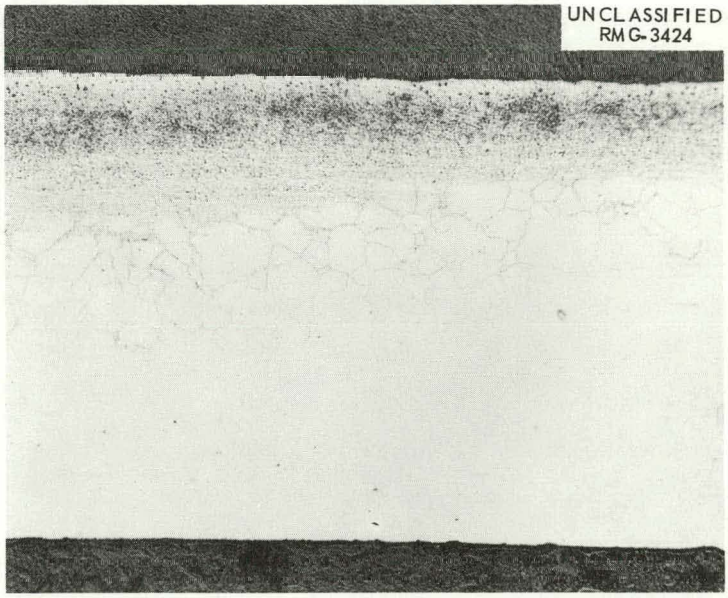

Fig. 6.2. Typical Area of Type 304 Stainless Steel Cladding from ETR-Irradiated Capsule E-9. Heavy precipitate is at the inner surface. Specimen lightly etched with picric and hydrochloric acids. 100X

LITR-Irradiated Capsules

Metallographic examinations have been made, when possible, of a UO_2 fuel pellet or a portion of a pellet selected from the center of each LITR-irradiated capsule. In each instance a transverse section was polished and examined, and unirradiated control samples were polished and examined for comparison. The photomicrographs presented here are typical of the microstructures observed unless otherwise stated.

Capsule L-11. The average central temperature at the start of irradiation in the a section of capsule L-11 was approximately 2575°F, whereas that of the b section was approximately 2700°F. The cladding was held at a nominal temperature of 1300°F.

Increases in porosity and grain size were noted in the hollow UO_2 fuel specimens from both the a and b sections in comparison with the control sample. Also, the grain size was larger at the outer surface than at the inner surface, as would be expected based on the temperature difference that existed across the pellet wall. Typical transverse sections of UO^2 pellets from sections a and b are shown in Figs. 6.3 and 6.4, respectively. An unusual area noted in the b section UO_2 specimen is shown in Fig. 6.5. The tantalum sheath of the internal thermocouple had apparently come in contact with the inner wall of the UO_2 pellet in this region. The resultant reaction can be seen as a second phase in the grain boundaries at the inner region. A radial crack can also be seen in this area.

Capsule L-23. LITR-irradiated capsule L-23 and capsules L-24 through L-28 and capsule L-32, to be discussed later, are of the model-3 type, which includes a depleted UO_2 sleeve around the hollow UO_2 pellets that acts as a thermal insulator. The central temperature at the start of irradiation in the a section of capsule L-23 was estimated to be approximately 2700°F and, in the b section, 2800°F.

The sample from the a section showed no signs of thermal fusion between fuel and insulator, whereas the fuel-to-insulator interface in the b section was no longer evident. The fuel in the a section showed no measurable increase in grain size, but there was an appreciable increase in porosity, whereas the microstructure of the fuel from the b section no

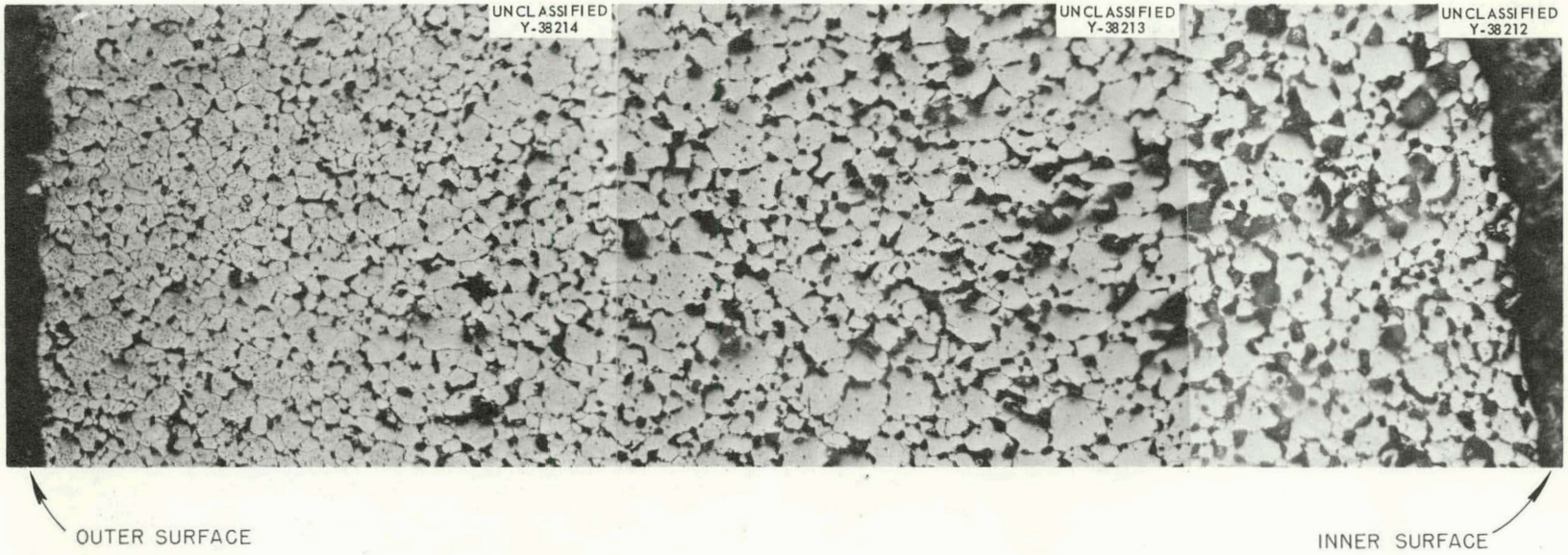

Fig. 6.3. Typical Transverse Section of a Hollow UO_2 Pellet from Section a of LITR-Irradiated Capsule L-11. Etched. 250X

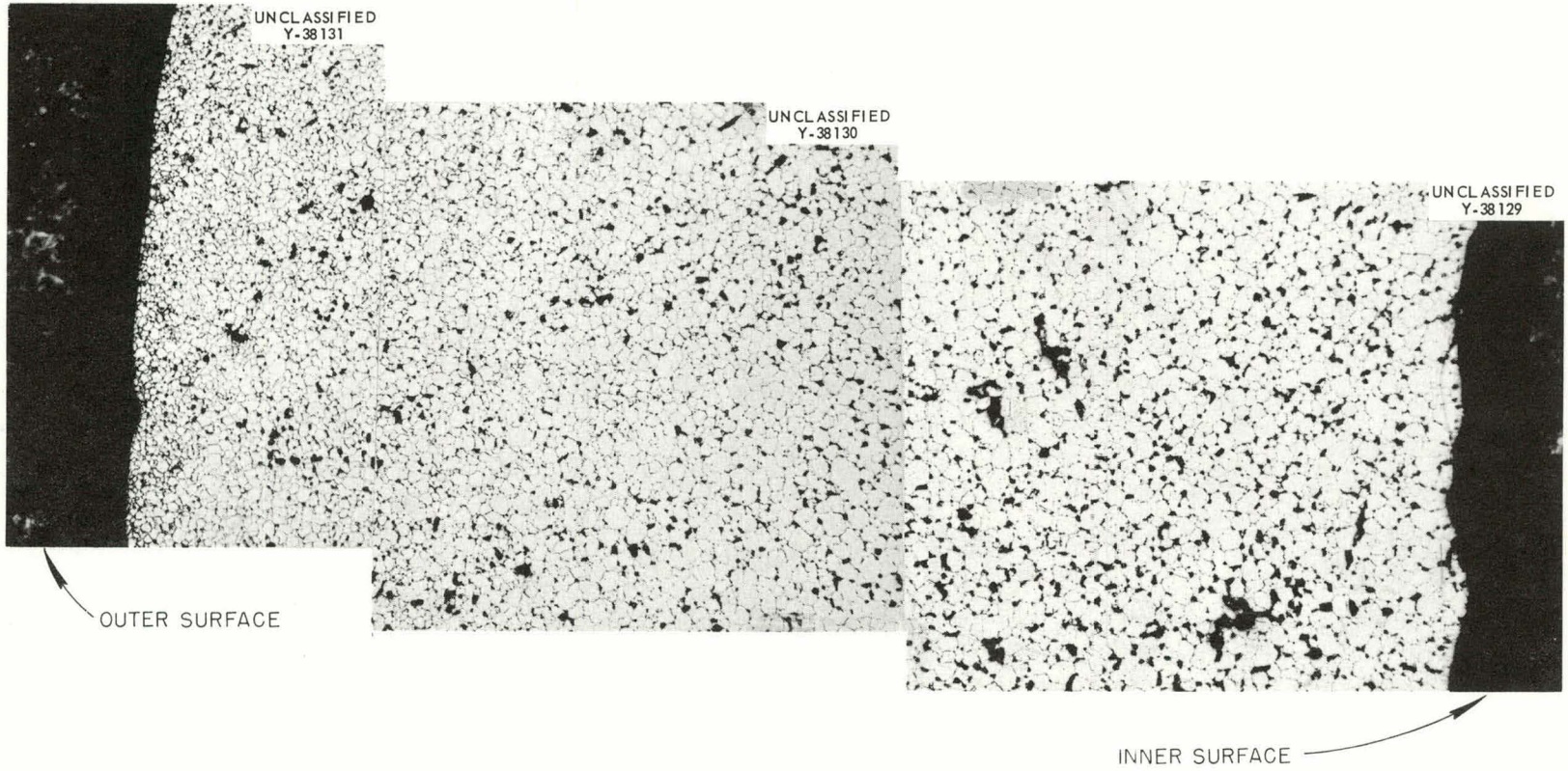

Fig. 6.4. Transverse Section of a Hollow UO_2 Pellet from Section b of LITR-Irradiated Capsule L-11. Etched. 250X

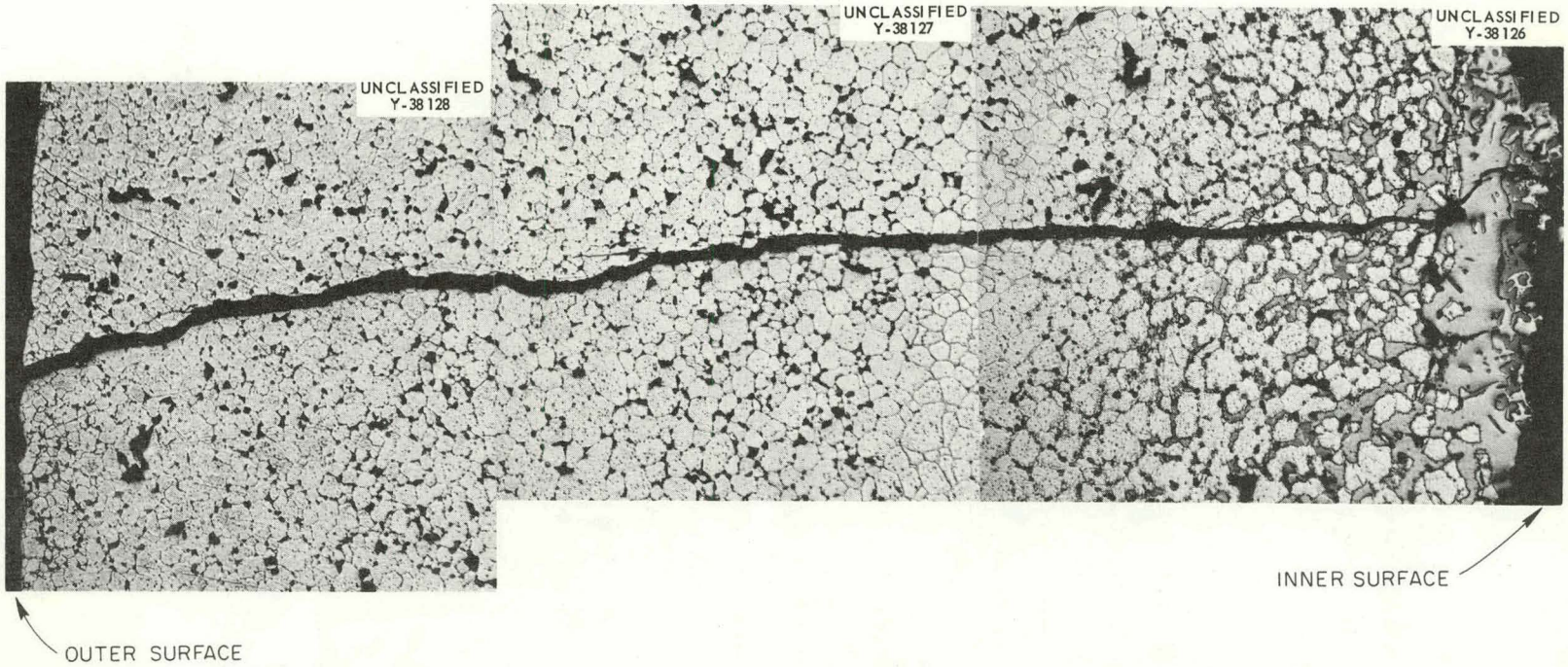

Fig. 6.5. Transverse Section of Unusual Area of a Hollow UO_2 Pellet from the b Section of LITR-Irradiated Capsule L-11. The tantalum thermoccuple sheath apparently reacted with the UO_2 at the inner surface. Etched. 250X

longer resembled the control. Typical areas from the a and b sections are shown in Fig. 6.6. Since failure of the seals allowed air to penetrate both sections of this capsule, the higher temperatures in the lower end (b section) probably account for the difference in the structure in the fuels from the two sections.

Capsule L-24. A piece of fuel from section a of capsule L-24 that had adhered to the depleted UO_2 insulator was selected as the representative sample. The average central temperature of this section at the start of irradiation was estimated to be approximately 2550°F. Adherence of the fuel to the insulator appears to have been a result of the migration of a second-phase material from the insulators into the fuel. The second-phase material is evident in Fig. 6.7.

Metallographic examination of a sample from the b section revealed a reaction similar to that which occurred in the b section of capsule L-23. Fission-gas-release experiments and visual inspection of the "as-opened" capsule indicated that a leak occurred in section b during irradiation. The large grains, large spherical porosity, and adherence of the fuel to the UO_2 insulator are shown in Fig. 6.8. The presence of the second phase material is not understood.

Capsule L-25. The average central temperature in the b section of capsule L-25 at the start of irradiation was estimated to be approximately 2300°F. A transverse section through the UO_2 insulator, UO_2 fuel pellet, tantalum thermocouple sheath, and BeO thermocouple insulator is shown in Fig. 6.9. Little or no difference in grain size was detected between the irradiated sample and the control material. There was some void agglomeration between grains in the irradiated fuel. A region at the outer surface of the fuel was practically devoid of porosity within the grains. This same region was separated from the remainder of the fuel pellet by a crack around the circumference of the pellet. The inner region of the fuel exhibited fine porosity within the grains. Evidence of a reaction was present in the outer half of the tantalum sheathing of the internal thermocouple.

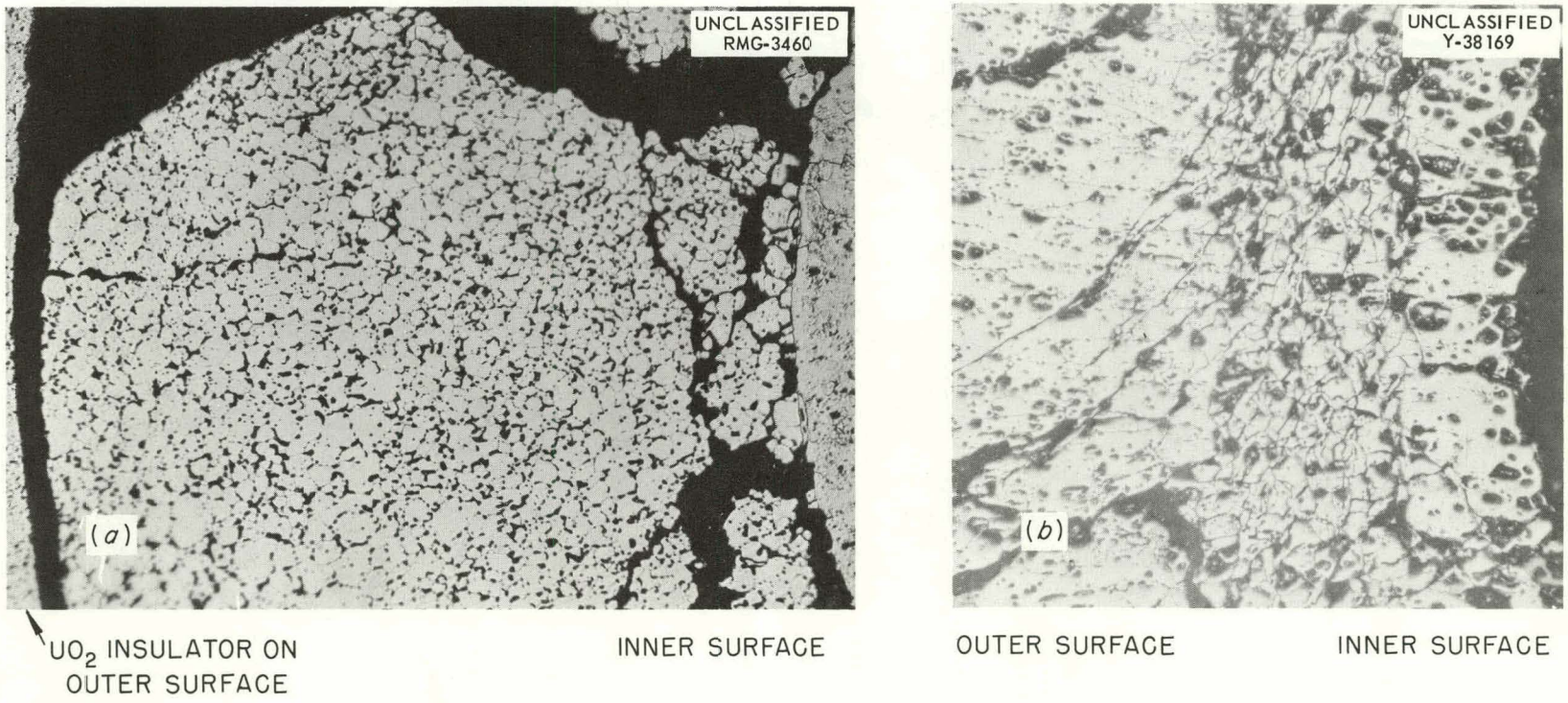

Fig. 6.6. Typical Microstructures of Hollow UO_2 Pellets from LITR-Irradiated Capsule L-23. (a) Pellet from a section. (b) Pellet from b section. Etched. 100X

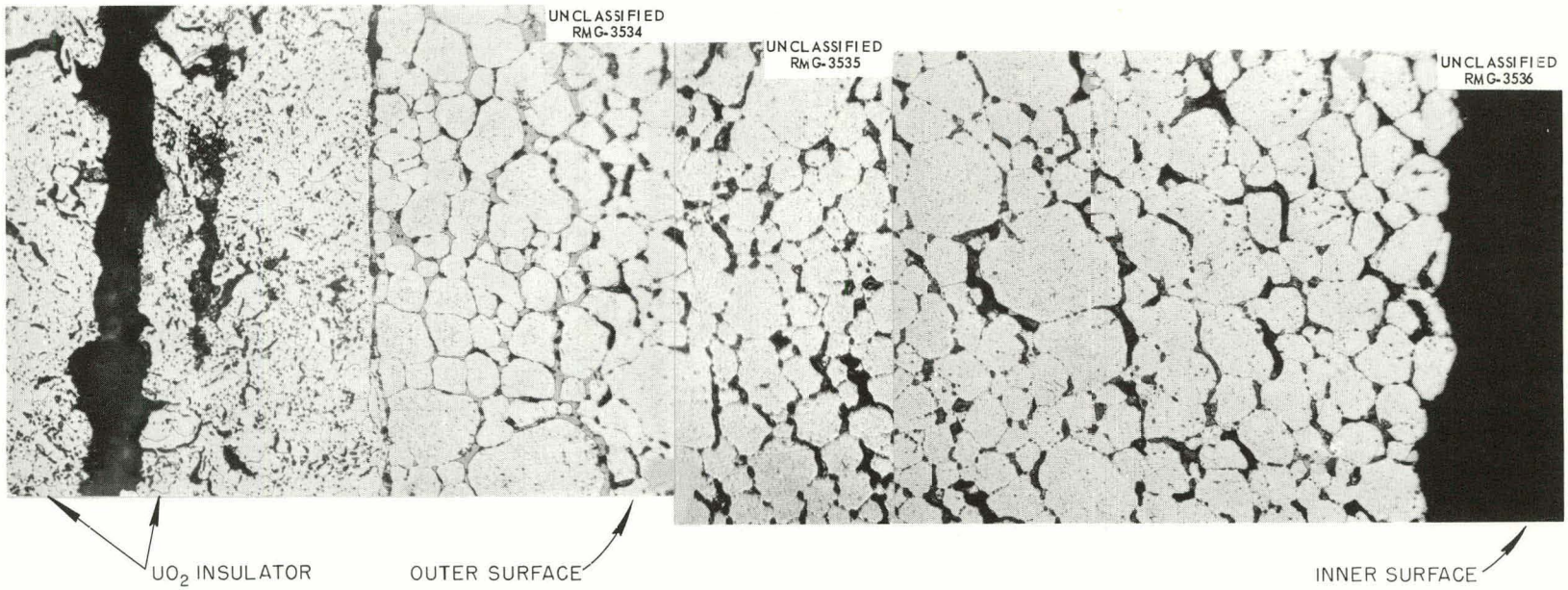

Fig. 6.7. Transverse Section of UO_2 Fuel Pellet and Insulator from a Section of LITR-Irradiated Capsule L-24. Etched. 250X

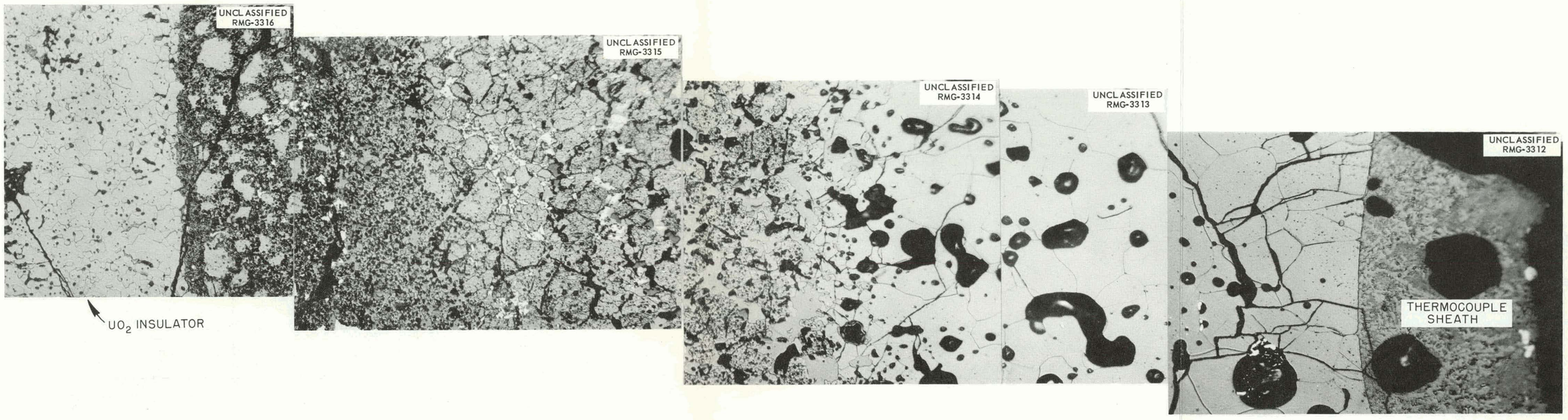

Fig. 6.8. Transverse Section of UO_2 Fuel Pellet and Insulator from b Section of LITR-Irradiated Capsule L-24. Etched. 250X

Fig. 6.9. Transverse Section Through the b Section of LITR-Irradiated Capsule L-25. Etched. 100X

Capsule L-27. The central temperatures at the start of irradiation of the a and b sections of capsule L-27 were estimated to be approximately 2000 to 2400°F, respectively. The bottom UO_2 fuel pellet from the a section was selected for metallographic examination. This pellet had not been in contact with the tantalum sheathing on the internal thermocouple and was not damaged to a great extent, as were the upper three pellets. The cross section revealed normal UO_2 fuel, with no evidence of a reaction at either the inner or outer surfaces. Most of the porosity was intergranular, and there was no evidence of grain growth. The top three fuel pellets, which showed evidence of having reacted with the internal thermocouples, were highly fractured, and no suitable sample for mounting for metallographic examination was available.

A UO_2 fuel pellet from the b section which remained intact was also examined. The fuel material did not appear to have undergone significant changes during irradiation. A large amount of intergranular porosity was noted that would seem to indicate a density of less than the measured 95% of theoretical.

Capsule L-28. The central temperatures at the start of irradiation of the a and b sections of capsule L-28 were estimated to be approximately 2200 and 3450°F. A portion of a pellet was selected from the center of the a section for the metallographic specimen. Comparison with the unirradiated control revealed little or no difference in the size of the grains and the amount of porosity.

A transverse section through the UO_2 insulator, UO_2 fuel, and thermocouple region was made at approximately the center of the b section (Fig. 6.10). A reaction of the UO_2 fuel with the tantalum sheath of the thermocouple was evident. The fuel was very porous and the grains were columnar. The columnar grains of the fuel extended into the UO_2 insulator. The second phase material noted in capsule L-24 was not seen.

Capsule L-32. The estimated central temperature at the start of irradiation of the b section of capsule L-32 was 3100°F. No a section central temperature was obtained because of failure of the thermocouple at startup. Very little difference was noted in the microstructures of

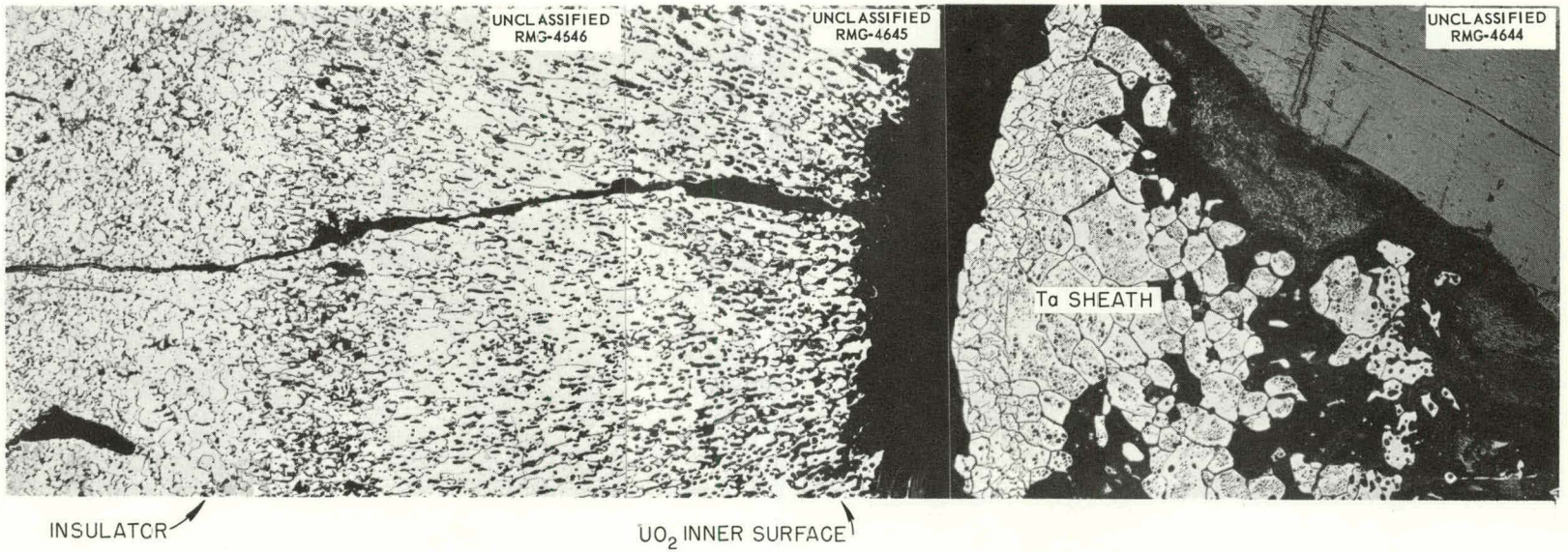

Fig. 6.10. Transverse Section Through the b Section of LITR-Irradiated Capsule L-28. Etched. 100X

the fuel specimens from the a section and the unirradiated control, except for extensive microfracturing in the irradiated sample. A typical area is shown in Fig. 6.11. Considerable difference was noted, however, between the microstructures of the fuel specimens from the b section (Fig. 6.12) and the a section. The grains of the b section fuel were of an irregular shape, and the fuel was quite porous, particularly in the region of radial cracks.

Conclusions. There appears to be no direct correlation of grain size increase and the integrity of the UO_2 fuel with irradiation temperature in the six model 3 LITR-irradiated capsules examined. This probably can be attributed to at least two things. First, the metallographic samples were not representative of fuel irradiated at the estimated temperatures either because of leaks in the capsules or reactions of the UO_2 with the tantalum thermocouple sheaths; and, second, there is some doubt that the recorded temperatures were accurate because of thermocouple drift.

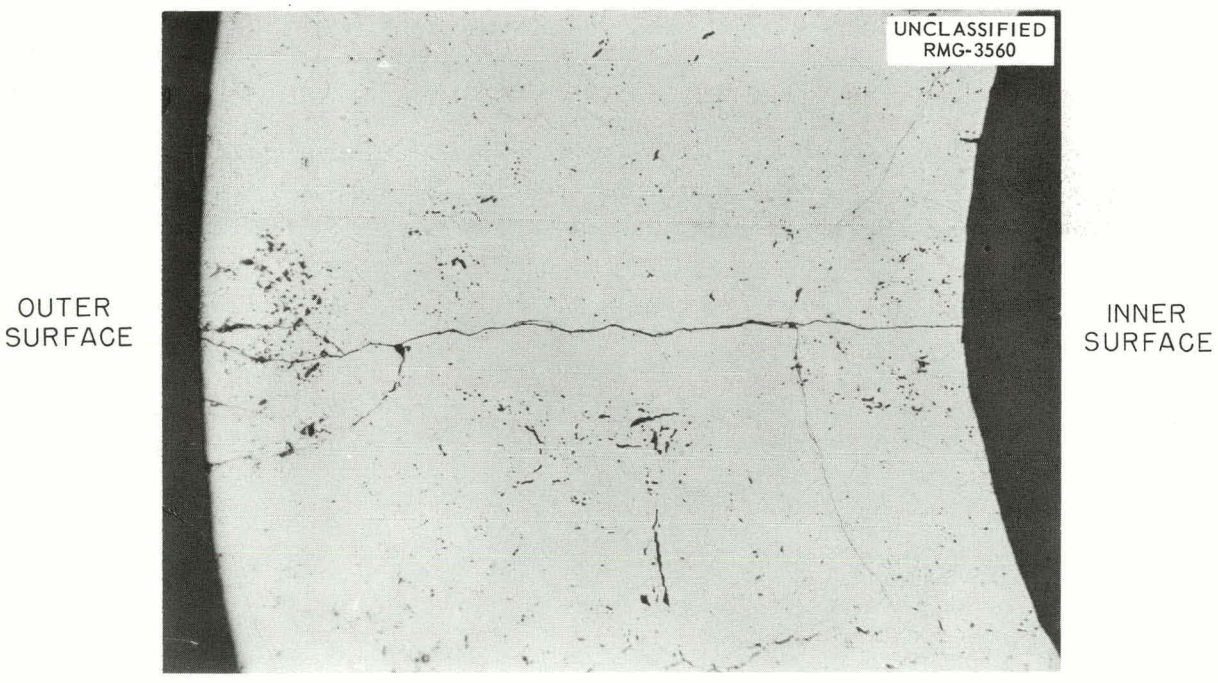

Fig. 6.11. Transverse Section of UO_2 Fuel Pellet from a Section of LITR-Irradiated Capsule L-32. Etched. 100X

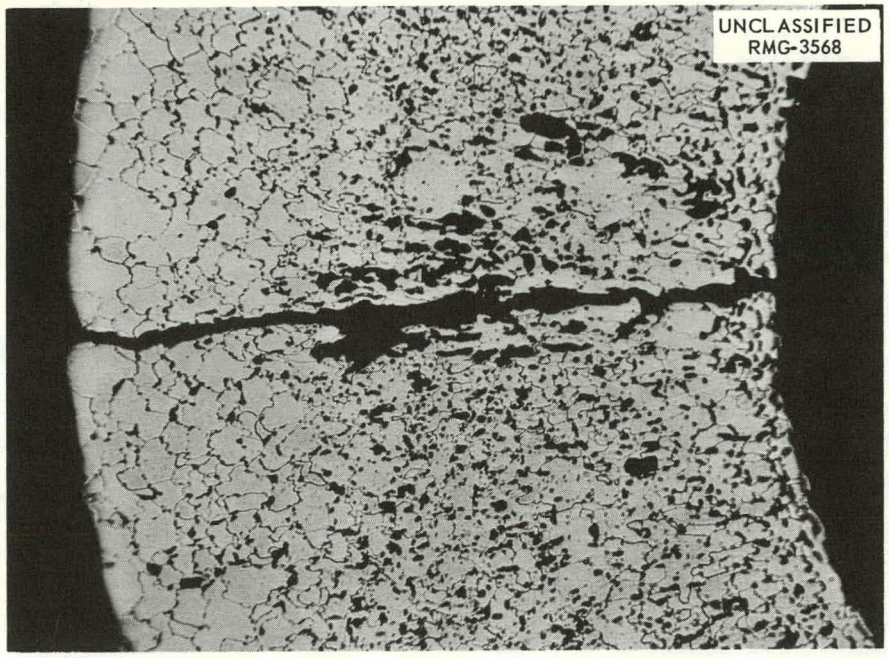

Fig. 6.12. Transverse Section of UO_2 Fuel Pellet from b Section of LITR-Irradiated Capsule L-32. Etched. 100X

Brittle Fracture of Irradiated Structural Metals

R. G. Berggren M. S. Wechsler

A critical point in large welded structures is the metallurgical condition of the weld metal and the heat-affected zone adjacent to the weld. It is possible to study the properties of the heat-affected zone by making use of a technique developed at Rensselaer Polytechnic Institute in which samples are subjected to the same thermal treatment as would be the case during welding. Preliminary results are presented here of an investigation of the effect of radiation on the notch ductility of such simulated heat-affected-zone samples.[5] The unaffected parent plate material was also studied. The material chosen corresponds to the steel used for the pressure vessels of many nuclear power reactors, including the EGCR, the EBWR, and various maritime and military reactors.

[5]This investigation was initiated by P. Patriarca, ORNL, who arranged for the preparation of the heat-affected-zone samples at Rensselaer Polytechnic Institute.

Charpy V-notch impact specimens were prepared from a 4-in. plate of ASTM A212, grade B, carbon-silicon steel. The steel was from an aluminum-treated heat produced according to ASTM Specification A-300 for fine-grain practice. The chemical analysis was: C, 0.25%; Mn, 0.74%; P, 0.013%; S, 0.025%; Si, 0.20%. The plate was normalized at 1625 to 1675°F, cooled with a water spray to 500°F, and stress-relieved at 1200 to 1250°F. One group of samples machined from the plate was characteristic of the parent base plate. Two additional groups of samples, prepared at Rensselaer Polytechnic Institute,[6] were synthetic weld-heat-affected material made under conditions corresponding to energy inputs of 100 000 joules/in. (2B series) and 50 000 joules/in. (4B series). Additional information concerning the pre-treatment of the samples is given in Table 6.6.

Table 6.6. Simulated Weld Thermal Cycles and Related Properties

	Series 2B Samples	Series 4B Samples	Parent-Plate Samples
Energy input in 1-in. plate, joules/in.	100 000	50 000	As received
Peak temperature, °F	2400	2400	
Initial plate temperature, °F	80	80	
Treatment after heating			
Temperature, °F	1150	1150	
Time, hr	4	4	
Cooling rate, °F/sec			
At 1000°F	13.6	43.8	
At 1300°F	31.9	83.4	
Hardness, VPN	229	280	164
Fracture transition temperature, °F			
10 ft-lb criterion	90	−35	−22
15-mil expansion criterion	125	4	−7
50% shear fracture criterion	210	25	70

[6]E. F. Nippes, W. F. Savage, and W. A. Brown, Progress Report No. 2, Study of the Weld Heat Affected Zone of A-212B Steel, Rensselaer Polytechnic Institute, February 1961.

The Charpy V-notch impact curves for the unirradiated heat-affected-zone samples and the parent-plate samples shown in Figs. 6.13 and 6.14 are quite consistent with the results of Nippes, Savage, and Brown.[6] It is of interest that the initial transition temperature was higher for the 2B series than for the 4B series (Fig. 6.13). Metallographic examination of the parent plate showed uniformly distributed regions of ferrite and fine pearlite. The synthetic heat-affected zones appeared to be tempered bainite or tempered martensite and proeutectoid ferrite at prior austenite grain boundaries. The major microstructural difference in the synthetic heat-affected zones appeared to be in the ferrite network. This network was discontinuous in the 4B series (50 000 joules/in.) and continuous in the

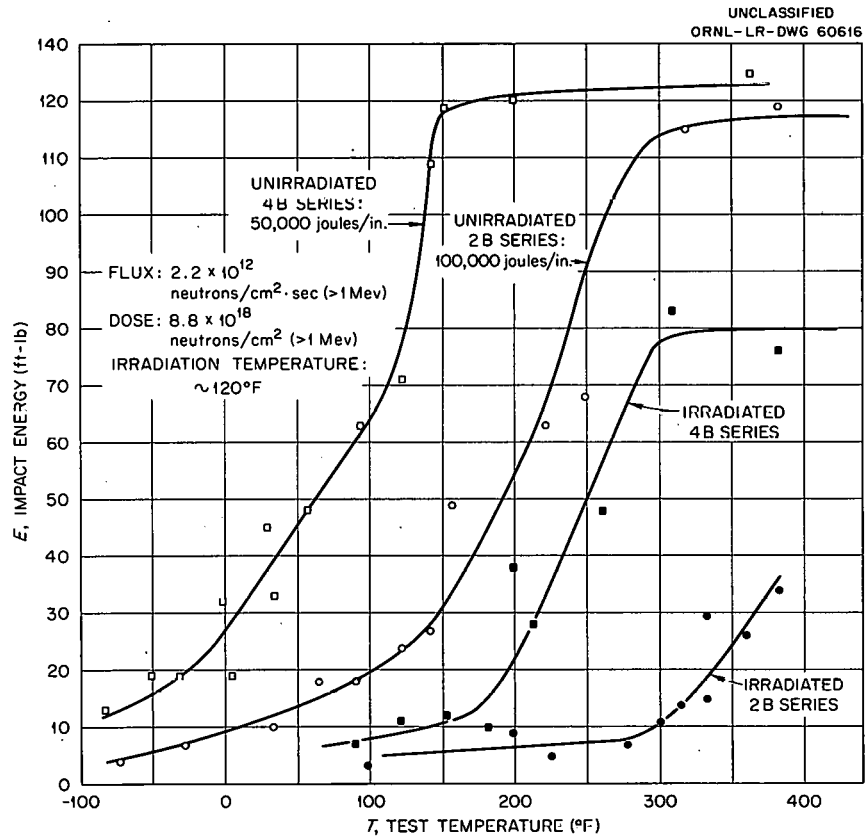

Fig. 6.13. Charpy V-Notch Impact Tests of Irradiated, Synthetic, Heat-Affected Zones in ASTM A212, Grade B, Steel (Item 147).

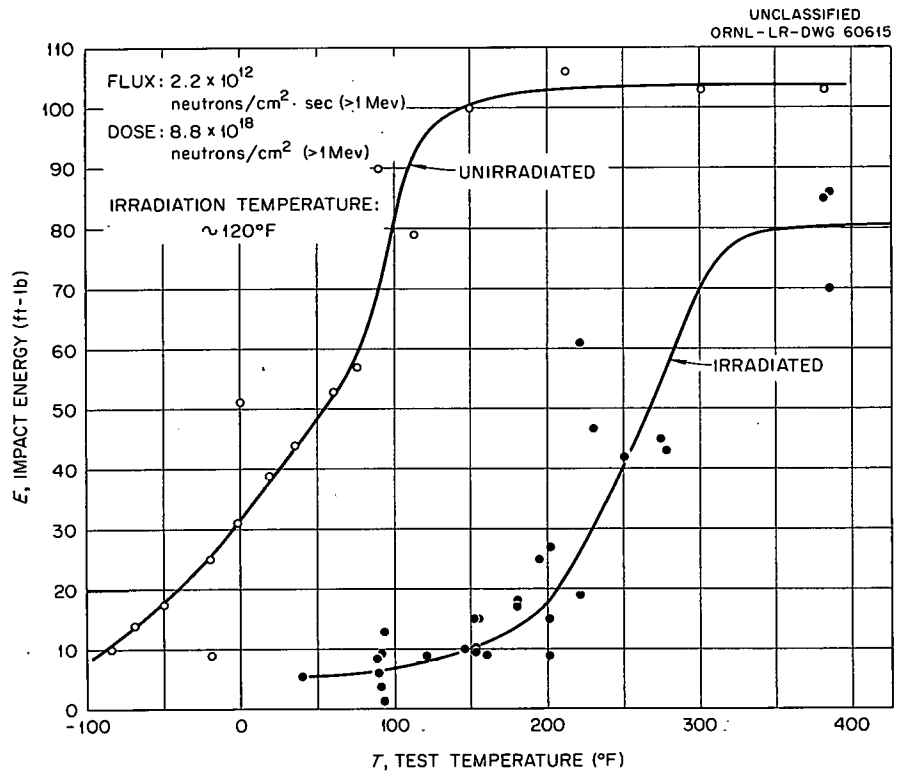

Fig. 6.14. Charpy V-Notch Impact Tests of Irradiated ASTM A212, Grade B, Steel Base Plate (Item 147).

2B series (100 000 joules/in.). Apparently this continuous ferrite network contributed to the higher initial notch-impact transition temperature of the 2B series.

The two types of synthetic weld-heat-affected-zone samples and the parent-plate samples were irradiated in the ORR pool-side facility for 1106 hr at 90 to 130°F to doses of 6 to 10 × 10^{18} neutrons/cm^2 (>1 Mev). The effects of the irradiation on the Charpy V-notch impact strengths for the three material conditions are presented in Figs. 6.13 and 6.14. A summary of the results on the basis of three transition temperature criteria are given in Table 6.7. The radiation-induced increases in transition temperature in these three materials are about equal and are nearly the same as for a variety of steels investigated by the Naval Research Laboratory[7]

[7]L. E. Steele and J. R. Hawthorne, Effect of Irradiation Temperature on Neutron-Induced Changes in Notch Ductility of Pressure Vessel Steels, ONRL Report 5629, June 28, 1961.

Table 6.7. The Effect of Neutron Irradiation at 90 to 130°F on Fracture Transition Temperature of ASTM A212, Grade B, Steel

Neutron dose: 6 to 10 × 10^{18} neutrons/cm^2 (>1 Mev)

Material	Transition Temperature (°F)		
	10 ft-lb Criterion	30 ft-lb Criterion	50% of Ductile Energy Criterion
Series 2B (100 000 joules/in.)			
Unirradiated	20	150	200
Irradiated	295	365	>400
Increase	275	215	>200
Series 4B (50 000 joules/in.)			
Unirradiated	−100	10	90
Irradiated	140	215	270
Increase	240	205	180
Parent plate			
Unirradiated	−80	−5	60
Irradiated	150	230	270
Increase	230	235	210

and the Oak Ridge National Laboratory.[8] A number of determinations remain to be made on the samples irradiated in this experiment. It is planned to measure the lateral contraction and expansion of the fractured samples and to determine their fracture appearance. Also, the microstructure of the irradiated samples will be examined metallographically. Finally, a number of samples from this irradiation experiment will be given a post-irradiation recovery treatment before testing, in order to determine the manner and extent of the annealing of the radiation effects.

Instantaneous Fission-Gas-Release Experiments

R. M. Carroll

The thin-plate samples of UO_2 sandwiched between ThO_2 plates that were used in the LITR instantaneous fission-gas-release experiments have

[8]R. G. Berggren, Radiation Effects in Ferritic Steel, p. 91–127 in Status of Radiation Effects Research on Structural Materials and the Implications to Reactor Design, TID-7588, October 1960.

been removed and examined. The oxygen-to-uranium ratio of the samples increased during irradiation from 2.002 to 2.66, which is the composition of U_3O_8. This in-pile oxidation almost certainly caused the fission-gas-release rate to slowly increase, as reported previously.[9] The sample had a flaky, burned appearance, and the increase in surface area as oxidation progressed was probably the primary cause of the increased fission-gas release.

Since the fuel was nonstoichiometric, the cooling bursts[9] may have been due to a phase change of the higher oxide states of the UO_{2+}. Cooling bursts have also been reported[10] for substoichiometric samples of UO_{2-}. A phase change of nonstoichiometric UO_2 during the cooling process appears to be the best explanation for the cooling bursts in both cases. The cooling burst may be an important factor in the total gas release. Rothwell[10] reported that as much as one-third the total gas in a substoichiometric sample was released in a burst while cooling from a temperature that had released comparatively little of the gas.

Another thin-plate sample of UO_2 in the form of 0.58-in.-diam disks, 0.032 in. thick, was installed in the facility. The sample consisted of high-density, small-grain material. It had an initial oxygen-to-uranium ratio of 2.01. In an attempt to prevent in-pile oxidation of the sample, a sweep gas was used that contained 3% hydrogen, with the remainder either argon or helium. When this sweep gas was used on a UO_2 sample that had already been oxidized, the sample crumbled as the UO_{2+} was reduced.[11] A sample which had not already been oxidized should retain its structure in the reducing atmosphere and also should not become oxidized.[12]

The atmosphere selected has apparently been effective in preventing in-pile oxidation of the UO_2 by trace amounts of oxygen in the sweep gas.

---

[9]GCR Quar. Prog. Rep. June 30, 1961, ORNL-3166, p. 153.

[10]E. Rothwell, The Release of Krypton^{85} From Irradiated Uranium Dioxide on Post-Irradiation Annealing, AERE-R-3672.

[11]R. M. Carroll and C. D. Baumann, Experiment on Continuous Release of Fission Gas During Irradiation (An Interim Report), ORNL-3050.

[12]J.A.L. Robertson, concerning the Effects of Excess Oxygen in UO_2 CRFD-973.

This was determined by allowing the sample to operate at constant conditions for one reactor cycle and observing that during this time the emission of Xe^{133}, Xe^{135}, Kr^{85m}, and Kr^{88} remained constant. Since oxidation of the UO_2 results in increased fission-gas release, this constant rate is considered evidence that the UO_2 was not oxidized.

The gamma-ray spectrum of the fission gas released was markedly different from that of fission gas released from UO_2 samples in a nonreducing atmosphere. A comparison of the fractional release rates for four isotopes is given in Table 6.8. Two fuel samples are compared in this table. The first two columns are for the constant condition run in a reducing atmosphere, and the data show that there was no increase in fractional release with time. The next three columns give the fractional release from the thin-plate sample of UO_2 irradiated in a nonreducing atmosphere. They show the increase of fission-gas release after 30, 60, and 90 days of irradiation and that the xenon-to-krypton fractional release did not change as the sample was progressively oxidized. If the ratio of the release of long-lived xenon to the release of short-lived krypton is compared for the two samples, the ratio may be seen to be higher for the oxidized sample. An explanation for this is being sought.

Table 6.8. Comparison of Fission-Gas-Release Rates in Reducing and Nonreducing Atmospheres

Fission Gas	Ratio of Release Rate to Production Rate				
	Reducing Sweep Gas		Inert Sweep Gas		
	June 8	June 29	After 30 Days	After 60 Days	After 90 Days
	$\times 10^{-4}$	$\times 10^{-4}$	$\times 10^{-4}$	$\times 10^{-4}$	$\times 10^{-4}$
Xe^{133}	14	11	17	123	760
Xe^{135}	4	5.2	5.0	40	370
Kr^{85m}	8.8	8.3	2.5	11	98
Kr^{88}	6.5	6.5	1.1	7.5	39

A disadvantage of using a trace-hydrogen atmosphere is that the hydrogen will affect the emf of the Pt vs Pt-Rh thermocouples by reacting with the high-temperature junctions. This reaction is temperature dependent, so the high-temperature thermocouples were affected the most. The thermocouple emf was reduced, but it stabilized quickly at constant temperatures. It was not possible to determine the true temperature of the sample, but the indicated temperature was from 100 to 200°C less than the actual temperature. Also, the thermocouples were embrittled from the hydrogen and failed early in the second reactor cycle. The sample was therefore withdrawn, and no further data were obtained.

A sample of single-crystal UO_2 has been prepared for the next irradiation. This also will be operated in a reducing atmosphere, but some of the thermocouples will be of the metallic-sheath type to protect the junction from the atmosphere.

7. EGCR EXPERIMENTAL FACILITIES

EGCR In-Pile Loops

F. H. Neill

Design Report (C. Michelson)

The preliminary design report for the EGCR in-pile loops was completed. The document summarizes the design of the small helium- or CO_2-cooled loops. These loops, which would utilize the two small (5 1/2-in.-o.d.) vertical through-tubes near the central axis of the EGCR, are designed to operate with helium or CO_2 at experiment powers up to 1500 kw, gas pressures up to 1000 psia, experimental section inlet temperatures up to 950°F, and experimental section outlet temperatures up to 1050°F. Several other documents were also completed in support of the loop design report. These include a compendium of selected preliminary design drawings representative of the various system flowsheets, component designs, piping arrangements, and electrical and instrumentation provisions. A two-volume set of design criteria presents the ground rules and starting basis for the loop design. A two-volume set of design analyses includes most of the design studies and analytical work performed during the establishment of basic design criteria and detailed design. Included are extensive stress analyses of the loop piping and components. A two-volume compendium of specifications includes loop component and material specifications.

Component Design (R. E. Helms, A. W. Culp, W. S. Chmielewski)

Studies were carried out to evaluate the credibility of reactor depressurization for several assumed loop experiments. Designs for catching products of an experiment meltdown in a geometry which would prevent through-tube meltdown and a filter system for rapid processing of the loop coolant and the reactor gas were considered.

Loop Fabrication (W. F. Ferguson)

All ORNL-procured EGCR in-pile loop materials, except 35 ft of 12-in. type 347H stainless steel pipe and the prefabricated process pipe

subassemblies, have been received. An order was placed with Taylor Engineering Company of Detroit, Michigan, for fabrication of the process pipe subassemblies. Delivery is scheduled to start in October 1961 and be completed during February 1962.

The experimental loop nozzle tees, which provide loop access through the pressure vessel, are being fabricated by Baldwin-Lima-Hamilton Corporation of Philadelphia, Pennsylvania. Essentially all machining of bottom tee subcomponents has been completed. Assembly and welding of subcomponents are scheduled to start during the week of September 5. Machining of subcomponents for the top tees is in progress.

Hydrogen-Cooled Loop Design (A. W. Culp, C. Michelson)

The preliminary design analysis for a hydrogen-cooled in-pile loop for operation in the EGCR is essentially complete. The hydrogen-cooled loop is designed to operate at a pressure of 300 psig and at a power level of 500 kw. Because of the use of complete secondary containment around the primary loop piping, including two in-pile through-tubes, the maximum credible accident in the case of the hydrogen-cooled loop will not leak reactor gas into the cell and there will not be over-pressurization of the cell accompanied by subsequent release of the gas to the reactor containment vessel. The maximum credible accident in the case of the hydrogen-cooled loop would simply dump the loop gas, plus the secondary containment gas, into the loop cell. This would raise the cell pressure to approximately 6 psig.

The problems of handling hydrogen as a coolant are not as formidable as first predicted. The loop would contain a maximum of 4 lb of loop gas. A mixture of this small quantity of gas with the cell atmosphere would give a hydrogen concentration well below the limits of combustion. Further, it is proposed to dilute the original cell atmosphere with CO_2 to a CO_2 concentration of 80%. Such an atmosphere would not form an explosive mixture with hydrogen, regardless of the hydrogen concentration. Fans mounted in the cell would ensure good mixing of the cell atmosphere and any hydrogen gas leakage. Once the gases were thoroughly mixed, they would not stratify, even though the fans subsequently stopped operating. This means that release

of the hydrogen to the cell could not form a flammable mixture and, likewise, subsequent release of the cell gas to the containment vessel could not form a flammable mixture. The cell would be kept at a positive pressure of 1 psig to prevent leakage of air into the cell and to assure secondary containment at all times.

The secondary containment system around the primary loop piping external to the cell would be pressurized with helium to 400 psig. Circulation of this gas might be required to prevent excessive temperatures of the inner in-pile through-tube as a result of gamma heating.

Because of the lower power level of the hydrogen loop, with respect of the other in-pile loops (500 kw instead of 1500 kw), the loop heater and cooler would be considerably smaller. The heater would be approximately 40% as long as those used in the helium-CO_2 loops, and the power transformer would have a commensurably lower rating. The cooler would be similar in design and operation to those used in the helium-CO_2 loops, except that it would only require 13 boiler tubes instead of 38.

The hydrogen loop offgas system would be similar to that for the helium-CO_2 system, except that provision would be made for oxidizing the hydrogen and condensing the steam before exhausting the noncondensibles up the stack. This would prevent inadvertent release of pure hydrogen to the ventilation system. The hydrogen would be reduced over a bed of copper oxide.

Through-Tube Orifice Development Tests

F. A. Flint

Pressure drop tests have been performed on six orifice plate configurations with air at 15 psia and 80°F over a flow rate range of 0 to 400 lb/hr, which is equivalent to a helium flow rate range of 0 to 670 lb/hr at reactor operating conditions. The orifice plate configurations, air flow rates, pressure drops, and corresponding predicted helium flow rates and pressure drops were reported previously.[1] Orifice plate No. 4 has been

[1]GCR Quar. Prog. Rep. June 30, 1961, ORNL-3166, p. 202.

tested for pressure drop in helium at reactor operating conditions. The results are given in Table 7.1. Further analytical and test work is under way to reduce the error in predicting the pressure drop across the orifice plate in helium at reactor operating condition based on the pressure drop measured in air at 80°F and 15 psia. A report is being prepared which will summarize the results of these tests.

Table 7.1. Results of Pressure Drop Tests of Orifice Plate No. 4

Number of scallops: 8
Scallop diameter: 0.25 in.
Flow area: 0.29 in.^{2}

Helium Flow Rate (lb/hr)	Helium Pressure Drop (in. Hg)		Error in Predicted Value (%)
	Predicted	Measured	
330	3.70	3.30	12
385	5.15	4.35	18
460	7.50	6.10	23

Through-Tube Bearing Tests

R. E. MacPherson A. M. Smith

Four additional cycling tests have been completed in the through-tube bearing test facility. Two tests were conducted with Linde Flame Plate LW-IN30 and two with Stellite No. 12 as the bearing material on both the sleeve that simulated the reactor tee section and the block that simulated the through-tube. As in the previous test,[2] the surfaces were maintained at 950 ± 25°F during thermal cycling, and loading was applied to simulate the thrust and bending loads existing in the reactor application.

[2]Ibid., p. 198.

Test No. 3 with Linde Flame Plate as the bearing material was terminated after 1000 cycles and an additional 170-hr period at temperature with the parts exposed to a static load. No galling or self-welding was evident during the test, but examination of the specimens after removal from the test stand revealed a wear pattern which indicated that contact between the parts had not been properly maintained. Further investigation showed that the weight clevis used to transmit the external load through the housing to the sleeve and block had been resting on the housing through a portion of the cycle. At best, only two-thirds of the load had been applied to the test pieces.

After alterations to the test rig to prevent the possibility of future binding or bottoming of parts, the test bearing was reassembled using a block and a sleeve coated with Stellite No. 12. The test (No. 4) of this bearing was terminated after 680 cycles, and the parts were examined. Some galling, as shown in Figs. 7.1 and 7.2, was again noted; however,

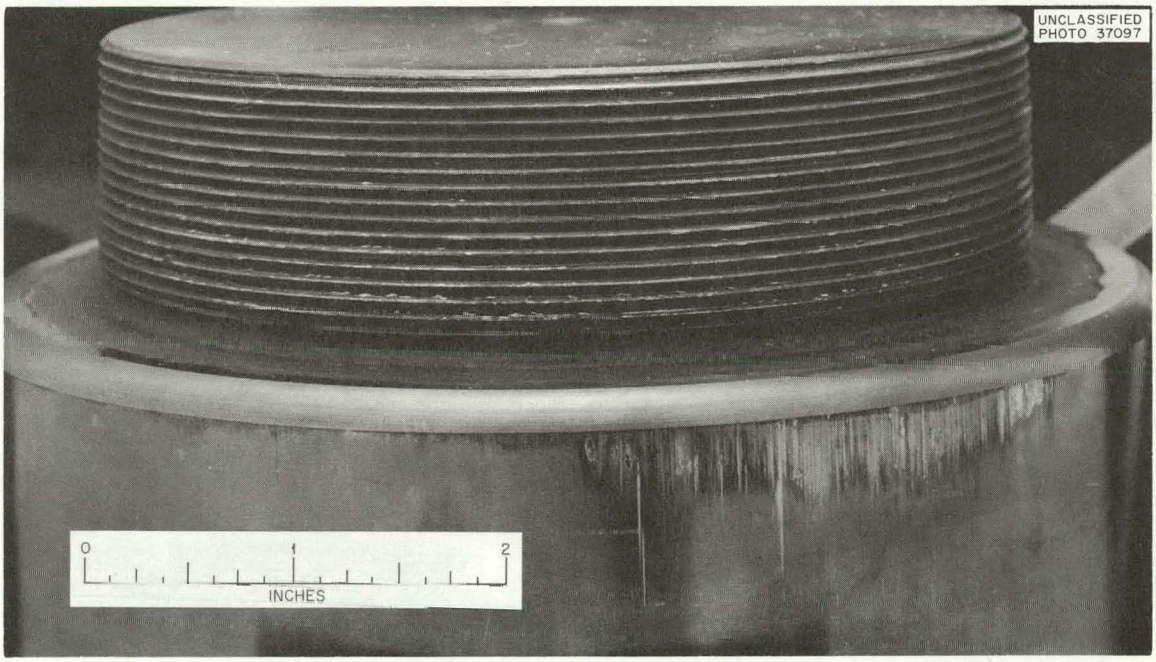

Fig. 7.1. Simulated Through-Tube Bearing of Stellite No. 12 After 680 Load Cycles with the Surface Maintained at 950°F.

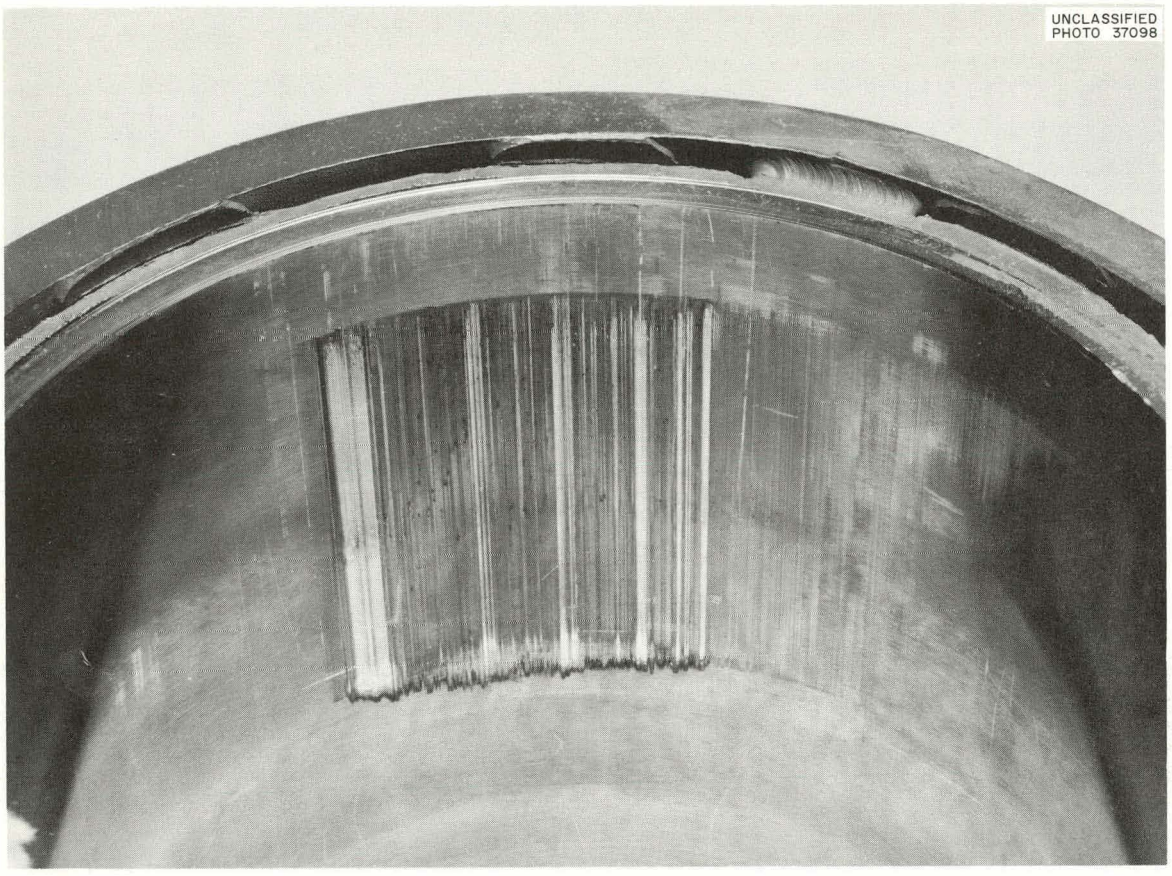

Fig. 7.2. Simulated Through-Tube Bearing Tee Section of Stellite No. 12 After 680 Load Cycles with the Surfaces Maintained at 950°F.

the abrasion was considerably less than that which occurred with Stellite No. 6.

The reworked parts coated with Linde Flame Plate LW-IN30 were then installed in the test facility in preparation for test No. 5. After 352 cycles at load and temperature, the test was terminated because of binding of the parts during cycling. As shown in Figs. 7.3 and 7.4, gross galling and flaking of the Flame Plate had occurred on both the sleeve and block.

Further testing of Stellite No. 12 is now in progress in test No. 6. Cycling of parts for 1025 cycles has been completed, and the parts are being subjected to a long-term static load to check for self-welding.

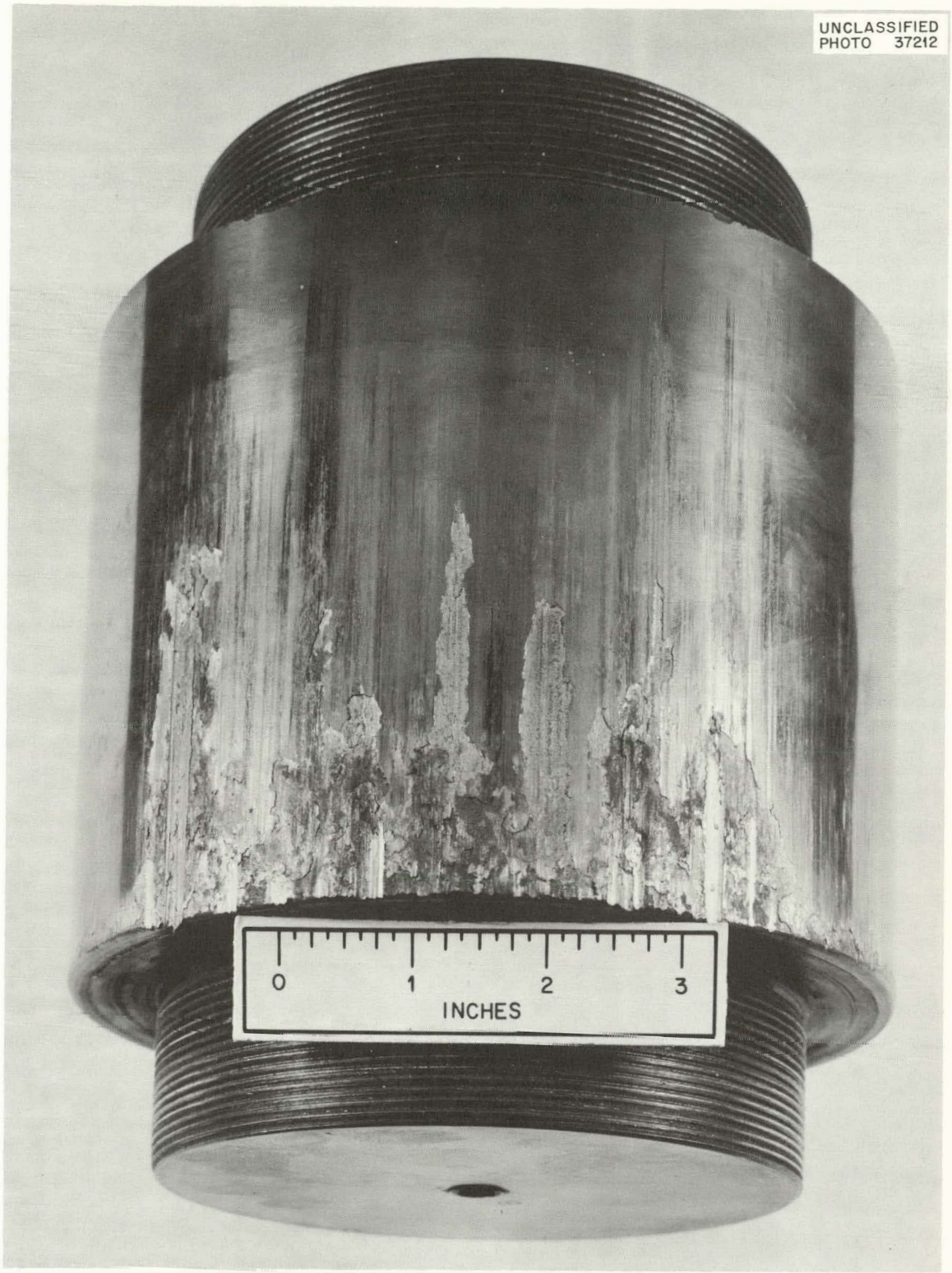

Fig. 7.3. Simulated Through-Tube Bearing of Linde Flame Plate LW-IN30 After 350 Load Cycles with the Surface Maintained at 950°F.

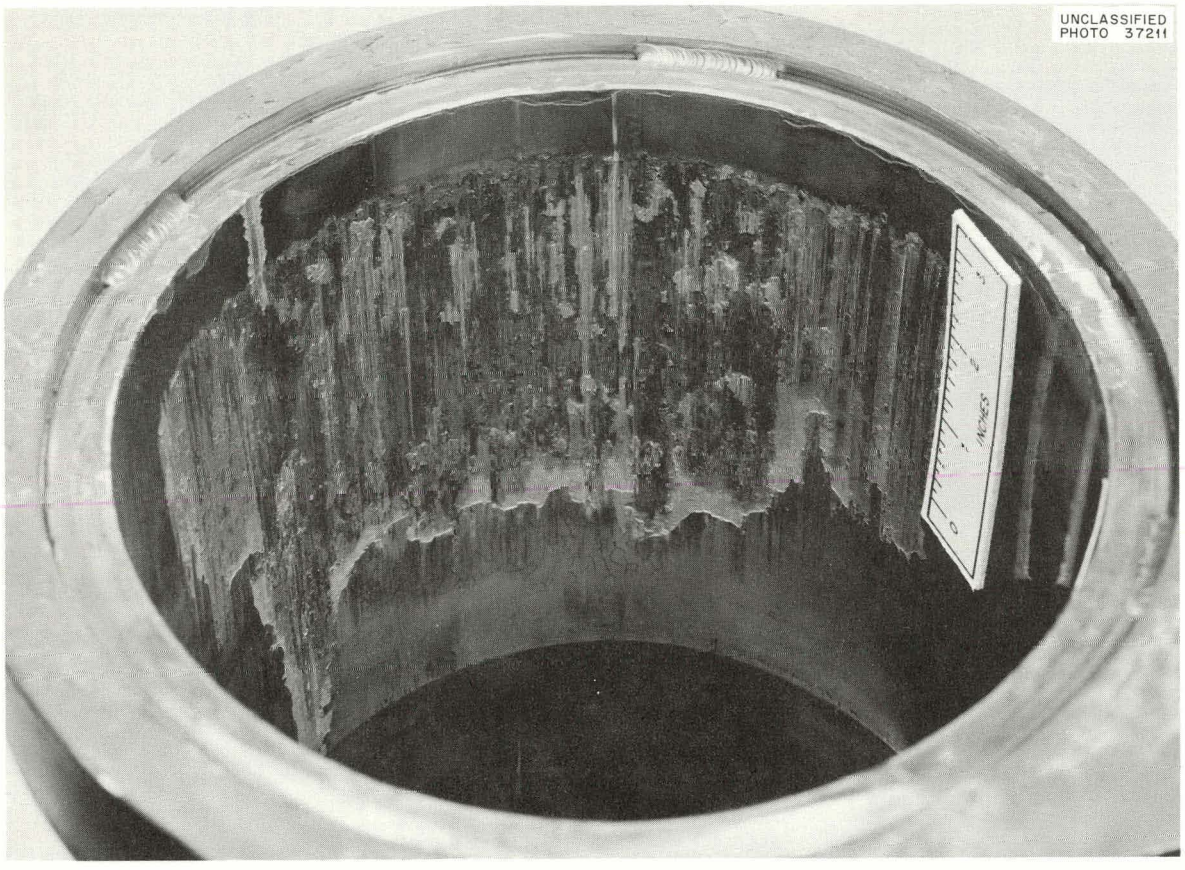

Fig. 7.4. Simulated Through-Tube Bearing Tee Section of Linde Flame Plate LW-IN30 After 350 Load Cycles with the Surfaces Maintained at 950°F.

Valve Tests

J. C. Amos

A 6-in. hermetically sealed gate valve, which was manufactured by Darling Valve & Manufacturing Company and described previously,[3] was prepared for high-pressure elevated-temperature tests by welding caps to the upstream and downstream nozzles. The body of this valve is a type 347 stainless steel casting. The machined portions of the weld necks were dye-penetrant inspected prior to welding, and no dye indications were observed. Numerous defects were detected, however, by dye penetrant

[3]GCR Quar. Prog. Rep. June 30, 1961, ORNL-3166, p. 196.

inspection of the heat-affected zone of the valve body casting during the course of welding. Although extensive weld repair was performed, the welds were accepted for test purposes with minor defects remaining. X-rays of both welds were acceptable in accordance with ASME Boiler and Pressure Vessel Code requirements. The repeated appearance of dye indications in the heat-affected zone of castings is consistent with previous welding experience.

A room-temperature mass-spectrometer leak check to verify the integrity of the over-all valve hermetic seal disclosed a leak in a seal weld between the valve body and the valve bonnet. This leak was repaired, and a second mass-spectrometer leak test demonstrated complete leaktightness of the valve at room temperature. During initial room-temperature seat-leakage tests, it was observed that, if upstream pressure were reduced to atmospheric pressure from 800 psig or above, the gate would jam in the closed position because of pressure trapped between the upstream and downstream gate disks. It was determined by installing a pressure tap and relief port in the valve bonnet that gate jamming could be eliminated by equalizing the upstream and bonnet pressure. This could be accomplished in future valve designs by adding a pressure-equalizing port in the upstream gate disk. Several valve-motor starter relays failed under jammed valve conditions, indicating that the relays provided did not have a sufficient contact rating to interrupt blocked rotor current to the drive motor. During room-temperature tests it was noted that a power interruption to the valve control panel resulted in erroneous counts registering on the electric counters provided for position indication and valve travel limit control. This is an undesirable feature which would result in loss of correct position indication in the event of a power system interruption. A room-temperature seat leakage test of this valve with 1000-psig upstream pressure gave a helium leakage rate of 7.6×10^{-3} cm^3 (STP)/sec. The valve is currently being installed in an electric furnace where thermal cycling and open-close cycling tests at elevated temperatures will be performed.

A 1-in.-IPS hermetically sealed harmonic-drive globe valve furnished for test and evaluation by United Shoe Machinery Corporation on a no-charge

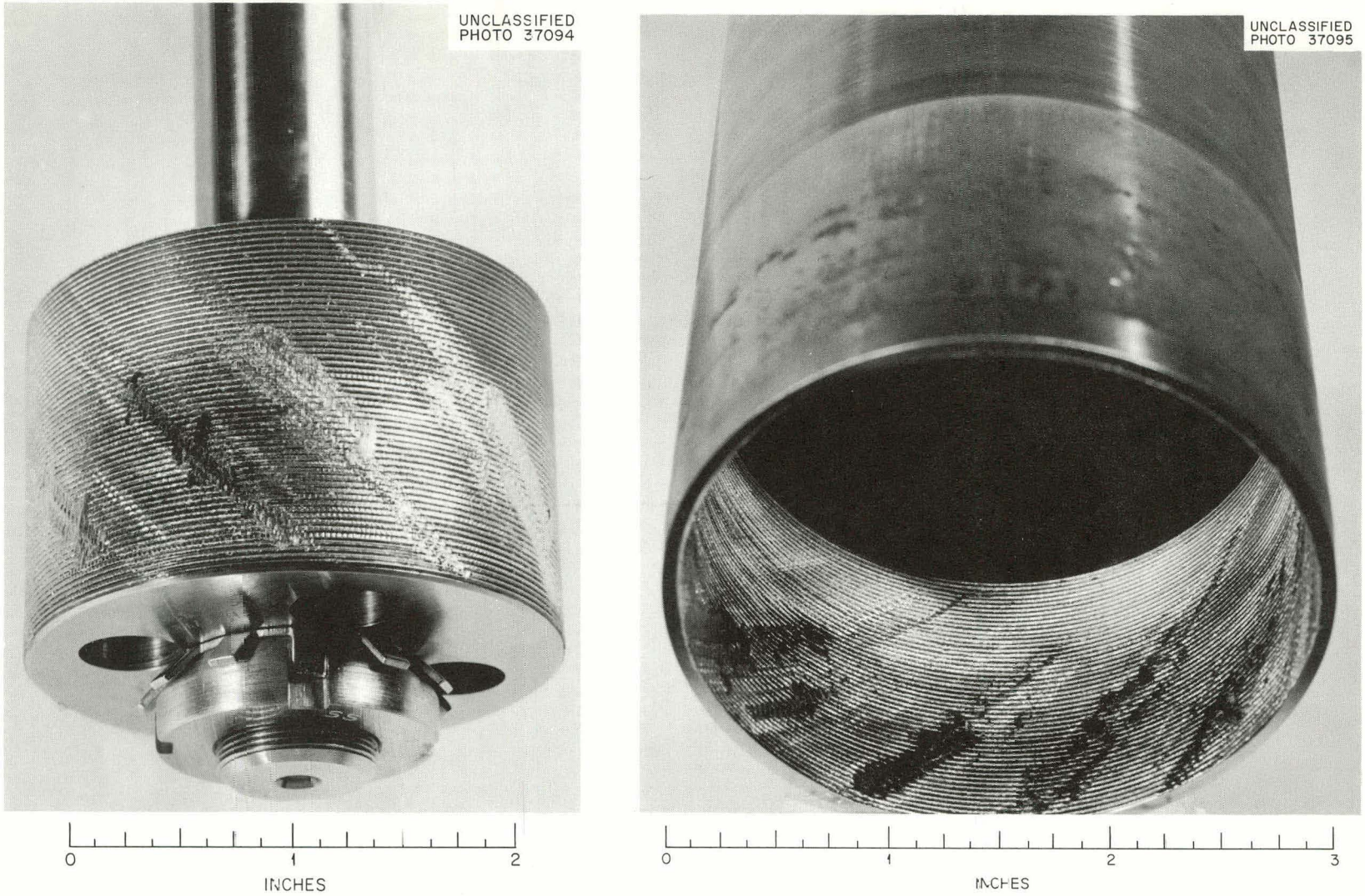

Fig. 7.5. Condition of Lead Screw and Flex Nut for Harmonic Drive Mechanism of 1-in.-IPS Globe Valve Manufactured by United Shoe Machinery Corporation After 2288 Open-Close Cycles.

basis (described previously[3]) has completed 100 thermal cycles between 200 and 1050°F followed by 2288 full open-close cycles with the valve body at 1050°F. A final mass-spectrometer leak test verified the integrity of the hermetic seal at the completion of the test. Initial seat leakage of helium at room temperature and 300 psig was less than 1×10^{-10} cm^3 (STP)/sec. After thermal cycling and 1000 open-close cycles, seat leakage had increased to 5.6 cm^3 (STP)/sec with 1000-psig upstream pressure and the valve body at 1050°F. Valve operation became progressively more difficult during the latter stage of the open-close cycling, and the test was terminated when the required operating torque became excessive. The valve was disassembled under the supervision of a United Shoe Machinery Corporation representative, and damage to internal parts of the harmonic drive mechanism, as shown in Fig. 7.5, was observed. The manufacturer has replaced the two damaged parts, and it is proposed to continue elevated-temperature open-close cycling until ultimate failure of the pressure-containing "flex" tube occurs. Manufacturers' tests have indicated that this tube will withstand in excess of 10 000 open-close cycles. ORNL initial tests have indicated that the valve will operate satisfactorily for 2000 cycles at a body temperature of 1050°F with no adverse effects other than an increase in seat leakage at shutoff conditions.

PAGES 106 to 108

WERE INTENTIONALLY

LEFT BLANK

8. PBRE PHYSICS

R. S. Carlsmith A. M. Perry

Calculations were started for determining the characteristics of a Pebble-Bed Reactor Experiment. The design will be similar in many respects to the one previously outlined by Fraas et al.[1] The principal differences affecting the physics of the system are that the current design will have a core 30 in. in diameter and 48 in. high instead of 18 in. in diameter and 97 in. high and the thermal power level of the current design will be 5 Mw rather than 10 Mw.

In the calculations, the critical core was found to have a composition, expressed as the atomic ratios of carbon to thorium to U^{235}, of 590:1.4:1. Since the reactor is largely reflector moderated, it appears appropriate for structural simplicity to utilize control rods located in the reflector. Two-dimensional, four-group calculations have been made to determine the effectiveness of rods located on a 40-in.-diam circle (with centers 5 in. from the core) in the vicinity of the maximum thermal-neutron flux. With B_4C control rods it was assumed that an approximate evaluation could be obtained with a calculational model in which the rods are black to neutrons of each energy group. The results of these calculations are given in Fig. 8.1 in which control rod effectiveness is plotted as a function of the diameter of the rods and the number of rods inserted the full length of core and reflector. It is believed that the total required effectiveness will be about 0.20 $\delta k/k$, including shutdown margin. On this basis, a tentative selection has been made of four rods, each 3 in. in diameter.

An approximate calculation has also been made of the fast flux in the inner portions of the reflector to aid in the estimation of damage to the graphite. The results are given in Fig. 8.2.

---

[1]A. P. Fraas et al., Preliminary Design of a 10-Mw(t) Pebble-Bed Reactor Experiment, ORNL CF-60-10-63 rev., May 8, 1961.

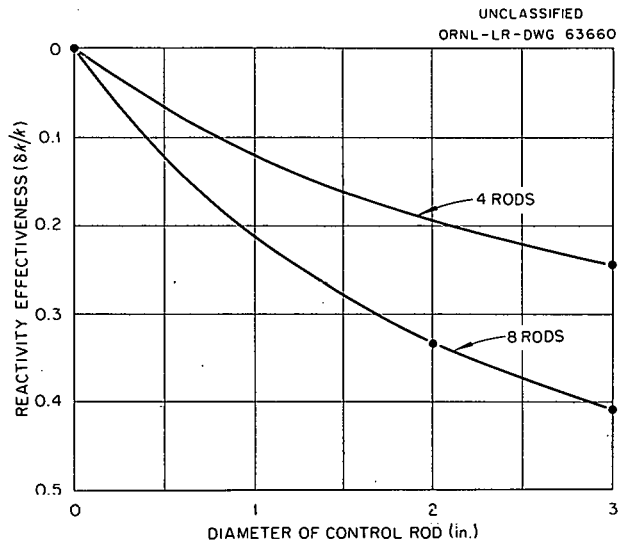

Fig. 8.1. Effectiveness of Block Control Rods Located in the PBRE Reflector on a 40-in.-diam Circle.

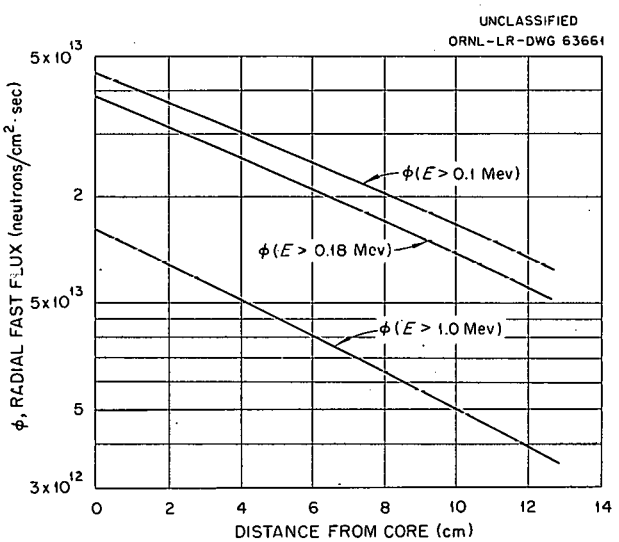

Fig. 8.2. Radial Fast Flux Distribution in PBRE Reflector.

9. PBRE DESIGN STUDIES

Core Design

J. W. Michel G. Samuels

A parametric study for determining the system pressure and core dimensions for a Pebble Bed Reactor Experiment was completed. The heat transfer and pressure drop relations used in the study were the same as reported by Fraas et al.[1] Two basic decisions which most influenced the core configuration were that the flow would be upward and that the pressure drop across the core would not exceed 80% of the weight of the bed, thus eliminating the need to hold the bed down to prevent levitation.

The system pressure was fixed at 500 psia. Although the exact choice of the pressure is rather arbitrary, the hazards problems associated with a relatively slow system loss-of-pressure are not so severe with an operating pressure of 500 psia or less. If a system operating at 500 psia is depressurized to atmospheric conditions, the mass flow of coolant through the core for the design blower speed will be about 2 to 3% of normal and sufficient to remove the afterheat.

The preliminary core design parameters are listed below:

Power Level	
Design power level	5 Mw(t)
Power density	9 w/cm^3 of bed
Core Dimensions and Characteristics	
Diameter of bed	2.5 ft
Height of bed	4.0 ft
Bed void fraction	39%
Bed face area	4.91 ft^2
Bed volume	19.6 ft^3
Bed weight	1305 lb

[1] A. P. Fraas et al., Preliminary Design of a 10-Mw(t) Pebble-Bed Reactor Experiment, ORNL CF-60-10-63 rev., May 8, 1961.

Number of spheres	11 700
Total heat transfer area	574 ft^2
Bed pressure drop	0.82 psi
Rate of temperature rise (no coolant flow)	565°F/min

Fuel Element

Sphere outside diameter	1.5 in.
Average heat flux	29 700 Btu/hr·ft^2
Maximum allowable power density (for 1500-psi stress and k = 8 Btu/hr·°F·ft)	45 w/cm^3 of bed

Coolant Characteristics

Gas	Helium
Pressure	500 psia
Inlet temperature	550°F
Mean outlet temperature	1250°F
Flow rate through core	19 500 lb/hr
Superficial mass velocity	3970 lb/ft^2·hr
Flow rate as percentage of levitation value	79%
Average heat transfer coefficient	200 Btu/hr·ft^2·°F

Reactor Parameters when Operated at Levitation Limit for 700°F Gas Temperature Rise

Power level	6.4 Mw
Power density	11.5 w/cm^3
Flow rate through core	24 700 lb/hr
Superficial mass velocity (based on pressure gradient equal to 87% of bed density using fuel density of 1.7)	5050 lb/ft^2·hr
Bed pressure drop	1.28 psi
Average heat flux	38 000 Btu/hr·ft^2
Rate of temperature rise (no coolant flow)	724°F/min
Average heat transfer coefficient	236 Btu/hr·ft^2·°F

Effect of Irradiation-Induced Stresses in Graphite Bodies on Reflector Design

B. L. Greenstreet W. A. Shaw F. T. Dodge

Graphite is essentially pure carbon, but it is not a specific material in the structural sense. There are differences in orientations of crystallites, the degree of graphitization, homogeneity, particle size, etc., depending upon the manufacturing processes. If the material is extruded, the long directions of the individual particles take a preferred orientation in the direction of extrusion. Thus, there is a difference in properties measured with the grain and against the grain because of the inherent anisotropy of the crystals. This lack of uniformity makes accurate stress analysis of graphite structures difficult. There are additional complications when graphite is used as a structural component in reactors, since under exposure to nuclear irradiation there are noticeable changes in most of the mechanical properties. Some of the changes are beneficial under certain circumstances; for example, the strength and stiffness increase and improve the ability of the material to resist mechanically applied loads. On the other hand, changes in the size of the individual particles (Wigner growth) can lead to induced strain of the material, analogous to thermally induced strain, which can conceivably lead to failure. When graphite is exposed to nuclear irradiation at 30°C, the length increases with the grain and decreases across the grain. There is a net increase in bulk volume. At temperatures above 100 to 300°C there is contraction in all orientations. The contraction is essentially linear with respect to exposure up to a "breakaway" point[2] at which the rate of contraction increases. The general shape of the curve beyond this point has not been established.

There is strong evidence that the fracture of graphite is determined by a critical magnitude of strain. If this strain is a result of a thermal gradient or nuclear irradiation, the increase in stiffness (Young's modulus)

---

[2]Personal communication to W. J. Larkin, AEC-ORO, from J. M. Davidson, HAPO, dated July 18, 1961, subject: Preliminary Results of Second Irradiation of EGCR Graphite.

has no effect on the fracture; that is, the increase in stiffness does not permit a higher temperature gradient or additional neutron exposure.

The cracking and rupture associated with differential Wigner growth strongly influenced the design of the reflector recommended for use in a full-scale pebble-bed power reactor.[3] In the specified reactor, the reflector pieces above the fuel region must be designed to provide the required gas flow area, to yield a reasonable lifetime before failure occurs, and to be replaceable. The chosen design (see Fig. 9.1) consists of closely packed 2-in.-diam cylindrical rods above and below the fuel region with their axes parallel to the core. The rods are to be supported by steel grids to which the rods will be attached by threaded studs, as indicated in Fig. 9.1. The rods are to be arranged in clusters that can be withdrawn through the service tube.

The induced shrinkage stresses will be a function of the rate of change of exposure with respect to the spatial coordinates. The stresses can, therefore, be reduced by keeping the diameters of the rods as small as possible consistent with handling convenience. For sufficiently small rods, the flux can be considered constant over a cross section. The only flux variation will therefore be in the axial direction.

The stresses induced in graphite reflector rods without tapered holes at the ends (shown in Fig. 9.1) were computed on the following bases:

1. The material is homogeneous and isotropic.

2. The flux distribution is constant over a cross section, that is, it does not vary either with the radial or circumferential direction. The variation in the axial direction is of the form

$$\phi = Ce^{-kz} ,$$

where ϕ is the fast neutron exposure in Mwd/AT per year at full power and C and k are constants.

---

[3]A. P. Fraas et al., Design Study of a Pebble-Bed Reactor Power Plant, ORNL CF-60-12-5 rev., May 11, 1961.

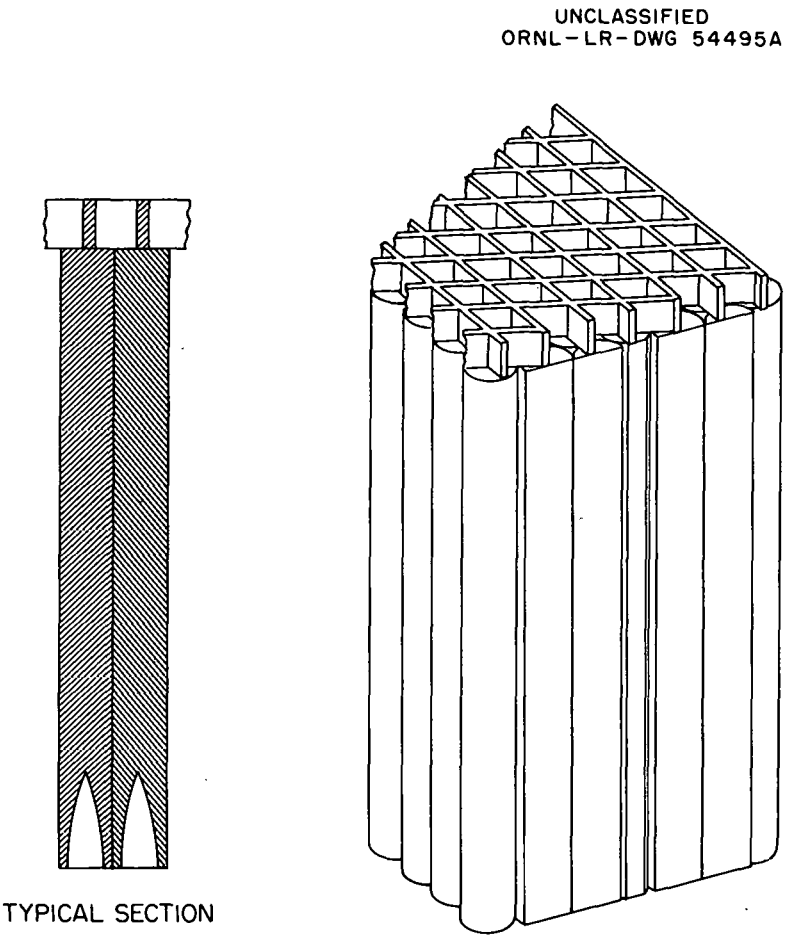

Fig. 9.1. Arrangement of Graphite Reflector Above Fuel Region.

3. The change in length of a line element, ϵ, is a linear function of the neutron exposure, that is,

$$\epsilon = \alpha\phi \quad ,$$

where ϕ is the fast neutron exposure and α is the coefficient of irradiation growth.

A closed form solution is terms of Bessel's functions was obtained for the solid cylinder. The solution can be made to satisfy all boundary conditions except identically vanishing stress components over the two ends. The nonzero stresses remaining are self-equilibrating and, therefore, by St. Venant's principle are of no concern a distance, say two

or three times the radius, removed from the ends. To investigate the effect in the vicinity of the ends, the nonzero stresses were removed by approximating a convergent series solution with the first term. The constant of integration of the approximating solution was chosen to give a best graphical fit to the desired form.

The stresses in a cylindrical rod were computed using the data[4] of Table 9.1. The flux was represented by

$$\phi = 7150\ e^{-0.19z}\ ,$$

and the mechanical properties used were $E = 1.53 \times 10^6$ psi, $\mu = 0.275$, $\alpha = -3.4 \times 10^{-7}$ (in./in.)/(Mwd/AT).

Table 9.1. Fast-Neutron Flux Distribution as a Function of Axial Distance Along a Rod

Axial Coordinate, z (in.)	Fast-Neutron Flux (Mwd/AT per Year at Full Power)
0	7150
3.583	3690
7.205	1800
10.787	848
14.409	391
17.992	173

The solution for the uncorrected stresses gave a maximum for all the stresses at the end z = 0 (Fig. 9.2). These stresses diminish with penetration into the cylinder, the magnitude at all positions being proportional to $e^{-0.19z}$. By correcting the axial stresses at the end z = 0 to give (nearly) zero stress, the magnitudes of the other stresses were increased appreciably near the end (Figs. 9.3 through 9.6). However, as stated above, after a very short distance all the stresses are essentially

[4]Data supplied by R. S. Carlsmith, November 21, 1960.

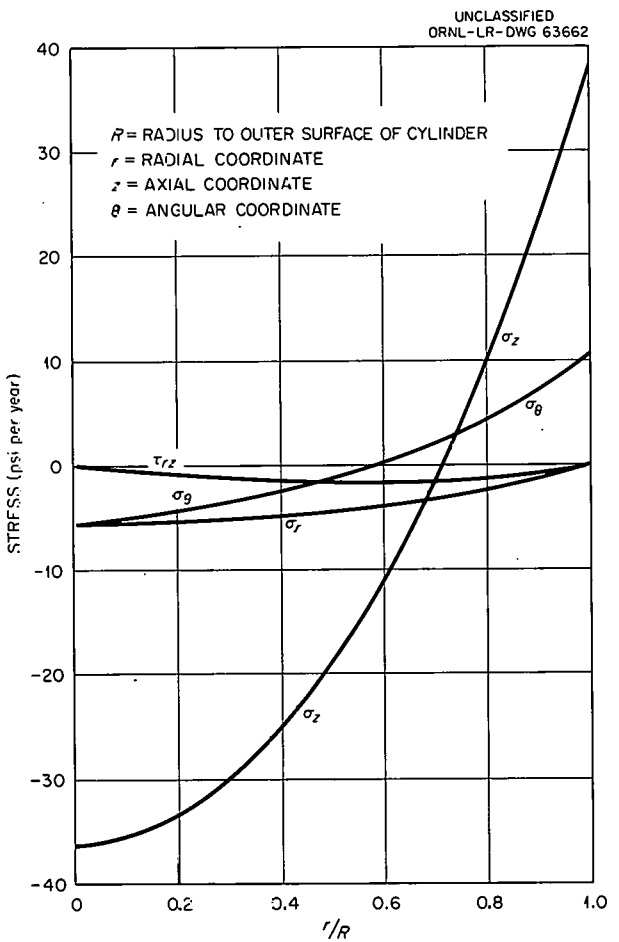

Fig. 9.2. Effect of Irradiation-Induced Stresses on PBRE Graphite Reflector Rods — Uncorrected Stresses at z/R = 0.

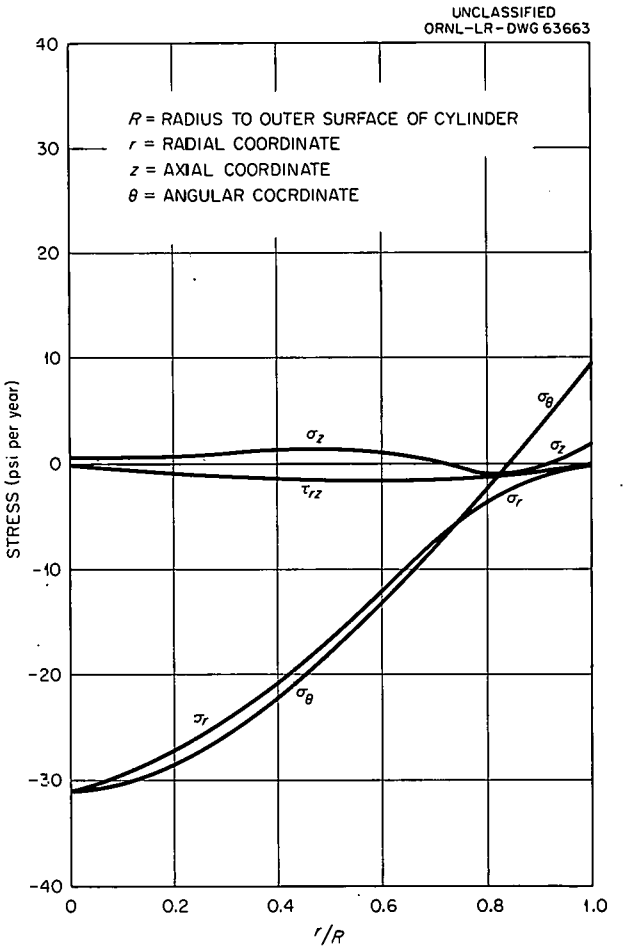

Fig. 9.3. Effect of Irradiation-Induced Stresses on PBRE Graphite Reflector Rods — Corrected Stresses at z/R = 0.

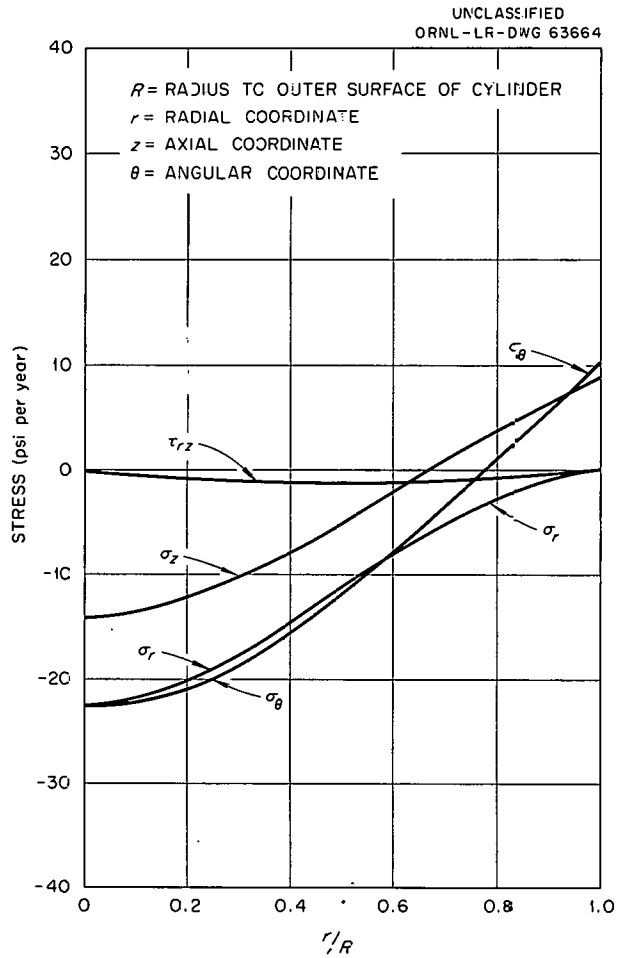

Fig. 9.4. Effect of Irradiation-Induced Stresses on PBRE Graphite Reflector Rods — Corrected Stresses at z/R = 0.1.

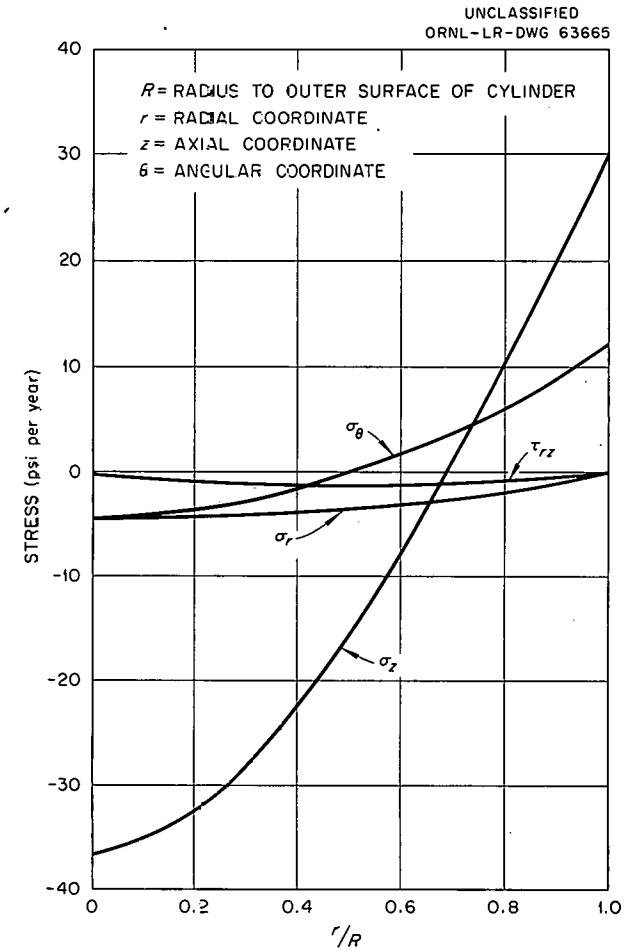

Fig. 9.5. Effect of Irradiation-Induced Stresses on PBRE Graphite Reflector Rods — Corrected Stresses at z/R = 0.5.

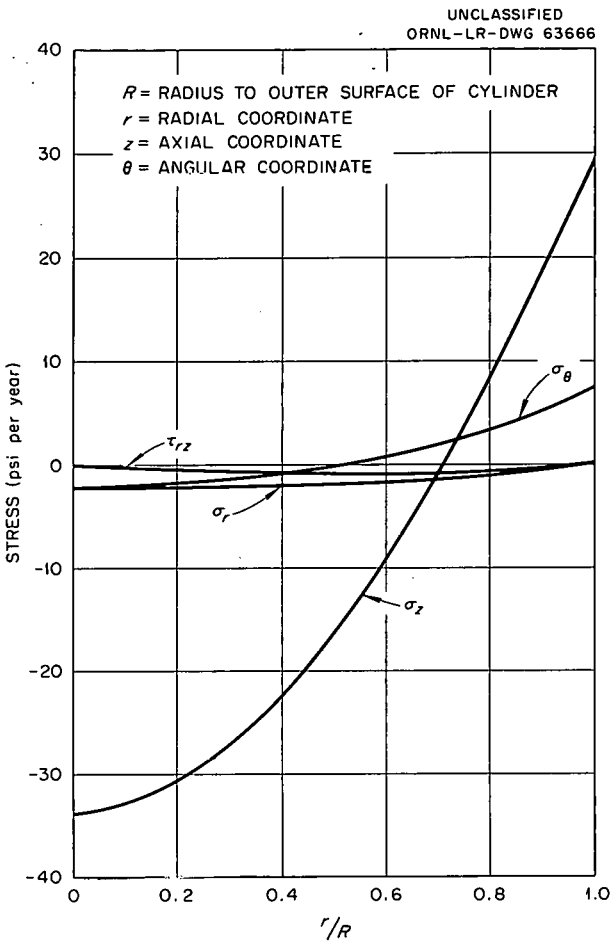

Fig. 9.6. Effect of Irradiation-Induced Stresses on PBRE Graphite Reflector Rods — Corrected Stresses at $z/R = 1.0$.

those corresponding to the uncorrected state. In attempting to satisfy the condition of zero stress over all surfaces, it was found that σ_z, the stress in the axial direction, and τ_{rz}, shear stress in radial direction on a plane perpendicular to the z direction, could not both be corrected to zero. It was decided to correct the σ_z stress and let the much smaller τ_{rz} stress remain uncorrected. The magnitude of the uncorrected τ_{rz} stress is about the same as the σ_z stress corrected to first term of the series solution (see Fig. 9.3).

The results indicate that the maximum stress accrual is about 36 psi per year and occurs at an axial distance equal to approximately one half the radius from the end. If the design lifetime of the reactor is 20 yr of full-power operation, the maximum stress will be approximately 720 psi. Hence, the graphite should not need to be replaced because of differential Wigner growth alone.

Heat Transfer Analysis of Pebble-Bed Reactors and Comparison with Prismatic Cores

R. B. Korsmeyer

A heat transfer analysis and a quantitative comparison of the pebble-bed reactor with the streamlined, or "prismatic", type of reactor has been

completed.[5] Although the radial-flow pebble-bed core has a characteristically low pressure drop, the radial mismatch of gas flow and power density and the neutron leakage at the center inlet make this design very unattractive compared with the much simpler axial-flow core. Of the latter, the downflow core is not subject to bed levitation, but the core support structure lies directly in the hot exit gas stream. Until the design of a reliable, dimensionally stable structure is demonstrated, therefore, only the axial-upflow core may be seriously considered.

The high heat transfer coefficients obtainable in pebble-bed cores or in cores with variable coolant flow cross sections are usually accompanied by high-pumping power requirements. This results from the eddy losses associated with expansion and contraction of the coolant passages in the direction of flow. In cores having prismatic fuel elements (that is, tubes, plates, etc.) the coolant flow passages are uniform longitudinally. Compared with the pebble-bed core, the heat transfer coefficient for a given mass flow rate is low in the prismatic core; but a high flow rate can be obtained for a given ratio of pumping power to heat removal in the prismatic core.

It is important therefore to compare the characteristic reactor sizes and operating pressures associated with these two types of core, for the same output, recognizing, of course, that the optimum design conditions are not the same. In other words the most meaningful comparison is one in which the two reactors have been independently optimized to deliver a given net power at fixed steam conditions. A fairly large power station for which reactors of these types might be attractive would be one designed to produce, say, 325 electrical megawatts (800 Mw thermal), at a steam temperature of 1050°F.[6] The coolant gas and its inlet and outlet temperatures would be the same in each case. For helium as the coolant and effective

---

[5]M. N. Ozisik, R. B. Korsmeyer, and G. L. Rhoden, Heat Transfer Analysis of Pebble-Bed Reactors and Comparison with Prismatic Cores, ORNL CF-61-6-16, June 19, 1961.

[6]A. P. Fraas et al., Design Study of a Pebble-Bed Reactor Power Plant, ORNL CF-60-12-5 rev., May 11, 1961.

inlet and outlet temperatures of 550 and 1250°F, respectively, equations have been developed relating the power densities and the gas-film temperature drop for these two reactors.[5]

Rather than to deal in terms of power density, however, the power station designer is more directly interested in the size of the reactor which he must enclose in a pressure vessel. The right-circular cylinder of largest volume which can be enclosed in a sphere of given diameter has a length-to-diameter ratio of 0.7. A reflected, cylindrical core which has the highest neutron efficiency, however, has a ratio of 0.92, although there is not much loss in economy for ratios between 0.7 and 0.92. Since very large pressure vessels of spherical form are cheaper than cylindrical vessels with domed ends, the shape of the pressure vessel does not enter into the comparison. The choice of length-to-diameter ratio does not, therefore, affect the comparison importantly, and equal values for the prismatic and pebble-bed cores have been arbitrarily chosen, although the choice biases the comparison slightly in favor of the pebble-bed concept.

A comparison of the core length, core volume, and film temperature drop for the prismatic and pebble-bed cores, as obtained in terms of the equivalent hydraulic diameters and fuel ball sizes, is presented in Fig. 9.7. The curves shown are for the particular combinations of pressure ratios and ratios of pumping power to heat removal shown. Subscripts S and P refer to the pebble-bed and prismatic reactors, respectively. The comparison shows immediately that the prismatic core is considerably smaller for the same power output than its pebble-bed counterpart or its operating pressure and pumping power are lower. On the other hand, the gas-film temperature drop is generally higher in the prismatic core if the core is much smaller than the pebble-bed core. Considering that prismatic fuel elements are easily designed to have much lower internal temperature drops than the matching pebble-bed fuel elements, higher surface temperatures can be tolerated without exceeding the maximum allowable fuel temperature. Furthermore, the core radial temperature distribution can be made quite uniform by orificing the fuel-channel inlets in the prismatic core, a step that is impractical for the pebble-bed core.

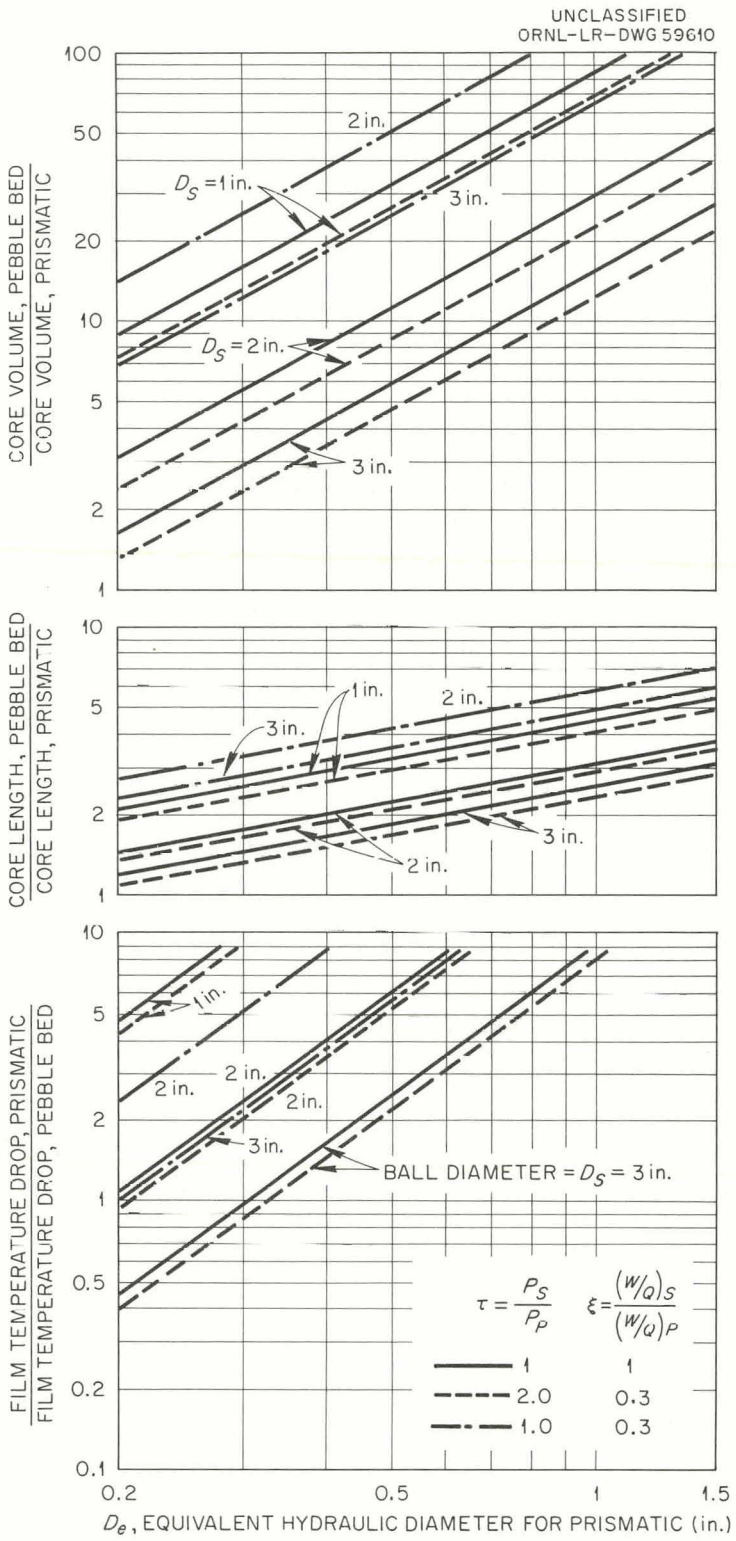

Fig. 9.7. Comparison of Axial-Flow Pebble-Bed Cores with Cores Having Prismatic Fuel Elements. (Prismatic core voidage = 0.20).

Since the fuel-levitation problem is aggravated as the fuel ball size is reduced, the designer is limited in the power densities he can achieve in unrestrained axial-upflow beds. As a result, either uneconomically low power densities and ratios of pumping power to heat removal are accepted or schemes of unproved feasibility are resorted to in order to prevent the fuel from fluidizing in the gas stream. In the pebble-bed reactor chosen here for comparison,[6] the design was optimized with respect to all these parameters, and even then it required fuel balls 2.5 in. in diameter and was limited to an average power density of 6.6 w/cm^3. The ratio of pumping power to heat removal had to be held to 0.003, whereas a value of 0.01 is acceptable for the prismatic cores. In this particular reactor the core height was 12.4 ft, the average gas-film temperature drop was 126°F, and the gas pressure was 700 psia. In conclusion, the fuel handling, and perhaps the reactor maintenance, for the pebble-bed reactor will have to be considerably easier and more economical than that for the prismatic reactors if the pebble-bed reactor is to be competitive.

10. PBRE EQUIPMENT DEVELOPMENT AND TESTING

Compressor Development

W. F. Boudreau

Main Blowers for PBRE

Preliminary design studies have been initiated to determine the general size and arrangement of the main PBRE blowers. Since there will be only one coolant flow path in this reactor, it may be possible to make use of two blowers connected in series, rather than in parallel, and thus eliminate the use of check valves. Two general types of compressors are being considered. One is a totally enclosed compressor with an electric motor and oil-lubricated bearings. A double labyrinth seal would be used with a small flow of helium to prevent oil from entering the reactor and fission products from entering the motor and bearing area. The second compressor being considered has a shaft seal and is driven directly by a small steam turbine. Each of these types of compressor appears to possess some particular advantages, and it will be necessary to develop further information for both of them, and for the reactor system as a whole, before it will be possible to make a choice.

In-Pile Loop Compressors (D. L. Gray)

Facilities for testing high-temperature grease-lubricated ball bearings were placed in operation. Three different tester configurations were used to permit starting the tests with readily available components. The bearings were tested at 12 000 rpm in a 300°F helium atmosphere. The results obtained are presented in Table 10.1.

It is believed that the short duration of run No. 1 in tester No. 1 was caused by a small flow of helium through the bearing. This condition was corrected before initiating run No. 2, which was substantially more successful. Two additional testers are now being assembled.

Heat transfer calculations for the compressor were checked by use of the general heat transfer computer code. The results indicate that the

Table 10.1. Results of High-Temperature Tests of Grease-Lubricated Ball Bearings

Tester No.	Run No.	Test Duration (hr)	Type of Grease	Cause for Termination	Bearing Inspection Results
1	1	144	Barden G-18	Excessive noise	Grease extruded past seals; bearing races and balls in good condition
	2	983	Barden G-18	Excessive noise	Grease base hard, no oil; races and balls in good condition
	3	456	Barden G-26	Excessive noise	Not inspected, will attempt to restart
2	1	333	Barden G-18	Inability to restart drive motor	Grease base hard, no oil; excessive wear of forward bearing retainer; balls and races in good condition
3	1	166	Barden G-26	Still operating	

rear bearings should operate at approximately 200°F and the forward bearings at 250°F. The losses in the motor appear to form an important heat source. Parts for the in-pile loop compressor and the loop for testing it have been fabricated and are now being assembled.

Equipment for Decontamination Operations

J. C. Amos

The feasibility of maintaining an all-ceramic gas-cooled reactor plant depends in large measure on the effectiveness with which equipment can be decontaminated in situ before beginning maintenance operations. Decontamination procedures proposed[1] for pebble-bed reactor components require

[1]A. P. Fraas et al., Preliminary Design of a 10-Mw(t) Pebble Bed Reactor Experiment, pp. 17.1–17.4, ORNL CF-60-10-63 rev., May 8, 1961.

hydraulic isolation of the component to be decontaminated. Since large valves in hot ducts are to be avoided if possible and since such valves would probably not be hydraulically leaktight, a promising method of isolating a component appears to be the insertion of some type of removable closure through an aperture provided in the duct wall for this purpose.

Gas stoppers of various types have been manufactured commercially and used for many years by the gas distribution industry to seal off gas mains during maintenance operation. Several vendors of such equipment were contacted and one or more of their standard items purchased for the purpose of determining their ability to seal large ducts containing aqueous decontamination solutions.

A 24-in. carbon steel pipe 5 ft long with a 4-in.-diam opening in the side and a Lucite mockup of a 24-in. sched-40 pipe to provide visual observation of stoppers were set up as shown in Fig. 10.1 for preliminary screening tests. A standard, rubber, 24-in. gas-main bag manufactured by Mulcare Engineering Company is installed in the Lucite pipe. The Goodman-Peden stopper is shown in Figs. 10.2 and 10.3 prior to installation and as installed in the carbon-steel pipe. A third type of temporary duct seal has been ordered from the LaFavorite Rubber Manufacturing Company. Standard items offered by all three vendors require 4-in.-diam openings for insertion of the 24-in. units and 6-in.-diam openings for insertion of 48-in. units.

Some water leakage was observed during initial tests of both the Mulcare and Goodman-Peden units. Leakage around the Mulcare unit followed a path along the seams of the rubber bladder. This leakage was subsequently stopped by continuing to inflate the bladder until a complete seal was accomplished by one section of the bag; however, this over-inflation ultimately resulted in failure of the bag. With the Goodman-Peden stopper installed in the steel duct, water was added to a depth of approximately 27 in. above the stopper, at which time the weight of the water forced the stopper out of position. It is evident that neither of these units would be suitable for retaining more than a few feet of head of an aqueous solution. However, since decontamination operations can be carried out by spray techniques,

the head of liquid imposed on the seal can be held to a minimum, especially in horizontal ducts.

Fig. 10.1. Gas Stopper Screening Test Setup Showing Mulcare Gas Bag Installed in Lucite Duct and Goodman-Peden Stopper Installed in Carbon Steel Duct.

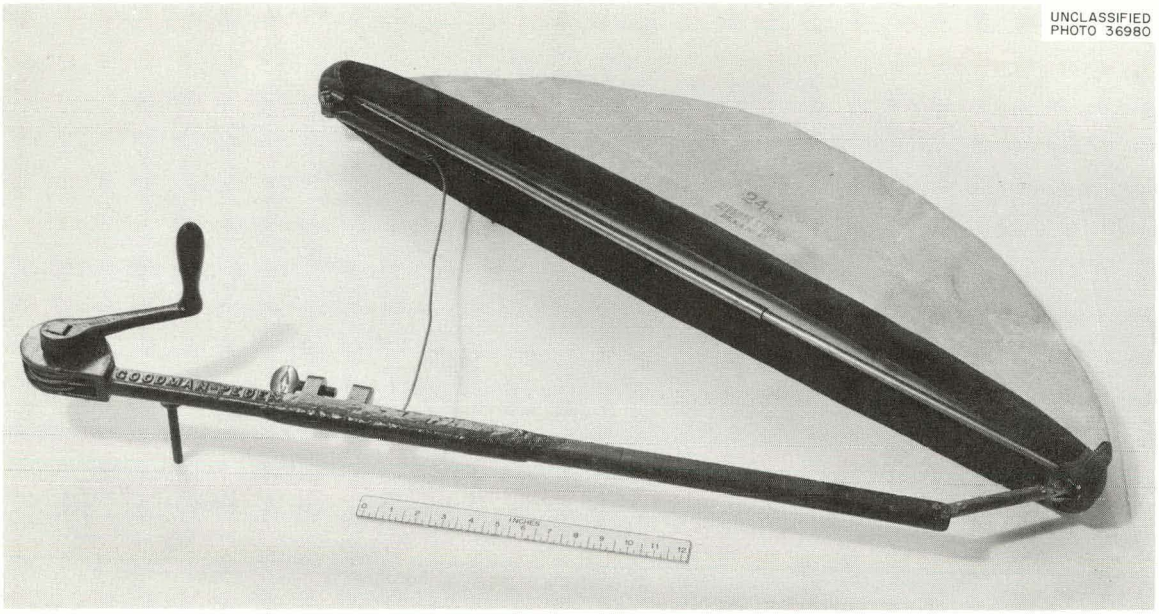

Fig. 10.2. Goodman-Peden Stopper for 24-in. Ducts; Manufactured by Safety Gas Main Stopper Co.

In the installed condition, both units tested were a full 24-in. in diameter. Since the inside diameter of a 24-in. pipe is less than 24-in., wrinkling of the bladder occurred in the case of the Mulcare unit and the gas stopper could not be positioned perpendicular to the pipe axis. This indicates that specially sized units may be necessary for proper sealing of standard pipe.

Initial water tests indicated that inflatable bladders may provide an economical method of sealing large ducts against small heads of aqueous decontamination fluids if the units are properly sized and seams can be either eliminated or arranged so that they do not provide a leakage path. Additional tests will be directed toward first obtaining a bladder that will provide an entirely satisfactory water seal. Tests will then be conducted to evaluate the resistance of these units to attack by the proposed decontamination solutions at actual operating temperatures. Installation and removal procedures will also be established during these tests.

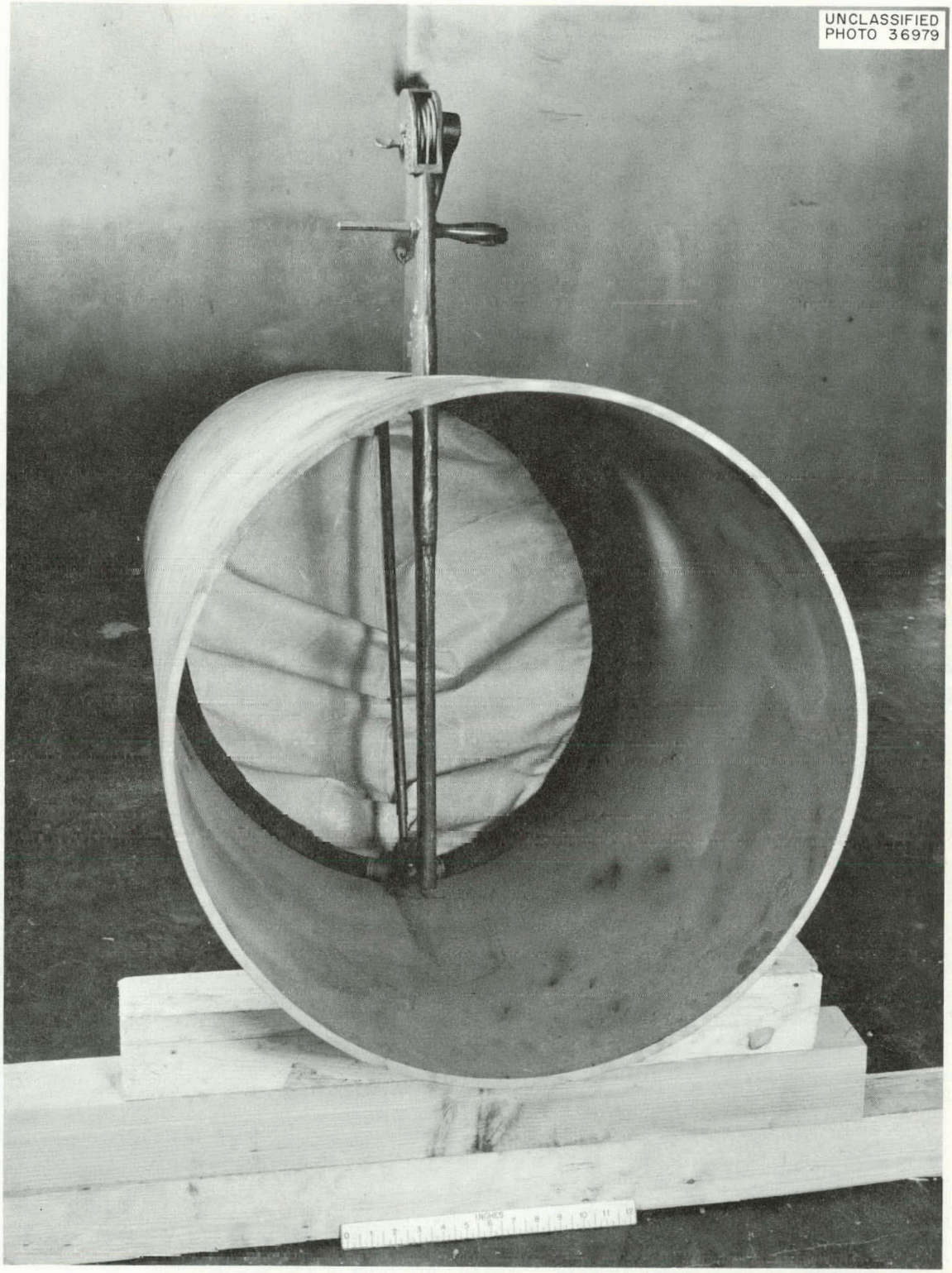

Fig. 10.3. Goodman-Peden Stopper Installed in 24-in. Carbon-Steel Duct.

THIS PAGE

WAS INTENTIONALLY

LEFT BLANK

PART 3. ADVANCED REACTOR DESIGN AND DEVELOPMENT

THIS PAGE

WAS INTENTIONALLY

LEFT BLANK

11. FUELED-GRAPHITE INVESTIGATIONS

W. O. Harms O. Sisman
D. B. Trauger

Materials Development

J. H. Coobs

Evaluation of Coated Fuel Particles (J. M. Kerr, F. L. Carlsen, Jr., T. Hikido)

The evaluation of spheroidal, coated fuel particles designed for use in graphite-matrix fuel elements in unpurged all-ceramic reactors has been continued. As previously reported,[1] coated particles from two different vendors were selected for irradiation in the LITR after thorough preirradiation evaluation. The first test capsule, designated LCP-1, which has been irradiated and is being examined, contained particles coated by High Temperature Materials, Inc. Irradiation of the second capsule (LCP-2), which contains coated particles from Minnesota Mining and Manufacturing Company (3M), was initiated on June 1, 1961, and will continue until October 17, 1961.

Two batches of fully enriched coated fuel particles have been received from a third vendor, the National Carbon Company, for evaluation and possible irradiation in the LITR. The uranium carbide particles were coated at two different temperatures, "A" and "B", which are reflected in the designations given to the two batches, "NCC-AD" and "NCC-BE." Metallographic examinations of particles from the two batches revealed an unusual coating structure, which consisted of three layers of different forms of carbon. A typical particle from batch NCC-BE is shown in Fig. 11.1, and Fig. 11.2 shows the representative microstructure of a particle from batch NCC-AD. The material immediately adjacent to the approximately 200-μ-diam carbide spheroids appears to be similar to layers that were identified to be graphite in other batches of coated and uncoated uranium carbide particles. It is

[1] GCR Quar. Prog. Rep. June 30, 1961, ORNL-3166, pp. 84–86.

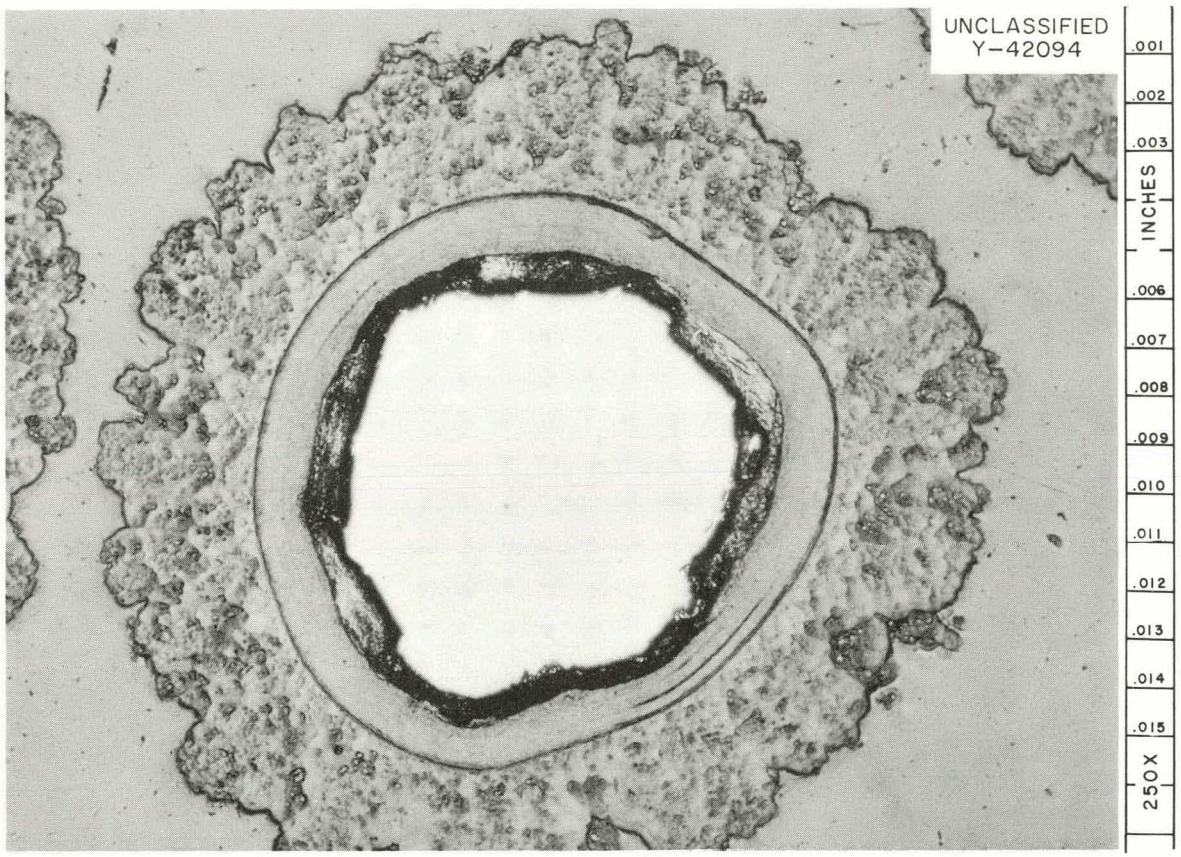

Fig. 11.1. Typical Microstructure of Pyrolytic-Carbon-Coated Uranium Carbide Particles from Batch NCC-BE, Illustrating Polyphase Structure of Coating. As polished. 250X

believed that this 10- to 25-μ-thick inner layer resulted from the carbide particle preparation step and was present before the particles were subjected to the coating operation. The coating has a duplex structure consisting of a 25- to 30-μ-thick laminar pyrolytic-carbon layer followed by an approximately 75- to 100-μ-thick layer of columnar pyrolytic graphite.

Evidence of an extensive reaction involving the two inner layers of particles from batch NCC-AD may be seen in Fig. 11.2. This reaction layer, which was observed in all the particles that were examined, is quite similar to the reaction layer found after a previous batch of coated particles was heated to 2170°C, with consequent coating failure. Therefore, the present plans are to irradiate only particles from batch NCC-BE in the LITR;

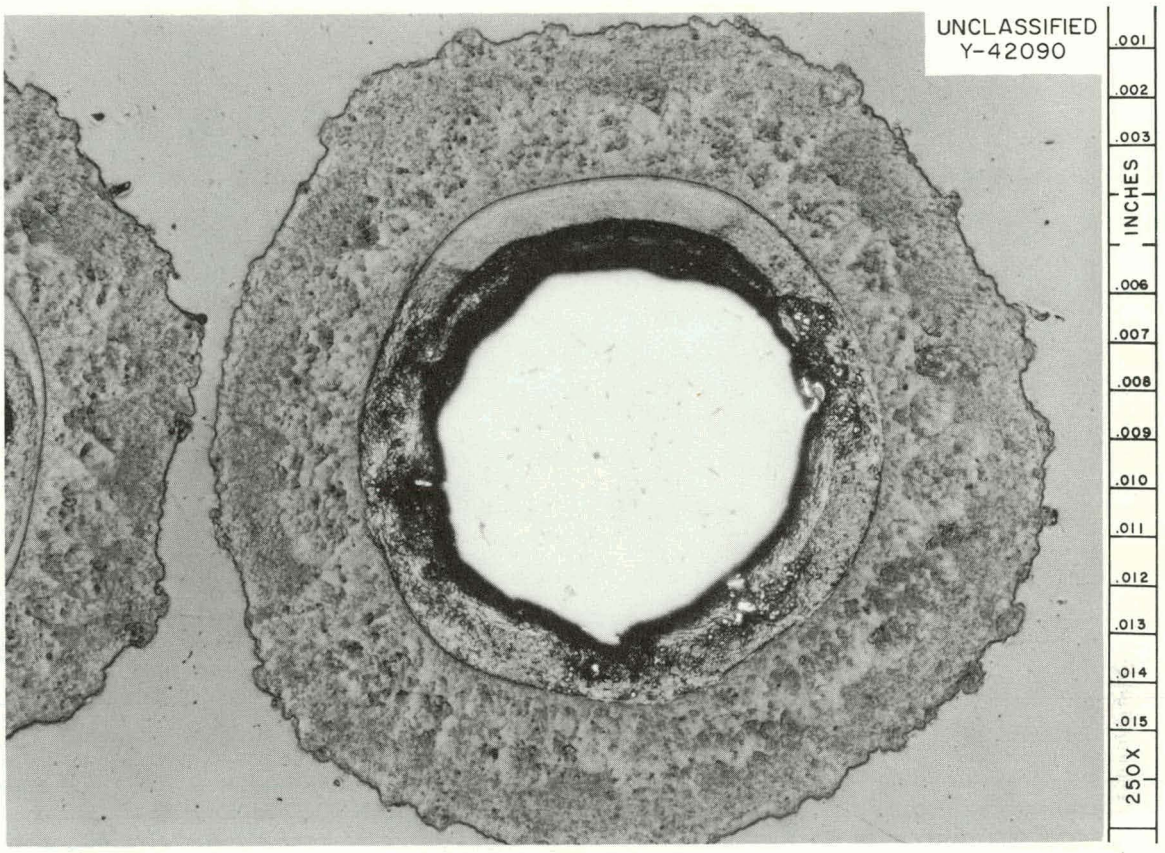

Fig. 11.2. Typical Microstructure of Pyrolytic-Carbon-Coated Uranium Carbide Particles from Batch NCC-AD, Illustrating Reaction at Inner Coating Surface. As polished. 250X

however, samples of both batches will be studied by the neutron-activation technique.

The uranium carbide spheroids of both batches appear to be of high quality and are essentially free of any phases other than UC and UC_2, which are present in the approximate ratio 1:5. Average values of the total weight per coated particle and the weight of uranium per particle are, respectively, 0.00017 and 0.00007 g for batch NCC-AD and 0.00014 and 0.00006 g for batch NCC-BE.

Preirradiation evaluations are being made of the two batches of coated particles according to the procedures described previously.[2] The results

[2]GCR Quar. Prog. Rep. March 31, 1961, ORNL-3102, pp. 104–7.

obtained thus far are presented in Table 11.1. The surface contamination on the particles from batch NCC-BE is somewhat higher than that observed on previous batches of coated particles and will make the analysis of fission-gas-release data more difficult. It was decided, however, to irradiate this material in the LITR because of the unusual structure of the coating, which combines the laminar and columnar types of pyrolytically deposited carbon.

The bulk densities of pyrolytic-carbon-coated uranium carbide and uncoated uranium carbide particles from the Minnesota Mining and Manufacturing Company (3M) were determined. The volume of the particles was determined using both the plastic embedment technique and the mercury porosimeter. The uncoated UC_2 particles were approximately 250 μ in diameter and those that were coated had a coating thickness of approximately 40 μ. Results for identical samples measured by the two techniques are given in Table 11.2.

Table 11.1. Preirradiation Evaluation Data for Pyrolytic-Carbon-Coated Spherical Uranium Carbide Particles from Batches NCC-AD and NCC-BE

	Batch NCC-AD	Batch NCC-BE
Uranium content, % U per gram of particles	41.2	43.4
Coated-particle diameter range, μ	417–495	417–495
As-received surface contamination, % of total uranium	1.2×10^{-3}	6.6×10^{-4}
Uranium dissolved in acid leaching (as-received), %	8.8×10^{-4}	1.3×10^{-3}
Surface contamination after three thermal cycles,[a] % of total uranium	(b)	8.2×10^{-4}
Uranium dissolved in acid leaching after thermal cycling, %	(b)	1.5×10^{-4}
Final surface contamination, % of total uranium	(b)	8.2×10^{-4}

[a] Thermally cycled to 1450–1500°C.

[b] Evaluation not yet completed.

Table 11.2. Density Data for Coated and Uncoated Uranium Carbide Particles

Sample Designation	Type of Particles	Number of Determinations	Average Bulk Density[a] (g/cm^3)	
			Embedment Measurement	Mercury Porosimeter Measurement
3M Lot F	Coated	4	5.641 ± 0.002	
		5		5.50 ± 0.18
3M Lot B	Uncoated	4	11.02 ± 0.33	
		3		10.98 ± 0.54

[a]Precision noted is based on 95% confidence level. Lot F particles contained 73.2% uranium.

Sweep capsule irradiation tests of coated-particle graphite-matrix fuel bodies are planned for the ORR Poolside Facility. The fuel specimens will be hollow graphite cylinders 0.600 in. o.d., 0.250 in. i.d., and 0.500 in. long, containing 0.178 g of U/cm^3 in the form of pyrolytic-carbon-coated uranium carbide spheroids. Fuel pellets for the first two experimental assemblies, which are scheduled for insertion in the ORR during the October shutdown, were received from the Minnesota Mining and Manufacturing Company and the National Carbon Company. After dimensional measurements, density determinations, and radiographic examination, two 12-pellet stacks were selected from each lot and loaded into the irradiation test capsules. The bulk densities of the 24 pellets selected from the lot received from the Minnesota Mining and Manufacturing Company averaged 1.90 g/cm^3, with a range from 1.88 to 1.92 g/cm^3. The pellets from the National Carbon Company had a slightly lower average bulk density of 1.84 g/cm^3, with a range from 1.82 to 1.86 g/cm^3. The fuel particle distribution, although not completely uniform, appeared to be satisfactory, according to radiographic examination.

Additional preirradiation evaluation tests are under way on pellets from the two lots. The tests will include alpha counting to determine surface contamination, leaching in 1:1 HNO_3-H_2O solutions, measurements of thermal expansion and thermal conductivity, chemical analysis, neutron-activation tests, and metallographic examination. Some pellets will be

subjected to thermal cycles and then re-examined. In addition, the feasibility of using a boiling 20 M HNO_3 treatment to detect damaged particles will be investigated (see later section, this chapter, on "Chemical Processing of Coated-Particle Fuels"). It has been observed in exploratory graphite fuel-element reprocessing studies that this acid treatment will disintegrate certain graphite matrices but will not attack the pyrolytic-carbon fuel-particle coatings, except for slight surface oxidation. If any coatings are cracked, or otherwise defective, the acid will attack the fuel particle and uranium will appear in the leach liquid.

A batch of 1/4-in.-diam, 1/4-in.-long graphite pellets containing normally enriched uranium carbide particles coated with pyrolytic carbon was also received from the 3M Company. These pellets were alpha counted on both ends, but no counts above background could be detected. Metallographic examination of the coated particles in the graphite matrix revealed the typical structure of coating and carbide particles. The radiographs of these pellets indicate nonuniform distribution, with agglomerations of coated particles occurring randomly in the pellets. The average density of these pellets, based on 20 determinations is 1.579 ± 0.006 g/cm^3 (95% confidence level), with a range of 1.56 to 1.60 g/cm^3. The results of acid leaching and thermal cycling tests of these pellets are presented in Table 11.3.

Diffusion Coefficients of Xe^{133} from Coated Particles (D. F. Toner, J. L. Scott)

Neutron-activation tests to measure fission-gas retention properties were run on UC_2 spheres coated with pyrolytic carbon (manufactured by High Temperature Materials, Inc.). The cumulative release of Xe^{133} from the spheres is plotted as a function of time at 2180°C in Fig. 11.3.

It was suggested previously[3] that above 2000°C the xenon release from coated UC_2 particles received from the 3M Company occurred by rupture of the carbon coating. Since the coatings on the present sample (HTM-1) did not rupture at 2180°C, it is concluded that the coating was probably applied at a higher temperature. The release of xenon from the HTM-1 sample appeared to occur by diffusion through the coating.

[3]GCR Quar. Prog. Rep. June 30, 1961, ORNL-3166, pp. 89–91.

Table 11.3. Preirradiation Evaluation of Coated-Particle Fueled-Graphite Pellets

Sample Designation	Uranium Removed by Leaching in 8 M HNO_3 (% of total uranium)	
	As Received	After Thermal Cycling[a]
3M-P4	7×10^{-4}	1×10^{-4}
3M-P6	1×10^{-3}	7×10^{-5}
3M-P8	1×10^{-3}	1×10^{-4}
3M-P10	7×10^{-4}	1×10^{-4}
3M-P12	1×10^{-3}	1×10^{-4}
3M-P15	7×10^{-2}	1.1×10^{-3}

[a]Pellets were cycled three times between 200 and 1500°C.

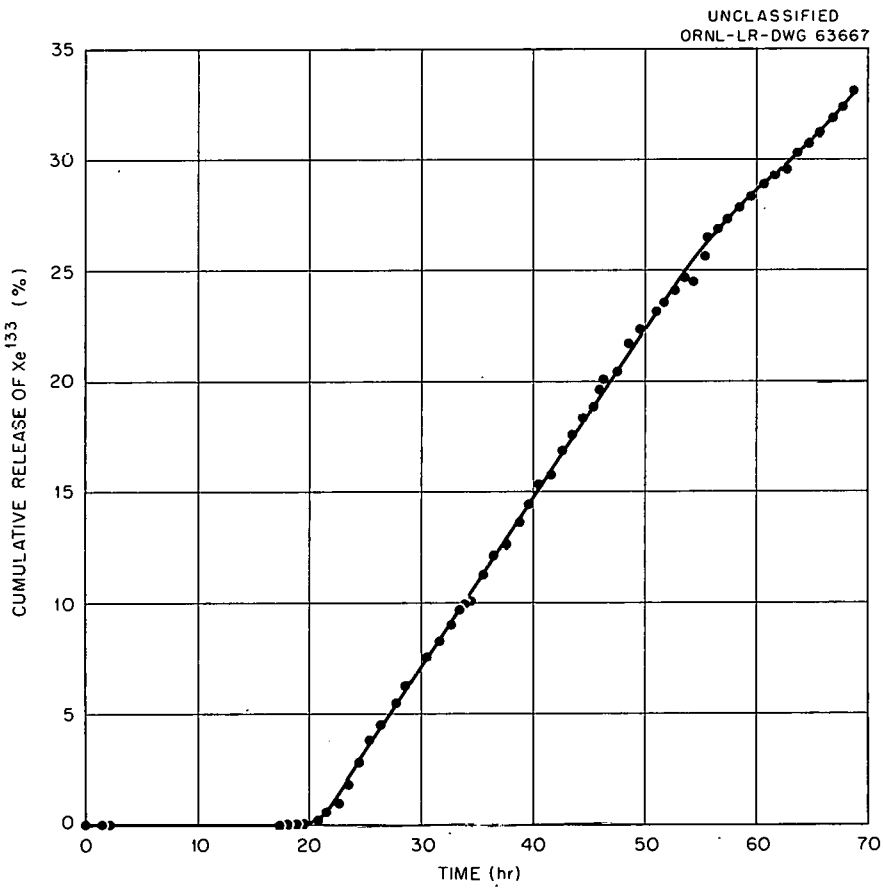

Fig. 11.3. Diffusion Release of Xe^{133} from Pyrolytic-Carbon-Coated UC_2 Spheres at 2180°C.

The model for release is diffusion through a uniform spherical shell. If a constant uniform concentration of Xe^{133} within the fuel and zero concentration at both surfaces of the coating are assumed, the equation of Crank[4] is applicable:

$$D = \frac{(b - a)^2}{6t_i} ,$$

where

b = the outer radius of the shell, cm,

a = the inner radius of the shell, cm,

D = diffusion coefficient, cm^2/sec,

t_i = time intercept (that is, the value of t extrapolated from the curve when the cumulative release is zero), sec.

With this equation, it is not necessary to specify the interface concentration. The calculated value of D at 2180°C was 1.41×10^{-10} cm^2/sec.

Model for the Release of Fission Products from Fueled Graphite Contained in a Low-Permeability Bottle (J. W. Prados)

A simple mathematical model was developed to describe the steady-state release of gaseous fission products from porous ceramic fuels in low-permeability containers.[5] The resulting equations were used to analyze experimental release-rate results obtained from a UC_2-fueled graphite body enclosed in a low-permeability impregnated graphite container (MTR-48-2). The relative release rates of the fission product species Kr^{85m}, Kr^{88}, and Xe^{133} were predicted with reasonable success. Absolute rate predictions were not possible because of lack of information on true permeability and porosity profiles in the graphite container.

Fission-Gas Release from Miniature Fueled-Graphite Bodies (D. F. Toner, J. L. Scott)

Four neutron-activation tests have been run on miniature 0.25-in.-diam, 0.25-in.-long solid cylinders of fueled graphite each containing

[4]J. Crank, Mathematics of Diffusion, p. 95, Oxford Press, 1956.

[5]J. W. Prados, A Model for Fission-Gas Release from Porous Fuels in Low-Permeability Containers, ORNL-3168, Aug. 11, 1961.

about 850 particles dispersed in the graphite matrix. The particles were manufactured and coated with pyrolytic carbon by the 3M Company and were from the same batch as the coated particles tested for fission-gas retention previously.[6] The purposes of the tests were (1) to determine the amount of Xe^{133} released from the pellets and (2) to determine the number of uncoated particles or particles with cracked coatings.

The results of the tests are summarized in Table 11.4. The data indicate that the fractional release of xenon below 2000°C is less than 10^{-3} during the times indicated. From these data and previous results of tests of coated particles not dispersed in a graphite matrix,[6] it may be concluded that some particles in all four fuel bodies were either uncoated,

[6]GCR Quar. Prog. Rep. June 30, 1961, ORNL-3166, pp. 86–88.

Table 11.4. Release of Xe^{133} from Miniature Fueled Graphite Bodies

3M Pellet No.	Heat-Treatment Conditions		Fractional Release of Xenon	Number of Exposed Particles
	Time (hr)	Temperature (°C)		
2	0–2	1075	5.81×10^{-5}	(a)
	2–4	1200	6.50×10^{-5}	(a)
	4–22	1400	2.26×10^{-4}	(a)
	22–27	1600	2.87×10^{-4}	(a)
	27–28	Room	3.28×10^{-4}	(a)
7	0–28.9	1500	3.51×10^{-4}	2
	28.9–51.7	2000	7.76×10^{-4}	2
	51.7–55.0	2100	2.29×10^{-3}	4
11	0–18.4	1300	1.89×10^{-4}	2
	18.4–24.4	2100	6.72×10^{-4}	3
	24.4–41.1	Room	7.89×10^{-4}	3
14	0–1.2	1000	3.69×10^{-5}	(a)
	1.2–2.7	1200	7.74×10^{-5}	(a)
	2.7–19.6	1400	2.47×10^{-4}	(a)
	19.6–50.4	1800	5.31×10^{-4}	(a)

[a]Not determined.

had cracked coatings, or both. In pellets 7 and 11, two particles in each pellet were exposed in the "as-received" condition. From the Xe^{133} released, it is estimated that two or three particles were exposed in pellets 2 and 14.

The total fraction, F, of gas released from one of these fuel bodies is a function of the gas released per particle, f, and the fraction of particles with imperfect coatings, f_p; thus

$$F = ff_p \quad .$$

In order to determine f_p, it is necessary to know by some independent means how much gas is released from a particle that has ruptured. Previously, it was reported that coatings on UC_2 particles fractured when heated over 2000°C and that the gas released upon fracture was composed of that which had diffused out of the UC_2 into the void or porous space between the particles and the coating prior to the fracture.[6] Thus, heating a sample to 2100°C and observing a particle rupture provides an independent means of determining the amount of Xe^{133} released per particle.

The data from a typical test are shown in Fig. 11.4. The release of Xe^{133} during the first 29 hr at 1500°C occurs by diffusion from particles with cracked coatings. The amount of gas released depends upon the number of cracked particles and the diffusion constant of xenon in UC_2 at 1500°C. The second part of the curve, at 2000°C, shows an increase in the diffusion rate; however, no coatings cracked during heating at the higher temperature. As the temperature was increased to 2100°C, two bursts of gas occurred, one followed by the other. This portion of the gas release is shown in an expanded time scale in Fig. 11.5. This release indicated that coatings of two particles had cracked. If the amount of gas released per particle is the same as the gas released by particles initially exposed, it may be concluded that after these two particle coatings had ruptured a total of four particles were unprotected, two of them in the as-received condition.

Fission-Gas Release from Large Fueled-Graphite Bodies (R. E. Adams)

Neutron-activation fission-gas-release tests were started using fueled-graphite specimens similar to those being irradiated in helium sweep capsules

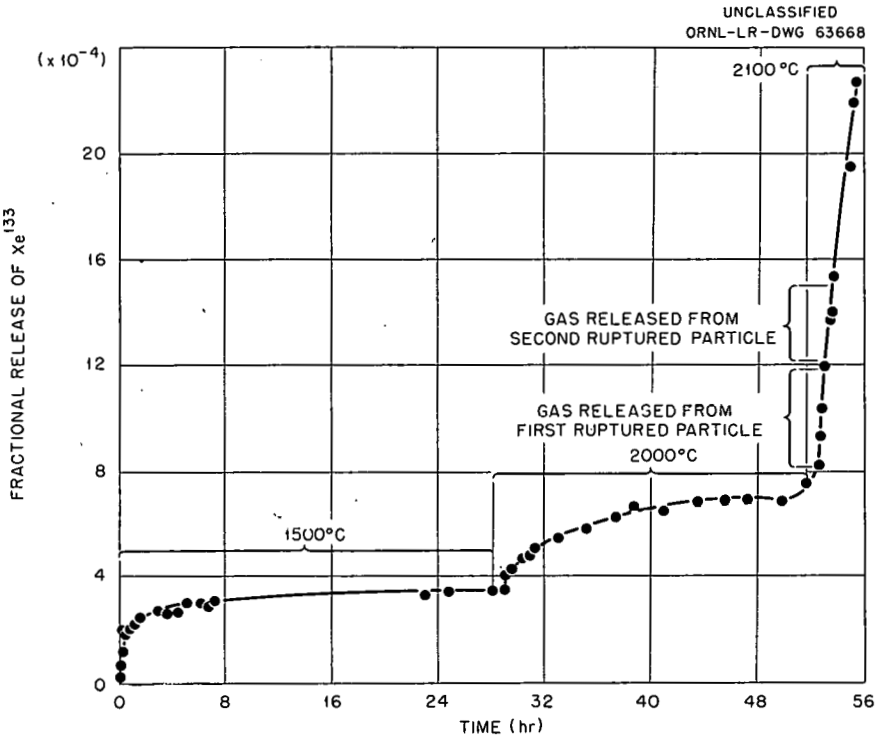

Fig. 11.4. Release of Xe^{133} at 1500, 2000, and 2100°C from Miniature Fueled-Graphite Pellet No. 7.

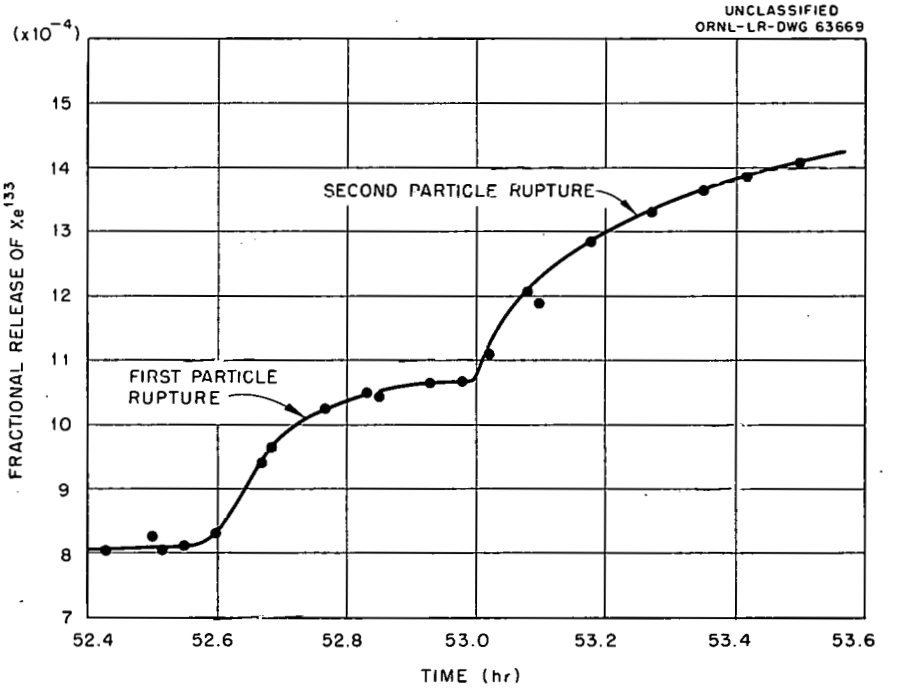

Fig. 11.5. Fractional Release of Xe^{133} from Pellet No. 7 at 2100°C. Expanded time scale.

in the MTR-48 facility. If a correlation between results from the two types of tests can be established, the relatively simple neutron-activation technique may be used as a screening test, so that specimens likely to release large amounts of fission products may be detected prior to use in sweep capsules. The specimens tested were 1-in. cylinders, 1 1/2 in. long, containing spherical 175- to 250-μ-diam UC_2 particles coated with pyrolytic carbon. The particles were dispersed in a porous graphite matrix and fired at 1800°C. Other information on the specimens is presented in Table 11.5.

Fission-gas-release tests are conducted by heating the specimens for various periods of time at increasing temperatures up to 1000°C. The first tests were made in vacuum (1 to 5 μ Hg), and the released Xe^{133} was collected in a charcoal-filled trap cooled by liquid nitrogen. The activity in the collection bulb was recorded continuously. At the end of the test the collection bulb was sealed, and the Xe^{133} was determined analytically. Appropriate correction for Xe^{133} decay and counter efficiency permits the fractional release at any time to be determined.

The data obtained from specimen 1060, plotted in Fig. 11.6, are typical of the data obtained in these experiments. The gas release that occurred in about 5 hr during heating to 600°C was about four times that which occurred during approximately 16 hr at 600°C. Similar effects were noted during the succeeding parts of the test.

Table 11.5. Data on Fueled-Graphite Specimens Used in Fission-Gas-Release Experiments

	Specimen No. 1060	Specimen No. 1081
Specimen weight, g	35.067	35.513
Uranium content, g	1.386	1.836
U^{235} content, g	0.010	1.710
Irradiated time, hr	36	0.80
Irradiated flux, neutrons/$cm^2 \cdot sec$	6.92×10^{11}	2.06×10^{11}
Calculated fissions	1.45×10^{15}	1.48×10^{15}

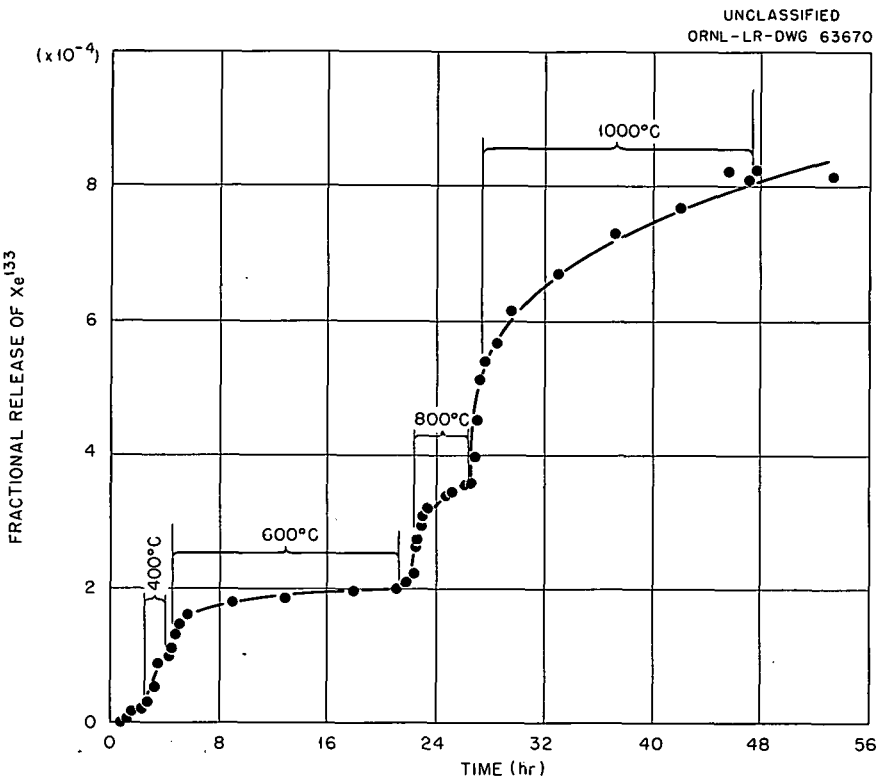

Fig. 11.6. Fission-Gas Release from Fueled-Graphite Specimen No. 1060.

The data from several experiments on the two specimens are summarized in Table 11.6. During initial heating of specimen No. 1081 (Test 1081-1), equipment malfunction caused temperature fluctuations between about 400 and 730°C during the first 27 hr of test, but the test was continued for 18 hr at 800°C. Test 1081-2 was then made using the same specimen. The fractional releases obtained during Test 1081-2, at 800°C and below, were much less than during the preceding test.

Significant results from these experiments may be summarized as follows:

1. The total fractional release of Xe^{133} from both fueled-graphite specimens during heating in vacuum for 50 to 100 hr at 1000°C or less was approximately 8×10^{-4} of the Xe^{133} in the specimens.

2. Two mechanisms of gas release apparently operated: (1) a diffusion mechanism, the rate of which increased with temperature, and (2) a mechanism which allowed rapid release during and shortly after the specimen temperature

Table 11.6. Data on Fission-Gas Release from Neutron-Activated Fueled-Graphite Specimens

Specimen	Heat-Treatment Conditions		Total Cumulative Fractional Release of Xe^{133}	Remarks
	Time (hr)	Temperature (°C)		
			$\times 10^{-4}$	
1060	0–2.5	200	0.2	
	3.0–4.0	400	1.0	
	4.5–21.7	600	2.1	
	22.1–26.1	800	3.6	
	26.7–47.7	1000	8.2	
1081	0–3.5	400	0.2	
	4.05–27.8	400–730	1.72	Temperature varied
	28.5–46.6	800	2.70	
1081	0–3	400	0.01	Specimen 1081 re-heated with new collection bulb
	3.25–21.5	600	0.22	
	22.4–27.1	800	0.50	
	27.7–49.2	1000	5.2	
1081	0–2.5	400	0.01	Specimen 1081 re-heated in CO atmosphere with new collection bulb
	3.0–25.2	600	7.65	
	26.0–28.5	700	8.80	

was increased for the first time to a given temperature level. It was postulated that the rapid gas release during initial heating might be associated with release of CO from the graphite upon initial heating, assuming that the CO could react with exposed UC_2 to allow rapid release of fission products. A third test was then made on specimen No. 1081 in which it was heated in an atmosphere of CO flowing at about 5 cm^3/min. The fission-gas collection trap was cooled to -78°C in a bath of dry ice and acetone. The results, also shown in Table 11.6, indicate that the fractional Xe^{133} release was much greater at 600°C than in the previous tests made in vacuum. It was concluded that the presence of CO definitely accelerated the gas release.

Postirradiation Examination of Fueled-Graphite Bodies

Physical Examinations (J. G. Morgan, M. F. Osborne, H. E. Robertson)

Postirradiation examinations have been completed of UC_2-graphite specimens irradiated in capsules MTR-48-1 and MTR-48-2. Core drilling for determining the uranium concentration and fission-product distribution was done on graphite can b from capsule MTR-48-1. The data obtained are plotted in Fig. 11.7. The concentration of fission products dropped over three orders of magnitude through the first 0.2 in. of the graphite wall. Additional samples will be taken on the outer surface. The results of core drilling of the fuel cylinders and graphite can a were reported previously.[7]

The second irradiation capsule (MTR-48-2) contained the fuel dispersion in a single graphite can. The uranium and fission-product gradient across the can wall is shown in Fig. 11.8. Core drill samples were also taken across the fuel pellet and were analyzed for uranium. The results of the uranium analyses are listed in Table 11.7. Some depletion of uranium at the outer wall of the fuel pellet is evident.

Metallographic Examinations (E. L. Long, Jr.)

Fuel Pellets of Capsule MTR-48-1. Metallographic examinations of fuel pellets a and b of capsule MTR-48-1 have been completed. The fuel pellets for the MTR-48-1 experiment were fabricated by converting the UO_2 to UC_2 by heating at approximately 2800°C. As can be seen in Figs. 11.9 and 11.10, which present microstructures of an unirradiated control sample, most of the UC_2 moved out of the space originally occupied by the UO_2 particles and into the graphite. At low magnification the microstructures of the irradiated a and b pellets were similar to the microstructures of the control specimen, but some differences could be seen at high magnification. The microstructures at the center and mid-radius of fuel pellet a are shown in Fig. 11.11. Areas near the center and mid-radius of fuel pellet b are shown in Fig. 11.12. It may be seen that the irradiated UC_2

[7] GCR Quar. Prog. Rep. June 30, 1961, ORNL-3166, p. 145.

particles are not as angular as those of the control specimen and that no UC_2 "fingers" were present after irradiation. This spheroidization could be a result of surface tension.

Fuel Pellets of Capsule MTR-48-2. The results of metallographic examination of fuel pellet a of capsule MTR-48-2 were reported previously.[8] An unirradiated control sample of the material used for pellet b is shown

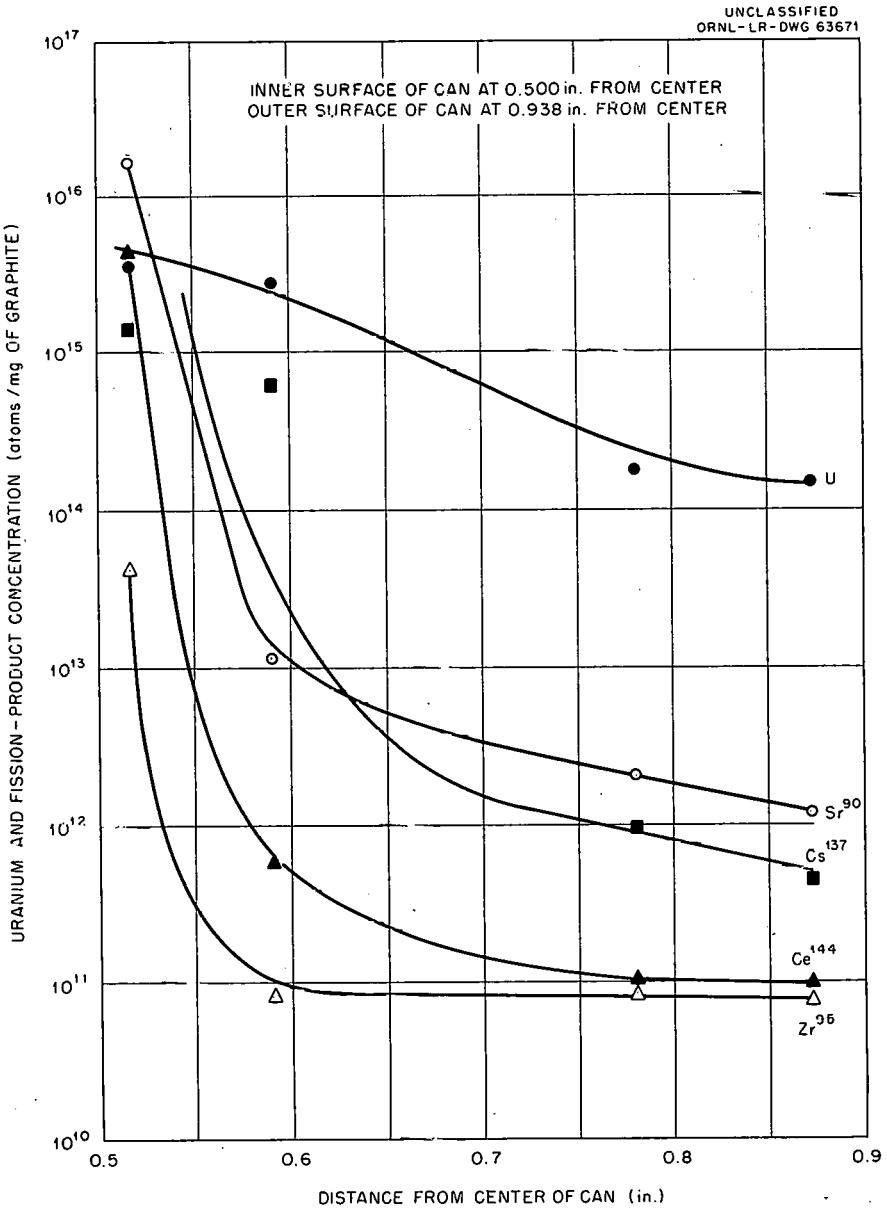

Fig. 11.7. Uranium and Fission-Product Concentrations Across Wall of Graphite Can of Capsule MTR-48-1.

in Fig. 11.13. Graphite crystals can be seen in the UC_2 particles. The UO_2 particles were converted to UC_2 at a lower temperature than for the pellets for the MTR-48-1 experiment. As a consequence, the UC_2 did not move out into the graphite as in the case of the fuel pellets for MTR-48-1.

[8]Ibid., p. 147.

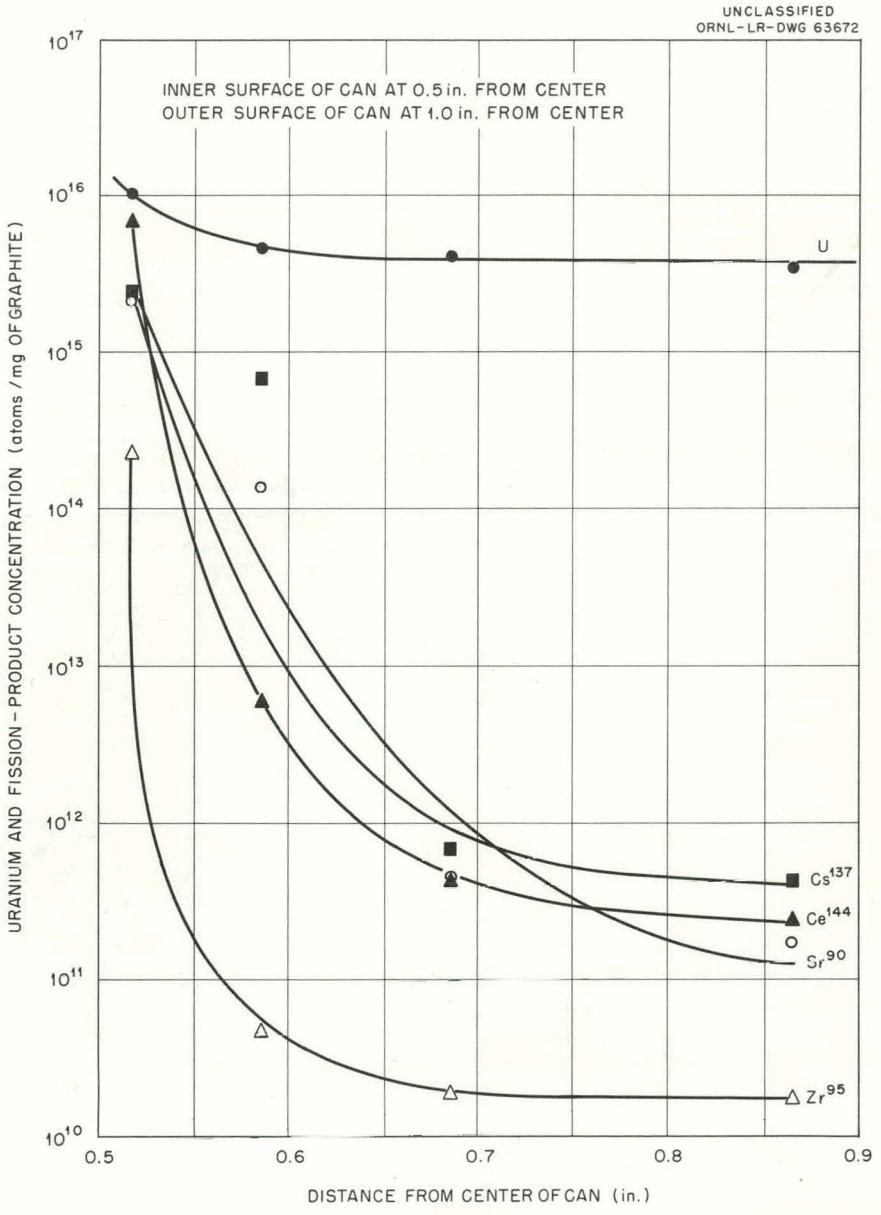

Fig. 11.8. Uranium and Fission-Product Concentrations Across Wall of Graphite Can of Capsule MTR-48-2.

Table 11.7. Uranium Concentration Across Fuel Pellets Irradiated in Capsule MTR-48-2

Position of Center of Drill (in. from center of pellet)	Uranium Concentration (atoms/mg of graphite)	
	Fuel Pellet A	Fuel Pellet B
0.000	9.0×10^{16}	1.6×10^{17}
0.095	6.5×10^{16}	1.5×10^{17}
0.190	8.8×10^{16}	1.6×10^{17}
0.285	(to be analyzed)	
0.380	9.8×10^{16}	1.0×10^{17}
	1.30×10^{17}[a]	1.86×10^{17}[a]

[a]Average preirradiation concentration.

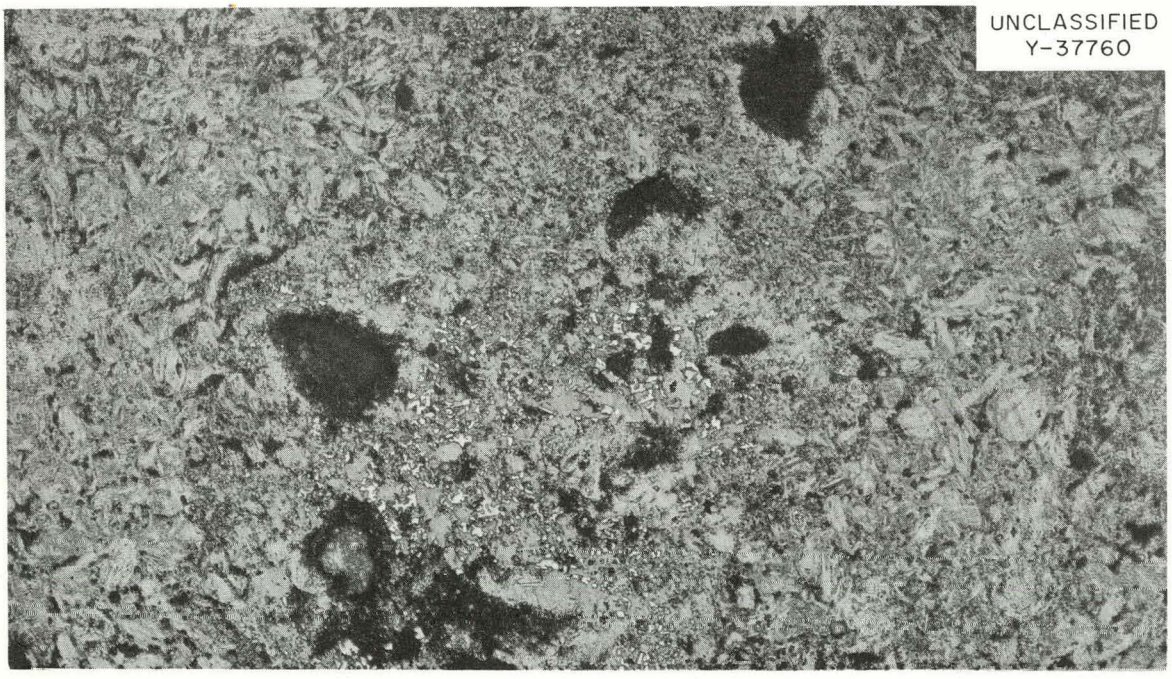

Fig. 11.9. Unirradiated Control Sample of Fuel Pellet Material for Capsule MTR-48-1. Fine UC_2 particles surround the large voids. As polished. 100X

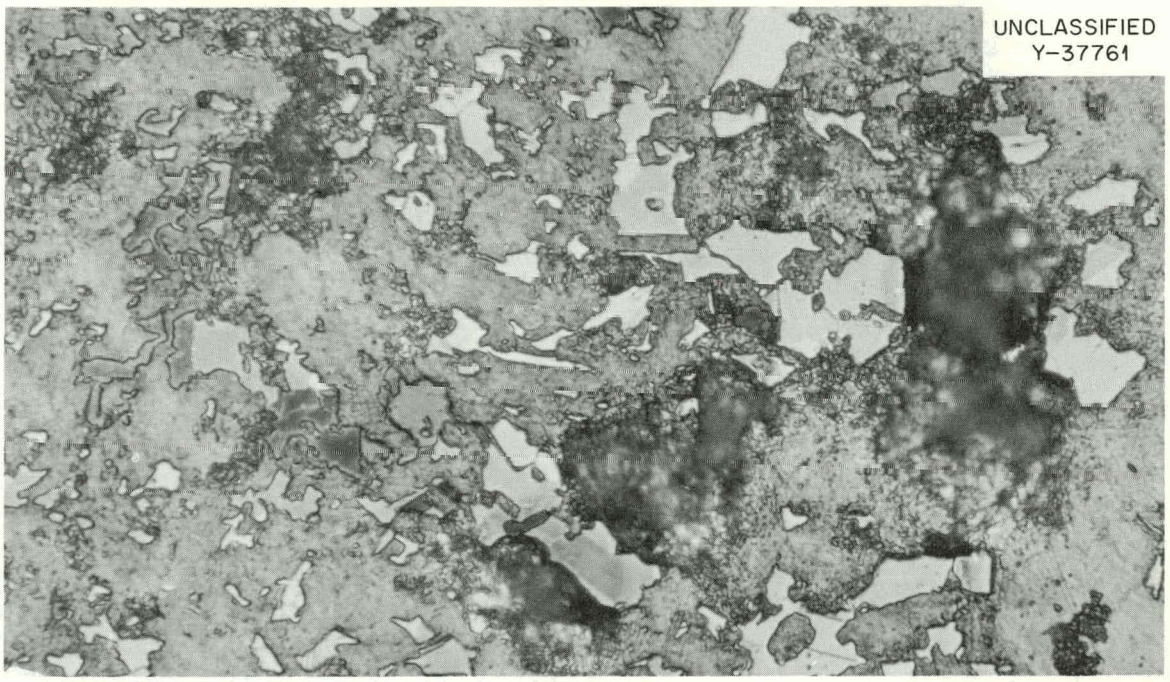

Fig. 11.10. Same as Fig. 11.9 but at a Higher Magnification. Etched. 750X

The postirradiation examination of fuel pellet b revealed a microstructure not unlike that of fuel pellet a. A portion of the UC_2 migrated into the graphite, while the remainder spheroidized, as may be seen in Fig. 11.14.

Graphite Cans of Capsules MTR-48-1, -2, -3. The low-permeability graphite fuel cans used in the MTR-48-1, -2, and -3 experiments have been examined. The plugs in the graphite cans from capsules MTR-48-1 and -3 were threaded, whereas the plug for the graphite can of capsule MTR-48-2 was tapered. All the plugs were sealed with silicon. The cans were sectioned as required to show the quality of the silicon seals, defect regions in the cans and seals, and the presence of any uranium compounds that might have migrated from the fuel pellets into the cans.

Capsule MTR-48-1 contained two fuel cans, designated as fuel cans A and B. Longitudinal sections were made through the plugs of both cans. Examination of the threaded seals disclosed that the silicon sealed only the first top thread in the A can, and, although the silicon bonded all threads in the B can, only the first thread was sealed. If the roots of

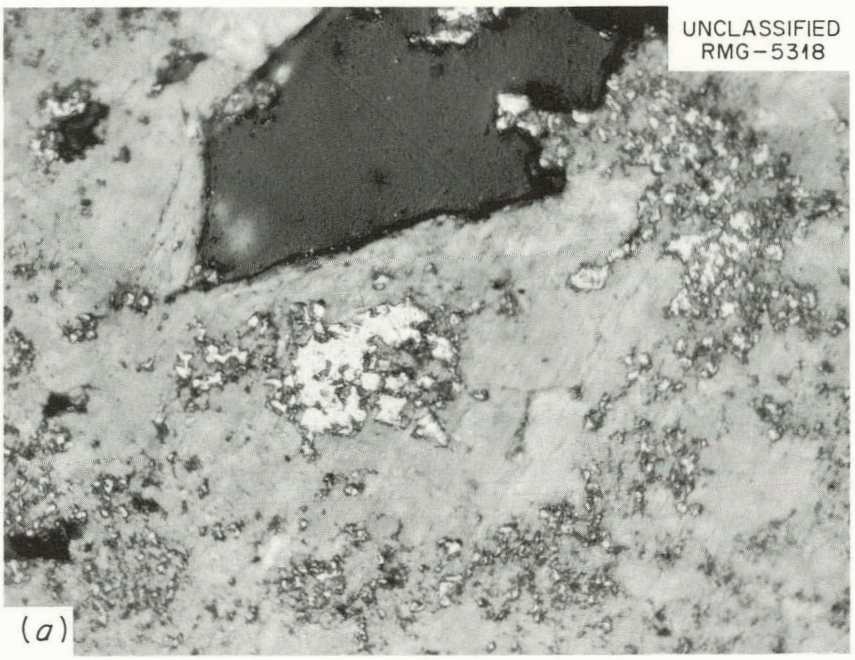

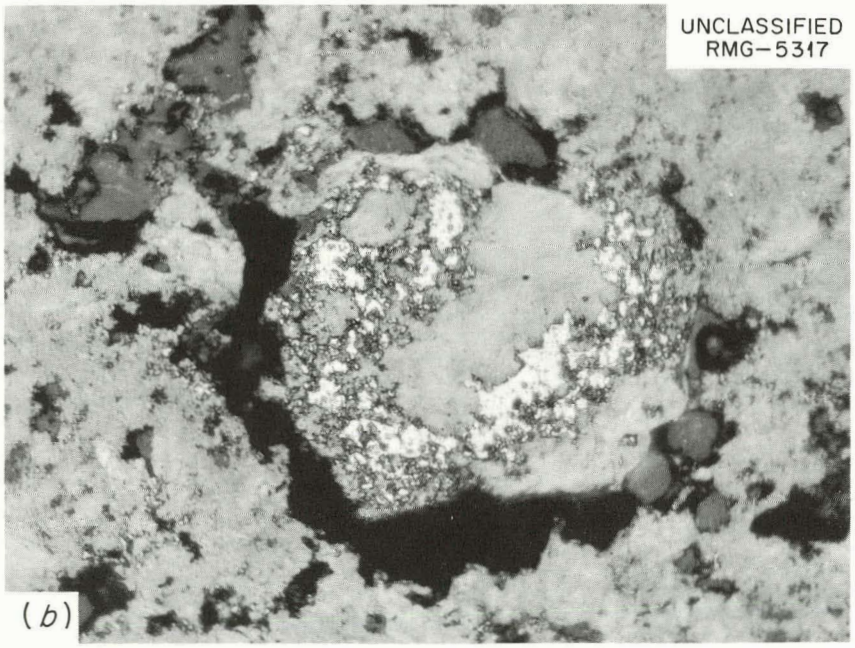

Fig. 11.11. Samples of Fuel Pellet a from Irradiated Capsule MTR-48-1. (a) Sample from near the center of the pellet. (b) Sample from mid-radius of the pellet. As polished. 500X

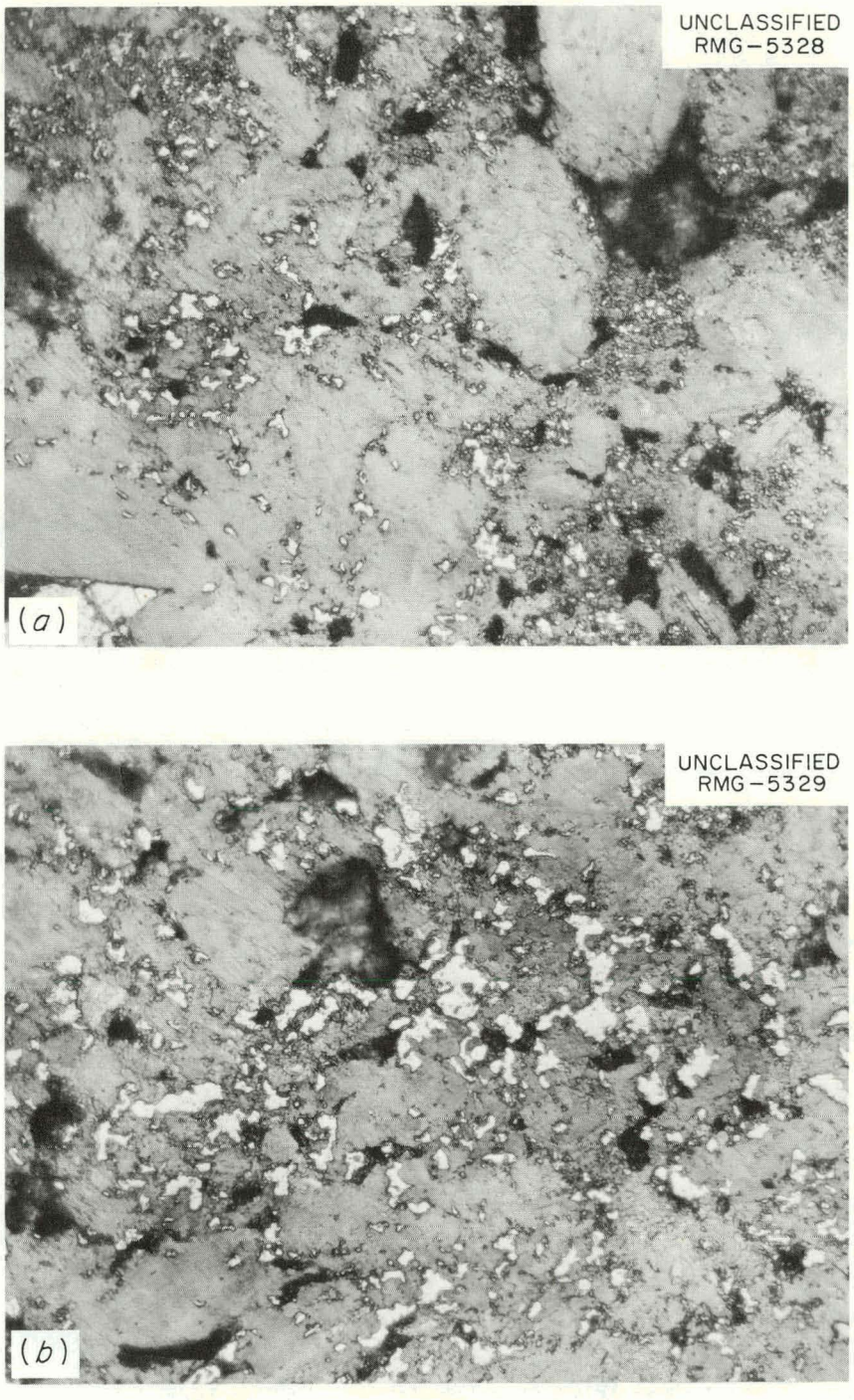

Fig. 11.12. Samples of Fuel Pellet b from Irradiated Capsule MTR-48-1. (a) Sample from near the center of the pellet. (b) Sample from mid-radius of the pellet. Etched. 500X

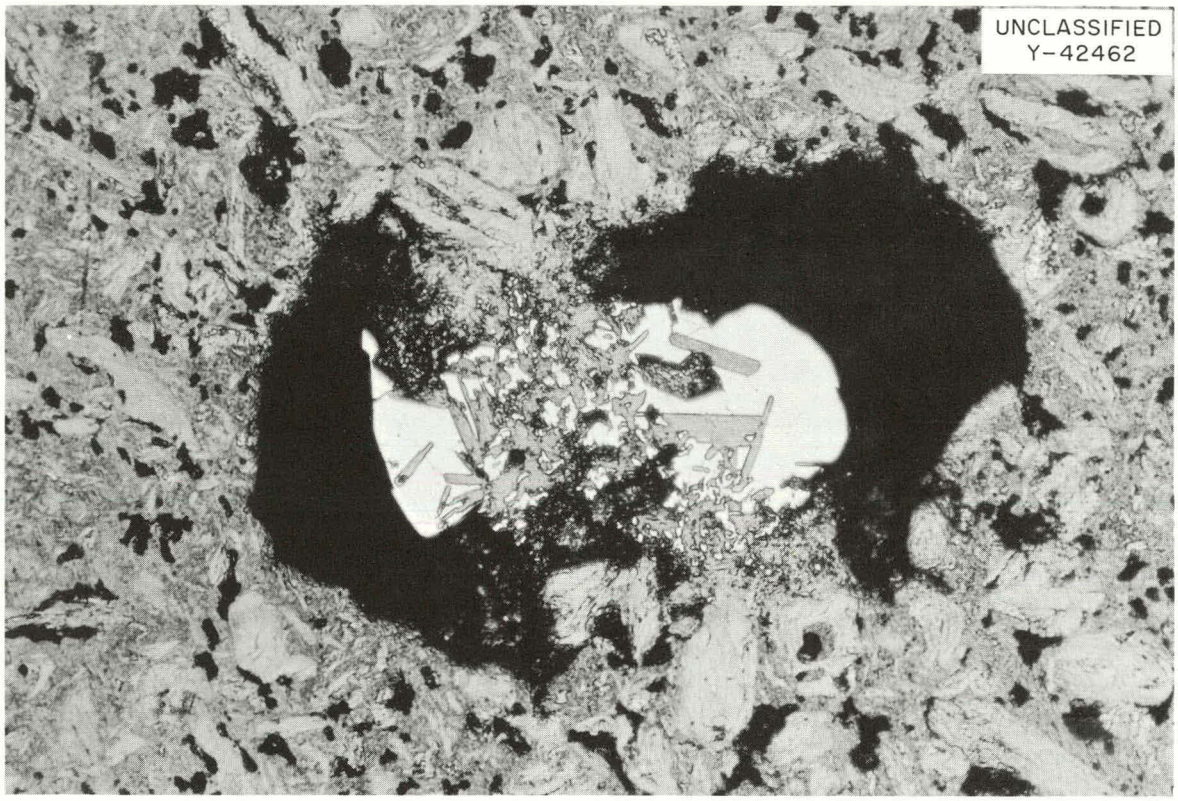

Fig. 11.13. Unirradiated Control Sample of Material from Fuel Pellet b of Capsule MTR-48-2. Note graphite crystals in the UC_2. Etched. 250X

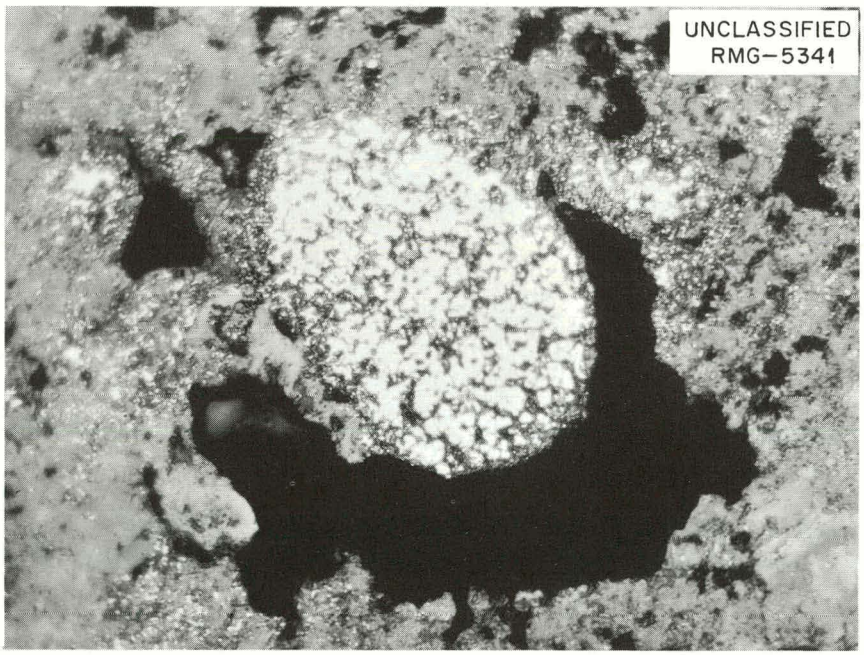

Fig. 11.14. Sample from Mid-Radius of Fuel Pellet b of Irradiated Capsule MTR-48-2. Note shade of UC_2 particle as compared with the control. As polished. 500X

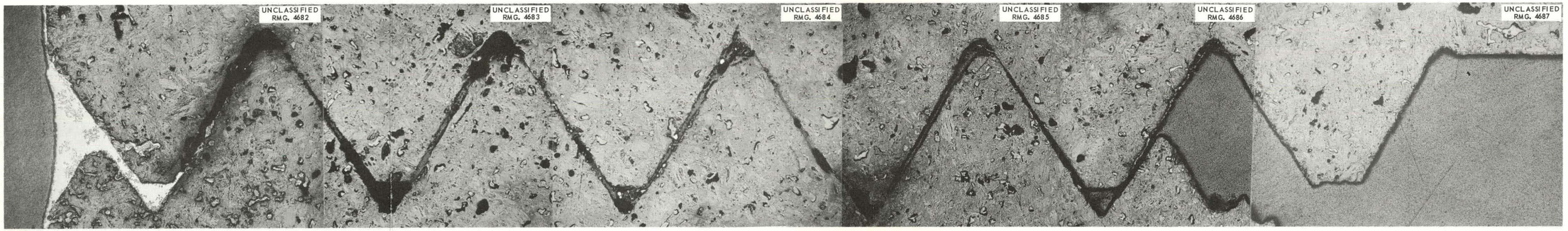

(a)

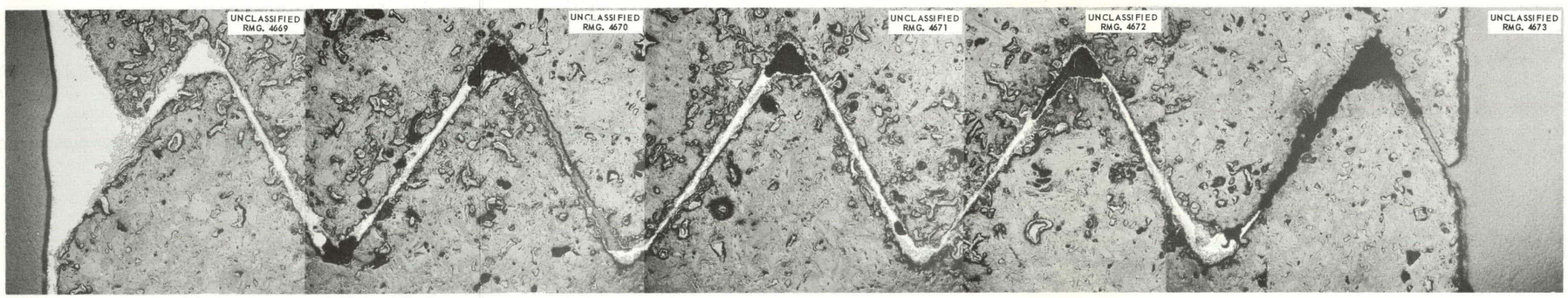

(b)

Fig. 11.15. Longitudinal Sections Through the Threaded Silicon-Sealed Plugs of Fuel Cans from Capsule MTR-48-1. (a) Fuel can A. (b) Fuel can B. As polished. 50X

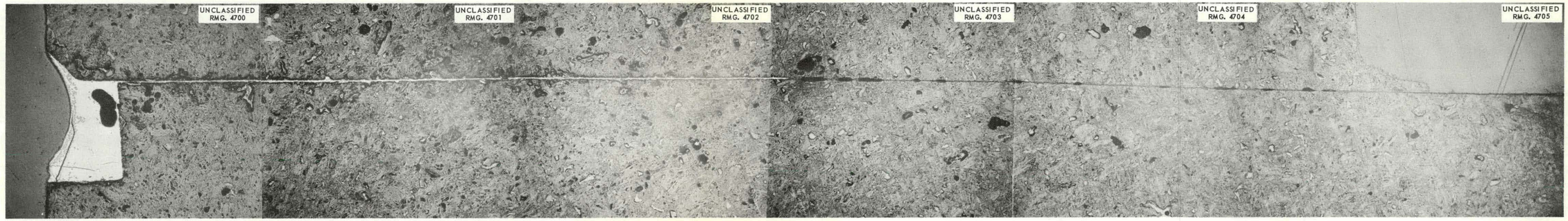

Fig. 11.16. Longitudinal Section Through the Tapered, Silicon-Scaled Plug of the Fuel Can from Capsule MTR-48-2. As polished. 50X

the threads are not sealed a spiral void results which extends the length of the threaded section. The silicon was also present throughout the pores in the graphite in the threaded regions. Longitudinal sections through the threaded regions of fuel cans A and B are shown in Fig. 11.15. Metallographic examination of a transverse section revealed no evidence of uranium compounds having migrated into the walls of the fuel cans, and there was no evidence of silicon migration down the inside walls of the cans.

The MTR-48-2 capsule contained only one fuel can, which was fitted with a tapered plug rather than a threaded plug and sealed with silicon. Metallographic examination of a longitudinal section through the plug showed that the silicon penetrated approximately half-way through from the top, as shown in Fig. 11.16.

As previously reported,[9] a leak was indicated during irradiation of capsule MTR-48-2. Metallographic examination revealed a fracture that originated at the gap between the tapered plug and the can (just below the termination of the silicon seal) and extended into the thermocouple hole. No evidence of uranium compound migration was found in the metallographic examination of a transverse section of the fuel can wall. However, an unidentified layer approximately 0.005 in. thick was noted on the inner wall of the fuel can, as shown in Fig. 11.17. The layer is not like silicon or silicon carbide in appearance; there was no evidence of a similar layer on the outer surfaces of the fuel pellets that were in this fuel can.

Capsule MTR-48-3 also gave evidence of a leak in the graphite can during irradiation.[10] A longitudinal section through the threaded, silicon-sealed plug and sequential examination revealed poor penetration of the silicon. None of the roots of the threads were sealed, as may be seen in Fig. 11.18. Additional grinding revealed a hairline crack in the silicon seal at the top of the plug (Fig. 11.18b). The leak probably followed the spiral cavity formed by the unfilled roots of the threads and continued via the hairline cracks in the silicon seal.

---

[9]GCR Quar. Prog. Rep. March 31, 1961, ORNL-3102, p. 178

[10]GCR Quar. Prog. Rep. June 30, 1961, ORNL-3166, p. 144.

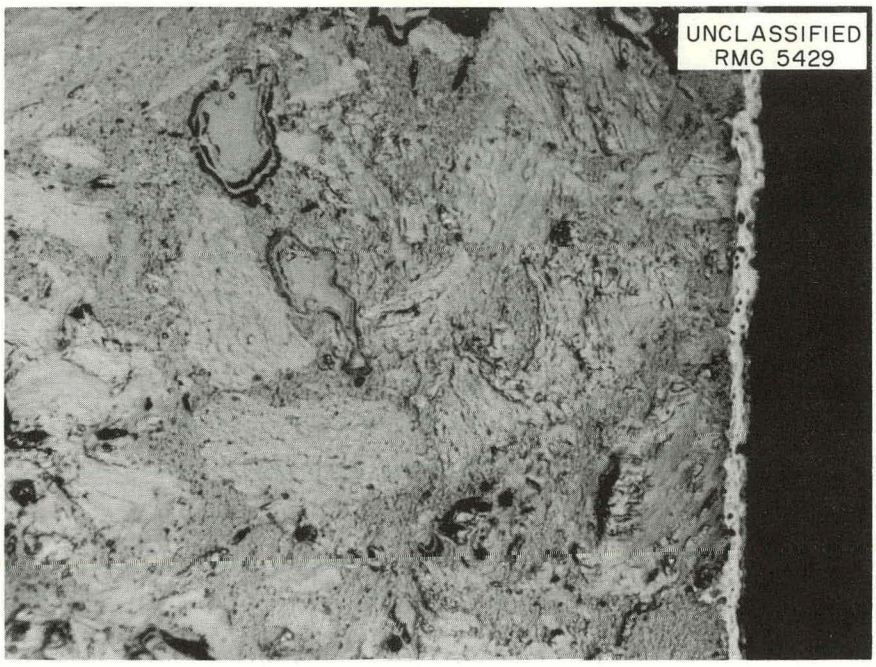

Fig. 11.17. Unidentified Layer on Inner Wall of Fuel Can from Capsule MTR-48-2. As polished. 250X

In summary, on all three threaded silicon-sealed plugs examined a spiral void remained as a result of the unfilled roots of the threads, and, at best, only the first thread was completely sealed. The tapered silicon-sealed plug revealed an integral seal that extended from the top of the can to about half-way through; however, a fracture developed in the graphite can at the termination of the seal, which also afforded an escape route for the fission gases. This was the only fuel can that gave indications of the silicon or a silicon compound having possibly migrated down the inner walls of the cans. There was no metallographic evidence of uranium compounds in the walls of the cans as a result of fuel migration.

Irradiation Tests

Miniature-Capsule Fission-Gas-Release Experiments in LITR (F. R. McQuilkin, W. E. Thomas)

Operating data for the miniature capsules recently irradiated in the LITR core are given in Table 11.8. As indicated, irradiation of four experimental capsules, LM-3, LM-4, LM-5, and LCP-1, was completed, and the capsules were removed for postirradiation analysis.

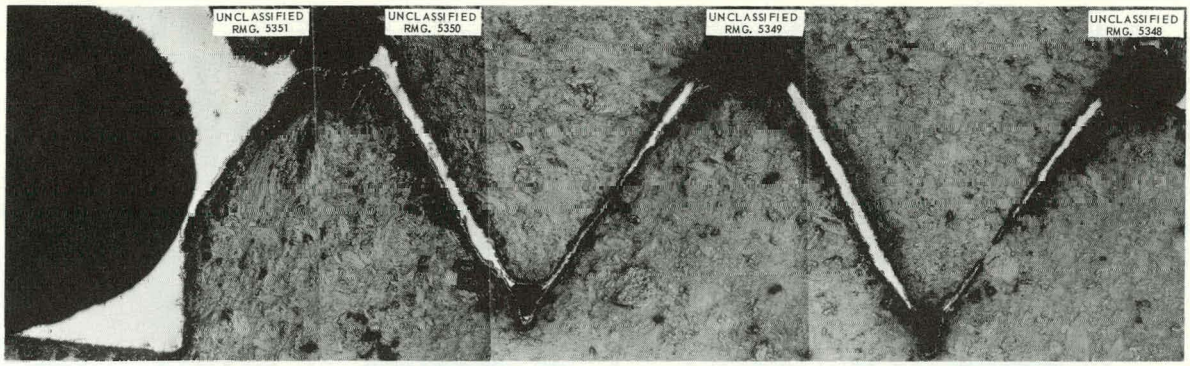

(a)

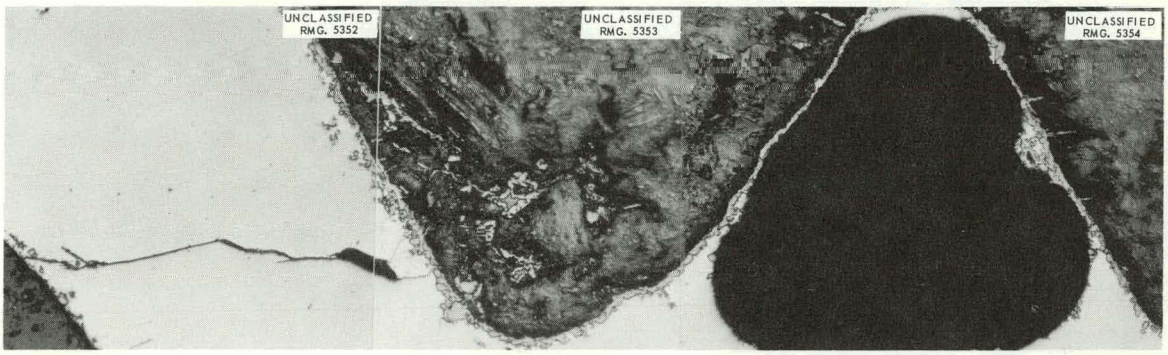

(b)

Fig. 11.18. Longitudinal Sections Through the Threaded, Silicon-Sealed Plug of Fuel Can from Capsule MTR-48-3. (a) Note roots of threads not filled with silicon. As polished. 50X (b) Additional polishing revealed hairline fracture in silicon seal. As polished. 250X

Temperature indications from the three external thermocouples (1/16-in.-diam, type 304 stainless steel-sheathed, Chromel-Alumel wires) used to measure the cladding surface temperatures of assembly LM-3 were erratic throughout the test period. The temperature indicated for the a (upper) specimen cladding increased 95°F, while the indication from one of the thermocouples on the b (lower) specimen increased 70°F and the indication from the other one in the same plane decreased 640°F. Throughout the test, the thermocouple that indicated the maximum cladding surface temperature was used for automatic control.

Both of the tungsten-rhenium thermocouples used to measure center fuel temperatures in coated-particle test assembly LCP-1 indicated a gradual temperature decline during the test period. The final temperatures were 100 to 200°F lower than at the initial temperatures.

Table 11.8. Operating Data for Miniature Fueled Capsules in LITR

Experimental Assembly No.	Fuel Composition	U^{235} Enrichment (%)	Central Fuel Temperature (°F)				Date Installed	Date Removed	Estimated Burnup
			Initial		Final				
			a Capsule	b Capsule	a Capsule	b Capsule			
LM-1	$BeO-UO_2$	20	1110	1395			10-20-60	In-pile	
LM-3	$BeO-UC_2-ThO_2$	93	1660	1895	1715	Open[a]	11-22-60	6-1-60	3.5 at. % of U + Th
LM-4	$BeO-UC_2$	50	1955	2300[b]	1900	(b)	2-8-61	7-25-61	5.1 at. % of U
LM-5	$BeO-UO_2-ThO_2$	93	1535	1900	1530	1880	4-11-61	8-22-61	3.1 at. % of U + Th
LCP-1	Pyrolytic-carbon-coated UC_2	93	1940	2120	2495[c]	1995	3-9-61	7-25-61	~8 at. % of U
LCP-2	Pyrolytic-carbon-coated UC_2	93	2355	2475			6-1-61	In pile	

[a]The central thermocouple indicated a gradual downward drift to 1860°F on 3-5-61, followed by an erratic increase to 2140°F on 3-26-61, and then failure.

[b]The central thermocouple was unreliable in operation, and failure occurred after 8 days service; the 2300°F value reported is estimated.

[c]The central thermocouple indicated a gradual downward drift to 1720°F on 6-29-61 followed by an erratic increase to 2495°F as of the date of removal.

Irradiation of a second coated-particle test assembly (LCP-2) containing loose pyrolytic-carbon-coated UC_2 spheres (~450 μ in diameter) prepared by the 3M Company was begun on June 1. The particle aggregates are contained within hollow cylindrical tantalum cans which in turn are encapsulated in an Inconel tube. The components of this test unit are shown in Fig. 11.19. A tantalum pin was used to mechanically fasten the can lid to provide for convenient hot cell disassembly and minimize the danger of damage to the irradiated particles during this step.

Specimen temperatures at the center of the tantalum can are measured by 0.072-in.-diam tantalum-sheathed tungsten-rhenium thermocouples. The b specimen central thermocouple failed shortly after startup and the a specimen central thermocouple has shown a gradual decline of 2 to 3°F per day of operation from an initial temperature of 1940°F.

A third coated-particle test assembly (LCP-3) containing pyrolytic-carbon-coated UC_2 spheres manufactured by the National Carbon Company has been designed. The loose particles will be contained in hollow cylindrical tantalum cans having dimensions suitable to provide specimen temperatures in the range 2000 to 2500°F.

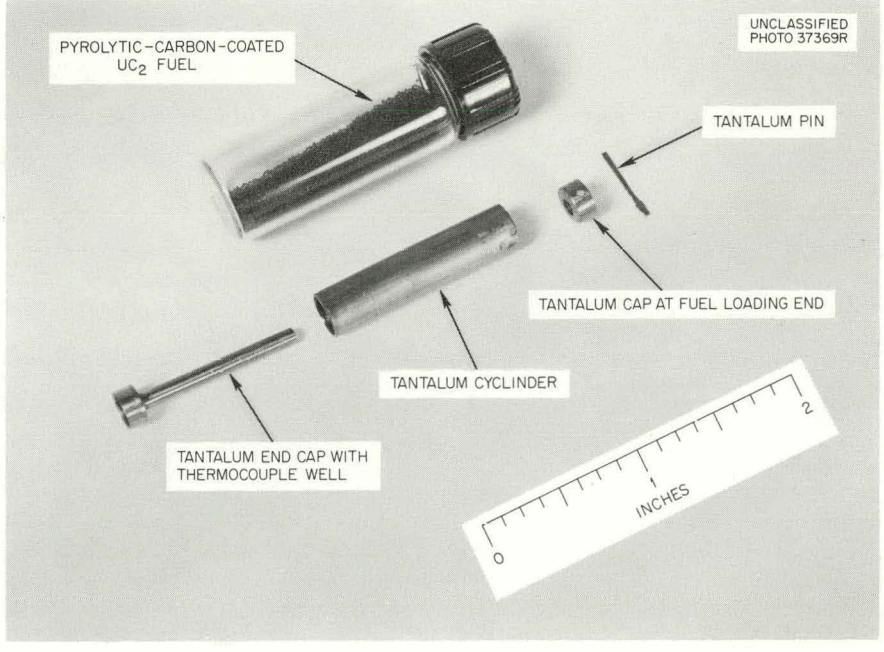

Fig. 11.19. Components of Experimental Assembly LCP-2.

MTR Irradiations (C. W. Cunningham and J. A. Conlin)

Experimental assembly MTR-48-5 containing pyrolytic-carbon-coated UC_2 particles dispersed in a graphite matrix was inserted in the MTR HB-3 beamhole on July 24 and is scheduled for operation through November 6. The test element in this assembly is similar to capsule MTR-48-2.[11] It has a single fuel cylinder 1 in. o.d. and 1.5 in. long. Unlike previous specimens, the encapsulating graphite bottle is porous, and the number of thermocouples for measuring the bottle wall temperature has been increased from three to six. Both assemblies were designed for a total fission power of 2.75 kw (140 w/cm^3) and to operate with a 1500°F wall temperature. The spherical UC_2 particles, supplied by the 3M Company, are 175 to 250 μ in diameter with 80- to 100-μ coatings. The graphite-matrix fuel cylinder and the bottle were supplied by the National Carbon Company. The fuel cylinder weighs 35.8 g and contains 2.0 g of 93% enriched UC_2 to give a U^{235} density of 0.0841 g/cm^3.

The assembly was operated in a retracted position during the first five days in-pile to obtain fission-gas-release data at low power and reduced temperatures. The fission power and central temperature are estimated to have been 1.85 kw and 1750°F, respectively, based on a measured bottle wall temperature of 1050°F. The assembly was then inserted to achieve the design conditions and an estimated 2500°F fuel central temperature.

Fission-gas-release rate data for assemblies MTR-48-2, -3, -4, and -5 are compared in Table 11.9. The data for assemblies 3 and 4 are uncertain because of possible graphite bottle leakage. Pinholes were found in specimen 3 and leaks are suspected in specimen 4. Because of the purge-gas activity, gas samples could be taken only at the conclusion of the tests, and a 14-hr delay was required for decay of activity before analyses could be made. Thus data for the short-lived fission products are somewhat inaccurate.

---

[11]GCR Quar. Prog. Rep. June 30, 1960, ORNL-2964, pp. 154–6.

Table 11.9. Fission-Gas-Release Data for Experimental Assemblies MTR-48-2, -3, -4, and -5

Experimental Assembly No.	Sampling Time (days)[a]	Estimated Fission Power (kw)	Graphite Bottle Wall Temperature (°F)	Estimated Maximum Central Temperature (°F)	Ratio of Release Rate to Birth Rate			
					Kr^{85m}	Kr^{88}	Xe^{133}	Xe^{135}
					$\times 10^{-3}$	$\times 10^{-3}$	$\times 10^{-3}$	$\times 10^{-3}$
48-2[b]	60	2.75	1500	2500	4.3	1.7	220	0.37
48-3	10	12.5	1050	2400	5.2	0.07	9.8	0.27
48-4	37	13.8	1150	2700	5.0	0.22	11	0.22
48-5	1	1.75	1050	1750	4.5	1.5	7.9	0.61
	5	1.85	1050	1750	2.4	0.49	2.7	0.74
	5	1.85	1050	1750	2.0	0.50	2.7	0.58
	13	2.75	1500	2500	2.9	1.11	4.1	0.43

[a] Days after start of test.

[b] See also Fig. 5.4, p. 128 of GCR Quar. Prog. Rep. June 30, 1961, ORNL-3166.

Chemical Processing of Coated-Particle Fuels

L. M. Ferris A. H. Kibbey

Chemical-processing methods are being developed for recovering uranium and thorium from irradiated high-temperature fuel elements containing coated fuel particles. Dissolution procedures which serve as head-end methods for decontamination and recovery of fissile and fertile material by tributyl phosphate–nitric acid solvent-extraction processes are being given first consideration, but alternative techniques, such as chloride volatility, are also being evaluated.

Three methods for processing pyrolytic-carbon-coated UC_2-ThC_2 and Al_2O_3-coated UO_2-ThO_2 fuel particles are being studied: (1) the grind-leach process in which the fuel element is mechanically ground to a fine powder to allow leaching of uranium and thorium with an acidic reagent; (2) the combustion-dissolution process in which the fuel is burned in oxygen followed by dissolution of the oxide ash in an acidic reagent; and (3) the HNO_3 leaching process in which the fuel element is disintegrated and the fuel simultaneously leached with boiling 21.5 M HNO_3.

The studies conducted thus far have indicated the following:

1. More than 99% of the uranium and thorium can be recovered from graphite-base fuel elements by leaching with fluoride-catalyzed nitric

acid if the fuel element is mechanically ground fine enough to ensure crushing of the fuel particles. This technique is applicable to elements containing either pyrolytic-carbon- or Al_2O_3-coated fuel particles.

2. Combustion in oxygen of elements containing pyrolytic-carbon-coated UC_2-ThC_2 particles, followed by dissolution of the U_3O_8-ThO_2 ash in boiling 13 M HNO_3–0.05 M HF, leads to complete recovery of the uranium and thorium if the fuel element does not contain iron as an impurity and is not coated with a refractory material such as SiC. The combustion-dissolution technique is not applicable to elements containing Al_2O_3-coated fuel particles.

3. Pyrolytic-carbon coatings are not affected by boiling 90% HNO_3 and other aqueous oxidizing agents, even when the graphite matrix is disintegrated. The HNO_3 leaching process is therefore not applicable as a processing method for elements containing coated fuel particles.

Digestion with 90% HNO_3 is being explored as a method for evaluating the integrity of coated fuel particles dispersed in graphite fuel bodies. The method appears to be applicable because sound coatings of pyrolytic carbon and Al_2O_3 are not attacked by 90% HNO_3 and other oxidizing solutions, although the graphite matrix is disintegrated to a powder. For example, boiling 3-g samples of UC_2 particles (BMI batch 16564-SP-5) having 160-μ pyrolytic-carbon coatings for 72 hr resulted in little solubilization of the uranium, as shown by the following data:

Oxidizing Solution	Amount of Uranium Leached (%)
2% HNO_3–98% H_2SO_4	0.20
5% HNO_3–95% H_2SO_4	0.25
98% H_2SO_4 saturated with $K_2Cr_2O_7$	0.15

Similar tests with General Atomic's UC_2 particles having 30- to 50-μ carbon coatings indicated that neither 90% HNO_3, 90% HNO_3–0.2% V_2O_5, nor 15 M HNO_3–5 M H_2SO_4 was effective in dissolving the carbon coatings. Except with the H_2SO_4-containing solution, where 13% of the uranium was solubilized, less than 0.5% of the uranium was leached from the particles.

In each of these experiments it is likely that the amount of uranium solubilized represents the extent to which the particles were cracked during handling and not the effectiveness of the various oxidizing solutions in dissolving the carbon coatings.

In contrast to the results cited above, uranium was apparently completely leached from irradiated graphite specimens containing carbon-coated UC_2 particles, after fission-gas-release tests (see preceding section, this chapter, on "Fission-Gas Release from Miniature Fueled-Graphite Bodies"). Each of the four cylindrical specimens (3M-P2, -P7, -P11, -P14) weighed about 0.3 g and reportedly contained 10% uranium. After two successive, 4-hr leaches with boiling 90% HNO_3, a total of about 0.3 g (~100%) of uranium was solubilized from each specimen. Uranium recoveries of less than 5% were obtained from similar specimens tested previously.[12] This difference in behavior may be due to each irradiated specimen having been heated to at least 1600°C during the fission-gas-release tests, and, consequently, enough damage to the coatings could have occurred to allow penetration of nitric acid. Since the other specimens had not been heat-treated, the particle coatings presumably remained essentially intact. Test to confirm this hypothesis are planned.

---

[12]L. M. Ferris, A. H. Kibbey, and M. J. Bradley, Processes for Recovery of Uranium and Thorium from Graphite Fuel Elements. Part II, ORNL-3186 (in press).

12. CLAD FUEL DEVELOPMENT

Beryllium-Clad Fuel Assembly Design Studies

G. Samuels R. S. Holcomb

The preliminary design of a beryllium-clad 19-element fuel assembly has been completed. The fuel element consists of 0.20-in.-i.d., 0.413-in.-o.d. UO_2 pellets contained in a 0.416-in.-i.d., 0.496-in.-o.d. beryllium tube which has six 0.040-in.-thick, 0.145-in.-high longitudinal fins twisted through 120 deg over the length of the tube. Magnesium oxide pellets are located at each end of the element to insulate the beryllium end caps from the high central temperature in the UO_2 pellets.

The 19 elements are spaced on a 0.79-in. equilateral triangular pitch by top and bottom spiders made of beryllium. The fuel-element bundle is held by the top and bottom spiders within a graphite sleeve which has a hexagonal hole with rounded corners that forms the gas flow passage. The weight of the elements is carried by the top spider resting on the graphite sleeve. The fuel element bundle is positioned within the graphite sleeve by six tabs on the top and bottom spiders which fit into slots in the sleeve. The fuel assembly is illustrated in Fig. 12.1.

The beryllium-clad fuel assembly is designed to produce 1.63 times the average channel power in the EGCR when a column of six assemblies is installed in a fuel channel. The mixed-mean exit gas temperature from the channel will be 1050°F with a flow rate of 2860 lb/hr, which is the maximum flow that can be provided with the total available pressure drop across the core.

Since the maximum channel power is only 1.36 times the average with uniform enrichment in the EGCR, the enrichment will have to be increased in the beryllium-clad fuel assembly to achieve the design power rating. The self-shielding effect causes a radial gradient in the power generation rate in the fuel element bundle that increases as the enrichment is increased. As a result of this radial power gradient, there are variations in the gas temperature and in the surface temperature between the center, intermediate, and outer rows of fuel elements. Such variations can be

UNCLASSIFIED
ORNL-LR-DWG 61919

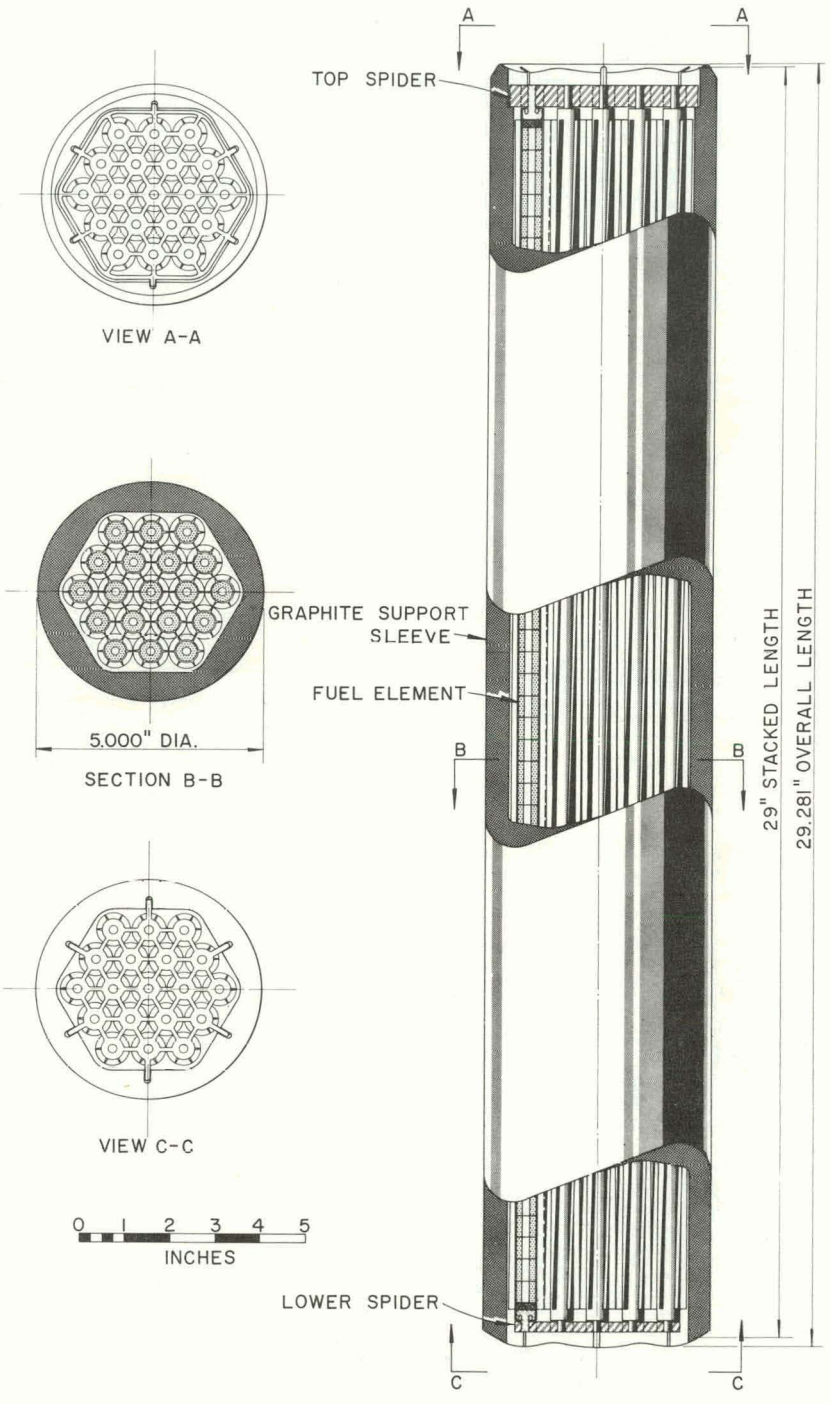

Fig. 12.1. EGCR Beryllium-Clad Fuel Assembly.

compensated for in the outer row by changing the spacing between the outer row of fuel elements and the graphite sleeve. Improvement of the temperature distribution of the intermediate row requires changing the enrichment or the fuel element pitch.

The calculated gas temperatures and fuel element surface temperatures for 3.5% and 5% enrichment are plotted in Figs. 12.2 and 12.3. The various

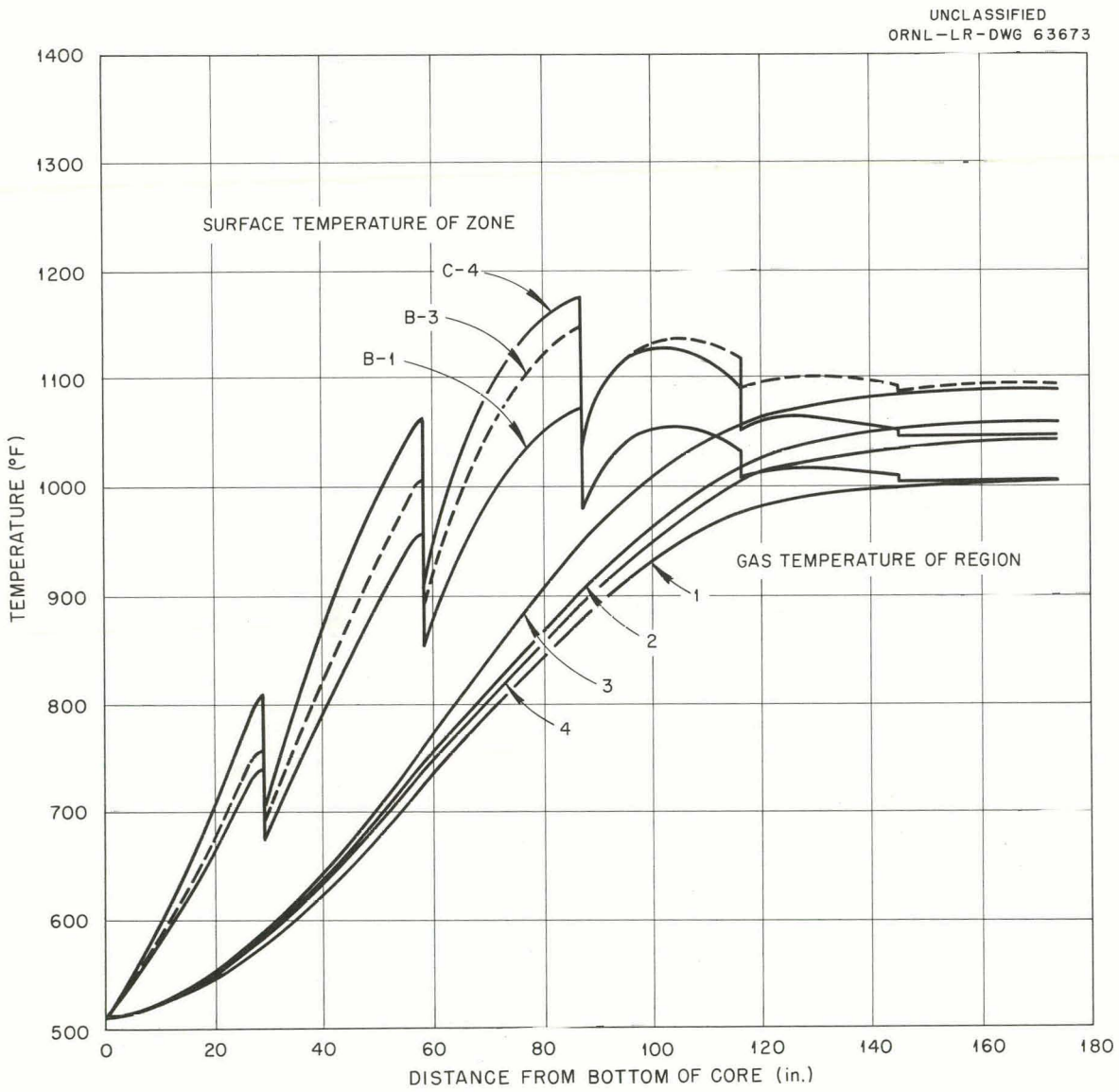

Fig. 12.2. Local Gas and Surface Temperatures of 19-Element Beryllium-Clad Fuel Assembly with 3.5% Enrichment.

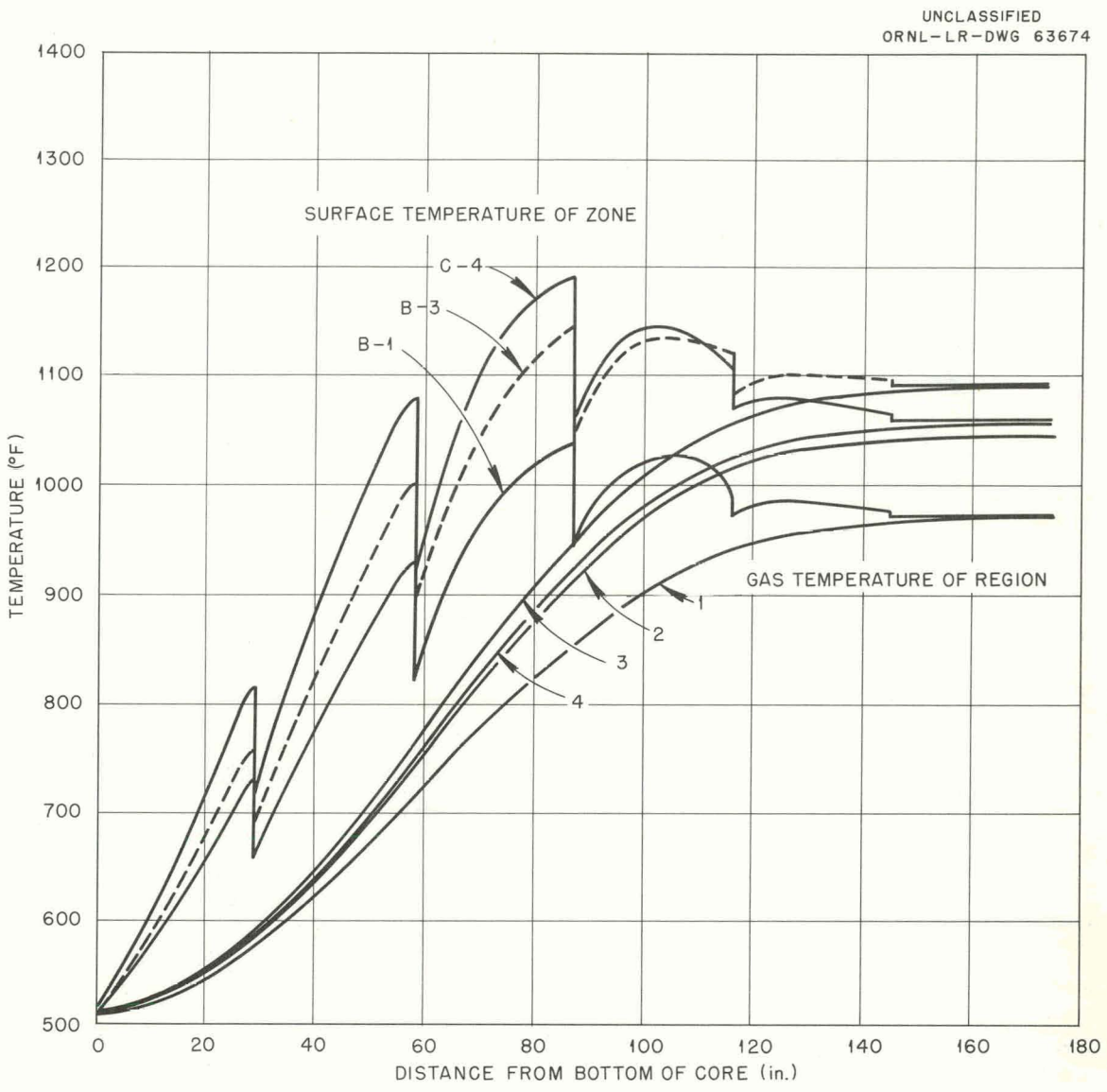

Fig. 12.3. Local Gas and Surface Temperatures of 19-Element Beryllium-Clad Fuel Assembly with 5% Enrichment.

curves refer to the designated surface area or flow region as identified in the sketch of Fig. 12.4. The calculations were made for the fixed reference design, so the temperature distribution is affected only by power variation from enrichment. It was assumed that the gas entering a particular flow region remained there and did not mix with any other gas along the entire length of the reactor. Radial heat flow was assumed in the UO_2, and

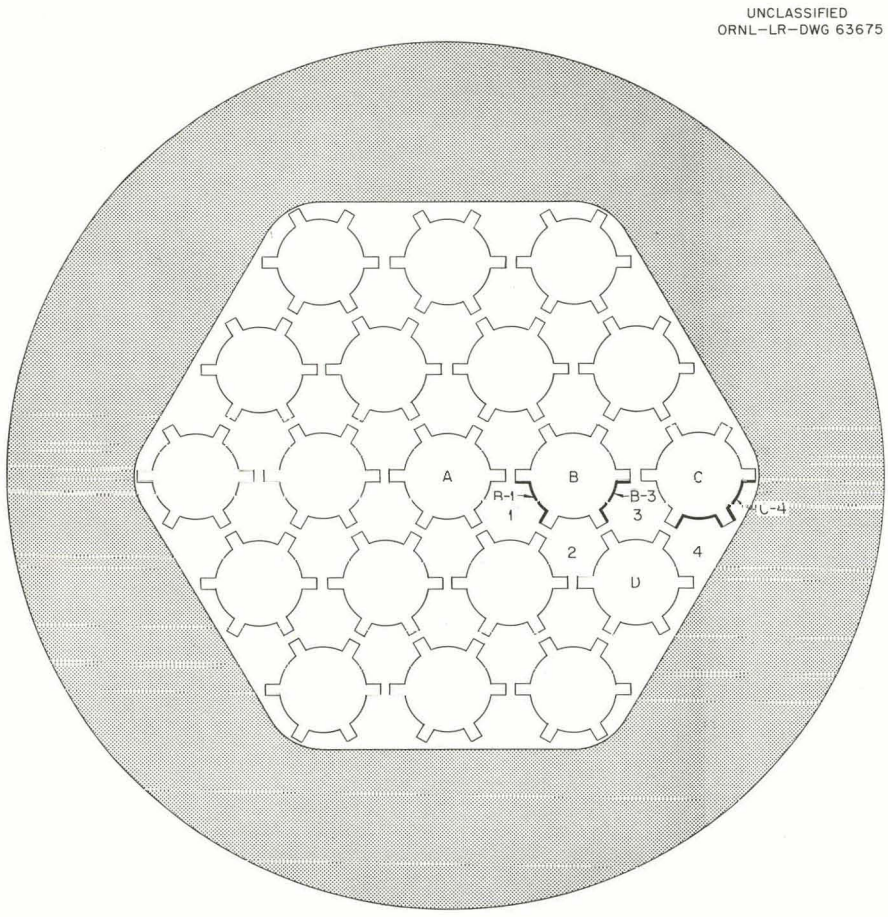

Fig. 12.4. Flow Region and Surface Zone Designation for Heat Transfer Calculations of 19-Element Beryllium-Clad Fuel Assembly.

axial conduction and circumferential conduction from one surface area to another in the beryllium tube was neglected.

In both cases, the maximum gas temperature rise occurs in region 3. The difference between the maximum and minimum gas temperature rise is 121°F for the 5% enrichment case as compared with 87°F for the 3.5% enrichment case. The maximum surface temperature occurs on surface area C-4, being 1190°F for the 5% enrichment case and 1172°F for the 3.5% enrichment case. The maximum temperature difference around a fuel element occurs on element B, being 122°F for the 5% enrichment case and 87°F for the 3.5% enrichment case.

Circumferential conduction will reduce the temperature variation around the fuel element surface, and some mixing of the gas streams should

occur between fuel assemblies. In any case, the temperature variations in the fuel assembly will be minimized by selecting a fuel channel in the high-flux region of the core in which to install the beryllium-clad fuel assembly column so that the least amount of increased enrichment will be required.

Materials Investigations

J. H. Coobs

Low-Temperature Fission-Gas Release from UO_2 (D. F. Toner, J. L. Scott)

It was reported previously that the release of Xe^{133} from sintered UO_2 at 400°C in a vacuum was dependent upon the rate of oxidation;[1] however, at 600°C, the Xe^{133} release was controlled by diffusion and was not dependent upon the rate of oxidation. In order to confirm these observations, another neutron-activation test has been run at 400°C on a sample of UO_2 designated as NUMEC 34-30. During the first 70 hr of the test, the specimen was heated in a vacuum of 1-μ Hg; for the last 30 hr, the specimen was heated in hydrogen at 1 atm. The fractional amount of Xe^{133} released during the test is plotted in Fig. 12.5 as a function of time. The sharp increase in the slope of the curve after about 62 hr is probably due to the saturation of the UO_2 by oxygen and the formation of a second phase. When hydrogen was admitted, the rate of xenon release was reduced considerably, but not to so low a value as the initial rate of release. This reduction in the rate of xenon release indicates that surface oxidation of the UO_2 is associated with the high xenon release between 62 and 70 hr.

Neutron-activation tests were run to determine the activation energy for Xe^{133} release below 1000°C in UO_2. Release measurements were made on a single fragmented pellet of NUMEC 34-30 between 500 and 1000°C in vacuum and at 400°C in hydrogen. The data were plotted as log D' versus $1/T$, as shown in Fig. 12.6, and the activation energy between 400 and

---

[1] J. L. Scott and D. F. Toner, GCR Quar. Prog. Rep. March 31, 1961, ORNL-3102, pp. 93–97.

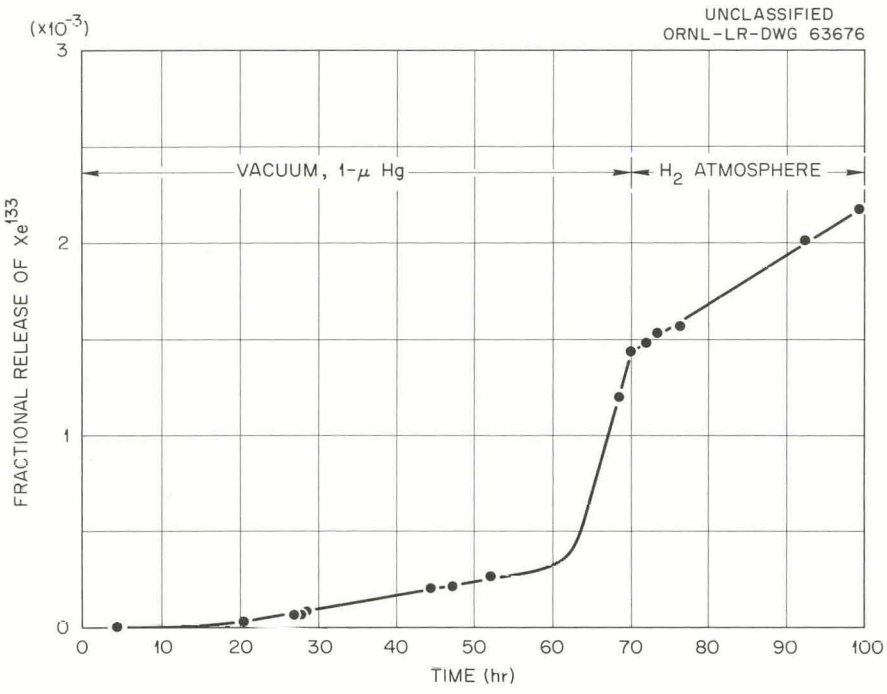

Fig. 12.5. Release of Xe^{133} from NUMEC 34-30 at 400°C in Vacuum and in Hydrogen.

800°C was calculated to be 14.7 kcal/mole. The value of D′ obtained at 1000°C is higher than indicated by the extrapolation of the data from lower temperatures; this result suggests that the mechanism by which Xe^{133} diffuses from UO_2 may be a function of the temperature range in which the process takes place. Activation energies of 70 to 80 kcal/mole have been reported by numerous investigators[2] for the range 1000 to 1600°C, and Anderson et al.[3] at Harwell observed three different activation energies in studying thoron emanation from UO_2 powder. Above 1100°C the activation energy was 81 kcal/mole; between 800 and 1100°C it was 38 kcal/mole; and below 800°C it was approximately 20 kcal/mole.

---

[2]Fission-Product Release from UO_2, Nuclear Safety, Vol. 3, No. 2 (in press).

[3]J. S. Anderson et al., The Properties and Microstructure of Uranium Dioxide: Their Dependence Upon the Mode of Preparation, AERE-C/R 886 (1954).

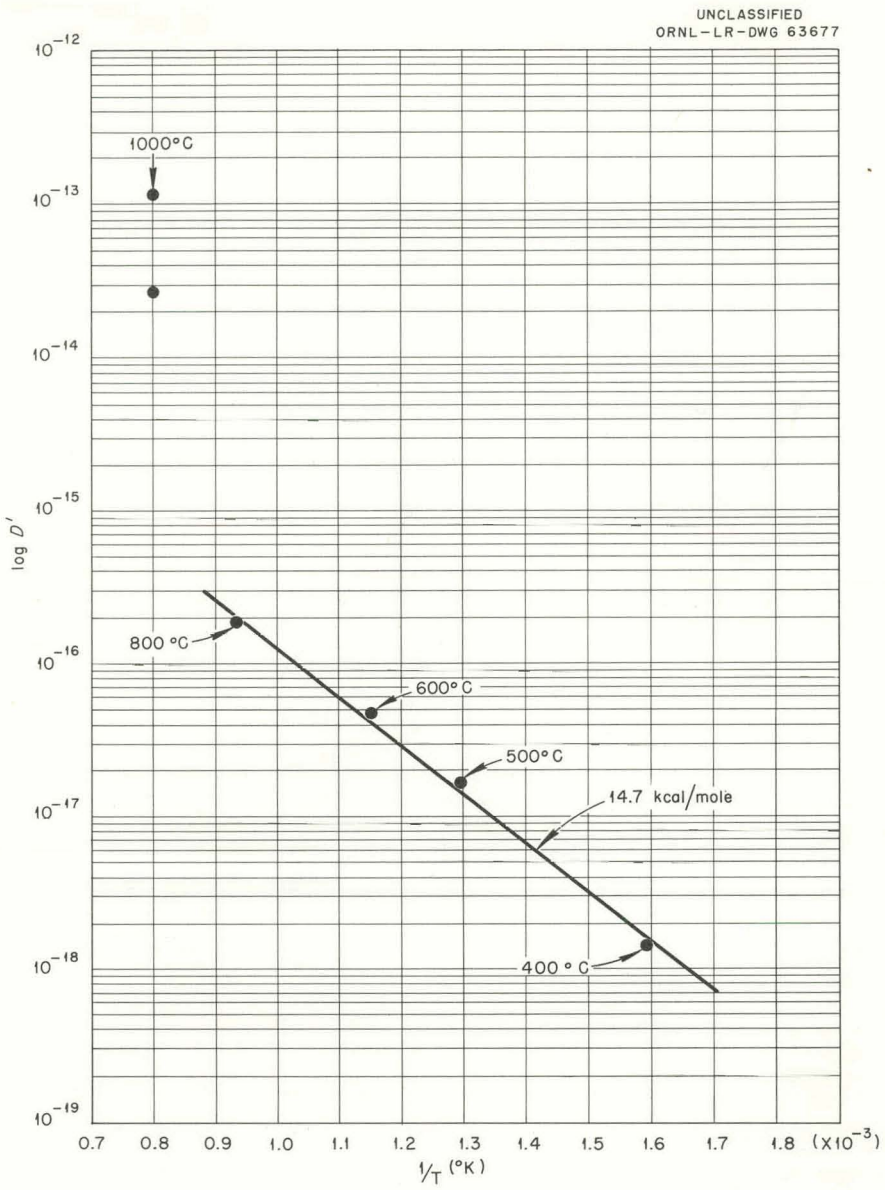

Fig. 12.6. Activation Energy for the Diffusion of Xe^{133} in UO_2.

A parallel situation has been observed with ThO_2. After a previous series of tests[4] it was reported that in ThO_2–5 wt % UO_2 the activation energy for diffusion of Xe^{133} was 75.9 kcal/mole in the temperature range 1440 to 2015°C. In pure thoria microspheres (35-μ diam) prepared by a

[4]J. L. Scott, D. F. Toner, and R. E. Adams, GCR Quar. Prog. Rep. June 30, 1961, ORNL-3166, pp. 89–91.

gel process, however, Morgan and Yust[5] found that the diffusion of O^{18} had an activation energy of 14.7 kcal/mole in the range 600 to 1400°C. The similarity of these data to those for UO_2 is not surprising, since these two compounds have the same crystal structure, form continuous solid solutions, and have the same atomic bonding.

It should be pointed out that at 800°C the D′ is at the intersection of the high and low activation-energy curves. The amount of xenon released by diffusion below 600°C is so small that large errors in D′ may occur. More tests are needed to definitely confirm a low activation energy below 800°C. It is thought that, if this low activation energy does exist, it may be associated with oxygen-ion vacancy movement.

Fabrication of UO_2 Irradiation Specimens (A. J. Taylor, J. M. Robbins)

Fabrication and inspection were completed on 250 UO_2 pellets for irradiation in GCR-ORR loop No. 1 at a heat rating of 27 000 Btu/hr·ft. These pellets are 3/8 in. in length, 0.706 ± 0.001 in. o.d., and 0.323 ± 0.005 in. i.d. The bulk densities are approximately 95% of theoretical. Metallographic examinations of these pellets revealed the presence of a discontinuous grain-boundary phase that was identified by x-ray diffraction analysis as iron-rich material containing Fe_3O_4 and alpha iron. Chemical analyses showed that the iron and silicon contents of the pellets were higher than the limit of 100 ppm specified for irradiation specimens. In the results of several analyses the iron content ranged from 110 to 294 ppm and the silicon content from 100 to 240 ppm. It was subsequently determined that the powder used in preparing the pellet was correspondingly high in iron and silicon.

A new high-temperature, continuous, hydrogen-atmosphere, sintering furnace has been installed for use in the development of techniques for fabricating ceramic components. Temperature profiles for the furnace have been obtained at hot-zone temperatures of 1400 and 1600°C using a W vs W–26% Re thermocouple, and a similar determination is in progress at 1750°C. The calibration of the thermocouple was corrected internally by visually observing through a viewing port at one end of the hot zone

[5]C. S. Morgan and C. S. Yust, Met. Div. Ann. Prog. Rep. May 31, 1961, ORNL-3160, pp. 41–42.

the thermal emf values at which samples of nickel (m.p., 1455°C) and iron (m.p., 1535°C) melted. It was established that at 1400 and 1600°C the temperatures at the extreme ends of the approximately 24-in. hot zone are not more than 15°C less than the temperature at the center.

Fabrication of Fueled BeO (R. L. Hamner)

The results of further studies made to consistently eliminate the microscopic cracking of BeO specimens containing large UO_2 particles have indicated two possible causes for this problem: (1) the release of binder residue during sintering and (2) laminations induced upon release of specimens from the forming dies.

Crack-free specimens were prepared by removing the epoxy resin binder in vacuum at 600°C prior to sintering and by reducing the angle of taper at the ejection end of the die. These specimens contained 20 vol % UO_2 as 150- to 250-μ particles and had bulk densities of 95% of theoretical. The reproducibility of the results has not been determined.

Thermal-Conductivity Studies (T. G. Godfrey, D. L. McElroy)

The thermal conductivity of 93.4% dense UO_2 in the temperature range 27 to 195°C was determined in the radial heat flow apparatus described previously.[6] The results are listed in Table 12.1. These results, together with prior experience,[6] indicate a precision of ±2% and an accuracy of ±5%. The corrected values are approximately 20% below those reported by Kingery et al.[7] but are in good agreement with recent work by Howard and Gulvin.[8]

Dispersion-Strengthened Fe-Al-Cr Alloys (B. King)

Methods for the preparation of dispersion-strengthened oxidation-resistant materials are being studied. A review of possible methods for

---

[6]GCR Quar. Prog. Rep. June 30, 1961, ORNL-3166, pp. 78–83.

[7]W. D. Kingery, J. Francl, R. L. Coble, and T. Vasilos, J. Am. Ceram. Soc., 37(2): 107–10 (1954).

[8]V. C. Howard and T. F. Gulvin, Thermal Conductivity Determinations on UO_2 by a Radial-Flow Method, IG Rep.-51 RD/C. UK-AEA, Culceth (Feb. 1961).

Table 12.1. Thermal Conductivity of UO_2 in the Temperature Range 27 to 195°C

Temperature[a] (°C)	Thermal Conductivity,[b] k (w/cm·°C)	
	Measured	Corrected to Theoretical Density
27	0.0732	0.0784
55	0.0674	0.0722
77	0.0660	0.0707
81	0.0656	0.0702
91	0.0648	0.0694
107	0.0640	0.0685
122	0.0634	0.0679
154	0.0608	0.0651
174	0.0596	0.0638
195	0.0582	0.0623

[a]Average specimen temperature.

[b]Values reported represent averages of 24 measurements, 12 based on absolute and 12 on differential determinations.

producing a fine dispersion of Al_2O_3 in a matrix of an alloy of 7 wt % Al, 5 wt % Cr, and the balance Fe has indicated that consolidation of surface-oxidized powders is feasible and is potentially an economical technique. Attempts are being made to prepare master alloy powders having the required high specific surface, proper oxidation behavior, and suitable base-metal composition. Three methods of preparing these powders are being investigated: (1) mechanical fragmentation of alloys containing 12 and 16% Al together with 5 to 10% Cr and the balance Fe, (2) mechanical fragmentation of a 58% Fe—38% Al—4% Cr alloy, followed by leaching with NaOH to remove excess aluminum and leave an alloy with 12% Al and 6% Cr that will contain 50% voids and has a high surface-to-volume ratio, and (3) spontaneous disintegration by the reaction $Al_4C_3 + 6\ H_2O \rightarrow 3\ CH_4 + 2\ Al_2O_3$ of alloys made up of 48% Al, 4% Cr, 1.5% C, and the balance Fe or 32% Al, 4% Cr, 1.5% C, and the balance Fe. The powdered material produced

by method 3 will be leached with NaOH to dissolve excess aluminum and produce a porous structure. The results of preliminary experiments indicate that the first method will be difficult to carry out; however, the latter two methods show considerable promise.

Experimental Tube-Burst Tests (J. T. Venard)

A correlation of tube-burst data on type 304 stainless steel at 1300, 1500, and 1600°F has been made using the Dorn parameter[9] and plotting σ versus $t_r e^{-Q/RT}$, where σ is the tangential stress, t_r the time to rupture, Q the activation energy, R the gas constant, and T the temperature in °K. The activation energy, Q, was found to be 110 000 cal/mole. The stress-rupture curves for 1100, 1300, 1500, and 1600°F predicted from this relation are shown in Fig. 12.7, along with the available experimental data. It may be seen that the experimental results correlate closely with the Dorn parameter for short rupture times (<1000 hr) but the experimental results deviate from linearity at longer times and the fit is somewhat negated.

Beryllium Corrosion (W. J. Werner)

A series of samples is presently being prepared for electron-microscopy studies of the films formed on Brush Beryllium Company hot-extruded tubing during exposure to approximately 4 vol % water vapor in flowing helium at 650°C. Sample preparation included the grinding of a longitudinal flat on the outer surface of each specimen for comparison with the ground surface of the original tube.

The reaction rate curve obtained in the exposure test for samples 1, 2, and 3 is shown in Fig. 12.8, and the limits of the presently available data for samples 4, 5, and 6 are indicated. Rate curves for the reactions of high-purity Pechiney flake beryllium powder with wet CO_2 and with wet helium at 650°C are also shown in Fig. 12.8 for comparison. In neither of the tests with Pechiney flake material was there a "break-away" reaction. The major differences between the two materials are the purity,

[9]R. L. Orr, O. D. Sherby, and J. E. Dorn, Correlation of Rupture Data for Metals at Elevated Temperatures, Trans. ASM, 46: 113–28 (1954).

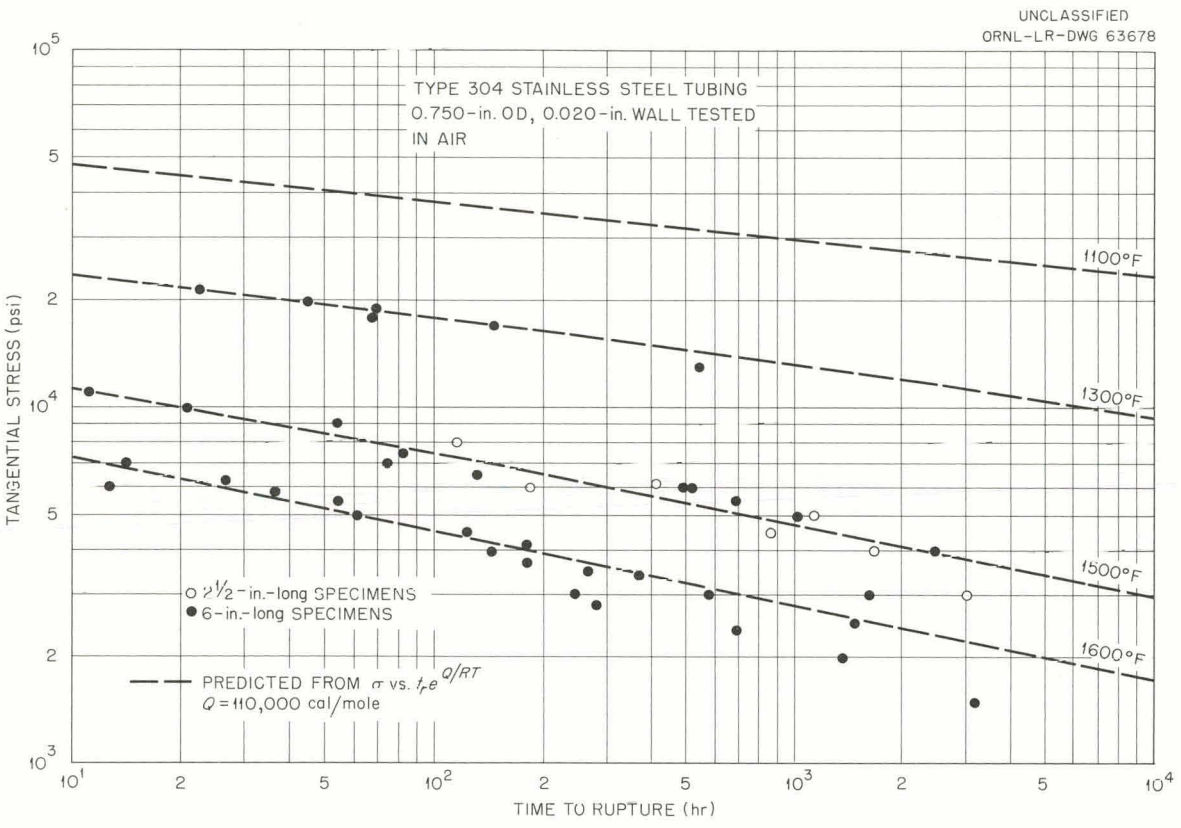

Fig. 12.7. Comparison of Tube-Burst Data with Stress-Rupture Curves Predicted by Use of the Dorn Parameter.

the orientation, and the relative absence of grain boundaries in the flake material as compared with the hot-extruded material. The chemical compositions of the two materials are compared in Table 12.2.

Beryllium Tubing Evaluation (R. W. McClung, C. V. Dodd)

Two hundred feet of 0.300-in.-o.d., 0.040-in.-wall beryllium tubing in 1-ft lengths was received from Imperial Chemical Industries, Ltd., for evaluation. The nondestructive evaluation tests used included fluorescent penetrants, low-voltage radiography, pulse-echo and resonance ultrasonics, eddy currents, and air gaging.

The penetrant technique revealed a few, shallow, scattered pinholes on all the tubing and two tubes with deep cuts or cracks. The radiographic procedure revealed the presence of numerous fine high-density

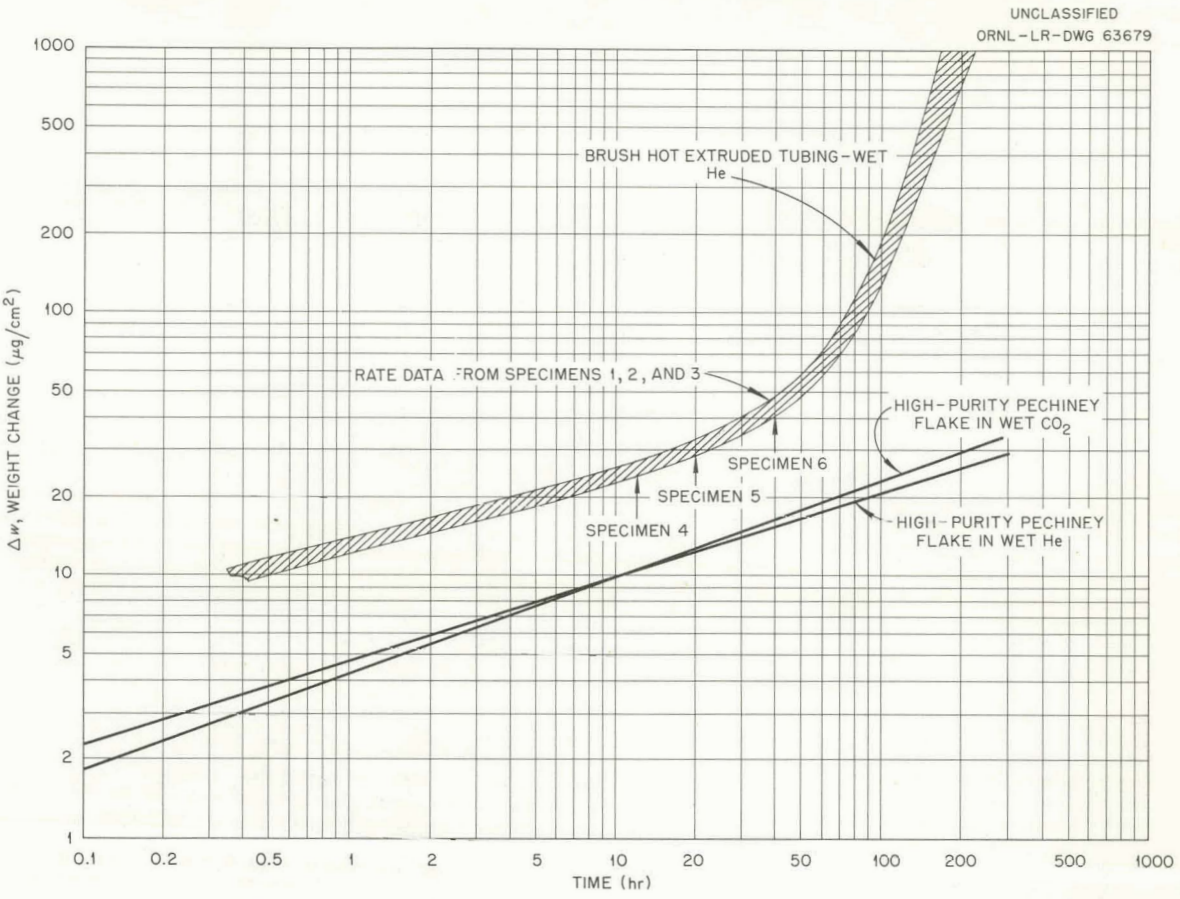

Fig. 12.8. The Reaction Rates of Beryllium in Wet He and Wet CO_2 at 650°C. Water vapor content of gas was approximately 4 vol %.

particles in less than half of the tubes. Approximately 12% of the tubes contained streaks or areas of high-density material. About half the tubing contained detectable extrusion marks in varying degrees. Most of these were rather shallow. Pits, gouges, or other localized conditions of wall thinning were observed in about 6% of the tubes.

Two of the 200 tubes were rejected by the pulse-reflection ultrasonic technique because of the presence of crack-like indications. These were the same two tubes in which cuts or cracks were found by penetrant examination.

The eddy-current technique was used with a longitudinal reference standard notch 0.006 in. deep and 0.250 in. long. Indications of suspected

Table 12.2. Results of Chemical Analyses of High-Purity Pechiney Flake Beryllium Powder and Brush Hot-Extruded Beryllium Tubing

Impurity	Impurity Analysis (ppm)	
	Pechiney Flake Beryllium Powder	Brush Beryllium Hot-Extruded Tubing
Fe	≤80	1300
Si	6	450
Mn	1	
Mg	≤1	100
Al	≤20	650
Cu	≤1	110
Ni	?	160
Ag	<0.2	2
Cr	<10	100
C	<90	1200–1300
Cl	~80	
BeO	200	15 400

discontinuities were compared with the indication from the reference defect. Two tubes were found to contain indications comparable to the reference standard, but, on the basis of the eddy-current examination, this is the best beryllium tubing that has been received.

Wall thickness variations were measured over the entire tubing length by the resonance-ultrasonic technique. Six tubes failed to comply with the specified thickness of 0.040 ± 0.008 in. Many of the tubes were near the minimum allowable thickness, and the six tubes mentioned above were only slightly below tolerance. The air-gage technique was used on randomly selected samples to measure variations in the inside diameter. The minimum and maximum were 0.3001 and 0.3036 in., respectively. The maximum inside diameter variation in any single tube was 0.0027 in.; the minimum was 0.0002 in. These nondestructive evaluation results show this tubing to be among the best that has been examined to date.

Destructive Evaluation of Discontinuities in Beryllium Tubing
(R. W. McClung, J. R. Weir)

Attempts are being made to correlate the results of nondestructive evaluation of small-diameter beryllium tubing with the destructive test

data.[10] A re-evaluation has been made of recorded data from eddy-current examination of 0.300-in.-i.d., 0.040-in.-wall tubing from Pechiney, the Chesterfield Tube Company, and the Brush Beryllium Company. Much of the tubing that exhibited discrete rejectable indications was then re-examined with eddy currents to locate the suspected defect accurately. Low-voltage radiographic examinations of these marked areas were made to obtain further information concerning the nature of the discontinuities. Pits, gouges, extrusion marks, and high-density particles were found in well over one-half of the tubes. At present it is not known whether the eddy-current indications were caused by the high-density particles or by some discontinuity that was not detected by radiography.

The defective areas have been further evaluated by the measurement of wall thicknesses by the resonance-ultrasonic technique. The tubing is now being fabricated into appropriate tube-burst capsules for destructive testing.

Welding of Beryllium (R. G. Gilliland)

A joint design similar in geometry to that used for fabricating beryllium tube-burst test specimens[11] is being studied for use in making end closures in beryllium tubing. The results of tests of such edge welds made using the tungsten-arc and the electron-beam welding processes are presented in Table 12.3. Preliminary evaluation of the room-temperature shear data indicates that the conventional tungsten-arc welding process produces stronger welds than does the electron-beam process. Specimens have also been prepared for shear-strength tests at 600°C.

Thermal-cycling tests were also performed on welds of the types of beryllium listed in Table 12.3. Beryllium tubes 0.300 in. i.d. with 0.040-in. walls were closed at one end with a tungsten-arc weld and were subjected to approximately 500 thermal cycles. The test conditions included a temperature change of 1000°F with a maximum temperature of 1380°F. A

[10]GCR Quar. Prog. Rep. June 30, 1961, ORNL-3166, pp. 115–6.

[11]GCR Quar. Prog. Rep. Dec. 31, 1960, ORNL-3049, pp. 233–4.

Table 12.3. Results of Room-Temperature Shear Tests on End-Closure Welds of 0.300-in.-i.d., 0.040-in.-Wall Beryllium Tubing

Tube Fabrication Method	Vendor	Ultimate Shear Strength (psi)	
		Tungsten-Arc Welded Joint	Electron-Beam Welded Joint
Machined from hot-pressed block	Brush Beryllium	25 700	21 000
Machined from hot-extruded rod	Brush Beryllium	24 400	20 000
Machined from warm-extruded rod	Brush Beryllium	26 000	16 100
Warm extruded to size	Brush Beryllium	22 300	19 400
Machined from hot-pressed block (0.15% C)	Brush Beryllium	27 700	17 600
Hot impact extruded	Pechiney	24 400	24 600
Hot extruded to size	Chesterfield	21 700	13 000
Extruded to size	Imperial Chemicals Industries	20 900	19 900

complete thermal cycle required 1 hr. The results of the tests were encouraging in that all the welded joints were helium leaktight after this rather severe thermal cycling. Radiographic and metallographic evaluation of these joints is currently under way.

Irradiation Effects Studies

Beryllium-Clad UO_2-Fueled Capsules (J. G. Morgan, M. F. Osborne, H. E. Robertson)

Six beryllium-clad UO_2-fueled capsules that were irradiated in the ORR (group III) were examined. Capsule fabrication and operating data for these capsules are summarized in Table 12.4.

Table 12.4. Fabrication and Operating Data for ORR-Irradiated Beryllium Capsules

Capsule No.	Fabricator	Average Outside Diameter (in.)		Pellet Enrichment in U^{235} (%)	External Pressure (psi)	Average Cladding Temperature[a] (°F)	Burnup[b] (Mwd/MT)
		Beryllium Can	UO_2 Pellets				
02-3	ORNL	0.594	0.513	1.82	450[c]	1048	2750
03-3	CEA	0.591	0.512	0.71	300[c]	1114	2350
04-3	CEA	0.592	0.516	0.71	450[c]	1072	2250
05-3	AEA	0.383	0.299	2.42	300	1140	3150
06-3	AEA	0.381	0.298	2.42	300	1112	2500
07-3	ORNL	0.380	0.299	2.42	300	1084	2300

[a]The design cladding temperature was 1112°F.

[b]Burnup calculated from previous experiments.

[c]Capsules 02-3, 03-3, and 04-3 began operation at 150 psi and the pressure was increased in 75-psi increments at one-month intervals to the indicated value.

Each capsule, after removal from its irradiation facility tube, was gamma scanned, dimensioned, drilled for fission-gas removal, and then cut open. Individual UO_2 pellets were measured and weighed where possible, and immersion density determinations were made in some cases. Samples of UO_2 were selected for radiochemical burnup analysis. Sections of beryllium tubing, end-cap weld areas, Be-UO_2 interfaces, and UO_2 pellets were mounted for metallographic examination.

Visual examination disclosed no obvious changes in five of the capsules, but one, capsule 05-3, had a circumferential break in the weld area at the bottom end cap, as shown in Fig. 12.9. Capsule 06-3 was shown by bubble testing to have at least two small leaks. The fission-product contamination of the NaK heat transfer bath surrounding each capsule confirmed the leakage.

Gamma scans indicated fairly uniform burnup along the capsules, with the exception of capsule 05-3 (see Fig. 12.10), which apparently suffered a 50% flux depression at the top end, probably due to faulty positioning of a cadmium shutter used in deliberate thermal cycling. In some cases, it was possible to distinguish each individual pellet, in addition to large gaps between pellets, by the small minima on the gamma-scran curve, as shown in Fig. 12.11.

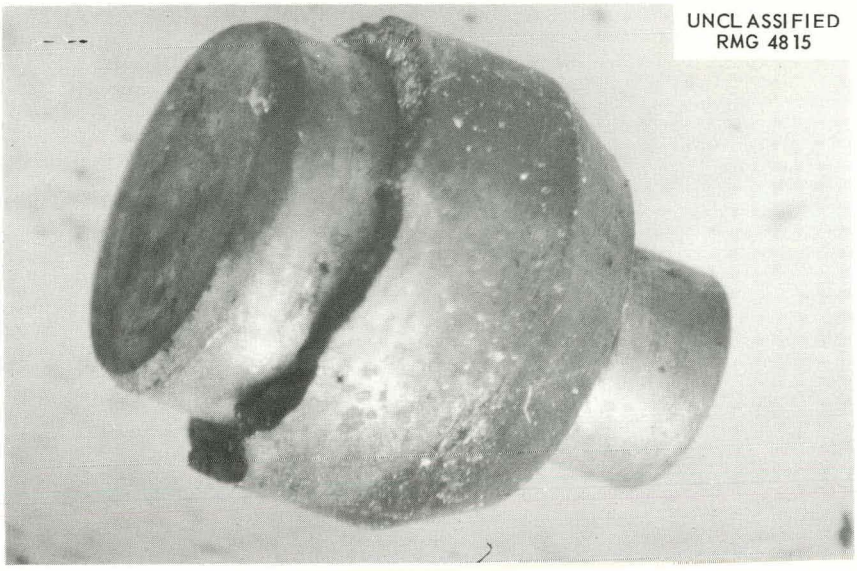

Fig. 12.9. End Cap From Beryllium-Clad Capsule 05-3 Showing Break in Weld Area. 7X

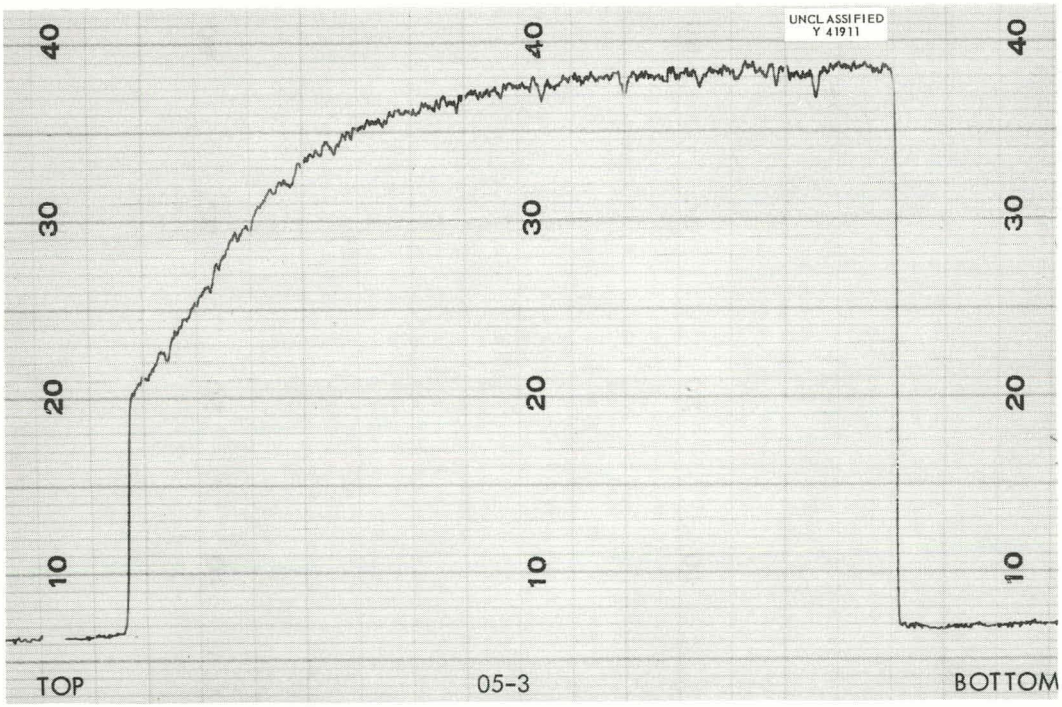

Fig. 12.10. Gamma Scan of Capsule 05-3 Showing Flux Depression Near Top End.

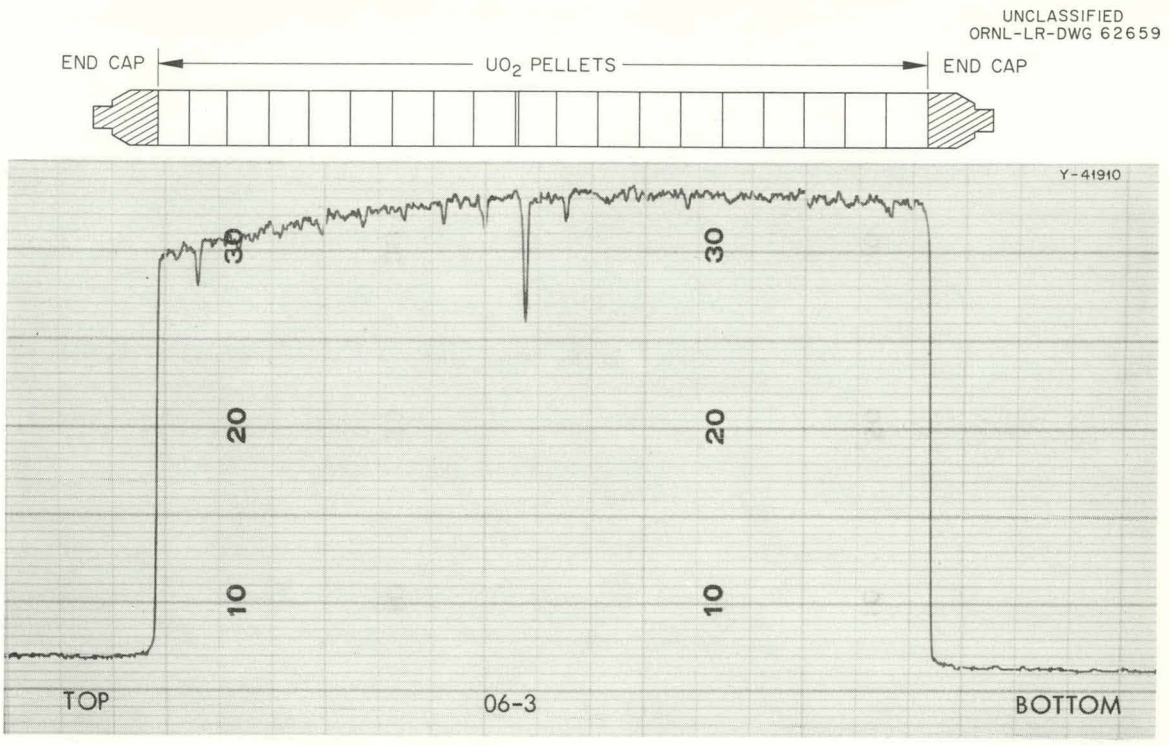

Fig. 12.11. Gamma Scan of Capsule 06-3 Showing Correlation with Fuel Pellet Position.

Significant changes were found in capsule dimensions, as shown in Table 12.5. All capsules had a general increase in diameter that reached a maximum near the center. Points of maximum bowing were in general not the same before and after irradiation. As expected, capsule 05-3 (the one with the broken end cap) had the largest dimensional changes. The only capsule on which accurate length measurements were made, capsule 06-3, showed a length decrease of 0.024 in.

Each capsule was drilled, and the contained gases were collected in an evacuated system. No gas was collected from the two capsules known to have leaked, and in addition no fission gas was found in capsule 04-3. It could not be determined whether this was due to an undetected leak or to a malfunction of the gas-collection system. The fission-gas release data, presented in Table 12.6, are consistent with data from similar previous experiments.

Table 12.5. Beryllium Capsule Dimensional Data

Capsule No.	Average Diameter (in.)		Maximum Change (mils)	Maximum Bow (mils)		Maximum Eccentricity (mils)	
	Before Irradiation	After Irradiation		Before Irradiation	After Irradiation	Before Irradiation	After Irradiation
02-3	0.5937	0.5944	+2.9	2.0	10.4	1.0	2.0
03-3	0.5912	0.5924	+3.6	10.7	18.4	1.6	2.0
04-3	0.5918	0.5923	+2.1	11.0	11.1	4.4	5.0
05-3	0.3825	0.3874	+9.2	9.1	33	1.0	4.0
06-3	0.3806	0.3828	+5.2	6.5	12.1	3.4	2.3
07-3	0.3804	0.3826	+3.6	0.6	5.9	0.2	1.5

Table 12.6. Release of Kr^{85} and Xe^{133} from UO_2 Irradiated in Beryllium Capsules

Capsule No.	Calculated Central UO_2 Temperature (°F)	Kr^{85} Release (%)	Xe^{133} Release (%)
02-3	~3000	0.12	0.01
03-3	~3000	0.34	0.05
07-3	~2000	0.32	0.05

Mass spectrometer analyses of the gases showed the presence of an unusually high hydrogen concentration, about 42%, in capsule 02-3. Since the capsules were filled with purified helium, it was assumed that this hydrogen evolved from the UO_2 during high-temperature irradiation. The UO_2 had been sintered in H_2, and the subsequent degassing may have been inadequate.

The capsules were disassembled by making circular cuts near the ends and longitudinal cuts over the central sections with a high-speed abrasive slitting wheel. One of the slit capsules and two of the pellets removed from that capsule are shown in Fig. 12.12. At least one pellet was removed intact from each capsule, except capsule 02-3, and the dimensions of the pellets were measured where possible. Small increases of up to about 1% were observed in 34 measurements. One exception, a length decrease of 0.4%, was probably due to measurements being made at different positions on an

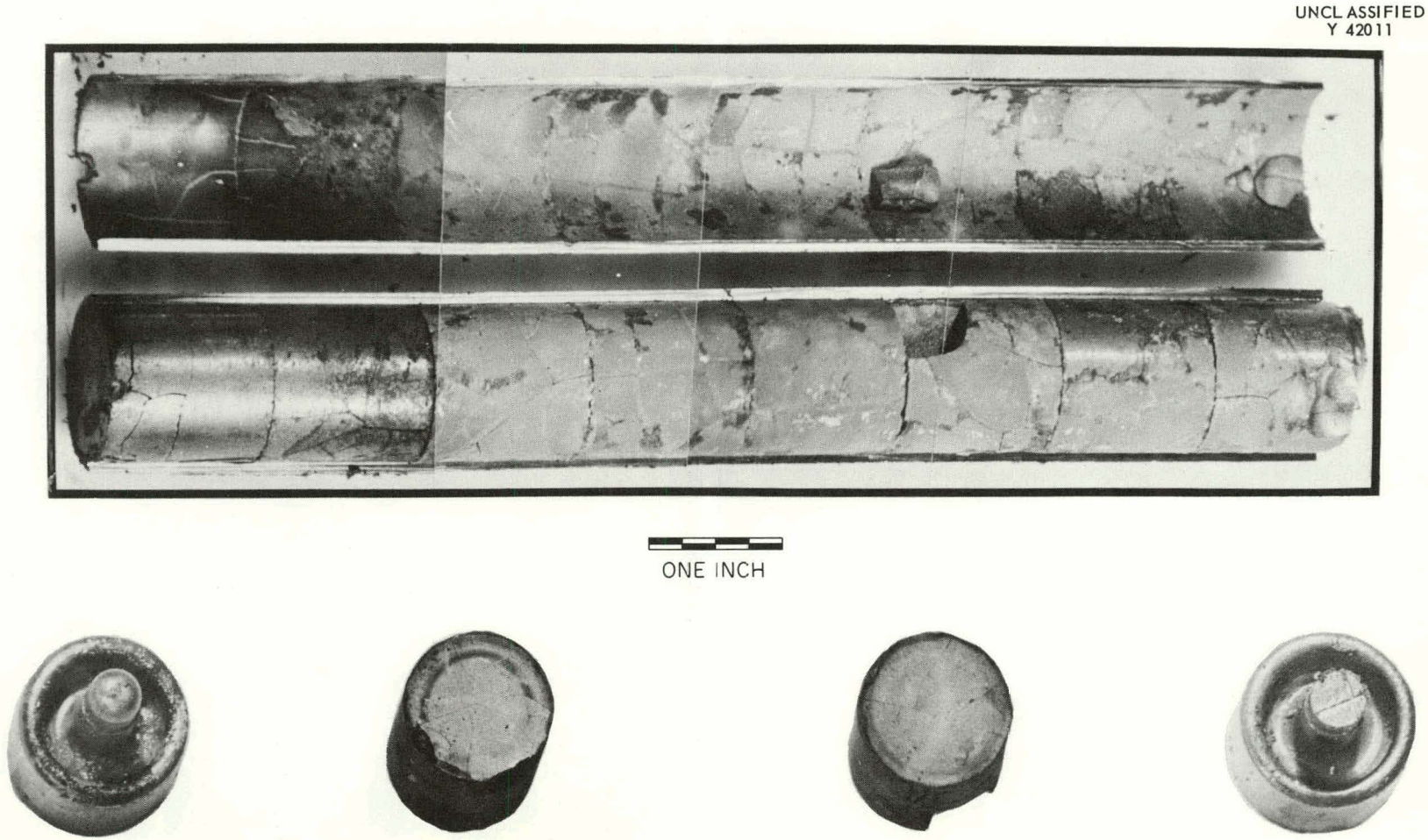

Fig. 12.12. Capsule 04-3, As Opened, Showing Cracked Pellets and End Caps.

asymmetrical pellet. The immersion density was determined for two pellets from each of capsules 05-3, 06-3, and 07-3. Small increases of about 0.5% were measured in all cases. This is in good agreement with data from similar previous experiments. The increases in dimensions combined with the increases in immersion density seem to indicate that the very small cracks in the UO_2 pellets, as may be seen in Fig. 12.12, expose some of the originally isolated voids as well as increase the bulk volume.

When an attempt was made to open capsule 02-3 in the described manner, one end cap broke off and the central portion of the beryllium can shattered, as shown in Fig. 12.13. This indicated that this beryllium capsule was under considerably more stress than any of the other five capsules. Similar behavior has been reported as a result of heat treatment under very high external pressure (the order of 60 atm) in the absence of irradiation.[12]

[12]M. Stobe, French CEA, personal communication.

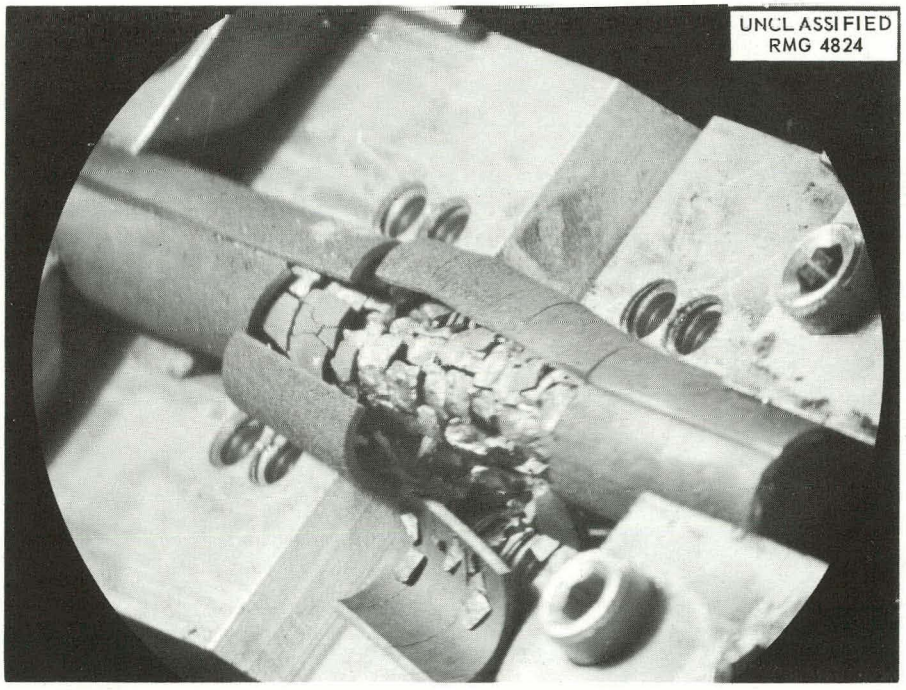

Fig. 12.13. Capsule 02-3 Showing Center Section that Shattered After a Partial Cut Had Been Made.

Both capsules 05-3 and 06-3 were found completely filled with NaK, indicating that leaks had developed during operation, since both a high pressure and thermal cycling would be required to force NaK throughout the capsules. Preliminary metallographic examination of the beryllium cladding has shown corrosion on both the inner and outer surfaces. Complete metallographic examination of all capsule components is under way.

BeO-UO_2 Pellets (J. G. Morgan, M. F. Osborn, H. E. Robertson)

Postirradiation examinations were conducted on the first of a series of irradiated capsules containing small hollow pellets consisting of 70 vol % BeO and 30 vol % UO_2. These samples had densities 92% of theoretical and were sealed in helium. The top, a section, operated at an average central temperature of 1900°F. The bottom, b section, operated at 2350°F. After irradiation all eight fuel pellets were intact, with no excessive cracking. Length and outside diameter measurements were made on each of the pellets, except one, which was prepared for metallographic examination. There was a general increase in dimensions, as shown in Table 12.7. The fission-gas release, listed in Table 12.8, was lower than that experienced with pure UO_2.

Beryllium (J. R. Weir)

Swelling data for beryllium irradiated to a neutron dose of 3.6×10^{20} neutrons/cm^2 (>1 Mev) have been obtained at 650 and 700°C on specimens manufactured by various techniques and having various compositions. The results of these measurements are shown in Table 12.9. Since the error in measurement of the density is probably ±0.2%, there is no conclusive evidence for composition-dependent swelling within this range of neutron exposure and temperature.

These results along with results obtained from previous irradiation experiments are summarized in Fig. 12.14. Two data points were deleted from this figure as it appeared in a previous report[13] because these data points, which showed 3.5 and 5.5% swelling, were in error as a result of

[13]GCR Quar. Prog. Rep. March 31, 1961, ORNL-3102, pp. 204–7.

Table 12.7. Dimensions of $BeO-UO_2$ Fuel Pellets of Capsule LM-2

Section	Pellet No.	Length (in.)		Change in Length (%)	Outside Diameter (in.)		Change in Outside Diameter (%)
		Preirradiation	Postirradiation		Preirradiation	Postirradiation	
Top, a	1–2	0.2484	0.2485	0	0.1562	0.1570	0
	2–4	0.2493	0.2535	+1.6	0.1560	0.1565 0.1570	<1
	3–7	0.2507	0.2595	+3.5	0.1565	0.1595 0.1585	+1.6
	4–9	0.2490	0.2525	+1.4	0.1560	0.1575 0.1575	+1
Bottom, b	8–16	0.2501	0.2565	+2.5	0.1565	0.1595 0.1595	+2
	6–11	0.2492	0.2575	+3.3	0.1558	0.1595 0.1595	+2.4
	5–10	0.2495	0.2535	+1.6	0.1561	0.1585 0.1585	+1.5

Table 12.8. Kr^{85} Release from UO_2-BeO Samples Irradiated in Capsule LM-2

Section	Average Central Temperature (°F)	Burnup (Mwd/MT of U)	Kr^{85} Released (%)
a	1900	41 000	0.5
b	2350	41 000	0.5

Table 12.9. Swelling Results for Beryllium Irradiated to a Neutron Dose of 3.6×10^{20} neutrons/cm^2 (>1 Mev)

Specimen	Specimen Composition Other than Beryllium	Specimen Configuration	Irradiation Temperature (°C)	Density Change (%)
1	3.75 wt % BeO	Sheet	700	−0.5
2	3.75 wt % BeO	Sheet	650	−0.2
3	1.7 wt % Be_2C	Sheet	650	−0.2
4	1.7 wt % Be_2C	Sheet	700	−0.2
5	1.2 wt % BeO	Rod	700	−0.4
6	1.2 wt % BeO	Rod	700	−0.7
7	0.6 wt % BeO	Block	700	−0.8
8	1.2 wt % BeO	Sheet	700	−0.4

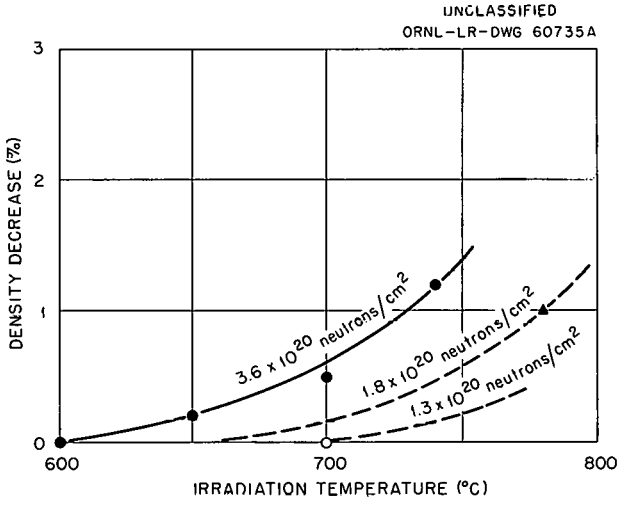

Fig. 12.14. Swelling of Beryllium Under Irradiation at Elevated Temperatures.

inability to remove the low-density corrosion products from the specimens prior to postirradiation density measurement.

Several in-pile stress-rupture experiments have been performed to investigate the relation of the integrated flux to the effect of irradiation on the stress-rupture strength of beryllium tubing. The manner in which these experiments are performed was described previously.[13] The results obtained thus far are summarized in Fig. 12.15. The fractional decrease in 100-hr rupture strength is plotted as a function of the integrated flux at 100-hr rupture time. The points on the figure represent data obtained at 600 and 700°C on tubing machined from hot-pressed beryllium (HPT), on warm-extruded tubing (WET), and on Pechiney tubing (PT). The equation representing the data from 600°C tests of hot-pressed tubing is

$$\Delta_{100} = 5.37 \times 10^{-14} \phi_I^{0.628} , \qquad (1)$$

where

$$\Delta_{100} = \frac{\sigma_{100}^{0} - \sigma_{100}^{\phi I}}{\sigma_{100}^{0}}$$

σ_{100}^{0} = 100-hr rupture stress in absence of irradiation,

$\sigma_{100}^{\phi I}$ = 100-hr rupture stress under irradiation after integrated flux (>1 Mev) of ϕ_I.

There is considerable scatter in the results at 700°C from both in-pile tests and the out-of-pile tests. It is believed that some of this scatter has been due to corrosion of the beryllium by small amounts of impurities in the argon or helium environment used in testing. Specimens tested at 600°C generally exhibit a thin protective oxide layer which should not affect the results significantly.

Inconel (W. E. Brundage, N. E. Hinkle, W. W. Davis, J. C. Zukas)

A second experimental assembly containing ten tube-burst specimens of "boron adjusted" heats of Inconel was operated in the poolside facility of the ORR. The time-to-rupture data obtained are listed in Table 12.10.

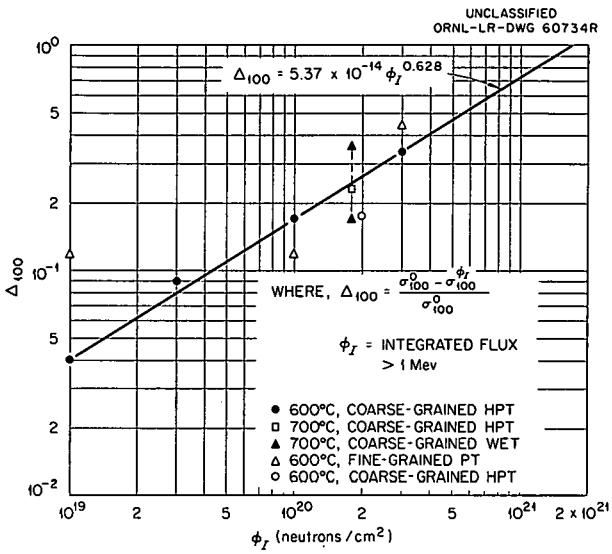

Fig. 12.15. Effect of Irradiation on the Stress-Rupture Properties of Beryllium.

These data substantiate the results previously reported[14] for these materials. When analyzed with respect to B^{10} concentration, however, the results do not show any supporting trend for the proposed damage mechanism; namely, that the rupture strength of Inconel is impaired by the helium generated during thermal-neutron bombardment of the B^{10}. The boron concentration, enrichment, and distribution are being investigated in order to aid in the analysis of these data.

Beryllium Oxide (G. W. Keilholtz, J. E. Lee, Jr.)

Beryllium oxide specimens irradiated in the ETR are being studied to obtain information on the stability of BeO under irradiation conditions.

[14]GCR Quar. Prog. Rep. June 30, 1961, ORNL-3166, p. 162.

Table 12.10. Effect of Neutron Bombardment on the Stress-Rupture Characteristics of "Boron Adjusted" Heats of Inconel Tested at 1500°F in Air

Material	Boron Content	Specimen No.	Stress (psi)	Time to Rupture (hr)
0B	<10 ppm, natural boron	29-8	4500	252
		29-3	3700	666
2B	20 ppm, natural boron	29-5	4500	151
		29-9	4000	123
10B	100 ppm, natural boron	29-2	4500	98
		29-6	3750	186
6B11	60 ppm, 98% B^{11}	29-1	3500	339
		29-7	3000	684
6B10	60 ppm, 95% B^{10}	29-4	3250	372
		29-10	2600	360

The cylindrical specimens were encapsulated in stainless steel and mounted in an annulus through which a mixture of argon and helium was circulated for temperature control during irradiation. Six experimental assemblies containing 63 specimens have been irradiated. The specimens from assemblies 1 through 5 have been examined, and assembly 6, which contains the largest specimens, including several unclad samples, has been partially disassembled.

Integrated fast neutron exposures in the range 1×10^{20} to 2×10^{21} neutrons/cm^2 were obtained with specimens 1 in. long and 0.4 to 1.1 in. in diameter at exposure temperatures from 100 to 1000°C. Serious deterioration of BeO specimens, ranging from fracture to disintegration into powder, has been observed.

The greatest damage appears in bodies irradiated to high neutron doses at low temperatures. Specimens irradiated at 110°C powdered at a dose of 1.5×10^{21} neutrons/cm^2. Specimens irradiated at 444°C to a dose of 1.1×10^{21} neutrons/cm^2 and at 737°C to a dose of 1.6×10^{21} neutrons/cm^2 remained intact. Specimens irradiated at 827 to 950°C to a dose of 2.1 to 2.6×10^{21} neutrons/cm^2 fractured.

Changes in linear dimension of up to 4% have been found. X-ray diffraction measurements revealed changes in the c-lattice parameter of up to 7×10^{-3} $\Delta c/c_o$ for material irradiated at 110°C but only 1 to 2×10^{-3} $\Delta c/c_o$ at 444 to 1025°C. The $\Delta c/c_o$ value appeared to saturate at a dose of 3×10^{20} neutrons/cm^2 in the higher temperature range. All temperatures above 444°C appeared equally effective in suppressing the $\Delta c/c_o$ value. Changes in the a-lattice parameter were smaller by a factor of 7.

Voids 0.1 to 0.3 μ in diameter that were not in the original material were found by electron microscopy in the interior of the grains and at grain boundaries. No evidence of chemical decomposition was observed. Radial temperature differences during irradiation increased by 50 to 100%, indicating a decrease in thermal conductivity.

The gases produced by transmutation were assayed after dissolving the specimens in molten salt. The tritium content of BeO irradiated at 110°C increased with neutron dosage; 6.4 parts of tritium per million parts of BeO were recovered from specimens irradiated to 2.1×10^{21} neutrons/cm^2. Specimens irradiated above 440°C contained much less tritium. Helium was

retained by the BeO even at irradiation temperatures of 1025°C. The helium content of the BeO increased linearly with fast irradiation dosage at a rate of 205 microliters per gram of BeO per 10^{21} neutrons/cm^2.

The cause of the observed changes cannot be determined with certainty from these experiments. The hypothesis that thermal stress alone is responsible for failure is rejected because the changes occur gradually over the irradiation period. It appears that atomic displacements or gas generation or some combination of these is the primary cause of failure.

It is probable that, for maximum life in a reactor, BeO bodies should be at temperatures above 400°C and that temperatures well above this figure are preferable. Physical deterioration of many of the specimens tested was such as to make the material unsuitable for use; however, the survival of some specimens after an exposure of 1.6×10^{21} neutrons/cm^2 at about 750°C suggests that conditions exist under which BeO may be used. It is clear that continued study of several experimental variables will be required before BeO moderators for long-lived reactors can be designed with confidence.

The next BeO irradiation test assembly, No. 7, is scheduled for insertion in the ETR in October 1961. Fabrication of the hardware is essentially complete and final assembly is currently in progress. This assembly will provide for irradiation of 48 specimen pellets, 0.800 in. in diameter and 0.50 in. thick. Forty of these pellets are of high-density material prepared at ORNL using cold pressing and sintering techniques. Eight pellets of similar size of high-density BeO material prepared by a hot-pressing technique and single crystals of pure BeO will also be included in the assembly. Beryllium oxide has a theoretical density of 3.02; the cold-pressed material density is 96% of theoretical and the hot-pressed material density is 92% of theoretical. Both are classified as high-density material. The irradiation temperatures will be 650, 950, and 1100°C at a peak fast-neutron flux of the order of 1 to 2×10^{14} neutrons/cm^2·sec.

A new arrangement of the temperature and dose rate variables has been designed which provides for exposure of high-temperature samples to a low flux and low-temperature samples to a high flux. This should permit an

evaluation of the temperature-annealing effects in relation to the neutron-flux effects.

Preliminary design work on experimental assembly No. 8 is also in progress. This assembly is to provide for irradiation of approximately 100 cylindrical pellets 1/2 in. in diameter and 1/2 in. long and approximately 200 pellets 1/4 in. in diameter and 1/4 in. long. These will be installed in four multiple-capsule columns that can be extracted from the core separately to allow large variations in the neutron dose. The pellets will be of more than one density and grain size and will be irradiated at two or more temperatures in the flux gradient of the reactor on a statistically designed arrangement. Irradiation of these specimens will require a major expansion of the experimental control equipment at the reactor site. The design work on this instrumentation has been completed.

13. DESIGN STUDIES OF ADVANCED POWER PLANTS

Preliminary Designs for Four Integrated Gas-Cooled Reactor Core and Steam-Generator Units

A. P. Fraas

Conceptual designs for four gas-cooled reactor plants have been prepared to investigate the possibility of reducing capital costs by exploiting the advantages of all-ceramic fuel elements. All four of these plants were designed to produce 500 Mw of electricity, and in all four the steam generator was placed directly above the reactor so that the two could be housed in a common pressure vessel. This arrangement gives a compact unit and reduces the cost of the pressure vessel, ducts, shield, and containment vessel.

A new type of axial-tube steam generator well suited to this basic configuration has been evolved. This can be designed to take advantage of the higher gas system pressures and temperatures to effect major reductions in the size and cost of the steam generator.

The most promising of the four designs is the HGCR-5, shown in Fig. 13.1. In comparing this with the large British CEA plants it was found that the weight of such important items as the pressure vessel, the graphite, and the steam generators is lower in the new design by a factor of about 10. The volume of the reactor building and the concrete in the shielding have been reduced by a similar factor. A comparison of the HGCR-5 with pressurized-water reactor and boiling-water reactor plants shows that the weight of steel required for the pressure vessel, the containment shell, and the steam generator can be reduced by factors of 3 or more. A comparison of the HGCR-5 with a modern coal-fired steam plant indicates that the weight of steel in the pressure vessel, the containment shell, and the steam generator is about one-third that required for the boiler portion of the coal-fired plant, and the building volume is reduced by a similar factor. A comparison of the HGCR-5 with the GCR-2 and the EGCR indicates that major savings in the weight and cost of the pressure vessel, steam generator, shield, and containment vessel can be effected through the use of all-ceramic fuel elements as opposed to stainless steel-encapsulated UO_2 fuel elements.

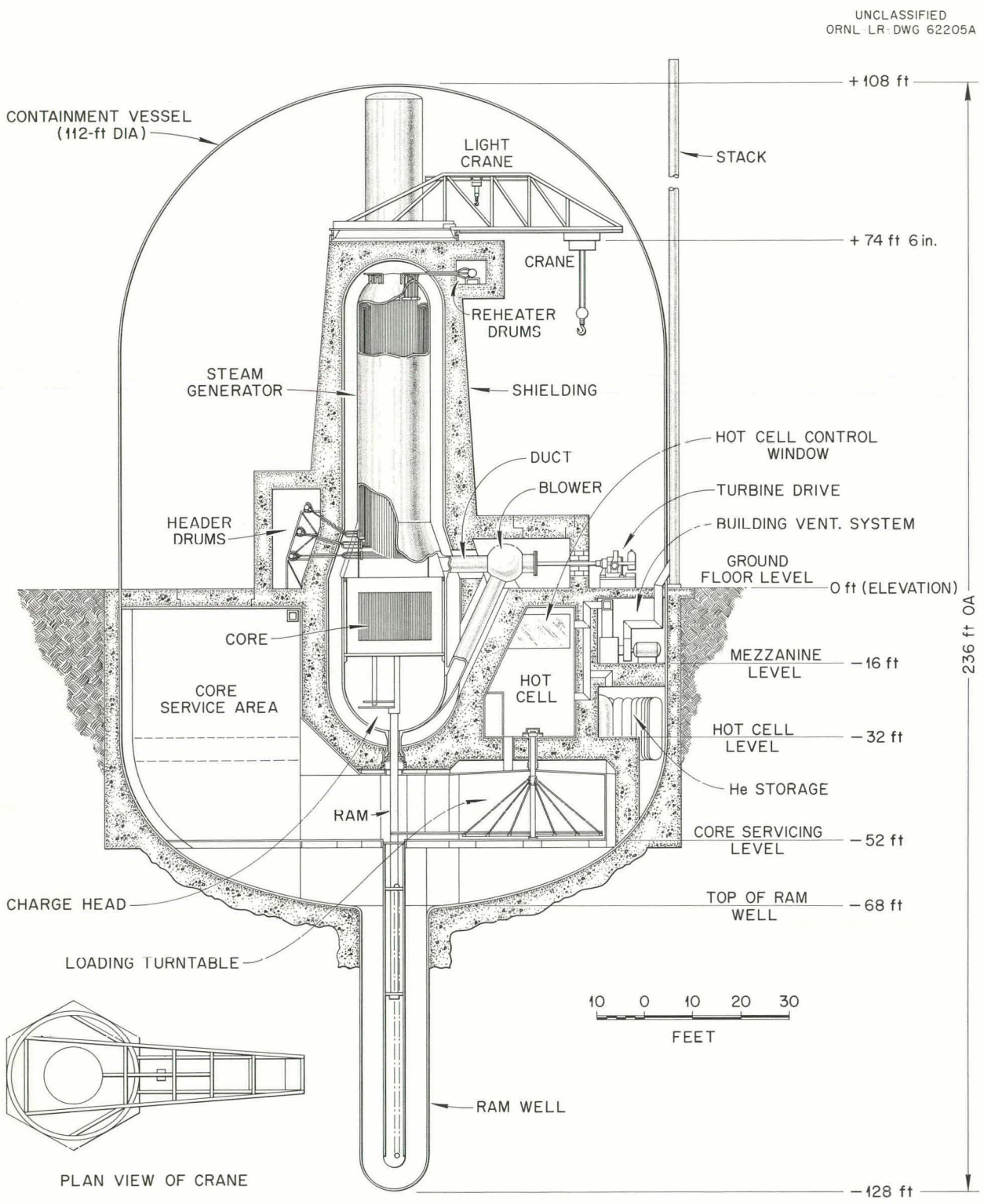

Fig. 13.1. HGCR-5 Reactor Elevation.

In the detailed report on this design study,[1] many of the design considerations associated with the evolution of the four designs are presented, together with discussions of fuel handling, maintenance, and hazards problems, particularly those associated with leakage from a high-pressure gas system containing roughly 100 000 curies of activity. The difficulty of coping with these problems on paper and the need for a reactor experiment such as the PBRE are emphasized.

Steam Generators for High-Temperature Gas-Cooled Reactors

A. P. Fraas M. N. Ozisik M. M. Yarosh

An analytical approach and an IBM machine code were prepared for the design of once-through steam generators for gas-cooled reactors for both axial-flow and cross-flow tube matrices. The codes were applied to investigate the effects of steam generator configuration, tube diameter, extended surface, type of cooling gas, gas and steam temperature and pressure conditions, and the pumping power-to-heat removal ratio on the size, weight, and cost of the steam generators.

The results indicate that the size and cost of steam generators can be reduced by increasing the gas system pressure and temperature. For gas system pressures and temperatures over 300 psi and 1100°F, mounting the tubes axially in the shell and directing the gas axially over the tubes yields smaller and less-expensive units than can be obtained with conventional cross flow over banks of serpentine tubes. With the axial-tube configuration there appears to be no great incentive to increase the gas system pressure above about 500 psi, and increasing the gas temperature above about 1250°F would entail a sharp increase in costs because stainless steel would have to be used rather than chrome-molybdenum steels.

For high-temperature high-pressure gas systems, the least expensive and most promising unit considered employs axial gas flow over 0.5-in.-diam bare U-tubes arranged with their axes parrallel to that of the shell. This

---

[1]A. P. Fraas, Preliminary Designs for Four Integrated Gas-Cooled Reactor Core and Steam-Generator Units, ORNL-2752 (to be published).

configuration is well suited to the installation of a reheater and can be built with conventional fabrication techniques. In the detailed report on this design study,[2] charts are presented to facilitate preliminary design calculations for a wide variety of steam generators for gas-cooled reactor applications.

A Comparison of Gas-Turbine and Steam Power Plants for Use with All-Ceramic Gas-Cooled Reactors

A. P. Fraas M. N. Ozisik

The most promising of the conceptual designs of gas-cooled reactors coupled to steam power plants, the HGCR-5, has been used as the point of departure for the preparation of a conceptual design for a gas-turbine plant.[3] The same basic reactor, fuel-handling system, and containment shell have been employed.

The first portion of the study was concerned with the design of suitable heat exchangers. Charts were developed for the cost and effectiveness of regenerators as functions of the principal design parameters. These were used to determine the effects of gas-turbine-cycle parameters on the cost of the major components of the plant. The results indicate that the most promising of the gas-turbine plants evolved would cost more than half again as much as the corresponding steam plant and would yield a net thermal efficiency about 75% of that for the steam plant. Since the reactors are basically similar, the capital charges and fuel cycle costs would be correspondingly higher for the gas-turbine plant.

Maintenance problems posed by a contaminated-gas system appear to be far more serious for the gas turbine and compressor than for the gas-circulating blower of the corresponding steam plant. Regeneration reduces the gas temperature rise through the reactor and increases the gas flow

---

[2]A. P. Fraas, M. N. Ozisik, and M. M. Yarosh, Steam Generators for High-Temperature Gas-Cooled Reactors, ORNL-3208 (to be published).

[3]A. P. Fraas and M. N. Ozisik, A Comparison of Gas Turbine and Steam Power Plants for Use with All-Ceramic Gas-Cooled Reactors, ORNL-3209 (to be published).

rate so that the compressor and turbine are larger in diameter, as well as over 10 times as long, as the circulating blowers. Not only is the surface area exposed to the contaminated gas greater, but the initial temperature drop in the gas system occurs in the turbine rather than a heat exchanger, and hence the amount of fission-product activity deposited in the turbine appears likely to be about 100 times greater than in a circulating blower. Further, the casing for the gas turbine would have to be split on the horizontal centerline, whereas the blower rotor assembly could be removed through a single circular flange separated from the hot portion of the casing by a heat dam. Thus the leaktightness problem would be far more difficult in the gas turbine. Further, the much greater complexity of the duct system for the gas turbine presents more severe thermal expansion problems, which inherently reduce the integrity of the gas-system pressure envelope relative to that for the steam system.

14. EXPERIMENTAL INVESTIGATIONS OF HEAT TRANSFER AND FLUID FLOW

H. W. Hoffman

Resistance-Heated-Tube Heat-Transfer Experiment

G. J. Kidd, Jr.

Initial experiments with the model 4 heat-transfer apparatus[1] have been completed. Circumferential temperature distributions as a function of axial distance along the cluster were obtained for all seven tubes of the downstream cluster at a Reynolds modulus of 54 000 and an average heat flux of 6610 Btu/hr·ft^2 with the upstream cluster unheated. (Heat fluxes for tubes 1 and 2 were ~4% above the mean; for tubes 3 and 5, ~1% below the mean; for tubes 6 and 7, ~2% below the mean; and for tube 4, ~3% below the mean.) The calculated mean circumferential heat-transfer coefficients are presented in Fig. 14.1. The curve for the peripheral tubes represent the average of the data for the six outer tubes; the gross discrepancy was 5%. The shift in the relative positions of the peripheral and central tube curves for the upstream and downstream sections of the cluster is attributed to a redistribution of flow between the inner and outer portions of the channel as the gas stream passes the mid-cluster spacer. This result is in agreement with previously reported conclusions based on the gas-mixing studies.[2]

An investigation of the cause of the discrepancies in heat generation between the several tubes of the cluster disclosed that tubes 1 and 2 were connected to the electrical power supply so that the current in these tubes was 180 deg out of phase with the current in the remaining tubes. Since the tubes constituting the cluster (as well as the power leads to these tubes) are in close proximity and carry high-amperage currents, this phase variation may have generated sufficient interaction

---

[1]GCR Quar. Prog. Rep. June 30, 1961, ORNL 3166, pp. 63–67.

[2]GCR Quar. Prog. Rep. March 31, 1961, ORNL 3102, pp. 87–88.

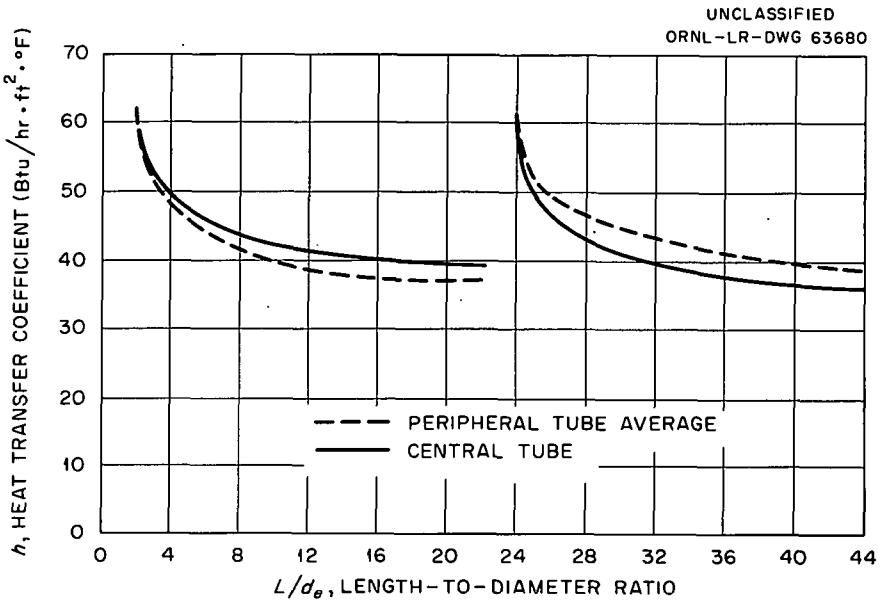

Fig. 14.1. Axial Variation of Heat-Transfer Coefficient in Downstream Cluster of Model 4 Apparatus. Series 4-1 experiments; nonuniform power; average heat flux of 6610 Btu/hr·ft^2; Reynolds modulus of 54 000.

between the electrical circuits to cause the observed heat-generation variation. This situation has been corrected by rewiring the apparatus. A second error source was eliminated by replacing the low-impedance voltmeter (11.1 ohms) used in the series 4-1 experiments by a precision high-impedance (10 megohm) vacuum-tube voltmeter.

Tests were then made (series 4-2) with a uniform power indication for all tubes. Circumferential temperature measurements at $L/d_e = 35$ indicate that there now exists substantial agreement (±0.75%) in the mean surface temperatures for the peripheral tubes (see Table 14.1).

Detailed temperature probing of the cluster (at 14 axial locations for all seven tubes) has been initiated for a uniform heat generation rate of 6500 Btu/hr·ft^2 and a Reynolds modulus of 54 000. This set of experiments is termed series 4-3. Measurements have been completed for tube 6; the data are presented in the form of the heat-transfer coefficient in Fig. 14.2. The results agree closely with the average peripheral-tube values for the nonuniform heat generation case (see Fig. 14.1); the series 4-3 data fall ~4% above those of series 4-1. The asymptotic Nusselt

modulus ($N_{Nu,\infty}$ = 122), with thermal properties evaluated at the bulk fluid temperature, corresponds to that calculated using a Dittus-Boelter correlation for "long" tubes.

Table 14.1. Comparison of Mean Surface Temperatures for Peripheral Tubes at L/d_e = 35

Tube No.	Mean Surface Temperature (°F)	
	Series 4-1	Series 4-2
1	324.5	285.7
2	322.8	285.5
3	291.8	288.7
4	291.6	287.8
5	294.8	286.4
6	291.4	284.4

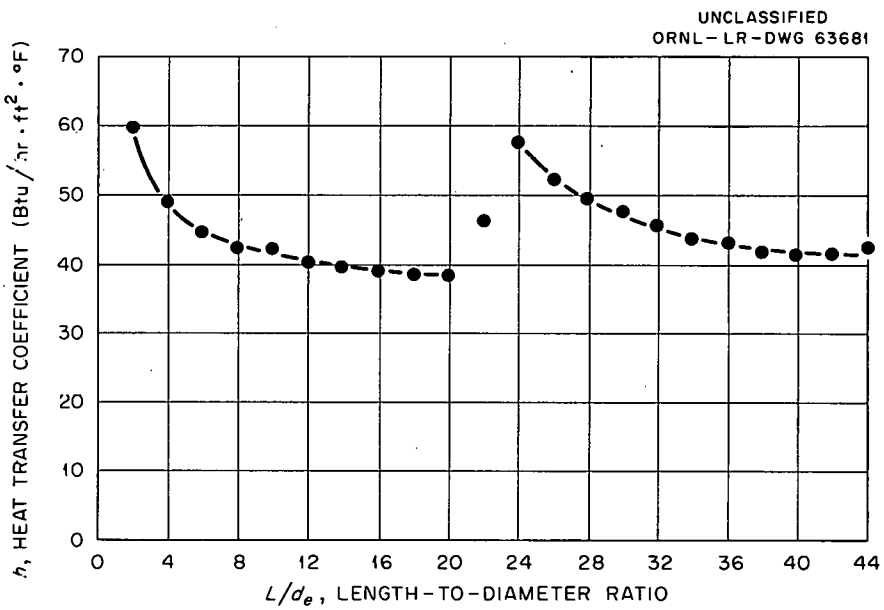

Fig. 14.2. Axial Variation of Heat-Transfer Coefficient for Tube 6 of Downstream Cluster of Model 4 Apparatus. Series 4-3 experiments; uniform power; average heat flux of 6500 Btu/hr·ft^2; Reynolds modulus of 54 000.

Unified Correlation for Heat and Mass Transfer in EGCR-Type Clusters

H. H. Sogin[3]

The experimental results for heat and mass transfer in models of EGCR clusters lead to the conclusion that entrance-region conditions prevail over essentially the entire length of the clusters.[4] Since entrance-region heat (or mass) transfer inside tubes has been successfully treated from the viewpoint of boundary-layer growth on a flat plate, it seems reasonable to suggest a similar approach for the situation of flow outside tubes. Thus, using as the characteristic length in the transport parameters (Reynolds, Nusselt, Sherwood moduli) the distance from the channel entrance (or from the point of initiation of the specific transfer process), the correlating equations take the form

$$N_{Nu,x} = \frac{qx}{\Delta t_x k} = N_{Re,x}^{n} \, f(N_{Pr}) \qquad (1)$$

for heat transfer, and

$$N_{Sh,x} = \frac{mx}{\Delta \rho_x D_v} = N_{Re,x}^{n} \, g(N_{Sc}) \qquad (2)$$

for mass transfer. In Eqs. (1) and (2), q and m are the heat and mass flux (in Btu/hr·ft^2), respectively; Δt_x is temperature difference (in °F) and $\Delta \rho_x$ is density difference (in lb/ft^3) evaluated at the position x (ft); N_{Nu} is the Nusselt modulus and N_{Sh} is the Sherwood modulus defined by Eqs. (1) and (2); N_{Pr} is the Prandtl modulus; k is the thermal conductivity (in Btu/hr·ft·°F); N_{Re} is the Reynolds modulus based on the length x; and N_{Sc} (the Schmidt modulus) is the ratio of the diffusivity of momentum (kinematic viscosity) to the diffusivity of mass, D_v (in

---

[3]Summer research participant.

[4]GCR Quar. Prog. Rep. Sept. 30, 1959, ORNL-2835, p. 57; GCR Quar. Prog. Rep. Sept. 30, 1960, ORNL-3015, p. 59.

ft^2/hr). Rewriting Eqs. (1) and (2) [with some algebraic manipulation] in terms of the more familiar diameter-Reynolds modulus gives

$$\frac{qd_e/k}{\Delta t_x} N_{Re}^{-n} = f(N_{Pr})\left(\frac{x}{d_e}\right)^{n-1} \tag{3}$$

and

$$\frac{m\rho_a/G}{\Delta\rho_x} N_{Re}^{1-n} = g_1(N_{Sc})\left(\frac{x}{d_e}\right)^{n-1}, \tag{4}$$

where N_{Re} is now the Reynolds modulus based on the equivalent diameter of the channel, d_e (in ft); ρ_a is the density of the bulk fluid; and G is the mass velocity (in $lb/hr \cdot ft^2$). For given N_{Pr} and N_{Sc} in a given geometry, $f(N_{Pr})$ and $g_1(N_{Sc})$ are constants (say B_1 and C, respectively). The problem is simplified further by considering only the mean values of the temperature and the mass removal at any x and by defining the temperature and concentration excess in terms of fluid conditions at the channel inlet. Thus, $\Delta t_x = \overline{t_{w,x}} - t_{a,i}$ and $\Delta\rho_x = \rho_{v,w} - \rho_{v,a,i}$. In the latter expression, $\rho_{v,w}$ is a constant over the entire surface, being derived from the vapor pressure of naphthalene in an isothermal system; and since the naphthalene concentration in the inlet air is zero, $\rho_{v,a,i} = 0$. Hence, $\Delta\rho_x = \rho_{v,w}$. The comparison between the heat and mass transfer experiments must be tempered somewhat by the fact that the heat-transfer measurements correspond most closely to a uniform wall heat (mass) flux situation, whereas the mass transfer studies relate to a uniform wall concentration (temperature) condition. For this analysis the heat-transfer data have been reduced to an isothermal condition on the basis that the ratio of the uniform flux coefficient to the uniform temperature coefficient is 1.043.

In the heat-transfer experiments, since the x origin of the Δt_x curve does not necessarily coincide with the origin of measurement (because of end losses and some heat generation in the electrodes that keep the tube

surface temperature upstream of the inlet from being equal to the fluid temperature), it is necessary to replace x by $x + \epsilon d_e$. (The quantity ϵ is determined by extrapolation of the Δt_x curve to the x axis.) Then, taking n for turbulent flow to be 0.8, Eq. (3) becomes

$$\frac{\frac{qd_e}{k}}{\overline{t_{w,x}} - t_{a,i}} N_{Re}^{-0.8} = B_1 \left(\frac{x}{d_e} + \epsilon \right)^{-0.2} , \qquad (5)$$

where B_1 and ϵ must be determined by experimental means.

Since the molecular diffusion ratio shifts from $N_{Pr} = 0.7$ in the heat-transfer tests to $N_{Sc} = 2.5$ in the mass-transfer studies, a change in the value of n in Eqs. (2) and (4) from 0.8 is to be expected. In the region of x-Reynolds modulus of interest, both the von Kármán analogy[5] and the Deissler and Loeffler analysis[6] suggest n = 0.83 for turbulent flow; this value has been confirmed by the experiments of Sherwood and Trass.[7] Equation (4) can then be written

$$\frac{m\rho_a/G}{\rho_{v,w}} N_{Re}^{0.17} = C \left(\frac{x}{d_e} + \epsilon \right)^{-0.17} . \qquad (6)$$

Further, in the mass-transfer experiments it is necessary to account for the inert starting sections (uncoated portions of the rods) which have no counterpart in the heat-transfer studies. Again, by analogy with both experiment and theory for flat-plate geometries, it is possible to obtain the expression

---

[5]J. G. Knudson and D. L. Katz, Fluid Dynamics and Heat Transfer, p. 424, McGraw-Hill, New York, 1958.

[6]R. G. Deissler and A. L. Loeffler, Jr., Turbulent Flow and Heat Transfer on a Flat Plate at High Mach Number with Variable Fluid Properties, ASME Paper No. 55-A-133 (1955).

[7]T. K. Sherwood and O. Trass, Sublimation Mass Transfer Through Compressible Boundary Layers on a Flat Plate, ASME Paper No. 59-A-137 (1959).

$$m(o,x) = m(x_1,x)\left[1-\left(\frac{x_1}{x}\right)^{0.915}\right]^{0.0926}, \qquad (7)$$

where $m(o,x)$ represents the mass flux ($lb/hr\cdot ft^2$) which would exist at x if naphthalene existed back to the geometric entrance, and x_i is the actual distance from the geometric entrance to the leading edge of the naphthalene. The quantity m in Eq. (6) corresponds to $m(o,x)$. For the situation in which the naphthalene-coated region extended from x/d_c = 2.7 to x/d_e = 21.8, the ratio $m(o,x)/m(x_1,x)$ varied nonlinearly, as indicated in Table 14.2.

Table 14.2. Correction for Inert Starting Length in Mass-Transfer Experiments

x/d_e	$m(o,x)/m(x_1,x)$	x/d_e	$m(o,x)/m(x_1,x)$
2.7	(naphthalene start)	17.4	0.982
3.8	0.885	19.6	0.984
6.1	0.942	21.8	0.985
9.8	0.967	22.5	(mid-cluster spacer)
13.6	0.976		

The data obtained thus far on heat and mass transfer in EGCR-type clusters have derived from studies with a number of significantly different experimental systems[8] (various entrance arrangements, spider and mid-cluster spacer designs, channel diameters, and tube spacings). However, for the purposes of this analysis, these several systems will be considered as a composite. It is further assumed that each mid-cluster spacer and end spider induces such violent mixing that fluid properties, including temperature and velocity, are virtually uniform at the inlet

[8]GCR Quar. Prog. Rep. June 30, 1959, ORNL-2767, pp. 75–76, 80; Dec. 31, 1959, ORNL-2888, pp. 59–60; June 30, 1960, ORNL-2964, p. 55; June 30, 1961, ORNL-3166, p. 55.

cross section of each cluster segment[9] (as physically defined by the spiders and spacers). These segments are designated I, II, III, and IV, referring, respectively, to the upstream and downstream sections of the inlet cluster and the upstream and downstream sections of the succeeding cluster. Fitting Eqs. (5) and (6) to the experimental data yields the results shown in Table 14.3; a typical comparison of the data with the reciprocal of the correlating equation [Eq. (5)] is shown in Fig. 14.3 for heat transfer in segment II. The weighted-mean value of B_1 in Table 14.3 is 0.0321, and the maximum deviation with respect to all tubes is ±6.4%. Thus,

$$N_{Nu,x_o} = 0.0321\ N_{Re,x_o}^{0.8} \pm 6.4\% \quad , \tag{8}$$

where x_o is the distance from the apparent origin of each segment, $x + \epsilon d_e$. For the downstream portion of the clusters (segments II and IV), the temperature difference is based on the calculated air temperature at the segment inlet. Equation (8) gives values for the heat-transfer coefficient which are ~14% higher than those recommended by Eckert and Drake[10] and ~28% higher than found experimentally by Reynolds et al.[11] In view of the differences in configuration and the high interstitial velocities existing at a given flow in the cluster geometry, this disagreement is not unreasonable.

Similarly, for the mass-transfer experiments, it is found that

$$N_{Sh,x_o} = 0.045\ N_{Re,x_o}^{0.83} \pm 15\% \tag{9}$$

---

[9]For the mass-transfer experiments, the data indicate that this assumption is not entirely correct. A more detailed discussion is to be found in a forthcoming memorandum by H. H. Sogin, "A Unified Correlation of Mean Heat and Mass Transfer Distributions in Seven-Tube Clusters."

[10]E. R. G. Eckert and R. M. Drake, Jr., Heat and Mass Transfer, pp. 173–6, 215–7, McGraw-Hill, New York, 1959.

[11]W. C. Reynolds, W. M. Kays, and S. J. Kline, Heat Transfer in the Turbulent Incompressible Boundary Layer, NASA Memoranda 12-1-58W, 12-2-58W, 12-3-58W, and 12-4-58W (1958).

is an adequate representation of the data. This result is ~31% greater than that obtained by Sherwood and Trass[7] for sublimation from a flat plate. The wide dispersion (±15%) has been included in order to account

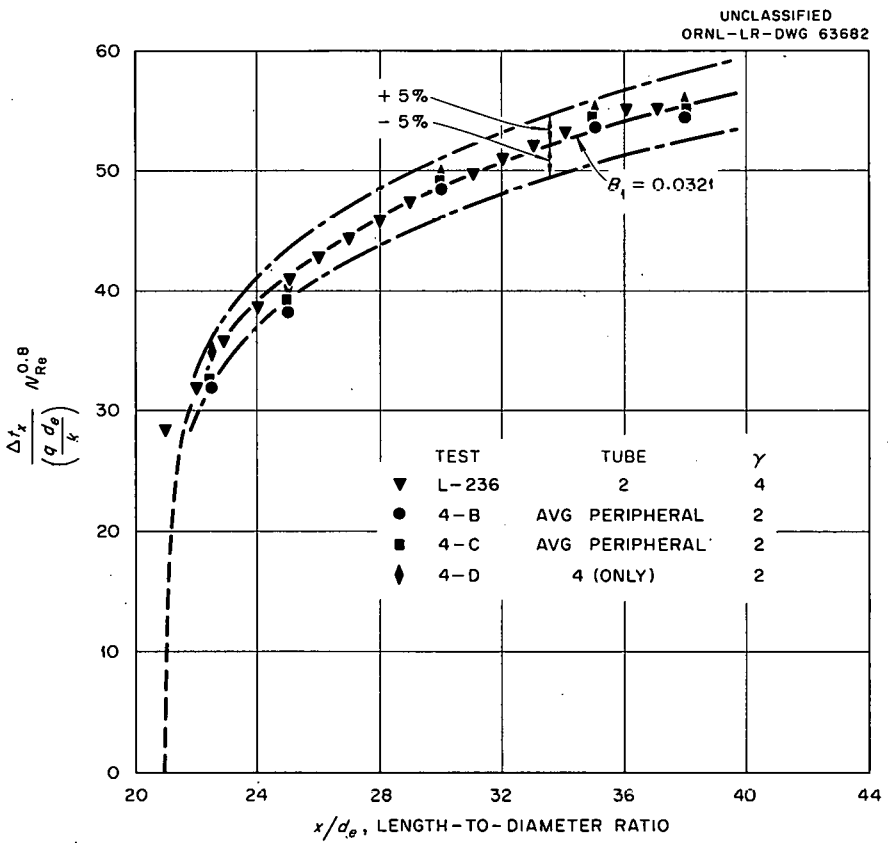

Fig. 14.3. Heat Transfer in Segment II of Model 3 Apparatus.

Table 14.3. Experimentally Determined Constants for Eqs. (5) and (6)

Segment	ϵ	Heat Transfer B_1	Mass Transfer C
I	1	0.0325	0.0184
II	−21	0.0317	No data
III	0	0.0307	0.0180
IV	−22.5	0.0333	0.0180

for all extremes at all cluster orientations in the downstream cluster. If only the 0-deg orientation were considered, the variability would be reduced to ±6%.

In view of the assumptions involved in this analysis and the manner in which the correlating equations were developed (N_{Pr} and N_{Sc} introduced in functional form and incorporated empirically into the constant), a comparison between Eqs. (8) and (9) to test the efficiency of the mass-transfer experiments in predicting heat transfer is not possible. However, the heat-transfer correlation (since it is independent of the equivalent diameter and the ligament ratio) should be useful in estimating the thermal characteristics for geometries similar to that of the EGCR cluster. Further experimental studies to examine the assumptions made are planned.

15. DEVELOPMENT OF EQUIPMENT AND TEST FACILITIES

Gas Chromatographic Analysis of Helium at Low Pressures

J. C. White A. S. Meyer, Jr. J. E. Attrill

Experiments are being conducted with a gas chromatograph for the purpose of evaluating its usefulness in continuously monitoring low-pressure (100 mm Hg) helium for H_2, O_2, N_2, CH_4, Co, and CO_2. A process gas chromatograph manufactured by Beckman Instruments, Inc. (Model 320C) has been adapted for these studies. This instrument is functionally similar to the process chromatographs of Greenbrier Instrument, Inc.,[1,2] which have been used for the analysis of helium from test loops and the helium-purification test facility. The instrument is equipped with a linear sampling valve, a dual-column valve, and a programmer-timer-control unit that can be used to carry out sampling and column switching operations according to a preset cycle and also to present the analytical data in bar-graph form. The chromatograph has a thermal conductivity detector equipped with filament elements rather than the 30K thermistors used in the Greenbrier instruments. The sensitivity of this detector is lower by at least an order of magnitude. In initial tests, the Beckman instrument has been found to be quite stable, and it appears to be of adequate sensitivity for application to studies of the reactions of structural metals and contaminants in helium.

The modifications necessary to adapt the instrument to the analysis of low-pressure samples are shown schematically in Fig. 15.1. The sample vent-line is capped off at the sampling valve and the sample inlet is connected to the three-way "vacuum" solenoid. During the period of the analysis cycle, in which the sampling switch is open, the sample loop is evacuated through the vacuum solenoid. When the sampling signal is received from the programmer control unit, the vacuum solenoid is energized to admit the sample at the pressure of the test system. After a few seconds delay,

---

[1]GCR Quar. Prog. Rep. Sept. 30, 1960, ORNL-3015, pp. 143–5.

[2]GCR Quar. Prog. Rep. June 30, 1961, ORNL-3166, pp. 178–80.

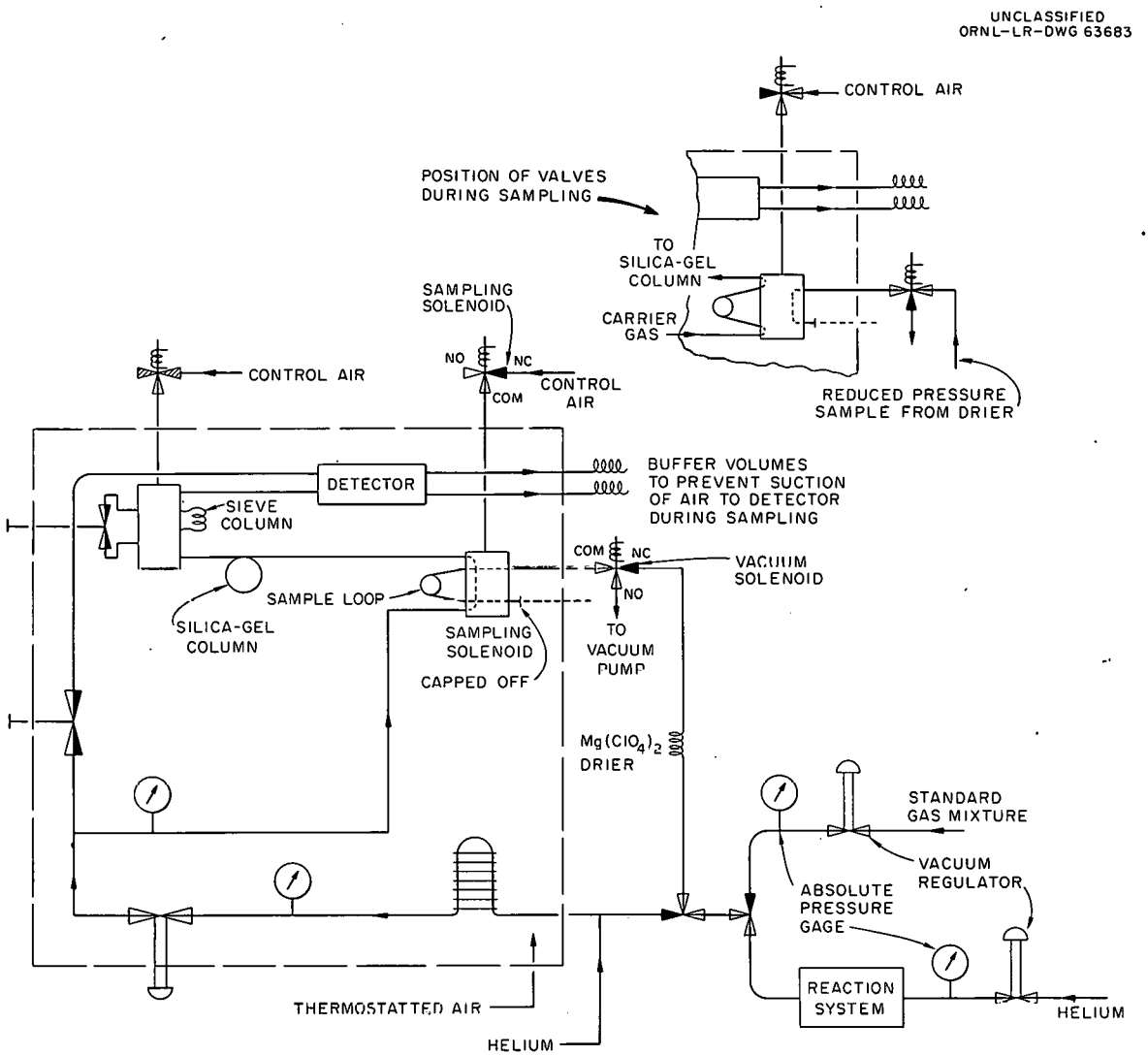

Fig. 15.1. Beckman Model 320C Process Chromatograph with Modifications for Sampling at Low Pressures (Valves of Sampling System Shown in Evacuation Position).

the sampling solenoid is switched to its normal position, and after a few seconds more the sampling valve is returned to the load position to evacuate the carrier gas from the sample loop during the remainder of the analysis cycle. The pressure in the reaction apparatus is maintained by makeup helium that is delivered through a vacuum-regulator valve (Matheson Co. Inc., No. 40). The gas for calibration purposes is

regulated to the same pressure as the test system so that identical volumes of sample are taken from each source.

Delay in the switching of the sampling valve is effected by the simple circuit shown in Fig. 15.2. The signal from the programmer control section immediately energizes the coil of the vacuum solenoid and the heater of the time-delay relay. When the time-delay relay closes, the sampling solenoid is energized. When the sampling switch in the control section is opened, the vacuum solenoid is immediately de-energized, while the sampling solenoid remains energized during the recovery period of the time-delay relay. Carrier gas from the sample loop therefore is not discharged back into the reaction apparatus.

The modified instrument has been assembled and made free of leaks. Excellent resolution of the six contaminants has been obtained with a silica-gel column (3 ft high and 3/16 in. o.d.) and a column (6 ft high and 3/16 in. o.d.) packed with type 5A molecular sieves using a 45 cm^3/min flow rate of carrier gas and at a temperature of 50°C. An analysis cycle can be completed every 15 min. Several as yet unexplained dips in the

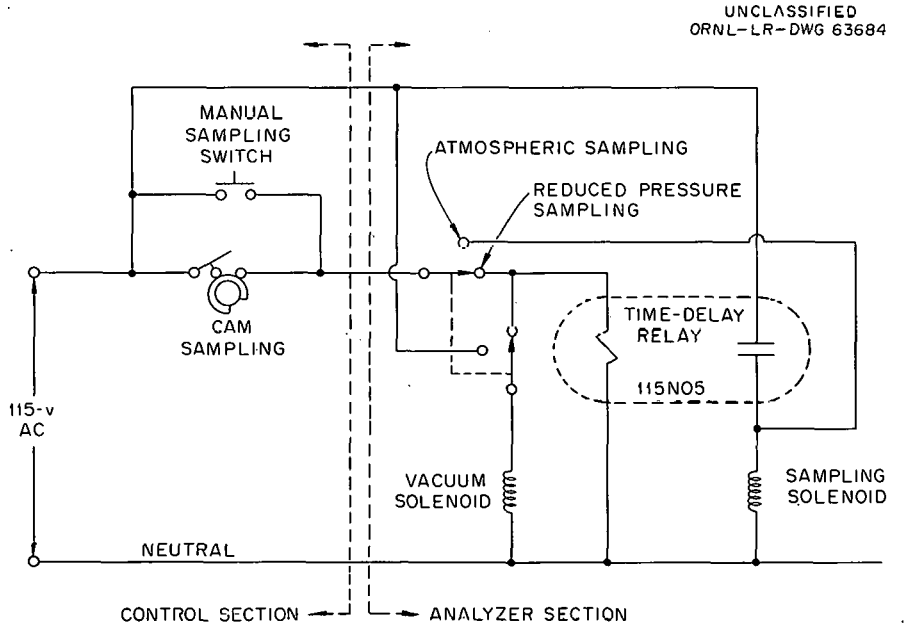

Fig. 15.2. Circuit for Delay of Sampling Valve Switching of Beckman Model 320C Gas Chromatograph.

base line have been observed after each sampling operation. Fortunately, however, none of these aberrations coincide with the peak of an eluted contaminant. Until the filaments, which were damaged during early tests of the instrument, are replaced, sensitivity and reproducibility of this chromatograph cannot be estimated precisely. As an indication of sensitivity, for 5-cm^3 samples at atmospheric pressure, full-scale deflection of the recorder is obtained for a 10% concentration of hydrogen and for concentrations of 1% or less for the remaining contaminants. Although the sensitivity is expected to vary in direct proportion to the absolute pressure, comparable sensitivity for samples at reduced pressure should be attainable by increasing the volume of the sample loop.

Measurement of High Temperatures

W. T. Rainey R. L. Bennett

Long term drift tests have been continued in an attempt to determine the causes of the rapid negative emf drifts noted during exposure of Chromel-P vs Alumel sheathed thermocouples to graphite-helium atmospheres at 870°C. As reported previously,[3] these drifts were shown to be closely associated with gaseous products desorbed from graphite.

The results of two series of tests in which sheathed thermocouples were exposed to pure gases are presented in Fig. 15.3. The Chromel-P vs Alumel thermocouples sheathed in type 304 stainless steel that were used in these tests were fabricated from the material obtained previously from Vendor A and all were grounded-junction thermocouples. They were checked by x-ray and dye penetrant techniques before use. No defects were found. Exposure to carbon monoxide at 7 psig and 865°C for 137 days has resulted in an average emf drift of +0.26 mv (6.5°C). Exposure to hydrogen under the same conditions (in the same furnace) has caused an average negative drift of -2.7 mv (-67.5°C) during 98 days. It should be noted that the thermocouples exposed to hydrogen showed the usual slight positive emf

[3] Ibid., p. 184.

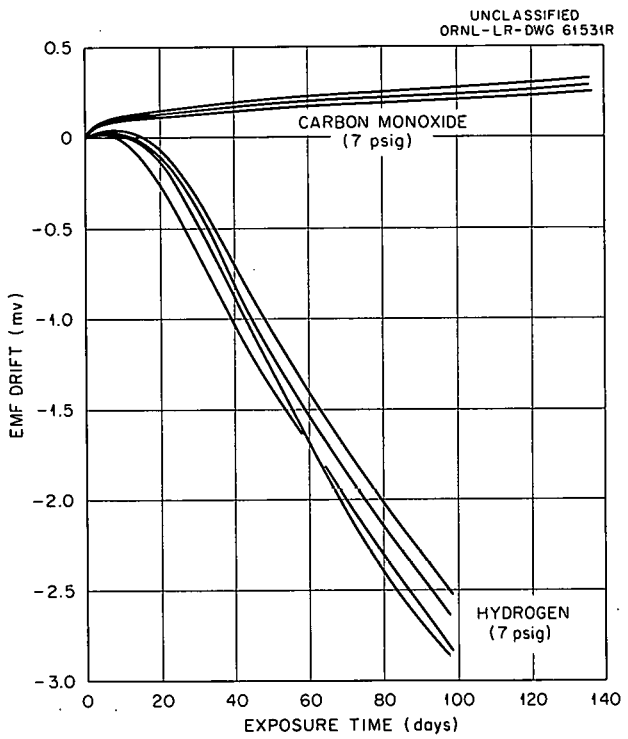

Fig. 15.3. EMF Drift of Chromel-P vs Alumel Sheathed Thermocouples in Hydrogen and Carbon Monoxide at 865°C.

drift during the first 10 days of exposure before the negative drift started.

Additional drift tests have been started under conditions similar to those expected in the EGCR. Sheathed (type 304 stainless steel from Vendor A) thermocouples are being exposed to a graphite-helium atmosphere at 704°C. All these thermocouples are 0.069 in. o.d. and were fabricated with grounded junctions. The tests have been under way for 18 days, and, as expected, no definite trend in emf drift has yet been observed.

Equipment has been set up for a high-pressure drift test to study the rate of emf drift under hydrogen pressures of 100 to 200 psig at 870°C. Two groups of thermocouples have been installed for this test. All the thermocouples have insulated junctions. The 0.069-in.-o.d. sheaths are type 304 or 347 stainless steel. Data have not yet been obtained.

Negative emf drifts are apparently caused by selective oxidation of the chromium in the Chromel-P wire. Hydrogen penetration of the sheath material at elevated temperatures is sufficient to set up the marginally oxidizing conditions necessary for such preferential oxidation. Hydrogen penetration of stainless steel is an accepted phenomenon and does not require defective welds or tubing. The differences in rates of emf drift noted for products from different vendors are probably due to internal differences rather than differences in rates of penetration of hydrogen. So far, no defects have been found in the sheath material which could cause differences in penetration. The oxidizing atmospheres set up inside

the sheath must be dependent upon the air and moisture content of the magnesia and its density, as well as hydrogen content. It is hoped that high hydrogen pressures will accelerate the rate of emf drift so that differences in thermocouple materials may be detected rapidly.

In-Pile Loops for Testing Ceramic Fuels

R. B. Korsmeyer

Two studies have been made of expendable, self-contained, gas-cooled in-pile loops for testing fission-product deposition from unclad reactor fuels. One loop was designed to fit into either the ORR-HN-1 beam hole or into the LITR-HB-2 hole,[4] and the other loop was designed for insertion into an outer experimental hole of the EGCR.[5] The purpose of the studies was to examine the possibilities of the greater experimental flexibility and ease of handling inherent in the operation of portable loops compared with permanent in-pile installations, recognizing, of course, that this approach entails acceptance of more limited objectives.

The package loop conceived for use in the LITR or the ORR has a fission-power capacity of about 5 kw. A schematic diagram of this loop is shown in Fig. 15.4. The design is based on fixed heat rejection to the circulating water, with supplemental heat supplied to the gas by the preheater for operation below design fission heat from the fuel. In this way, it is possible to keep the gas flow and exit temperature from the fuel at design values. Although intended for operation at constant gas flow regardless of fuel heat output, the flow may be reduced by reducing the pump speed through a variable-frequency power supply.

Since the loop was conceived as a device for testing fission-product deposition from unclad fuel elements, such as pebble-bed reactor fuels, a comparison of its characteristics with those of the pebble-bed reactor

---

[4]R. B. Korsmeyer, An In-Pile Loop for Testing Ceramic Fuels, ORNL CF-61-6-67, June 30, 1961.

[5]R. B. Korsmeyer, EGCR Package Loop, ORNL CF-61-8-69, Aug. 23, 1961.

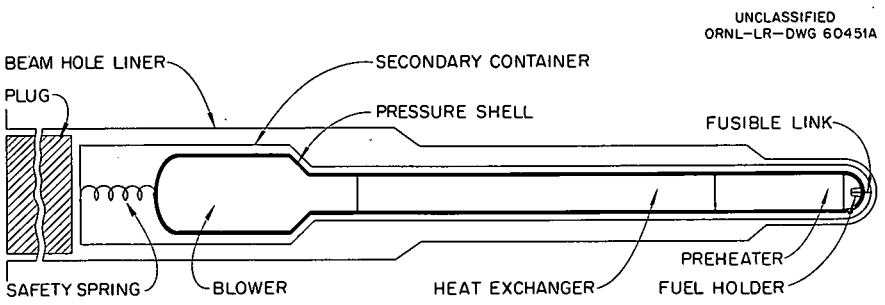

Fig. 15.4. Schematic Diagram of Loop In-Pile Testing of Unclad Fuels.

GCR-ORR loop No. 2 provides some indication of the degree to which loop experiments could be made to simulate large reactor operations.

It is not clear at the present time what parameter is most useful for scaling fission-product deposition data from loop tests to the conditions visualized in large power reactors. Two parameters which have been generally considered are surface-to-total power and surface-to-volume ratios. However, heat transfer specialists indicate that another parameter, the length-to-equivalent diameter ratio, is controlling. This view stems from the belief that the mechanism of fission-product deposition is related to the mechanism governing mass transfer and heat transfer in fluid streams. These parameters for the corresponding zones of the pebble-bed reactor, GCR-ORR loop No. 2, and the package loop are listed in Table 15.1, along with descriptions of the zones, the approximate gas temperature ranges, and the percentage of total surface in each case. It is apparent that the simulation between the pebble-bed reactor and the loops with respect to surface-to-power or surface-to-volume ratios is not very good, although the length-to-diameter ratios in the main heat exchangers in each case are of the same order.

The loop for use in the EGCR is shown in schematic outline in Fig. 15.5. The main heat sink for the loop is furnished by the helium supply for through-tube cooling, which is available at 125°F and 175 lb/hr in the horizontal pipe chase. This helium passes first through the cooler in countercurrent exchange with the loop gas and then enters the regenerator in parallel but not mixed with the pump discharge. The regenerator reduces

Table 15.1. Comparison of Loop and Pebble-Bed Reactor Surfaces, Volumes, and Some Length-to-Diameter Ratios

Zone	Zone Temperature Conditions	Pebble-Bed Reactor (800 Mw)					GCR-ORR Loop No. 2 (76 kw)					Package Loop (5 kw)				
		Zone Description and Temperature (°F)	Surface (%)	Surface-to-Volume Ratio, S/V (ft^{-1})	Surface-to-Power Ratio, S/P (ft^2/Mw)	Length-to-Diameter Ratio, L/D	Zone Description and Temperature (°F)	Surface[a] (%)	S/V[b]	S/P	L/D[b]	Zone Description and Temperature (°F)	Surface (%)	S/V	S/P	L/D
1	Hottest, contains fuel	Core, 550–1350°F	0.4	0.2	1.0		Fuel chamber, 1250–1500°F	0.6	16	0.01		Fuel chamber, 1200°F	1.0	75	0.06	
2	Hot gas, nearly isothermal	Hot plenum, 1350°F	0.3	0.2	0.5	<1.0	Hot piping between fuel chamber and regenerator, 1370°F	5.3	16	0.09	54	Preheater[c] hot gas return duct, ~1200°F	0.5	41	0.03	56
		Steam generator stack, 1250°F	0.3	1.2	0.5	14.0										
3	Gas cooling	Steam generator, hot gas side, 1250–550°F	68.5	22.0	153.0	850	Regenerator (hot side), 1360–870°F	29.3	434	0.50	220	Regenerator, hot side, 1200–500°F	43.6	520	2.6	420
							Evaporator, 870–600°F	2.9	77	0.05	58					
4	Cool gas, nearly isothermal	Vessel shell, thermal barrier, piping, blowers, 550°F	4.1	2.9	9.2		Piping compressors, ~600°F	17.4	19	0.30	216	Compressor, pressure shell, 500°F	11.4	15	0.7	
		Cool graphite shield, 550°F	13.2	31.0	29.0		Filter, ~600°F		High	High						
5	Gas preheating	None					Regenerator, cold gas side, 620–1230°F	29.3	434	0.50	220	Regenerator, cold gas side 500–900°F	43.0	510	2.6	420
6	Intermediate gas temperature nearly isothermal	None					Preheater, 1300°F	11.1	70	0.19		Preheater 900–1200°F	0.5	43	0.03	37
							Piping, ~1250°F	4.1	19	0.07	39					

[a] Excluding filter.

[b] Data furnished by T. S. Kress.

[c] Pressure vessel shell in this region and in the region of the fuel chamber will probably need to be insulated from the hot gas sufficiently to assure a maximum metal temperature no higher than about 1100°F; otherwise this passage of the preheater would be classed in zone 3.

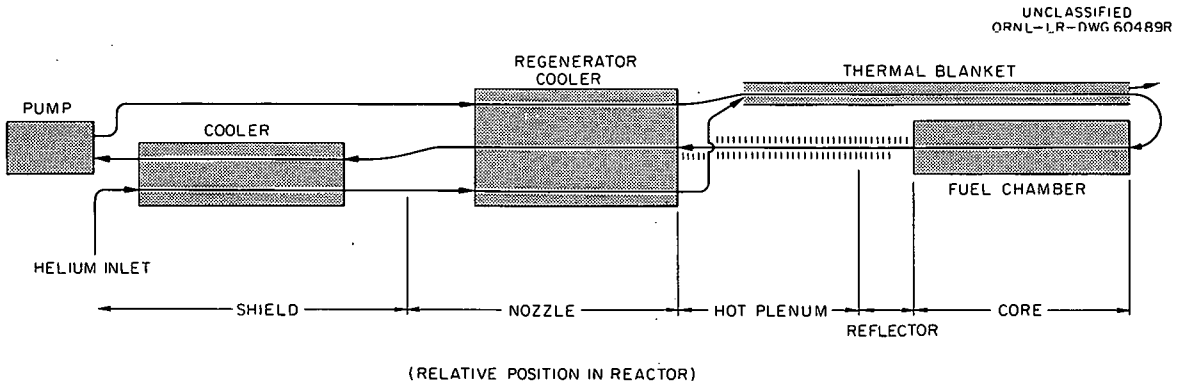

Fig. 15.5. Schematic Diagram of EGCR Package Loop.

the temperature of the hot gas, entering at a maximum of 1150°F, by simultaneous regenerative heat exchange with the pump discharge and heat rejection to the helium coolant. The loop gas (pump discharge stream) leaves the regenerator surrounded by the helium coolant in concentric ducts.

The concentric streams are ducted through the hot plenum and down into the core to the loop fuel chamber inlet where the cooling helium stream is discharged directly into the reactor. Thus the cooling stream holds the temperature rise of the loop to a minimum during passage to the fuel chamber inlet. The loop gas passes upward through the fuel and leaves the fuel chamber through a bare pipe in order to cool down to the reactor hot gas temperature before entering the regenerator.

THIS PAGE

WAS INTENTIONALLY

LEFT BLANK

PART 4. TEST FACILITIES, COMPONENTS, AND MATERIALS

16. TEST FACILITIES DESIGN AND CONSTRUCTION

GCR-ORR Loop No. 2

J. Zasler

Design and Construction (P. A. Gnadt, W. R. Huntley, S. Kress, E. E. Wade)

Construction of the ORR facility has been essentially completed. All components have been set and the main piping between them has been welded in place. The main components and piping, except for the compressors and heater, are shown in Fig. 16.1. The side-stream cleanup system, except for some special valves not yet received, and the flange buffer gas system are complete and ready for checkout.

The full-flow mainstream filter has been pretested, assembled in its shield, and installed at the ORR. Pretesting consisted of thermal cycling three times to 700°F. After this test the first unit and a spare tested 99.885 and 99.93% efficient on 0.3-μ smoke particles.

The cell ventilation and associated offgas piping have been installed in the basement. The offgas piping for main loop gas dump and pressure relief has been installed. The cell-cooling and fission-gas-trap refrigeration units have been installed and are ready for checkout.

The cell viewing window and the control stations for remotely operated cell maintenance equipment have been installed. The shielding door for the experimental assembly removal hole has been installed (Fig. 16.2).

The main electric control panels have been set in the basement of the ORR Building. Shop work on the auxiliary electrical and the pneumatic control panels is continuing. The electrical and instrument penetrations have been installed and are ready for the cell leakage rate test. The primary electrical supplies and switchgear have been installed. The motor-generators and associated speed-control equipment for the compressors have been installed and checked out. Cable runs between the power supplies, main control panels, and the cell penetrations are now being installed.

Piping for the beam hole and experimental assembly cooling water is approximately 30% complete. The remaining portion of this water system

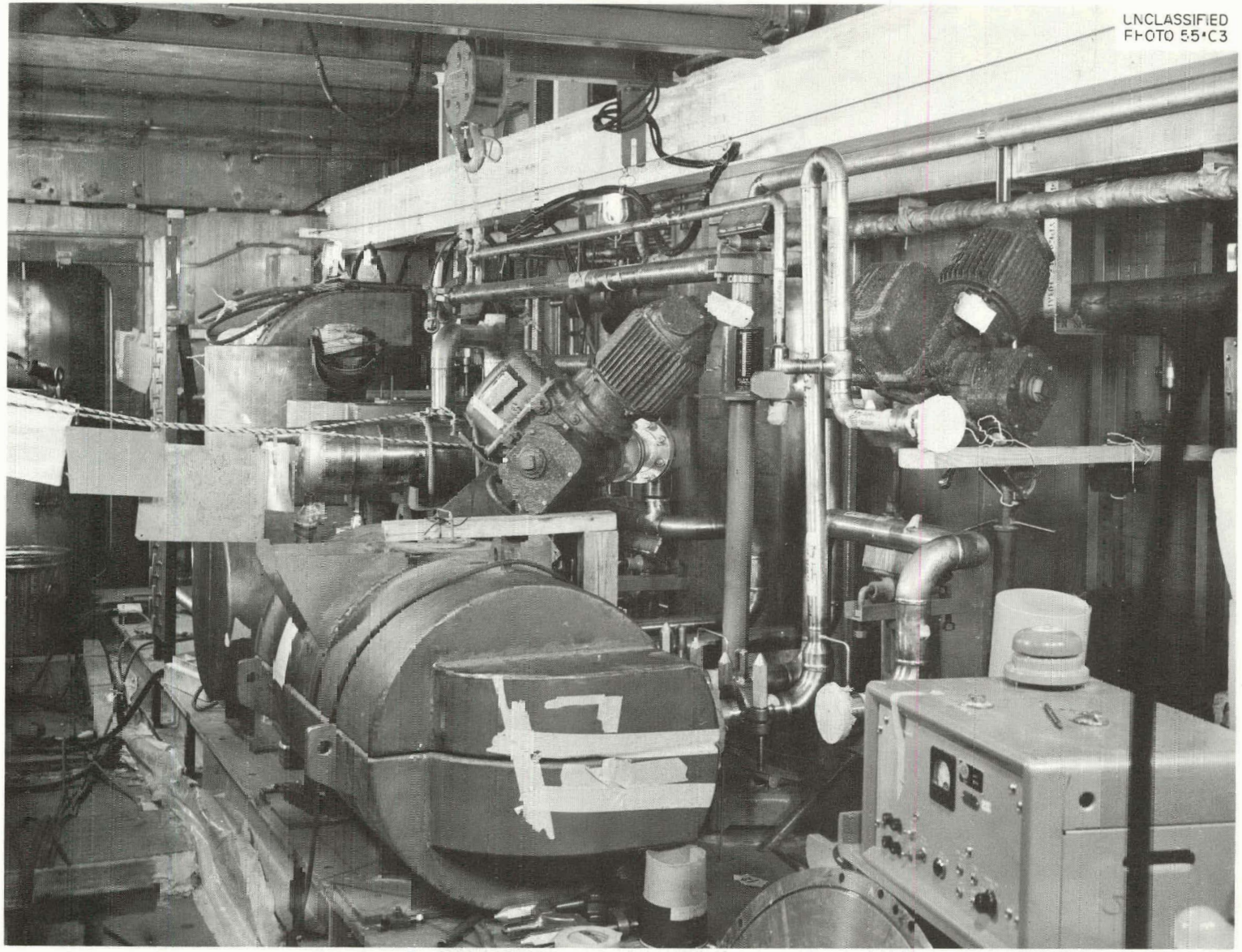

Fig. 16.1. Main Components of GCR-ORR Loop No. 2 Facility as Viewed Through Cell Window.

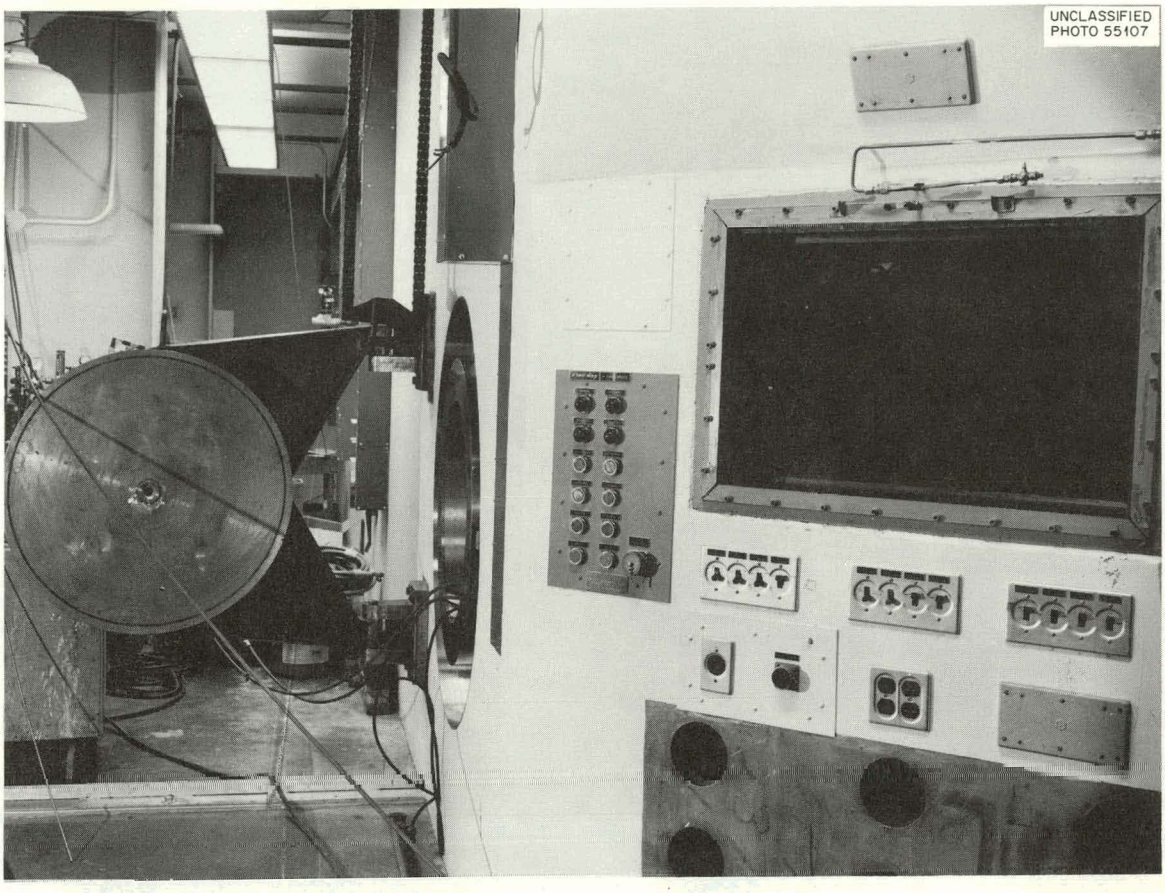

Fig. 16.2. View of GCR-ORR Loop No. 2 Facility Showing Shielding Door for Removal of Experimental Assemblies and Viewing Window.

will be installed during the reactor shutdown scheduled for October. All main piping for the on-rack water systems and the supplies has been installed.

Detailing was completed on the 24-in. shielding plug, and the unit is now being fabricated. Work has continued on the 35-ton experimental assembly and pressure piping carrier. The carrier dollies have been finished. The transfer table, which provides for withdrawal of the test plugs across the cell, is also nearing completion. The inner seal door of the test-plug removal sleeve is complete. Three ion-chamber shields were fabricated and lead filled and work was started on two more.

The ORNL-designed compressors with grease-lubricated bearings, which are to be used initially in the loop, have been delivered and installed at the ORR.

Performance tests of the prototype 1 1/2-in. sched-80 pipe cutting and sealing die were completed. A pipe cut made with the die is shown in Fig. 16.3. Helium leakage rates of the severed ends of the pipe of the order of 10^{-2} to 10 cm^3 (STP)/sec were obtained. During testing, the forming blocks shifted, and it is believed that a more consistent and, on the average, lower leakage rate is obtainable with fixed blocks. Adherence of the pipe metal to the knife did not increase after the first three cuts and is not a problem. One die for use on the loop is on hand and the other was returned to the vendor for correction.

Preliminary tests on connectors for the thermocouple leads which go in the fuel tube show that they will withstand 720 psi without failure

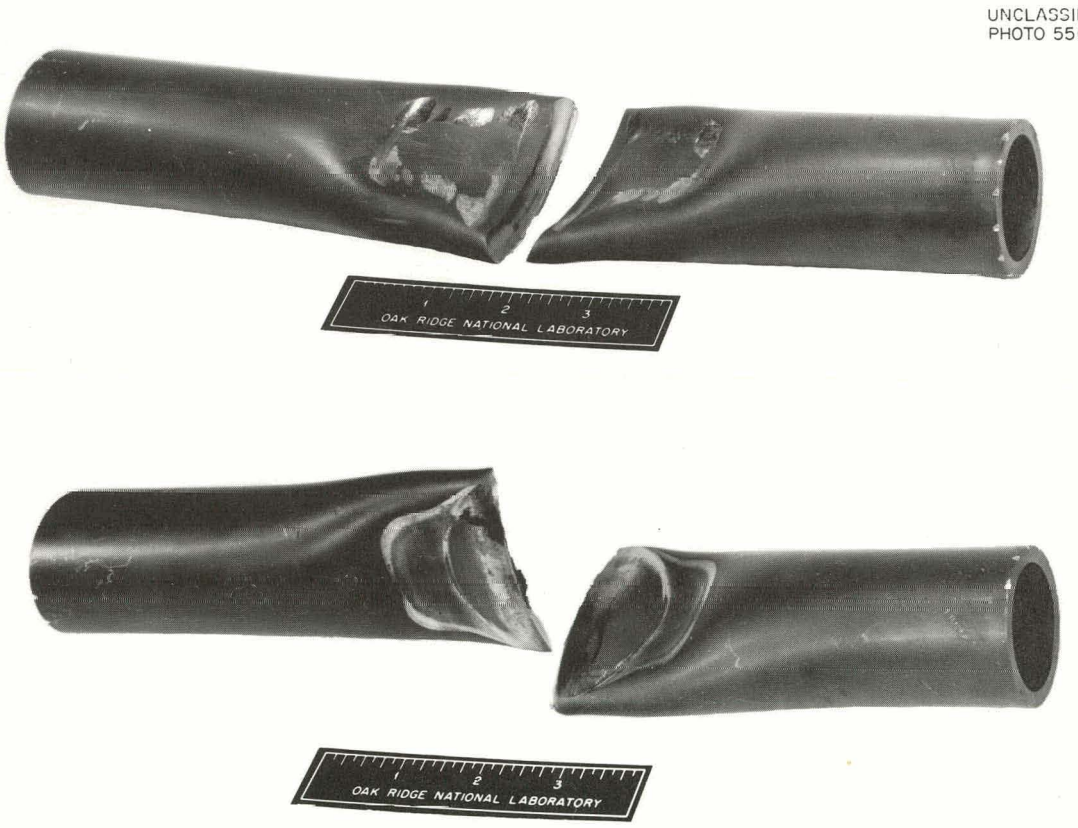

Fig. 16.3. Cuts and Seals Made in 1 1/2-in. Sched.-80 Type 347 Stainless Steel Pipe with Prototype Die.

or leakage. The connector tested had a carbon steel flange. Tests are to be made on connectors with stainless steel flanges.

A slip joint is required in the 18-in. pressure piping plug to allow insertion and removal of the test specimens. This joint is approximately 4 in. in diameter and 8 in. in length, and it must operate at temperatures up to 1500°F. The female member is fabricated from Haynes 25 alloy and the male is type 347 stainless steel flame-spray-coated with aluminum oxide. The slip joint has been tested by thermally cycling it 10 times between 80°F and 1550°F. The inner part was moved longitudinally during the cycling. The results indicate that the joint will be satisfactory in the loop. Dimensional stability was good. X-ray, dye check, and radiography show no cracks. There was no abrasion or self-welding of the materials.

Detailing of the 18-in. pressure piping plug is now complete. A number of design changes have recently been made to provide for better gamma-heat removal in the forward portions of the plug.

Designs were completed of loop auxiliaries such as the sampling system, water-cooling systems, and pressure-transmitter racks. Design work is in progress on the equipment to be used at the segmenting cell for sectioning both the 4-in.-diam fuel tube and the pressure-piping plug after irradiation.

An analysis was made to determine the pressure-relief capacity of the annulus between the 24-in. plug and the test plug. It was concluded that the capacity is sufficient to relieve the test region in the event of a rupture of the main loop pressure shell.

The side-stream cooler was eliminated because it was determined that adequate cooling was obtained by radiation and natural-convection heat transfer from the length of tubing leading from the rack to the first side-stream component.

The 7090 code (TOSS) has been successfully revised and extended so that multiple modes of heat transfer (e.g. radiation, convection, and conduction) from a single surface can be considered. This will be made available through the SHARE organization after a finished report is written. This code has been used extensively in several studies for loop No. 2:

The axial "in-pile" location on the pressure shell at which exterior insulation may begin was determined with the extended code; also determined were temperatures and pressures existing in the transfer cask during transfer of a fuel element, temperature distributions in the concrete behind the thermal shield for two values of gamma heat, tentative results for the hazardous condition of loss of loop coolant and no subsequent ORR action, and results for the similar condition of loss of loop coolant accompanied by a scram of the ORR. The latter condition was also simulated on the analog computer, and the results will be compared with the 7090 data.

New input data were compiled for analog computer simulation of the loop in its more advanced stages of design. Results were obtained but have not yet been evaluated.

Filter Tests (R. E. MacPherson)

Tests have been conducted on both Flanders Airpure and Cambridge Absolute filters for use as full-flow primary coolant filters. Efficiency tests were conducted on the filters in the "as received" condition, after "canning," and after thermal cycling of the canned units. Also, air pressure drop tests were performed on the canned filters over a flow range of 150 to 530 lb/hr.

Results of the tests on the Flanders Airpure filters were reported previously.[1] Results of tests on the Cambridge Absolute filters are given in Table 16.1. Although the three filters did not meet the design criterion of 99.97% efficiency for removal of 0.3-μ particles, they are considered to be satisfactory for the intended application. The efficiency of the filters was not impaired during thermal cycling. In fact, post-thermal cycling efficiency tests showed a slightly higher efficiency than that of the "as received" filters. It was also demonstrated that some volatile material would be given off for a limited time when the filter was initially heated. A curve of filter pressure drop versus gas flow rate for unit No. 1 is shown in Fig. 16.4.

[1]GCR Quar. Prog. Rep. March 31, 1961, ORNL-3102, p. 268.

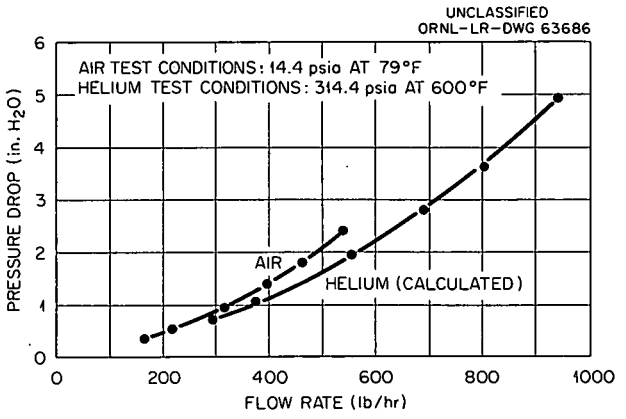

Fig. 16.4. Pressure Drop Versus Flow Rate Across Filter Unit No. 1.

Table 16.1. Results of Efficiency Tests of Cambridge Absolute Filters

Unit	Condition	D.O.P. Filter Efficiency[a]
1	As received	99.926
2	As received	99.540
3	As received	99.850
1	Canned (before thermal cycling)	99.991
2	Canned (before thermal cycling)	99.930
1	Canned (after thermal cycling)	99.964
2	Canned (after thermal cycling)	99.885
1	Canned (after "bake out" at 705°F)	99.993

[a]Dioctylphthalate, 0.3-μ particle size.

Modification of GCR-ORR Loop No. 1

J. K. Franzreb

All equipment and instrumentation installed in the newly reconstructed loop has performed as designed. The loop has been used to irradiate

pressure vessel steel weld samples for two seven-week cycles. The maximum specimen temperature has been held at 555°F and the temperature spread from top to bottom of the specimen column has been only 50 to 60°F.

The additional instrumentation necessary for fuel capsule tests in the rebuilt loop is nearly complete. The secondary containment around the compressor piping has been completed, and a satisfactory helium leakage rate has been obtained. Shielding of the secondary containment around the surge tank and duct is also complete. The design report and the safeguards questionnaire were completed, and the loop design was accepted by the ORNL Reactor Experimental Review Committee.

Compressor Development

W. F. Boudreau

Regenerative Compressors with Grease-Lubricated Bearings

Compressors for GCR-ORR Loops. (I. K. Namba) An evaluation of the condition of the bearings that were removed from the two compressors which had operated[2] for 3300 hr in GCR-ORR loop No. 1 was received from the manufacturer (Barden Corp.). The report indicated that the bearings could have operated for some additional period of time in a satisfactory manner, without relubrication. The compressors now installed in this loop have accumulated about 2300 hr of running time at helium conditions of 275 psig and 550°F, and it is planned to continue operating them for a further period of at least 1200 hr before removing them for inspection.

Two regenerative compressors are being installed in GCR-ORR loop No. 2, and the components for a third unit are being procured. The rotating assemblies for these compressors are identical to those being used for GCR-ORR loop No. 1, except that two-pole motors are being used in the new units to match the output of the presently installed motor-generator sets. Two of these compressors will be operated in parallel to provide about 80% of the original design mass flow for loop No. 2. Each of these

[2]GCR Quar. Prog. Rep. June 30, 1961, ORNL-3166, p. 214.

compressors is installed in its own individual pressure vessel to conform to the loop operating and maintenance criteria.

Compressor for Control Rod Drive Test Facility. (H. C. Young) A small regenerative compressor is being fabricated to ORNL drawings, and a loop has been designed for testing it.

Compressors with Gas Bearings

Bristol Siddcley Experimental Compressor. (D. L. Gray) Based on temperature measurements in the critical area of the compressor housing between the volute and the cooling water jacket, it was decided to accept the experimental compressor from Bristol Siddeley with the maximum operating temperature at the normal design pressure of 406 psia limited to 356°F. The installed thermocouples, speed detector, and shaft touch indicators were left intact. The compressor was received on July 31, and final electrical and instrument work are under way on the loop for testing it.

Continental Bearing Research Corporation Experimental Compressor. (D. L. Gray) A gas-lubricated bearing system designed and fabricated by the Continental Bearing Research Corporation was tested. The rotating unit was accelerated to approximately 18 000 rpm before the electrical supply was temporarily lost. During the 4 to 5 min required to restore the power supply, the unit decelerated smoothly to approximately 6000 to 8000 rpm. When the power supply was restored, the unit accelerated to 24 000 rpm and then stopped abruptly. Inspection revealed that the bronze end rings of the motor rotor (supplied by ORNL) had ruptured and rubbed against the stator.

Since the bearings appeared to have operated successfully, plans are being made to rebuild the test unit, either with a similar rotor furnished by ORNL or with a new motor procured from a vendor to be selected by the compressor fabricator. The rebuilt unit will be tested in Oak Ridge, where a variable-frequency power supply is available for testing at lower speeds.

Compressors for GCR-ORR Loop No. 2. (H. C. Young) Bristol Siddeley has revised the delivery date for the first two compressors from July 31 to October 15, 1961. One compressor was operated at full speed, pressure,

and temperature for a short period; however, bearing touching terminated the test. Modifications to the cooling system to reduce thermal stresses have resulted in excessive operating temperatures at the front bearing, and a number of modifications to provide greater internal cooling are in progress.

Thermocouple readings in the area of the flange and motor barrel junction indicate that, even with an electric heater, the total maximum stress exceeds the allowable stress. The heater is to be relocated closer to the flange undercut in an effort to reduce the temperature gradient.

Development of Shaft Seals

W. F. Boudreau W. K. Stair

Subcontract arrangements have been made for the development of basic information on the design and operation of shaft seals. The mechanical Engineering Department of the University of Tennessee will undertake a study that will include:

1. a critical screening survey of known devices for gas dynamic sealing,
2. detailed theoretical analyses of those devices which hold the greatest promise of practical utilization,
3. design and fabrication of a reduced-scale seal testing facility,
4. a test program for the experimental evaluation of the parameters developed under item 2.

17. FABRICATION STUDIES

J. H. Coobs

Fabrication of Unfueled BeO

R. L. Hamner

High-purity specimens of unfueled BeO are being prepared for irradiation experiments designed to evaluate BeO as a moderator material for reactors in which high fast-neutron doses would be accumulated. A total of 115 cylindrical BeO specimens, 0.800 ± 0.002 in. in diameter and 0.500 ± 0.002 in. long, were prepared for irradiation experiment ORNL-41-7 in the ETR (see chapter 12, this report). These specimens were fabricated to the specified dimensions by cold pressing and sintering in hydrogen at 1750°C. The bulk densities obtained were 2.90 ± 0.01 g/cm^3, or approximately 96% of theoretical. Additional BeO specimens of the same dimensions and with a bulk density of 2.80 ± 0.03 g/cm^3 were machined from hot-pressed blocks for use in this experiment. The conditions in the proposed irradiation experiment will be similar to those obtained in a prior (ORNL-41-5) test in which low-density, 0.8-in.-diam specimens cracked and powdered at a fast-neutron dose of greater than 10^{21} neutrons/cm^2 (>1 Mev).

In preliminary development work it was observed again[1] that the bulk density of BeO bodies was affected markedly when the heating rate to the sintering temperature was varied. Starting with the same green density, the final bulk density obtained was decreased from 96 to 64% of theoretical when the time to reach the sintering temperature was increased from 2 to 24 hr. It is noted that these results are directly opposite to those reported by Lively et al[2] based on sintering studies of BeO conducted in an air atmosphere. This anomaly is not understood, but it might be caused by prolonged exposure of the BeO to trace amounts of moisture in the hydrogen atmosphere during sintering.[3]

---

[1]GCR Quar. Prog. Rep. June 30, 1961, ORNL-3166, pp. 83–84.

[2]D. T. Livey, N. Brett, I. Denton, and P. Murray, Factors Affecting the Density of Sintered and Hot Pressed Beryllia, Progr. in Nuclear Energy Tech., Engr., and Safety, 3(IV): 111–34 (1960).

The preparation of small, cylindrical, 0.25-in.-diam, 0.25-in.-long BeO specimens of four different types for irradiation experiment ORNL-41-8 was begun, based on the specifications and fabrication developments previously reported.[1] This experimental assembly is designed for studying the effects of density, grain size, and temperature on BeO bodies irradiated at high fast-neutron doses. The 120 specimens designed to meet the low-density large-grain-size specifications were cold pressed and sintered in hydrogen at 1750°C to a dimension approximately 0.003 in. oversize and to a bulk density of approximately 2.6 g/cm^3. It is calculated that with the extended heat treatment required to increase the grain size the specimens will shrink to meet the dimensional specification and that the bulk density will be increased to approximately 2.7 g/cm^3. An additional 118 specimens for this series that were designed to meet the high-density fine-grain-size specification were sintered under the same conditions to a bulk density of 2.90 ± 0.01 g/cm^3 and are now being characterized.

Fabrication studies were initiated on the preparation of larger BeO specimens of the same type with densities of 2.7 and 2.9 g/cm^3 and two significantly different grain sizes for each density. These specimens, nominally 0.5 in. in diameter and 0.5 in. long, are to be included in experimental assembly ORNL-41-8 to evaluate the additional variable of thermal stress.

Compatibility of Selected Ceramics and Metals

J. M. Kerr

Nine different combinations of ceramics and metals were heated to 1400°C in flowing argon for a minimum time of 100 hr. The combinations were Al_2O_3-Re, BeO-Re, MgO-Mo, ThO_2-Re, UO_2-Re, ZrO_2-Mo, pyrolytic graphite-Mo, pyrolytic graphite-Ta, and UO_2-Ta. The first six couples of the above list were heated for 100 hr, the pyrolytic graphite-Mo and pyrolytic graphite-Ta

[3]C. A. Aitken, Initial Sintering Kinetics of Beryllium Oxide, J. Am. Ceram. Soc., 43: 630 (Dec. 1960).

couples were heated for 345 hr, and the UO_2-Ta couple was heated for 772 hr. Metallographic examination revealed reaction only between MgO-Mo and pyrolytic graphite-Mo. No reaction was observed between any of the other ceramic-metal combinations. A duplicate run of the pyrolytic graphite-Ta couple will be made.

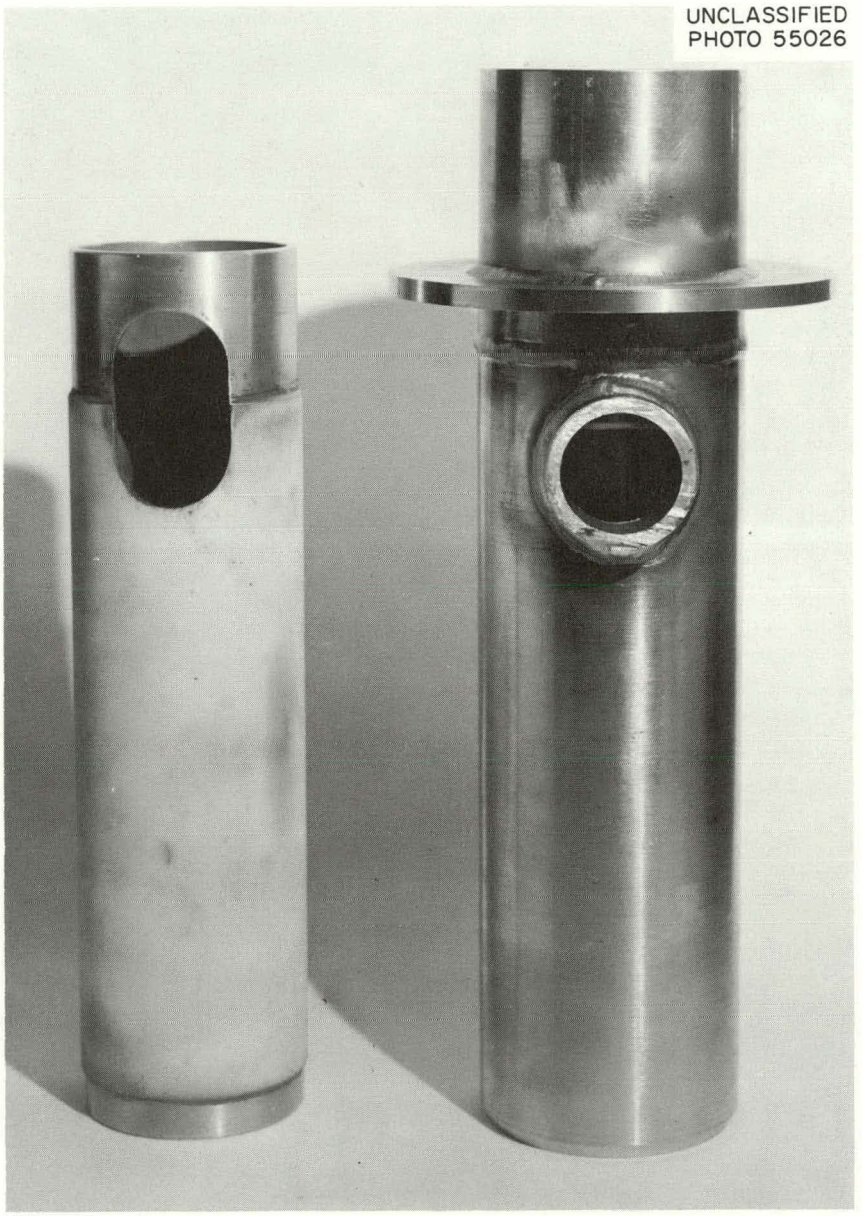

Fig. 17.1. GCR-ORR Loop No. 2 Slip-Joint Test Assembly. The nozzle "T" section is on the right and the aluminum oxide-coated inner tube is shown on the left.

GCR-ORR Loop No. 2 Fabrication Assistance

E. A. Franco-Ferreira

A nozzle slip-joint test assembly for ORR loop No. 2 use has been fabricated. The two sections of this unit are shown in Fig. 17.1. On the right is shown the nozzle T section and on the left is the Al_2O_3-coated, stainless steel inner tube. The lower portion of the T section is made of Haynes 25 alloy; two dissimilar-metal welds were required between the Haynes 25 alloy and the stainless steel.

All welds were inspected and the critical dimensions of the parts have been measured. The test assembly is presently being thermally cycled through ten cycles from room temperature to 1550°F in a helium atmosphere. While the assembly is at temperature, the inner tube is moved to determine whether self-welding or galling occurs. After the cycling tests are completed, the parts will be measured to check dimensional stability, and all welds will be inspected again. If the unit successfully passes the examination, the T section will be installed in the ORR loop No. 2 facility.

Previous reports in this series are:

ORNL-2500 Parts 1–4, issued April 1, 1958
ORNL-2505 Issued June 19, 1958
ORNL-2510 Issued September 18, 1958
ORNL-2676 Period Ending December 31, 1958
ORNL-2767 Period Ending June 30, 1959
ORNL-2835 Period Ending September 30, 1959
ORNL-2888 Period Ending December 31, 1959
ORNL-2929 Period Ending March 31, 1960
ORNL-2964 Period Ending June 30, 1960
ORNL-3015 Period Ending September 30, 1960
ORNL-3049 Period Ending December 31, 1960
ORNL-3102 Period Ending March 31, 1961
ORNL-3166 Period Ending June 30, 1961

THIS PAGE

WAS INTENTIONALLY

LEFT BLANK

ORNL-3210

Reactor Technology
TID-4500 (16th ed.)

INTERNAL DISTRIBUTION

1. G. M. Adamson
2. S. A. Beall
3. M. Bender
4. R. G. Berggren
5. D. S. Billington
6. E. P. Blizard
7. E. C. Bohlmann
8. C. J. Borkowski
9. G. E. Boyd
10. R. B. Briggs
11. W. E. Browning
12. F. L. Carlsen
13. E. L. Compere
14. J. H. Coobs
15. W. B. Cottrell
16. J. A. Cox
17. F. L. Culler
18. J. H. DeVan
19. D. A. Douglas
20. R. B. Evans
21. D. E. Ferguson
22. J. L. Fowler
23. A. P. Fraas
24. J. H. Frye, Jr.
25. W. R. Gall
26. A. E. Goldman
27. B. L. Greenstreet
28. W. R. Grimes
29. J. P. Hammond
30. W. O. Harms
31. M. R. Hill
32. H. W. Hoffman
33. A. Hollaender
34. A. S. Householder
35. W. H. Jordan
36. C. P. Keim
37. M. T. Kelley
38. P. Lafyatis
39. J. A. Lane
40. C. E. Larson (K-25)
41. R. S. Livingston
42. H. G. MacPherson
43–62. W. D. Manly
63. R. W. McClung
64. C. J. McHargue
65. F. R. McQuilkin
66. H. J. Metz
67. J. G. Morgan
68. K. Z. Morgan
69. F. H. Neill
70. M. L. Nelson
71. N. Ozisik
72. P. Patriarca
73. A. M. Perry
74. D. Phillips
75. M. E. Ramsey
76. M. W. Rosenthal
77. G. Samuels
78. H. W. Savage
79–80. A. W. Savolainen
81. J. L. Scott
82. O. Sisman
83. E. D. Shipley
84. M. J. Skinner
85. G. M. Slaughter
86. A. H. Snell
87. E. Storto
88. J. C. Suddath
89. J. A. Swartout
90. E. H. Taylor
91. D. F. Toner
92. D. B. Trauger
93. C. S. Walker
94. J. L. Wantland
95. G. M. Watson
96. M. S. Wechsler
97. A. M. Weinberg
98. J. R. Weir
99. J. C. White
100. C. E. Winters
101. J. Zasler
102–105. ORNL – Y-12 Technical Library Document Reference Section
106–172. Laboratory Records Department
173. Laboratory Records Department ORNL R.C.
174–176. Central Research Library

EXTERNAL DISTRIBUTION

177–179. W. F. Banks, Allis-Chalmers Mfg. Co.
180–182. P. D. Bush, Kaiser Engineers
183. R. A. Charpie, UCC Research Administration, New York, N. Y.
184–185. David F. Cope, Reactor Division, AEC, ORO
186–187. R. W. Coyle, Vallecitos Atomic Laboratory
188. E. Creutz, General Atomic
189–191. R. B. Duffield, General Atomic
192. D. H. Fax, Westinghouse Atomic Power Division
193. M. Janes, National Carbon Research Laboratories, Cleveland, Ohio
194. T. Jarvis, Ford Instrument Co.
195. James R. Johnson, Minnesota Mining and Manufacturing Company, Saint Paul, Minn.
196. Richard Kirkpatrick, AEC, Washington
197. C. W. Kuhlman, United Nuclear Corp.
198–199. H. Lichtenburger, General Nuclear Engineering Corp.
200. J. P. McGee, Bureau of Mines, Appalachian Experiment Station
201. S. G. Nordlinger, AEC, Washington
202. R. E. Pahler, High-Temperature Reactor Branch, Reactor Division, AEC, Washington
203. H. B. Rahner, Savannah River Operations Office
204. Corwin Rickard, General Atomic
205. M. T. Simnad, General Atomic
206. Nathanial Stetson, Savannah River Operations Office
207. Donald Stewart, AEC, Washington
208. Philip L. Walker, Pennsylvania State University
209. R. E. Watt, Los Alamos Scientific Laboratory
210–211. W. L. Webb, East Central Nuclear Group, Inc.
212. Division of Research and Development, AEC, ORO
213–813. Given distribution as shown in TID-4500 (16th ed.) under Reactor Technology category (75 copies – OTS)